Advances in Biochemical Engineering/Biotechnology 150
Series Editor: T. Scheper

Bo Mattiasson
Lei Ye *Editors*

Molecularly Imprinted Polymers in Biotechnology

Springer

150
Advances in Biochemical Engineering/Biotechnology

Aims and Scope

This book series reviews current trends in modern biotechnology and biochemical engineering. Its aim is to cover all aspects of these interdisciplinary disciplines, where knowledge, methods and expertise are required from chemistry, biochemistry, microbiology, molecular biology, chemical engineering and computer science.

Volumes are organized topically and provide a comprehensive discussion of developments in the field over the past 3–5 years. The series also discusses new discoveries and applications. Special volumes are dedicated to selected topics which focus on new biotechnological products and new processes for their synthesis and purification.

In general, volumes are edited by well-known guest editors. The series editor and publisher will, however, always be pleased to receive suggestions and supplementary information. Manuscripts are accepted in English.

In references, Advances in Biochemical Engineering/Biotechnology is abbreviated as *Adv. Biochem. Engin./Biotechnol.* and cited as a journal.

More information about this series at http://www.springer.com/series/10

Bo Mattiasson · Lei Ye
Editors

Molecularly Imprinted Polymers in Biotechnology

With contributions by

Richard J. Ansell · Sara Axelsson · Johan Billing
Brian Boyd · Swapnil Chavan · Kerstin Golker
Shan Huang · Björn C.G. Karlsson · Rüstem Kecili
Yukiya Kitayama · Zhuo Li · Yibin Liu · Bin Lu
Hui-ting Ma · Bo Mattiasson · Fosca Mirata
Ian A. Nicholls · Carina Nilsson · David Nivhede
Gustaf D. Olsson · Anthony Rees · Marina Resmini
Annika M. Rosengren · Hirobumi Sunayama
Subramanian Suriyanarayanan · Eri Takano
Toshifumi Takeuchi · Ying-chun Wan
Jesper G. Wiklander · Lei Ye · Ecevit Yilmaz
Meiping Zhao

Springer

Editors
Bo Mattiasson
Department of Biotechnology
Lund University
Lund
Sweden

Lei Ye
Department of Pure and Applied Biochemistry
Lund University
Lund
Sweden

ISSN 0724-6145 ISSN 1616-8542 (electronic)
Advances in Biochemical Engineering/Biotechnology
ISBN 978-3-319-20728-5 ISBN 978-3-319-20729-2 (eBook)
DOI 10.1007/978-3-319-20729-2

Library of Congress Control Number: 2015942812

Springer Cham Heidelberg New York Dordrecht London

Printed on acid-free paper

Springer International Publishing AG Switzerland is part of Springer Science+Business Media (www.springer.com)

Preface

Molecular recognition plays a critical role in numerous living systems. Protein-based receptors, nucleic acids, enzymes and antibodies are well-known examples of biological materials that have high molecular binding selectivity. Because of their well-defined molecular recognition properties, these biological macromolecules have been exploited in many technical applications to offer efficient purification for therapeutic products and to develop analytical methods for monitoring drugs, toxic chemicals in food and environmental pollutants. Although widely used, biological macromolecules are limited by their high production costs and low stability. This problem has stimulated the development of synthetic materials that can be designed to have tailor-made molecular selectivity. Molecular imprinting, a synthetic technique that uses molecular templates to create selective binding sites in cross-linked polymers, has become one of the most efficient methods for preparation of selective recognition materials. Molecularly imprinted polymers (MIPs) are robust, they can even be sterilized without loosing their unique properties. MIPs can be produced in large quantities and can be re-used many times. These features make MIPs suitable in particular for a number of biochemical applications and recently the stability properties have attracted interest from the environmental sector since biomolecules are degraded in non-sterile environments while MIPs may be stable over extended periods of time.

The history of molecular imprinting can be dated back to the 1930' although it is generally accepted that the modern era of the technique started some forty years ago. Over the past twenty years, the interest in this synthetic technique and its applications has increased exponentially, as reflected from the number of annual publications until 2014 (Fig. 1). Initially most focus was on making molecular imprints of small molecules but during the last decade more and more activities have been observed concerning MIPs against macromolecules and even particulate matter such as cells. During this development a trend towards use of less apolar solvents have been seen since e.g. proteins tend to precipitate when exposed to hydrophobic solvents

The development in literature gives interesting observations concerning the areas of applications. Initially, high resolving separations were the focus, later on MIPs

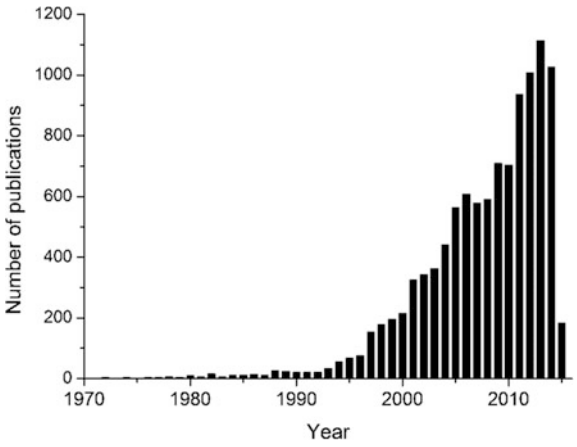

Fig. 1 Number of publications related to the topic of molecular imprinting. The data include research papers, conference abstracts, book chapters and review articles. *Source* www.mipdatabase.com (courtesy Dr. Michael J. Whitcombe)

were used for solid phase extraction as a pre-step before analysis and more recently nano-MIPs are studied as tools in biological systems.

In the past, application of MIPs has been limited to organic solvent-based systems due to the intrinsic hydrophobicity of the synthesized materials. The recent development in molecular imprinting technique started to bring in many novel MIP materials that can be applied directly under aqueous conditions. For the first time, synthetic MIPs start to act as "antibody mimics" to enable direct analysis and treatment of biomedical/biochemical samples under aqueous conditions. This important step has been realized thanks to a number of breakthroughs that are reviewed in the present volume: new synthetic chemistry (Chaps. 313 and 318) and analytical characterization (Chap. 316), computational design (Chap. 314). After introducing the fundamental aspects in material synthesis, we provide expert reviews on the use of MIPs for treating aqueous samples from an academic (Chap. 319) and industry angle (Chap. 317). MIPs for catalysis (Chap. 312), in environmental biotechnology (Chap. 311) and for biotransformation (Chap. 315) are also reviewed with the intention to provide further updated progresses.

We hope that this volume can provide a useful background for interested researchers and can inspire future development of MIPs for biotechnology and biomedical applications. We thank all the authors for their excellent contributions.

March 2015

Bo Mattiasson
Lei Ye

Contents

Adv Biochem Eng Biotechnol (2015) 150: 1–24
DOI 10.1007/10_2015_313

Published Online: 4 April 2015

Synthetic Strategies in Molecular Imprinting

Lei Ye

Abstract This chapter introduces the basic principle and the synthetic aspects of molecular imprinting. First, the use of a molecular template to guide the location of functional groups inside molecularly imprinted cavities is explained. Three different mechanisms that ensure a molecular template associates with functional monomers or the imprinted polymers, that is, through reversible covalent, noncovalent, and sacrificial covalent bonds, are then described. The main] focus is put on noncovalent molecular imprinting using free radical polymerization. The merits of using classical radical polymerization and more sophisticated, controlled radical polymerization are analyzed. After these synthetic chemistry aspects, the chapter continues to discuss the different polymerization processes that can be used to prepare well-defined polymer monoliths, microspheres, and nanoparticles. New top-down processing techniques that produce micro- and nanopatterns of imprinted polymers are also reviewed. The chapter finishes with a brief introduction to using imprinted polymers as building blocks to construct new functional materials and devices, which we consider as one important direction for further development.

Keywords Affinity separation · Free radical polymerization · Molecular imprinting · Molecular recognition · Template

Contents

L. Ye (✉)
Division of Pure and Applied Biochemistry, Lund University, 221 00 Lund, Sweden
e-mail: lei.ye@tbiokem.lth.se

1 Introduction

In nature, molecular recognition plays a critical role in many processes, in particular for living organisms. Well-known examples are found in DNA replication, cell differentiation, and immune responses. The therapeutic function of drugs is largely based on their highly selective molecular interaction with the biological targets. Biological molecules that have high molecular selectivity, such as antibodies, receptors, and aptamers, have been used for a long time in technical applications spanning diagnostic assays, biosensors, purification of high-value products, and controlled delivery of therapeutics. Despite their high molecular selectivity, biological recognition materials are limited by low stability and high production cost, and therefore cannot be used on a large scale or under harsh conditions. In this respect, synthetic materials with predesigned molecular recognition capability become very attractive due to their high stability and much lower production cost compared to biological recognition materials.

Over the past decades, molecular imprinting has become one of the most effective techniques to synthesize materials with predictable molecular selectivity. Molecularly imprinted polymers (MIPs) are often called artificial antibodies, synthetic receptors, and enzyme mimics because of their similar functional performances. The basic principle of molecular imprinting is using a selected molecular template to create well-defined binding sites in crosslinked polymers or inorganic materials. The process involves crosslinking functional monomers or inorganic precursors around the selected molecular template, which controls the location and orientation of the molecular building blocks via covalent or noncovalent interactions. After the crosslinking reaction, the molecular template is removed to leave a complementary binding site in the crosslinked material (Fig. 1). The finished material now contains template-defined sites and is ready to accept the original molecular template as well as its closely related analogues. The degree of molecular selectivity is determined by how well the binding sites are defined through the whole process.

According to the above general definition, MIPs can be created in both organic and inorganic materials. In fact, the early examples of molecular imprinting were carried out in inorganic silica, where organic dyes were used as templates and the crosslinked silica were obtained through sol-gel condensation reactions [1]. Although imprinted materials based on silica or metal oxide networks are still being exploited [2, 3], the majority of molecular imprinting today uses organic polymers as the solid matrix, as the free radical polymerization is more compatible with various template structures, and therefore has more general applicability for different types of molecular templates.

Depending on the types of chemical bonds that maintain the template–monomer complexes (Fig. 1), there are three distinct molecular imprinting approaches for preparing MIPs: covalent molecular imprinting, noncovalent molecular imprinting,

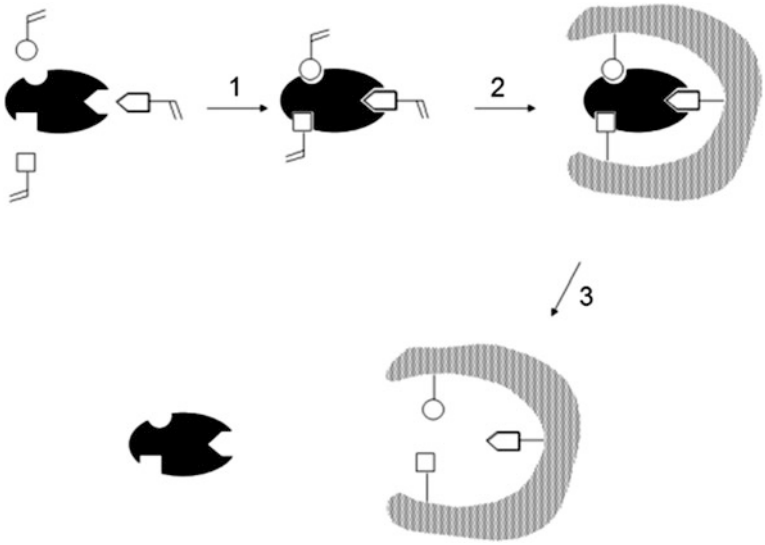

Fig. 1 Schematic representation of molecular imprinting process: (*1*) preassembly template-functional monomer, (*2*) crosslinking polymerization, (*3*) template removal

and semi-covalent molecular imprinting (Fig. 2). The covalent imprinting approach was first described by Wulff and coworkers [4]. It uses a reversible covalent bond to link the molecular template with the functional monomer. After polymerization, the covalent bond is broken to free the template from the solid polymer to furnish an imprinted site. In the rebinding process, the template associates with the site via the same covalent bond.

In the 1980s, Mosbach and coworkers [5] first demonstrated the use of noncovalent interactions for molecular imprinting in organic polymers. In this approach noncovalent interactions are utilized to stabilize the template-functional monomer complex during the crosslinking reaction. The rebinding of template to the furnished sites is also realized by the same noncovalent interactions. Because many functional monomers are available and the synthetic process is less complicated, the noncovalent approach has become the mainstream of molecular imprinting, and for almost all known molecular templates there are successful noncovalent MIPs existing in the literature. Still, it is worth mentioning the semi-covalent imprinting approach invented by Whitcome and coworkers [6], who used a covalent bond to form a template–monomer complex during polymerization, but noncovalent interaction to realize template rebinding. The covalent and semi-covalent approaches are more demanding for synthetic skills although they promise, in principle, better-defined recognition sites in a finished MIP. In reality, the selectivity, affinity, and capacity of MIPs are affected not just by the stability of the molecular complex in a prepolymerization mixture. The improvement of MIP performance gained by using complicated covalent or semi-covalent approaches still remains open for debate.

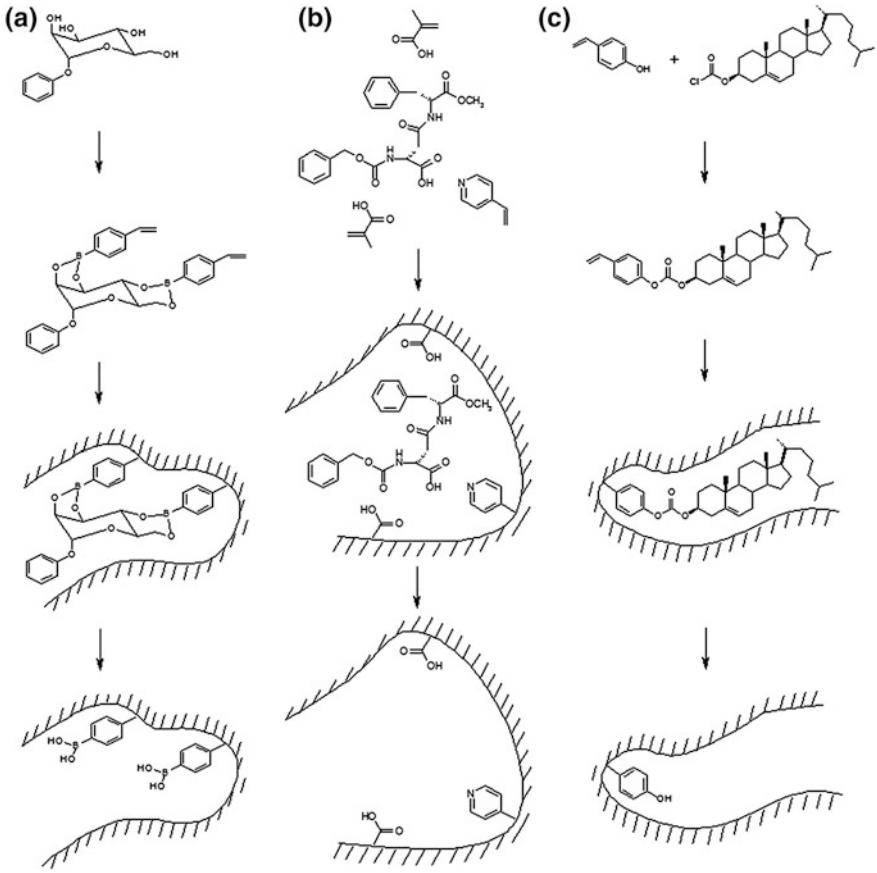

Fig. 2 Synthetic approaches of **a** covalent, **b** noncovalent, and **c** semi-covalent molecular imprinting. The molecular templates used in these approaches are represented by derivatives of **a** monosaccharide, **b** dipeptide, and **c** cholesterol

In this chapter, we focus on the noncovalent approach for preparation of molecularly imprinted polymers. Due to space limitations we do not present a comprehensive list of molecular templates, but rather explain the basic principles of noncovalent molecular imprinting, and address the most important new polymer chemistry and micro-/nanofabrication techniques that are being introduced into the molecular imprinting area. For more extensive discussions on topics uncovered in this chapter, we refer to several excellent reviews already existing in the literature, for example, on general radical polymerization [7], specialized and noncommercial functional monomers [8, 9], and molecular imprinting using condensation cross-linking reactions [10].

2 Noncovalent Molecular Imprinting

Noncovalent molecular imprinting is the most commonly used approach in research laboratories today. The popularity of this approach is due to its simplicity, easy access to a large number of functional monomers, and the faster binding kinetics of the resulting polymer compared to covalent MIPs. Figure 2b shows the schematic process of noncovalent imprinting of using a dipeptide derivative, Cbz-Asp-Phe-OMe as a molecular template [11]. The two functional monomers, 4-vinylpyridine (Vpy) and methacrylic acid (MAA) are used because Vpy interacts with the carboxyl group, and MAA forms a hydrogen bond with the carbonyl moiety, both present in the template. The crosslinking is achieved by copolymerization with excess crosslinking monomer, for example, ethylene glycol dimethacrylate (EGDMA). To increase porosity and surface area, additional solvent is often added. Depending on the actual reaction condition, polymers of different morphologies can be obtained. After the polymerization, the template is removed by solvent extraction to give the finished MIP.

Figure 3 illustrates the classical process of preparing MIP particles in test tubes. The process is only feasible on a small laboratory scale and generates irregular particles. Nevertheless, MIPs prepared by this classical process are still being used for applications where their physical shape and particle size are not critical, for example, for solid-phase extraction aiming at clarifying analytical samples [12]. In other applications, it is more attractive to develop a synthetic process that is scalable and can give well-defined MIPs in terms of physical shape and size distribution.

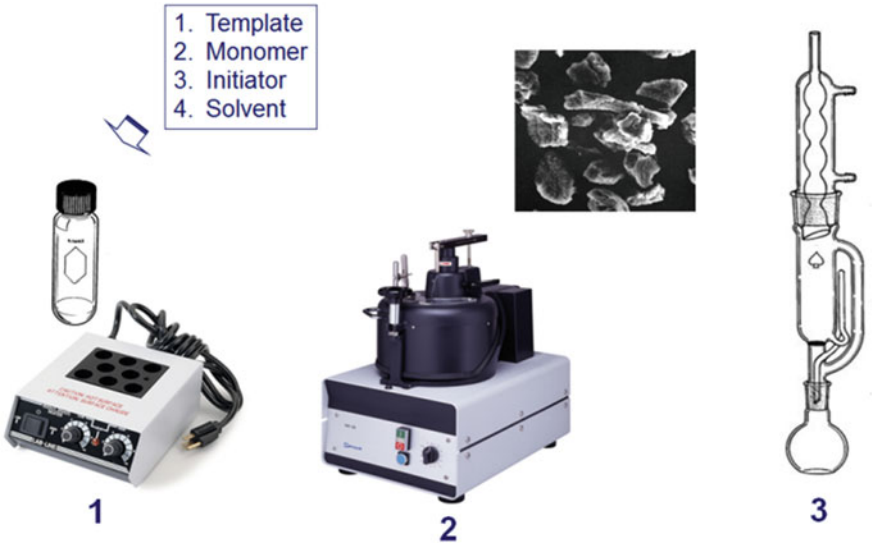

Fig. 3 A classical process for preparing MIP particles: *1* Dissolution of reagents in solvent followed by crosslinking polymerization, *2* mechanical grinding, *3* solvent extraction to remove the molecular template

2.1 Building Blocks for Noncovalent Molecular Imprinting

The easy access to a large number of functional monomers and crosslinkers is part of the reason that noncovalent molecular imprinting has become the most popular approach. In Fig. 4 we list some commonly used functional monomers and crosslinkers that are commercially available. Normally, for a given template the functional monomers are selected based on their capability to form a strong interaction with the template. One particular functional monomer is MAA, which can act both as a hydrogen bond donor and as a hydrogen bond acceptor, or as a negatively charged carboxyl ion to form a stable complex with different templates. The methyl group appended to the vinyl carbon makes the C–C bond a poor Michael acceptor, so that side reaction between MAA and templates containing amino or thiol groups can be avoided. In the group of basic functional monomers, 4-vinylpyridine (4-Vpy) is frequently used for imprinting of acidic templates because of its low cost and good solubility in common solvents.

Because most MIPs have a high crosslinking density, the main composition of a finished MIP is contributed from the crosslinker. Therefore, the surface polarities and chemical stabilities of MIPs are mainly determined by the crosslinker. The common feature of crosslinkers is the presence of multiple polymerizable vinyl groups in a single molecule. The ones that find frequent use in organic solvents are EGDMA, divinylbenzene (DVB), and trimethanolpropane trimethacrylate (TRIM). For preparation of hydrophilic MIPs, more water-soluble crosslinkers such as *N,N′*-methylenebisacrylamide (MBA) and 1,4-bis(acryloyl)piperazine (BAP) can be used.

In addition to many commercially available functional monomers, functional monomers designed to form strong interactions with special template structures have also been reported. These “specialty” functional monomers are often inspired by studies in the supramolecular chemistry area, where specific molecular interactions in noncovalent molecular complexes are the main focus [13]. For the crosslinkers, the distance between two adjacent polymerizable vinyl groups has great impact on the rigidity of the MIP and its microporosity. All the crosslinkers shown in Fig. 4 have a short spacer between the two adjacent vinyl groups and have been used to prepare MIPs for small organic molecules. For larger templates such as proteins, it is often necessary to use more spacers, for example, poly(ethylene glycol) dimethacrylate (**1**). The combined use of flexible crosslinker and low crosslinking density can lead to soft, gel-like MIPs that offer fast enough diffusion for protein to bind to imprinted sites [14].

The standard use of crosslinker is to ensure that functional groups providing template binding are fixed in well-defined positions in a polymer network. For this reason oftentimes the crosslinker is considered “inert” and barely contributes to selective molecular binding. As in most MIP preparations the added crosslinker counts for a large portion in the obtained MIPs; the nonspecific binding caused by this part of the material cannot be overlooked. This problem leads to a dilemma of balancing between binding specificity and capacity: whereas increasing crosslinking density can improve specificity, it can lead to reduced capacity for the same MIP. To solve this problem, Spivak and coworkers developed hybrid crosslinking

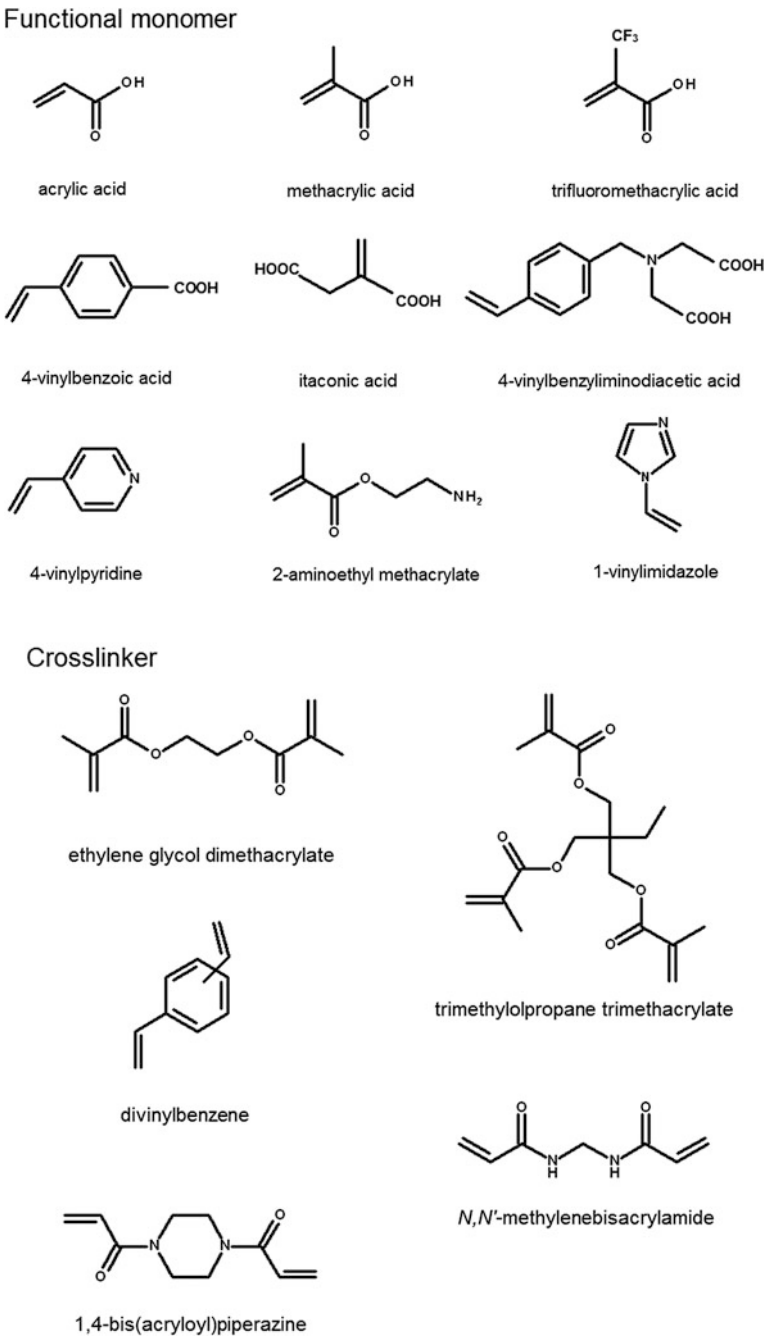

Fig. 4 Common functional monomers and crosslinkers used in noncovalent molecular imprinting

monomers that contain template-binding functional groups [15]. This type of functional-crosslinking monomers has brought an obvious improvement for noncovalent MIPs. In particular, the hybrid monomer *N,O*-bismethacryloyl ethanolamine (NOBE) has proven superior results for MIPs designed to bind carboxyl-containing templates.

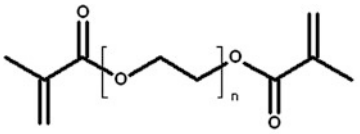

1

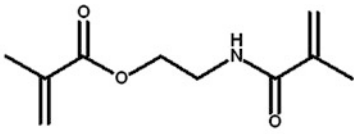

2

The reaction solvent used in noncovalent molecular imprinting affects not only template-functional monomer complexation, but also surface polarity and pore structure of the obtained MIPs. As noncovalent interactions such as hydrogen bonds can be interrupted by polar solvents, noncovalent molecular imprinting is frequently carried out in nonpolar organic solvents such as toluene, chloroform, and dichloromethane. The use of organic solvent also incurs major limitations, such that the obtained MIPs are normally very hydrophobic and display high nonspecific binding when they are applied in an aqueous environment. To obtain water-compatible MIPs, it is therefore necessary to consider synthesizing MIPs directly in water or in water-miscible solvents. Here, noncovalent interactions other than simple hydrogen bonds must be exploited, for example, the inclusion complexes formed between nonpolar organic groups and cyclodextrin [16], and between cations and crown ether [17, 18]. Imprinting of biological macromolecules (e.g., proteins) is mainly carried out in aqueous solvent, where combined hydrogen bonds, ionic forces, and hydrophobic effects have been suggested to contribute to a positive imprinting effect.

Although imprinting solvent does not constitute the final polymer composition, it influences the pore structure of MIPs from different length scales. The reason is that formation of solid MIPs involves phase separation of the growing polymer chain from a previously homogeneous monomer solution. Depending on at what reaction stage the polymer forms a separated phase, the resulting solid material can have a very different structure on the micro ($\phi < 2$ nm), meso ($\phi = 2$–50 nm), and macro domain ($\phi > 50$ nm). It is generally accepted that phase separation is affected by the solubility parameters of the polymer and the solvent, and also by the quantity of the added crosslinking monomer. Despite some empirical guidelines, optimizing pore structure of MIPs through adjusting reaction solvent still requires tedious trial-and-error experiments.

2.2 *Classical Versus Controlled Radical Polymerization Chemistry*

Under most noncovalent imprinting conditions, free radicals do not react with functional groups such as amino, carboxyl, hydroxyl, carbonyl, ester, or amide groups that frequently occur in organic molecules. This functional group tolerance

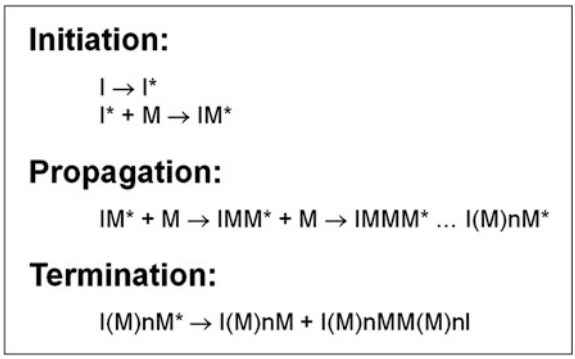

Fig. 5 Main process of classical free radical polymerization: initiation, propagation, and termination. *I* and *M* represent the initiator and the monomer; *I** and *M** symbolize the corresponding free radicals

is the reason for the broad use of free radical polymerization for MIP preparation. Radical polymerization can be initiated by heat, photo irradiation, and occasionally by a redox reaction. The chemical process is routinely used in the chemical industry to synthesize commodity polymers. In general, the polymerization process involves three steps: initiation, chain propagation, and termination (Fig. 5). In most classical radical polymerization processes, radicals are generated continuously by heat or photo homolysis, leading a slow initiation accompanied by fast chain propagation. Due to the relatively high concentration of radicals, premature termination cannot be avoided. This characteristic of radical polymerization leads to a very heterogeneous mixture of polymer chains of varying lengths; that is, the obtained polymer product has a broad distribution of molecular weight. In the case of crosslinking polymerization, it means an inhomogeneous network structure that is impossible to control by adjusting the monomer feed. In addition, it is common that the functional monomer and crosslinker used in an imprinting system have different radical reactivity, which can cause nonstatistical distribution of functional groups in the final polymer structure. Apart from these complications, abundant evidence supports that by using a template molecule, it is indeed feasible to tune the molecular selectivity of crosslinked polymers.

In most noncovalent imprinting systems, the strength of template-functional monomer interaction is moderate (with an experimental K_D of template–functional monomer complex $\geq 10^{-3}$ M). Nevertheless, high affinity MIPs (with $K_D \leq 10^{-6}$ M for the template) are common in the literature. One possible reason for the significant enhancement of affinity is that the growing polymer network develops multidentate interactions with the template during the imprinting reaction. The initially flexible chains of oligomers enable their sufficient conformational change to maximize interaction with the template. The new initiator radicals generated later are helpful for forming a more rigid 3D network around the template through further crosslinking the remaining vinyl groups.

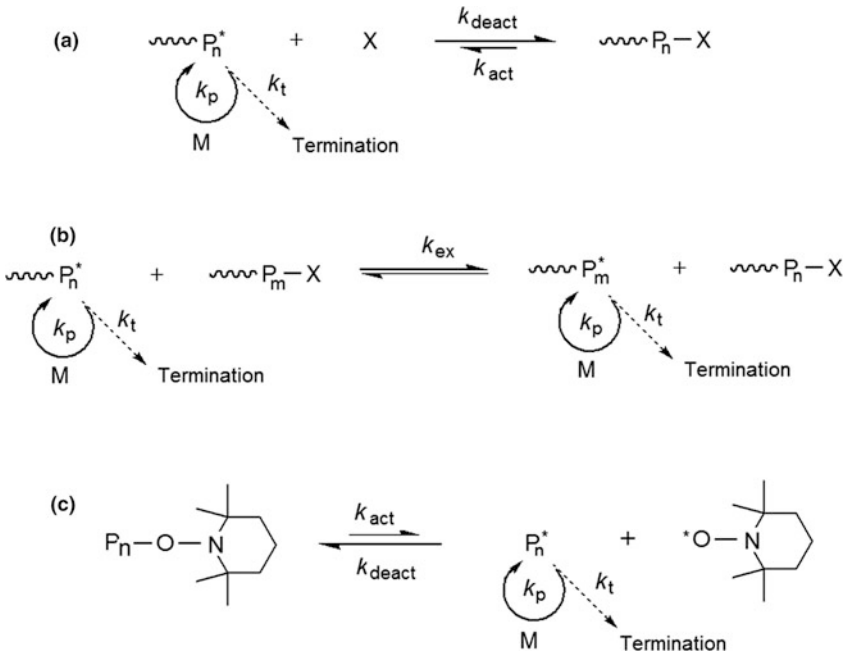

Fig. 6 Simplified reaction mechanisms for the CRPs used in noncovalent molecular imprinting: **a** ATRP, **b** RAFT polymerization, **c** NMP. The initiation step is not shown

The lack of precise control over the classical radical polymerization process, although offering a large number of successful MIPs, has attracted much research interest in using more sophisticated polymer chemistry. Controlled (living) radical polymerization (CRP) is a rapidly evolving advancement in modern polymer chemistry [19]. The basic principle of CRP is to have all polymer chains grow at the same pace until final termination is reached. To realize this, CRP comprises fast radical initiation combined with a slow but simultaneous chain propagation, using temporary capping agents to protect the propagating chain radicals and prevent them from premature termination. As propagation takes place for all chains in parallel, the final polymer product normally has a very narrow molecular weight distribution. Three most important CRP chemistries have been exploited in molecular imprinting: atom transfer radical polymerization (ATRP), reversible addition-fragmentation chain transfer (RAFT) polymerization, and nitroxide-mediated polymerization (NMP) (Fig. 6). Among these CRPs, ATRP leaves easily convertible functional groups on the MIP surface and makes further surface modification the most straightforward [20]. The disadvantage of ATRP is its low functional group tolerance due to the involvement of metal catalyst and ligand. Although NMP has good functional group tolerance, the polymerization requires a high reaction temperature (>100 °C) to activate the dormant radicals, which makes NMP a slow process and only applicable for some special template systems [21].

RAFT polymerization, characterized by its good functional group tolerance and giving convertible end-functional groups, can be considered the most suitable CRP for noncovalent molecular imprinting [22].

Whether CRP alone can lead to better noncovalent MIPs remains open to debate. Although some studies claim that a more homogeneous polymer structure (synthesized using CRP) has resulted in improved MIP performance, the available experimental data are limited and do not offer sufficient evidence. According to the general CRP mechanism, the network rigidity of a MIP prepared by CRP remains unchanged with monomer conversion. As a result, the fidelity of the imprinted sites is already defined at the beginning of the imprinting reaction. If this is true, then the classical, uncontrolled radical polymerization should produce better-defined imprinted sites. The use of CRP for molecular imprinting appeared only a decade ago, therefore the extent to which CRP can affect the quality of noncovalent MIPs remains to be clarified. After all, CRP processes require (expensive) specialty reagents and are in general slower than classical radical polymerization. Before dramatic improvement of MIP performance is clearly demonstrated, the use of CRP for MIP preparation will remain largely an academic interest. Nevertheless, the "living" characteristic of CRP is useful for continuous grafting of polymer on a MIP surface, and offers a convenient means for modifying a MIP surface to minimize nonspecific binding under different solvent conditions [23]. The terminal functional groups derived from the CRP reagents can also be used directly to conjugate MIPs with other functional materials without involving an additional polymer layer [24].

When free radical polymerization is used, noncovalent molecular imprinting can be considered a kinetically controlled process, as the crosslinked network, once formed, does not change its 3D structure. The fidelity of imprinting depends on the status of the template-functional monomer complex when the actual crosslinking reaction is taking place. Apparently, any free functional monomer (not associated with the template) that is being added to the polymer network does not contribute to imprinting; it instead causes nonspecific binding of the MIP. Because the noncovalent template–functional monomer complex exists in an equilibrium with the free template and free functional monomer, there are always free functional monomers in the reaction system. In consequence, noncovalent MIPs always display some level of nonspecific binding.

Thermodynamic control over the molecular imprinting process has been attempted in some intriguing studies, where reversible polymerization–depolymerization reactions were exploited. The basic idea is to maximize the interaction of the template with functional monomers and reversible polymer chains, the two components that exist in equilibrium under one special condition. After a long enough equilibration time, the reaction condition is altered to freeze the 3D structure of the MIP. In this way it is hoped that the MIP can have a self-optimized network structure to give optimal template recognition. This synthetic methodology is similar to that used in dynamic combinatorial chemistry (DCC), where reversible covalent bonds are employed to build up synthetic receptors (host molecules) for

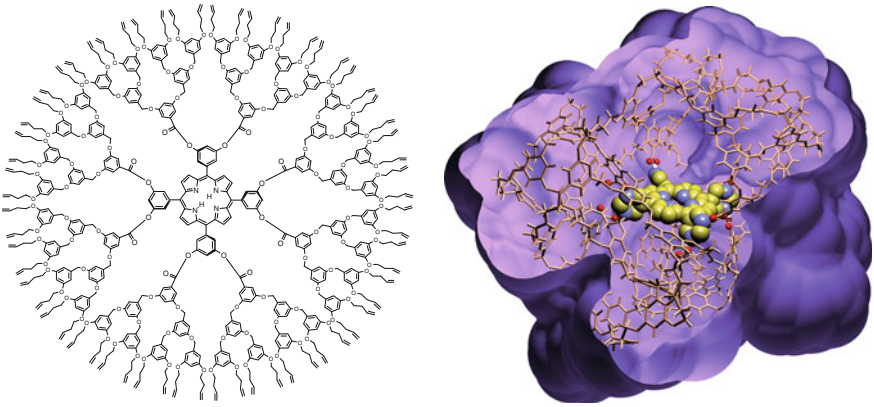

Fig. 7 Monomolecular imprinting inside dendrimers. *Left* pre-assembled dendrimer prior to crosslinking of the peripheral vinyl groups. The porphyrin template is covalently attached to the core. *Right* the finished dendrimer containing a single binding site for the porphyrin template (reproduced with permission from *Nature* 2002, *418*, 399. Copyright 2002 Nature Publishing Group)

different guest molecules [25]. As prominent examples, Steinke and coworkers synthesized enantioselective MIPs using ring-opening metathesis polymerization [26], and Zimmerman and coworkers [27] synthesized monomolecularly imprinted dendrimers using ring-closing metathesis polymerization (Fig. 7). In both cases the reversible metathesis polymerization was suggested to allow the reaction systems to approach a minimum energy status, thereby leading to self-optimized binding sites in the crosslinked polymers. Because the existing examples used a semi-covalent imprinting strategy, it still remains unclear how noncovalent MIPs can be improved by using similar thermodynamic control.

2.3 Reaction Systems Offering MIPs with Controlled Formats

For preparation of MIPs, free radical polymerization can be carried out in both homogeneous and heterogeneous systems. Because of the crosslinked structure, most MIPs are obtained as solid particles at the end of the polymerization. In some special cases, very small MIP particles (nanoparticles) can be synthesized and these particles are sometimes considered "soluble" in the corresponding solvent. Here, the distinction between homogeneous and heterogeneous systems is used to describe the initial state of the molecular imprinting process: a homogeneous system means that molecular imprinting starts from a homogeneous solution, whereas a heterogeneous system involves more than one phase in the reactor.

The classical molecular imprinting process shown in Fig. 3 gives porous particles with irregular shapes and a broad size distribution. To make the MIP particles

suitable for practical applications, it is often necessary to fractionate the particles according to their sizes. This bulk polymerization method involves minimal reaction parameters that need optimization, and is suitable for preparing a small quantity of MIPs, for example, for analytical applications. The main drawback of this method is its poor repeatability in terms of controlling particle shape and particle size distribution, which are important when a large amount of MIP is needed. The classical bulk polymerization method is still in use, particularly in miniaturized reactors such as in capillary columns and nanochannels to give in situ prepared MIPs [28]. In the past decade more research has shifted to the use of new polymerization techniques that are scalable and can offer MIPs with well-defined size and formats.

2.3.1 Bulk Polymerization in Confined Spaces

By carrying out the classical bulk polymerization in miniaturized reactors, MIPs can be prepared with a finished physical format defined by the small reactors. Early examples are MIP-filled capillary columns that can be used to separate analytical samples using capillary electrochromatography. To maintain sufficient liquid flow through the column, it is important that the in situ prepared MIPs have a macroporous structure. The macroporous structure can be obtained by terminating the polymerization before complete conversion of the monomers [29], or by using special solvent conditions to affect the reaction-induced phase separation [30].

The first free-standing MIP monolith was reported by Yan and coworkers [31]. In this work, the authors first used a patterned poly(dimethylsiloxane) (PDMS) stamp on silicon wafer to form microchannels, then polymerized MAA and EGDMA in the presence of 2,4-dichlorophenoxyacetic acid (2,4-D) as a template. Because the elastomer PDMS stamp can be easily removed, it was straightforward to prepare the well-defined MIP micromonoliths. The soft lithography method was further developed by Haupt and coworkers using UV-initiated polymerization to fabricate MIP patterns with submicrometer resolution. The MIP pattern showed chiral selective recognition for a fluorescent analogue of the amino acid template, Boc-L-Phe [32]. The soft lithography method for creating MIP arrays is attractive for developing biomimetic sensors, particularly for analyzing complex samples where response patterns from the arrays can be utilized to improve selectivity [33].

Compared to other microfabrication methods, nanoimprint lithography (NIL) can generate MIP patterns with the smallest feature size. Because NIL uses more chemically resistant stamp (made from silicon) than PDMS, the technique can be used to pattern MIPs made from a large variety of monomer/solvent compositions. The first example of NIL for MIP patterning was reported by Forchheimer et al. [34] using propranolol as a template. The MIP pattern displayed clear chiral selectivity when it was tested in radioligand binding assays (Fig. 8).

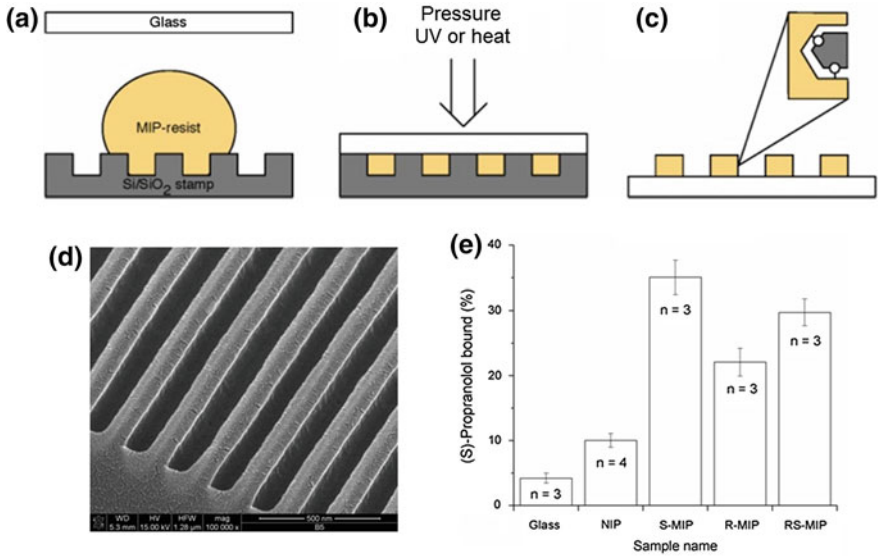

Fig. 8 Fabrication of MIP nanostructures using reactive NIL and surface characterization. **a** A monomer mixture containing the molecular template is deposited on a patterned stamp. **b** A substrate is pressed against the stamp, causing the reaction mixture to fill up the empty space defined by the stamp pattern. The monomers are polymerized by UV or thermal polymerization. **c** Releasing the stamp (de-molding) furnishes a MIP pattern containing molecularly imprinted binding sites. **d** SEM image of MIP pattern. **e** Uptake of chiral molecular probe ((S)-propranolol) by different surfaces. The sample S-MIP was imprinted against (S)-propranolol, and displayed the highest uptake for the template enantiomer

2.3.2 Grafting MIPs on Defined Structures

One straightforward approach to control the physical form of MIP is by grafting a thin layer of imprinted polymer on predefined structures. If the thickness of the grafted MIP layer is controlled to be low, the obtained composite material will have a physical form similar to the original structural scafold. Two grafting chemistries have been utilized: "grafting to" means that the initial radicals are generated in solution, which react with surface-immobilized vinyl groups to allow the growing polymers to be captured on the surface (Fig. 9a), and "grafting from" uses surface-bound free radicals to initiate the imprinting polymerization (Fig. 9b, c) [35]. When imprinting is carried out in dilute solution, the "grafting from" chemistry is more suitable as it avoids the slow diffusion of oligomers/polymers before they reach the structural scafold. Use of surface-immobilized iniferter to graft the MIP layer has attracted great interest, as the iniferter can be conveniently fixed on the surface, and the radical polymerization can be induced by simple UV irridation. The UV-induced polymerization may be used to gain both temporal and spatial control over the grafted MIP layer. Some well-defined MIP srtructures prepared by grafting

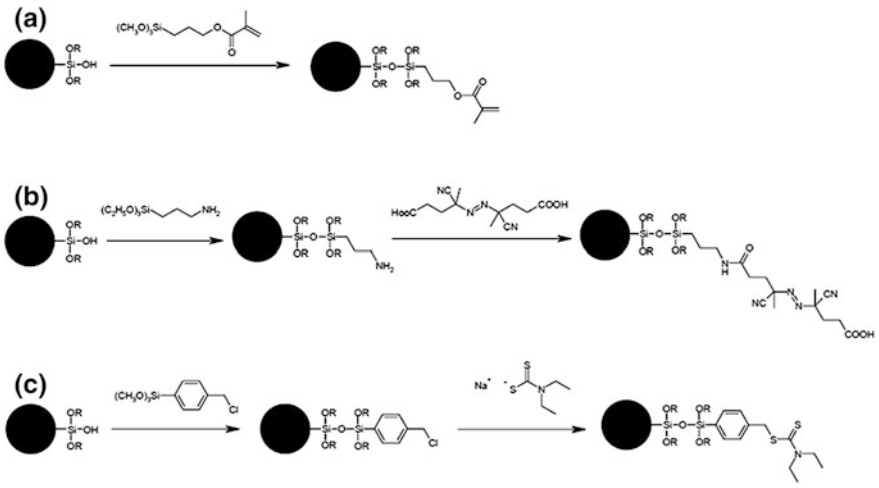

Fig. 9 Surface modification of the structural scaffold for grafting of the MIP layer. **a** The structural scaffold is first modified with a polymerizable vinyl group. **b** A free radical initiator. **c** Or an iniferter

polymerization are composite beads with well-defined core-shell structures [36–38], micro- and nanochannels [39, 40], and periodic mesoporous organosilica [41].

2.3.3 Preparation of MIP Nanoparticles and Microspheres

Spherical MIP particles in the nano- and micrometer range can be synthesized directly from low-molecular–weight building blocks. The imprinting reaction can be carried out in both homogeneous and heterogeneous systems. For synthesis of MIP nanoparticles, emulsion polymerization, miniemulsion polymerization, microemulsion polymerization, and precipitation polymerization can be utilized [42]. Each of these techniques has its own advantage and disadvantage, so the choice is based on the required particle size and uniformity of the MIP, and the compatibility of the reaction condition with noncovalent molecular imprinting (Table 1). Classical emulsion polymerization, miniemulsion polymerization, and microemulsion polymerization use water as the continuous phase, and special surface-active reagents to assist maintaining a stable dispersed phase during the polymerization. The presence of water and the surface-active reagents can interrupt hydrogen bond interactions between most templates and functional monomers, therefore noncovalent MIP nanoparticles synthesized by these techniques often have a lower template affinity and selectivity than MIP particles obtained from bulk polymerization.

Despite the poor compatibility of water with most noncovalent imprinting systems, a number of interesting studies have exploited the surface-active reagents (surfactants), so that the template constitutes part of the amphiphilic reagent and is

Table 1 Reaction systems for synthesis of MIP nanoparticles

Reaction systems	Use of surface-active reagent	Location of crosslinking reaction	Compatibility with noncovalent imprinting
Emulsion polymerization	Yes	In latex particles	−
Miniemulsion polymerization	Yes	In monomer droplets	−
Microemulsion polymerization	Yes	In monomer droplets	−
Precipitation polymerization	No	In latex particles	+

fixed on the surface of monomer droplets during the imprinting reaction. In this way surface-imprinted sites are generated on the nanoparticles, allowing fast-binding kinetics to be realized for the MIP nanoparticles [43–45].

Precipitation polymerization starts from a homogeneous solution of monomer in a near Θ solvent [46]. With the progress of the polymerization, the growing and crosslinked polymer chains phase separates from the solvent to form colloidal particles. The choice of reaction solvent is critical for obtaining uniform MIP nanoparticles: the solvent should be a good solvent for the monomer but should be a poor solvent for the polymer, so that the obtained polymer can phase-separate from the solution in a controlled manner [47]. For noncovalent molecular imprinting, acetonitrile is the most useful near Θ solvent to prepare polymethacrylate-type nanoparticles. Because no interfering reagent is used, precipitation polymerization is the most suitable process for preparing high-quality MIP nanoparticles (Fig. 10). Using solution NMR and dynamic light-scattering techniques, Long et al. [48] have studied the dynamic process of particle nucleation and growth during precipitation polymerization, and the impact of monomer conversion on the

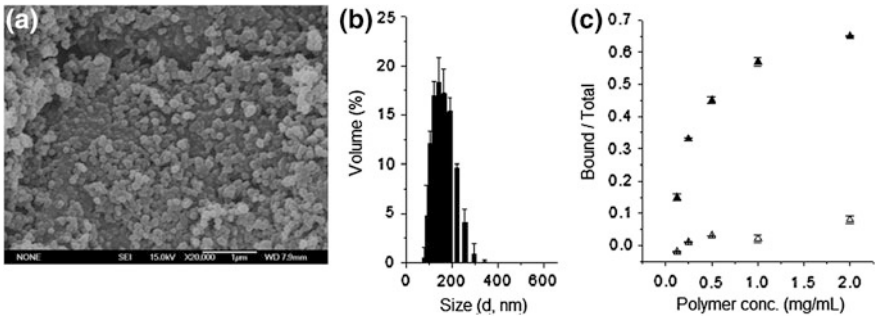

Fig. 10 Propranolol-imprinted poly(MAA-co-TRIM) nanoparticles. **a** SEM image. **b** Particle size distribution measured by dynamic light scattering in acetonitrile. **c** Binding of tritium-labeled (*S*)-propranolol by the imprinted (*filled triangle*) and nonimprinted nanoparticles (*black dot*) in acetonitrile containing 50 % buffer (from Ref. [47])

molecular selectivity of the obtained MIP nanoparticles. This study brought new insights to the molecular imprinting process: under well-controlled precipitation polymerization conditions, particle nucleation occurs during the first reaction period, and in the second period the polymerization mainly contributes to increasing intraparticle crosslinking. As no secondary nucleation takes place, it becomes possible to synthesize hydrophilic core-shell MIP particles using a simple one-pot reaction with sequential monomer addition [49].

MIP microspheres can be synthesized using suspension polymerization [50, 51], precipitation polymerization [47], and seeded suspension polymerization [52]. To avoid the interruption of the hydrogen bond by water, Mayes et al. used non-aqueous suspension polymerization to prepare MIP microspheres [53, 54]. Using seeded suspension polymerization, MIP microspheres with a narrow size distribution can be obtained, although the synthetic process is more complicated due to the multistage swelling process. More recently, Ye and coworkers reported the use of Pickering emulsion polymerization to synthesize MIP microspheres [55–57]. In these Pickering emulsion systems, solid particles are used as stabilizers to replace the surfactants used in conventional suspension polymerization. Because of the high emulsion stability, the Pickering emulsion polymerization can be carried out without agitation. In addition, by immobilizing a template on the surface of the stabilizing particles, truly surface-exposed and water-compatible MIP microspheres have been realized [58, 59]. Figure 11 shows the SEM images of some representative propranolol-imprinted microspheres prepared using the different polymerization methods.

2.4 MIPs as Building Blocks for Multifunctional Materials

Although preparation of MIPs often requires synthetic skills from organic and polymer chemists, oftentimes the final application is in the hands of researchers in analytical chemistry, enviromental science, biology, and medicine. Although for different applications it is possible to design and synthsize specialized MIPs for their intended use [60–63], it is in practice very inconvenient because the reaction conditions for MIP synthesis, for example, the use of high temperature, organic solvents, and protection gas, cannot be fulfilled. To solve this problem, one feasible approach is to develop MIPs as modular building blocks that can be handled like antibodies for different applications. In this respect MIP nanoparticles are particularly interesting, as they can be prepared in large quantity with high molecular selectivity [64], and their small physical size allows the material to be easily handled with standard liquid dispensers.

Compared to antibodies, MIP nanoparticles have significantly larger size that makes them more difficult to be conjugated with other functional materials, or to be integrated into functional devices. It is understandable that the coupling reaction kinetics between nanoparticles is much slower than between small molecule reagents. Nevertheless, the recent results have shown that it is indeed feasible to use

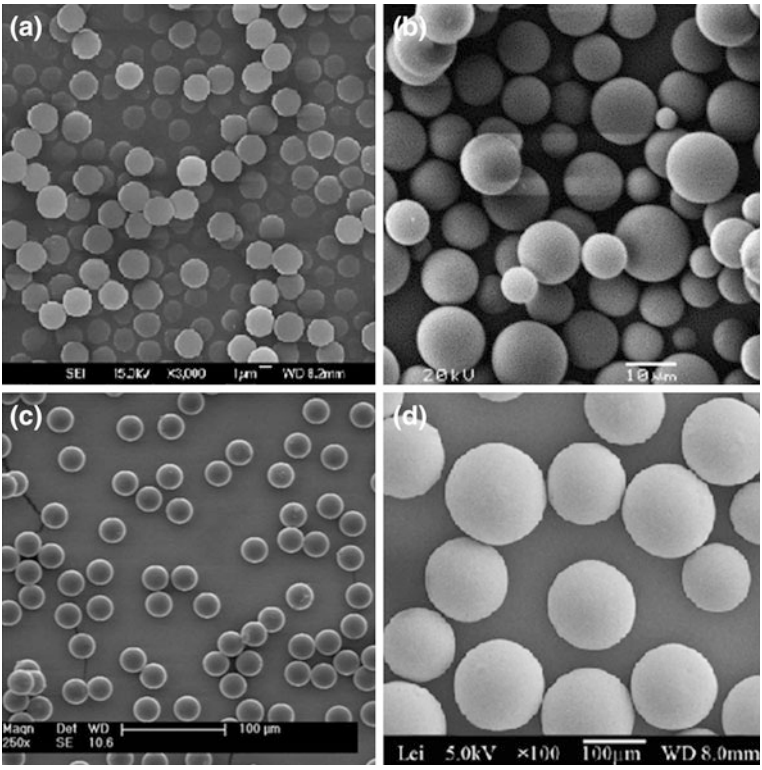

Fig. 11 Propranolol-imprinted polymer microspheres prepared by **a** precipitation polymerization (from Ref. [47]), **b** suspension polymerization in perfluorocarbon (from Ref. [54]), **c** suspension polymerization carried out in microfluidic reactor (from Ref. [51]), and **d** Pickering emulsion polymerization (from Ref. [55])

modular MIP nanoparticles as antibody mimics in many interesting applications. In the following examples, the common critical point is to maintain the intrinsic molecular selectivity when the MIPs are combined with other functional materials.

One simple method to assemble MIP nanoparticles into a defined structure is by using a polymer as an physical "adhesive". Using this method, MIP nanoparticles have been encapsulated into electrospun nanofibers to act as solid-phase extraction material for analytical sample preparation and optical sensing (Fig. 12) [65–67].

Reimhult et al. [68] spin-coated MIP nanoparticles suspended in poly(ethylene terephthalate) (PET) solution on a quartz crystal surface to obtain a stable QCM sensor surface. In a more recent work, Hajizadeh et al. [69] used hydrogel polymer to crosslink MIP nanoparticles under frozen condition and obtained macroporous nanoparticle cryogels. The high molecular selectivity of the MIP nanoparticles allowed the cryogel sponge to remove β-blockers from the biological sample with high efficiency.

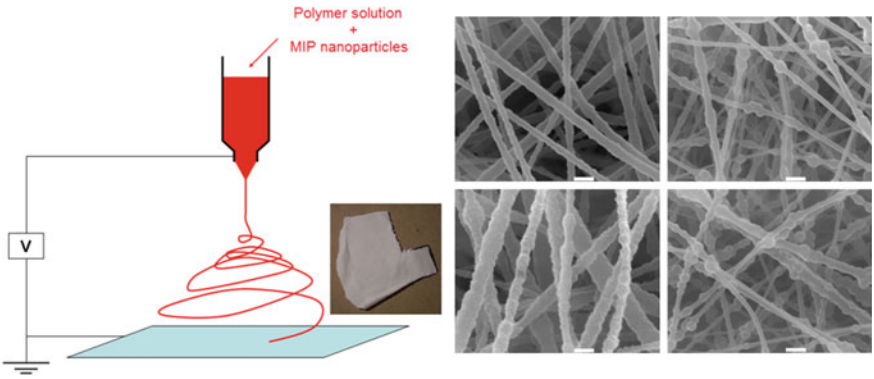

Fig. 12 Encapsulation of MIP nanoparticles in nanofibers by electrospinning. The schematic drawing to the left shows the basic electrospinning setup. The SEM images to the right show PET nanofibers loaded with different amounts of MIP nanoparticles (from Ref. [66])

As mentioned earlier, MIP nanoparticles with well-defined core-shell structure can be synthesized using one-pot precipitation polymerization [49]. Using the same method, we introduced terminal alkynyl groups on the surface of propranolol-imprinted nanoparticles [70], and used these "clickable" MIP nanoparticles as building blocks to prepare magnetic composites [71] and multifunctional colloidosomes [72]. In these examples, the interparticle conjugation was achieved by Cu (I)-catalyzed 1,3-dipolar cycloaddition between organic azide and alkyne groups (the CuAAC click chemistry; Fig. 13).

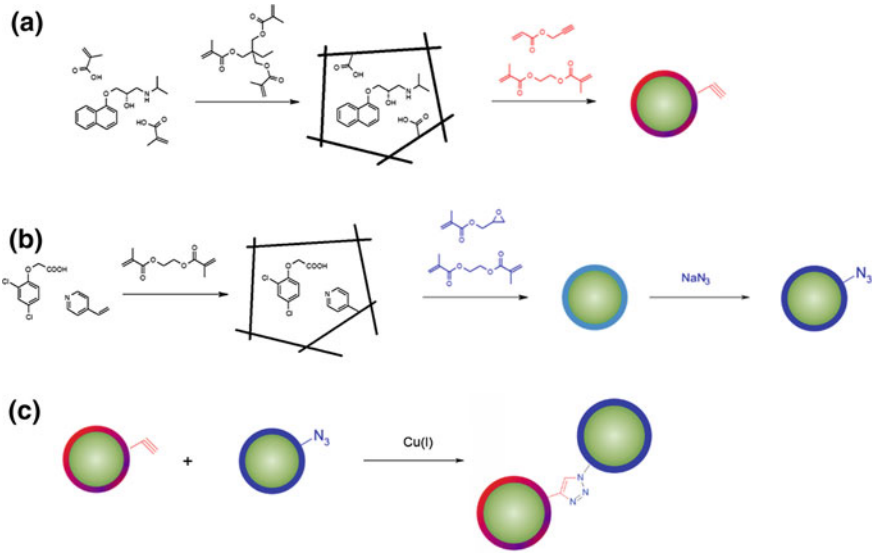

Fig. 13 Synthesis of clickable MIP nanoparticles using propranolol (**a**) and 2,4-D (**b**) as the templates. **c** Conjugation of the two MIP particles using CuAAC click reaction

Unmodified MIP nanoparticles can be linked to other materials or surfaces more directly. Direct linkage between functional nanoobjects is important as it allows more efficient transfer of electrons and photons, which are critical for chemical sensing and energy conversion. To realize direct fixation of MIP nanoparticles on a surface, we used photoactivated conjugation between an organic polymer and a perfluorophenylazide (PFPA)-modified surface [73]. As the PFPA reagent can be easily immobilized on a large variety of surfaces and the photoactivated nitriene can react with all organic materials [74, 75], the photoconjugation method has a general applicability for linking MIP nanoparticles with other functional materials. More important, the high-efficiency click chemistry and photoconjugation method does not affect the molecular recognition of the MIP building blocks.

3 Conclusions

After more than five decades of development, molecular imprinting in organic polymers has proven a very reliable method for preparing synthetic materials with predictable molecular selectivity. The high stability and relatively low synthetic cost make MIPs ideal for a broad range of applications including affinity separation, chemical sensing, catalysis, and controlled drug delivery. In addition, even in vivo application of MIPs is being conceived and it will not be surprising to witness new exciting results. The synthetic chemistry used in molecular imprinting has progressed significantly over the past years, resulting in new formats and unprecedented functional performance of MIPs. Controlled (living) polymer chemistry, new heterophase polymerization process, click chemistry, and photocontrolled conjugation have played important roles in making new MIP materials. Micro- and nanofabrication of MIPs has become routine practice in many laboratories. Despite MIPs having a long application history in nonaqueous media, truly water-compatible MIPs are finding increasing applications in biology-related areas. With better understanding of basic molecular recognition in water, new insights into the molecular details of the imprinting process, and exploitation of modern synthetic and polymer chemistry, more MIPs are expected to act as qualified artificial antibodies in the coming years.

References

1. Dickey FH (1949) The preparation of specific adsorbents. Proc Natl Acad Sci USA 35: 227–229
2. Katada N, Niwa M (2006) The re-birth of molecular Imprinting on silica. In: Piletsky S, Turner A (eds) Molecular imprinting of polymers. Landes Bioscience, Georgetown, USA
3. Díaz-Gacía ME, Laíño RB (2005) Molecular imprinting in sol-gel materials: recent developments and applications. Microchim Acta 149:19–36

4. Wulff G, Sarhan A (1972) The use of polymers with enzyme-analogous structures for the resolution of racemates. Angew Chem Int Ed 11:341
5. Arshady R, Mosbach K (1981) Synthesis of substrate-selective polymers by host-guest polymerization. Macromol Chem Phys 182:687–692
6. Whitcombe MJ, Rodriguez ME, Villar P, Vulfson EN (1995) A new method for the introduction of recognition site functionality into polymers prepared by molecular imprinting—synthesis and characterization of polymeric receptors for chloresterol. J Am Chem Soc 117:7105–7111
7. Matsumoto A (1995) Free-radical crosslinking polymerization and copolymerization of multivinyl compounds. Adv Polym Sci 123:41–80
8. Wulff G, Knorr K (2002) Stoichiometric noncovalent interaction in molecular imprinting. Bioseparation 10:257–276
9. Sellergren B, Hall A (2013) Synthetic chemistry in molecular imprinting. In: Ye L (ed) Molecular imprinting: principles and applications of micro- and nanostructured polymers. Pan Stanford Publishing, Singapore
10. Lieberzeit PA, Glanznig G, Jenik M, Gazda-Miarecka S, Dickert FL, Leidl A (2005) Soft lithography in chemical sensing—analytes from molecules to cells. Sensors 5:509–518
11. Ye L, Ramström O, Mosbach K (1998) Molecularly imprinted polymeric adsorbents for byproduct removal. Anal Chem 70:2789–2795
12. Ye L (2005) Molecularly imprinted polymers for solid phase extraction and byproduct removal. In: Yan M, Ramström O (eds) Molecularly imprinted materials. Science and Technology, Marcel Dekker Inc., New York
13. Cragg PJ (2010) Supramolecular chemistry: from biological inspiration to biomedical applications. Springer, London
14. Takeuchi T, Hishiya T (2008) Molecular imprinting of proteins emerging as a tool for protein recognition. Org Biomol Chem 6:2459–2467
15. Sibrian-Vazquez M, Spivak DA (2004) Molecular imprinting made easy. J Am Chem Soc 126:7827–7833
16. Hishiya T, Asanuma H, Komiyama M (2002) Spectroscopic anatomy of molecular imprinting of cyclodextrin. Evidence for preferential formation of ordered cyclodextrin assemblies. J Am Chem Soc 124:570–575
17. Andersson HS, Ramström O (1998) Crown ethers as a tool for the preparation of molecularly imprinted polymers. J Mol Recogn 11:103–106
18. Viton F, White P S, Gagné MR (2003) Crown-ether functionalized second coordination sphere palladium catalysts by molecular imprinting. Chem Commun 39:3040–3041
19. Tsarevsky NV, Sumerlin BS (2013) Fundamentals of controlled/living radical polymerization. RSC Publishing, Cambridge
20. Wei X, Li X, Husson SM (2005) Surface molecular imprinting by atom transfer radical polymerization. Biomacromolecules 6:1113–1121
21. Boonpangrak S, Whitcombe MJ, Prachayasittikul V, Mosbach K, Ye L (2006) Preparation of molecularly imprinted polymers using nitroxide-mediated living radical polymerization. Biosens Bioelectron 22:349–354
22. Titirici M-M, Sellergren B (2006) Thin molecularly imprinted polymer films via reversible addition-fragmentation chain transfer polymerization. Chem Mater 18:1773–1779
23. Zhang H (2014) Water-compatible molecularly imprinted polymers: promising synthetic substitutes for biological receptors. Polymer 55:699–714
24. Zhou T, Jørgensen L, Mattebjerg MA, Chronakis IS, Ye L (2014) Molecularly imprinted polymer beads for nicotine recognition prepared by RAFT precipitation polymerization: a step forward towards multi-functionalities. RSC Adv 4:30292–30299
25. Corbett PT, Leclaire J, Vial L, West KR, Wietor J-L, Sanders JKM, Otto S (2006) Dynamic combinatorial chemistry. Chem Rev 106:3652–3711
26. Patel A, Fouace S, Steinke J H G (2003) Enantioselective molecularly imprinted polymers via ring-opening metathesis polymerization. Chem Commun 39:88–89

27. Zimmerman SC, Wendland MS, Rakow NA, Zharov I, Suslick KS (2002) Synthetic hosts by monomolecular imprinting inside dendrimers. Nature 418:399–403
28. Iacob B-C, Bodoki E, Oprean R (2014) Recent advances in capillary electrochromatography using molecularly imprinted polymers. Electrophoresis 35:2722−2732
29. Schweitz L, Andersson LI, Nilsson S (1997) Capillary electrochromatography with predetermined obtained through molecular imprinting. Anal Chem 69:1179–1183
30. Svec F, Fréchet JMJ (1999) Molded rigid monolithic porous polymers: an inexpensive, efficient, and versatile alternative to beads for the design of materials for numerous applications. Ind Eng Chem Res 38:34–48
31. Yan M, Kapua A (2001) Fabrication of molecularly imprinted microstructures. Anal Chim Acta 435:163–167
32. Lalo H, Ayela C, Dague E, Vieu C, Haupt K (2010) Nanopatterning molecularly imprinted polymers by soft lithography: a hierarchical approach. Lab Chip 10:1316–1318
33. Shimizu KD, Stephenson C (2010) Molecularly imprinted polymer sensor arrays. Curr Opinion Chem Biol 14:743–750
34. Forchheimer D, Luo G, Montelius L, Ye L (2010) Molecularly imprinted nanostructures by nanoimprint lithography. Analyst 135:1219–1223
35. Minko S (2008) Grafting on solid surfaces: "grafting to and "grafting from" methods. In: Stamm M (ed) Polymer surfaces and interfaces. Springer, Heidelberg
36. Sellergren B, Bückert B, Hall AJ (2002) Layer-by-layer grafting of molecularly imprinted polymers via iniferter modified supports. Adv Mater 14:1204–1208
37. Pérez-Moral N, Mayes AG (2007) Molecularly imprinted multi-layer core-shell nanoparticles —a surface grafting approach. Macromol Rapid Commun 28:2170–2175
38. Gonzato C, Courty M, Pasetto P, Haupt K (2011) Magnetic molecularly imprinted polymer nanocomposites via surface-initiated RAFT polymerization. Adv Funct Mater 21:3947–3953
39. Qu P, Lei J, Ouyang R, Ju H (2009) Enantioseparation and amperometric detection of chiral compounds by in situ molecular imprinting on the microchannel wall. Anal Chem 81:9651–9656
40. Wang H-J, Zhou W-H, Yin X-F, Zhuang Z-X, Yang H-H, Wang X-R (2006) Template synthesized molecularly imprinted polymer nanotube membranes for chemical separations. J Am Chem Soc 128:15954–15955
41. Lofgreen JE, Ozin GA (2014) Controlling morphology and porosity to improve performance of molecularly imprinted sol-gel silica. Chem Soc Rev 43:911–933
42. Ye L, Yilmaz E (2005) Molecularly imprinted polymer beads. In: Yan M, Ramström O (eds) Molecularly imprinted materials. Science and Technology, Marcel Dekker Inc., New York
43. Awino JK, Zhao Y (2013) Protein-mimetic, molecularly imprinted nanoparticles for selective binding of bile salt derivatives in water. J Am Chem Soc 135:12552–12555
44. Zeng Z, Hoshino Y, Rodriguez A, Yoo H, Shea KJ (2010) Synthetic polymer nanoparticles with antibody-like affinity for a hydrophilic peptide. ACS Nano 4:199–204
45. Gruber-Traub C, Weber A, Dettling M, Herz M, Herold M, Brunner H, Tovar GEM (2006) NANOCYTES—inverse miniemulsion polymerization technology for specific protein recognition. Polym Preprints 47:901–902
46. Downey JS, Mclsaac G, Frank RS, Stöver HDH (2001) Poly(divinylbenzene) microspheres as an intermediate morphology between microgel, macrogel, and coagulum in cross-linking precipitation polymerization. Macromolecules 34:4534–4541
47. Yoshimatsu K, Reimhult K, Krozer A, Mosbach K, Sode K, Ye L (2007) Uniform molecularly imprinted microspheres and nanoparticles prepared by precipitation polymerization: the control of particle size suitable for different analytical applications. Anal Chim Acta 584:112–121
48. Long Y, Philip JYN, Schillén K, Liu F, Ye L (2011) Insight into molecular imprinting in precipitation polymerization systems using solution NMR and dynamic light scattering. J Mol Recogn 24:619–630
49. Yang K, Berg MM, Zhao C, Ye L (2009) One-pot synthesis of hydrophilic molecularly imprinted nanoparticles. Macromolecules 42:8739–8746

50. Lai J-P, Lu X-Y, Lu C-Y, Ju H-F, He X-W (2001) Preparation and evaluation of molecularly imprinted polymeric microspheres by aqueous suspension polymerization for use as a high-performance liquid chromatography stationary phase. Anal Chim Acta 442:105–111
51. Zourob M, Mohr S, Mayes AG, Macaskill A, Pérez-Moral N, Fielden PR, Goddard NJ (2006) A micro-reactor for preparing uniform molecularly imprinted polymer beads. Lab Chip 6:296–301
52. Haginaka J, Takehira H, Hosoya K, Tanaka N (1999) Unifor-sized molecularly imprinted polymer for (S)-naproxen selectively modified with hydrophilic external layer. J Chromatogr A 849:331–339
53. Mayes A, Mosbach K (1996) Molecularly imprinted polymer beads: suspension polymerization using a liquid perfluorocarbon as the dispersing phase. Anal Chem 68:3769–3774
54. Pérez-Moral N, Mayes AG (2006) Direct rapid synthesis of MIP beads in SPE cartridges. Biosens Bioelectron 21:1798–1803
55. Shen X, Ye L (2011) Molecular imprinting in Pickering emulsions: new insight into molecular recognition in water. Chem Commun 47:10359–10361
56. Shen X, Zhou T, Ye L (2012) Molecular imprinting of protein in Pickering emulsion. Chem Commun 48:8198–8200
57. Zhou T, Shen X, Chaudhary S, Ye L (2014) Molecularly imprinted polymer beads prepared by Pickering emulsion polymerization for steroid recognition. J Appl Polym Sci 131:39606
58. Shen X, Ye L (2011) Interfacial molecular imprinting in nanoparticle-stabilized emulsions. Macromolecules 44:5631–5637
59. Shen X, Bonde JS, Bülow L, Leo JC, Linke D, Ye L (2014) Bacterial imprinting at Pickering emulsion interfaces. Angew Chem Int Ed 53:10687−10690
60. Bompart M, De Wilde Y, Haupt K (2010) Chemical nanosensors based on composite molecularly imprinted polymer particles and surface-enhanced Raman scattering. Adv Mater 22:2343–2348
61. Zhao M, Zhang C, Zhang Y, Guo X, Yan H, Zhang H (2014) Efficient synthesis of narrowly dispersed hydrophilic and magnetic molecularly imprinted polymer microspheres with excellent molecular recognition ability in a real biological sample. Chem Commun 50:2208–2210
62. Ma Y, Li H, He S, Zhang H, Zhang H (2014) Efficient one-pot synthesis of water-compatible and photoresponsive molecularly imprinted polymer nanoparticles by facile RAFT precipitation polymerization. J Polym Sci A Polym Chem 52:1941–1952
63. Piacham T, Josell Å, Arwin H, Prachayasittikul V, Ye L (2005) Molecularly imprinted polymer thin films on quartz crystal microbalance using a surface bound photo-radical initiator. Anal Chim Acta 536:191–196
64. Poma A, Guerreiro A, Caygill S, Moczko E, Piletsky S (2014) Automatic reactor for solid-phase synthesis of molecularly imprinted nanoparticles (MIP NPs) in water. RSC Advances 4:4203–4206
65. Chronakis IS, Jakob A, Hagström B, Ye L (2006) Encapsulation and selective recognition of molecularly imprinted theophylline and 17β-estradiol nanoparticles within electrospun polymer nanofibers. Langmuir 22:8960–8965
66. Yoshimatsu K, Ye L, Linberg J, Chronakis IS (2008) Selective molecular adsorption using electrospun nanofiber affinity membranes. Biosens Bioelectron 23:1208–1215
67. Yoshimatsu K, Ye L, Stenlund P, Chronakis IS (2008) A simple method for preparation of molecularly imprinted nanofiber materials with signal transduction ability. Chem Commun 44:2022−2024
68. Reimhult K, Yoshimatsu K, Risveden K, Chen S, Ye L, Krozer A (2008) Characterization of QCM sensor surfaces coated with molecularly imprinted nanoparticles. Biosens Bioelectron 23:1908–1914
69. Hajizadeh S, Xu C, Kirsebom H, Ye L, Mattiasson B (2013) Cryogelation of molecularly imprinted nanoparticles: a macroporous structure as affinity chromatography column for removal of β–blockers from complex samples. J Chromatogr A 1274:6–12
70. Xu C, Ye L (2011) Clickable molecularly imprinted nanoparticles. Chem Commun 47: 6096–6098

71. Xu C, Shen X, Ye L (2012) Molecularly imprinted magnetic materials prepared from modular and clickable nanoparticles. J Mater Chem 22:7427–7433
72. Shen X, Xu C, Uddin KMA, Larsson P-O, Ye L (2013) Molecular recognition with colloidosomes enabled by imprinted polymer nanoparticles and fluorogenic boronic acid. J Mater Chem B 1:4612–4618
73. Chaudhary S, Kamra T, Uddin KMA, Snezhkova O, Jayawardena HSN, Yan M, Montelius L, Schnadt J, Ye L (2014) Controlled short-linkage assembly of functional nano-objects. Appl Sur Sci 300:22–28
74. Liu L-H, Yan M (2010) Perfluorophenyl azides: new applications in surface functionalization and nanomaterial synthesis. Acc Chem Res 43:1434–1443
75. Xu C, Uddin KMA, Shen X, Jayawardena HSN, Yan M, Ye L (2013) Photoconjugation of molecularly imprinted polymer with magnetic nanoparticles. ACS Appl Mater Interfaces 5:5208–5213

Adv Biochem Eng Biotechnol (2015) 150: 25–50
DOI 10.1007/10_2015_318

Published Online: 19 March 2015

Theoretical and Computational Strategies for the Study of the Molecular Imprinting Process and Polymer Performance

Ian A. Nicholls, Swapnil Chavan, Kerstin Golker, Björn C.G. Karlsson, Gustaf D. Olsson, Annika M. Rosengren, Subramanian Suriyanarayanan and Jesper G. Wiklander

Abstract The development of in silico strategies for the study of the molecular imprinting process and the properties of molecularly imprinted materials has been driven by a growing awareness of the inherent complexity of these systems and even by an increased awareness of the potential of these materials for use in a range of application areas. Here we highlight the development of theoretical and computational strategies that are contributing to an improved understanding of the mechanisms underlying molecularly imprinted material synthesis and performance, and even their rational design.

Keywords Chemometrics · Molecular dynamics · Molecular imprinting · Multivariate statistical analyses · Quantum mechanics · Rational design

Contents

I.A. Nicholls · S. Chavan · K. Golker · B.C.G. Karlsson · G.D. Olsson · A.M. Rosengren · S. Suriyanarayanan · J.G. Wiklander
Bioorganic and Biophysical Chemistry Laboratory, Linnaeus University Centre for Biomaterials Chemistry, Department of Chemistry and Biomedicine, Linnaeus University, 39182 Kalmar, Sweden

I.A. Nicholls (✉)
Department of Chemistry—BMC, Uppsala University, Box 576, SE-75123 Uppsala, Sweden
e-mail: ian.nicholls@lnu.se

1 Introduction

Recent years have seen a rapid increase in both fundamental studies of the molecular imprinting process and in the number of areas in which molecularly imprinted polymer (MIP)-based applications are being explored [1–9]. Major driving forces for this development have been interested in the establishment of in silico rational MIP design strategies, and the interest in tailoring polymers and their formats for particular application areas. This has in turn increased interest in elucidating the physical mechanisms underlying MIP formation and MIP–ligand recognition. This necessitates knowledge of the molecular level events occurring in pre-polymerization mixtures, the polymerization reactions, and of the factors influencing polymer-ligand recognition. Ideally, such insights will lead not only to better-performing polymers, but even to a better understanding of the origin of MIP polyclonality and the often low yields of high-fidelity sites, and the relationship between recognition properties and morphology.

While the molecular imprinting concept is at the surface eye-catching because of its apparent simplicity, researchers have quickly become aware that the complexity of the pre-polymerization mixtures, the heterogeneity of the polymeric recognition sites, and the amorphous nature of the materials together made elucidating mechanisms a challenge. Initially, conclusions regarding the underlying mechanisms were drawn from empirical studies, in particular of ligand-polymer recognition characteristics.

The limits of computational tools for assessing molecularly imprinted polymerization systems led to the earliest attempts to model the molecular imprinting process being based upon the use of thermodynamic models [10–14]. An interesting and relatively recent contribution to the literature in this area reported stochastic simulations being used to study the interaction of pre-polymerization mixture components [15]. Here, monomer-template binding affinities were used in a stochastic algorithm [16] to position the monomer and template units in a lattice matrix. Subsequently, the cross-linker was added, the template removed and the binding sites analyzed for heterogeneity. This modelling resulted in simulated MIPs that display the same trends as MIPs formed under the corresponding imprinting conditions.

The rapid increase in computing power that has taken place over the past decade, and the concurrent establishment of new and improved software, has made the use of simulations based upon mathematical descriptions realizable. Computational techniques can today be used to investigate both polymer performance and intimate aspects of the molecular imprinting process per se. Currently, a broad range of

computational techniques is being used in the study of various aspects of the molecular imprinting [17]. These techniques span from statistical treatments to quantum mechanical simulations. Here we provide a brief background on the use of computational methodologies in the study of molecular imprinting, and we present the state-of-the-art in terms of the types of computational methodologies currently in use. In particular, we address the use of computational means for studying electronic structure and molecular dynamics (MD), and we provide a brief presentation of the use of statistical methods in the study of molecular imprinted polymer systems.

2 Electronic Structure Methods

Computational methods for the study of electronic structure have become increasingly more common in aspects of the design and evaluation of MIPs. This class of methods includes semi-empirical, ab initio, and density functional strategies. In most cases, these methods and basis sets have been developed with the aim of describing a system to a high degree of accuracy, while at a reasonable computational cost. As these methods, in contrast to less sophisticated models and to other theoretical approaches, are able to describe the electronic structure, they generally yield considerably better representations of non-covalent interactions present in the system under study. In most studies these methods have been used to describe interactions present in pre-polymerization mixtures, in particular aiming to investigate the interaction between the template molecule and candidate functional monomers. In some studies, however, their use was extended beyond the pre-polymerization mixture, e.g, where these techniques have also been applied to the evaluation of recognition and rebinding of templates to MIPs.

As stated, the most common application of electronic structure methods in the design of MIPs is in the determination of putative complexes between templates and monomers. Examples of this strategy include the use of the semi-empirical AM1 method for the calculation of a complex between (*S*)–nilvadipine and 4-vinylpyridine (4VP) [18], the optimization of a complex between 2,4,6-trichlorophenol and four molecules of 4VP [19], and the PM3 method for describing two complexes formed between (*S*)-naproxen and one or two molecules of acrylamide, respectively [20]. This strategy was employed in conjunction with density functional methods by Pietrzyk et al. [21] to model a complex between melamine and three functional monomer molecules on a B3LYP/3-21G(d) level of theory. The B3LYP functional was also used by Demircelik et al. [22] with a 6-31G(d,p) basis set, and by Riahi et al. [23], with a 6-311+G(d,p) basis set, for the modelling of template-monomer complexes; the latter study also included the effect of solvent using a polarizable continuum model (PCM). In PCM calculations, the effect of the solvent is approximated by placing the system in a cavity with a surface that is polarizable according to the dielectric constant of the modelled solvent.

More recently, Holdsworth et al. [24] have demonstrated that the binding energies calculated by the AM1 method for complexes of a cocaine molecule and 1–14 molecules of either methacrylic acid (MAA) or 4VP could be used to guide optimization of the polymerization mixture composition (template—functional monomer ratio). The proposed optimal template and functional monomer relationship was subsequently validated both by NMR and rebinding studies on a series of synthesized MIPs, thus confirming the viability of this computational approach.

A number of examples of MIP-design based upon electronic structure techniques have been presented over recent years. The use of binding energies obtained from calculations on complexes between the template and a set of different functional monomers has become a more frequently used strategy for choosing functional monomers. This approach was adopted by Luliński et al. [25] in the design of a dopamine-imprinted polymer system using a PM3 level of theory. Similarly, an AM1 level of theory was used to design a MIP selective for *N*,*O*-dibenzylcarbamate [26], as was the case for studies using theophylline as template [27] in conjunction with the more sophisticated B3LYP/6-31+G**//B3LYP/3-21G level of theory. Other adaptions of this strategy include work by Gholivand et al. [28], using HF/6-31G(d) calculations in the design of a furosemide-imprinted polymer, by Alizadeh [29] for developing a pyridoxime-imprinted polymer using B3LYP/6-31G calculations, by Yao et al. [30], using MP2/6-31++G(d) calculations on an aniline template system, and by Li et al. [31], who chose functional monomers for a polymer system imprinted with chlorophenols based on results from B3LYP/6-31G (d,p) calculations. In a similar study by Kowalska et al. [32], the interactions of harmane various functional monomers were investigated using B3LYP/6-31G(d,p) calculations.

The design of a polymer system imprinted with nicotinamide was undertaken using a broad range of calculations, e.g., different density functional methods and MP2 in combination with different basis sets, by Del Sole et al. [33]. This strategy was also used by Azenha et al. [34] in the design of a silicate-based polymer selective for β-damascenone, in this case using HF and B3LYP in combination with different basis sets.

A growing number of other examples can be found in the literature, including the calculations of the structures of the complexes formed between a series of compounds and two molecules of MAA [35]. In this case, the structural parameters obtained by AM1 calculations could be correlated to the results of experimental data in the form of chromatographic studies. In a study by Lai and Feng [36], molecular geometries of buffer acids and bases optimized on the AM1-level were related to the metformin template binding in the respective media using an assumed mechanism for competitive binding. Moreover, Wu et al. [37] were able to demonstrate a relationship between experimentally determined capacity factors and the binding energies found by MP2/6-31G//HF/6-31G and PM3 calculations of complexes of various functional monomer-templates.

A number of other noteworthy examples include the use of B3LYP/6-311+G**//B3LYP/6-31G* and including solvent effects in the energy calculations of complexes in the pre-polymerization mixture of Diñeiro et al. [38, 39]. Here, the authors

were able to rationally select both the functional monomer and porogen for the successful preparation of a homovanillic acid-imprinted polymer. An extended strategy for optimization of both functional monomer and solvent was presented by Dong et al. [40], who complemented B3LYP/6-31G(d) calculations with a preceding step in which candidate systems were chosen using MD simulations (see later).

Electronic structure methods have also been used for cases where a template that differs from the target structure of the MIP is used. These methods can also assist in the choice of the template itself. One example of such a study, published in 2005 by Rathbone et al. [41], concerned the design of a MIP-based mimic of cytochrome CYP2D6. Here, the templates to be imprinted were chosen on the basis of superposition studies of a series of PM3-optimized candidate molecule geometries on known CYP2D6 substrates with the selected templates.

Quantum chemical calculations have also been used in the design of an ester hydrolysis-catalyzing polymer based on PM3 calculations. These calculations provided support for the hypothesis that the template used in the MIP synthesis is a mimic of the transition state of the reaction to be catalyzed [42]. Finally, using a very different approach, Voshell and Gagné [43] used HF/6-31G* and AM1 computational studies to determine the conformational rigidity of a dendritic system used in the imprinting of BINOL. Based on these results, a more rigid dendrimer structure was identified that afforded enhanced enantioselectivity and decreased binding site heterogeneity.

A significant limitation in the application of electronic structure methods to MIP systems is the difficulty in handling the large numbers of atoms necessary to provide a comprehensive picture of the pre-polymerization or polymer system. One particular complication appears to be the problems that can arise from the lack of an explicit solvent [44, 45]. For electronic structure methods, the inclusion of a reasonable number of solvent molecules makes the calculation rather time- consuming; as a result, solvent effects are often omitted completely. However, methods such as PCM provide the possibility of including solvent effects without the inclusion of explicit solvent molecules [46]. Nonetheless, the validity of this assumption appears limited in light of a recent report [44]. The method was recently applied by Wu et al. [47], in an MP2/6-311+G*//B3LYP/6-311G* study of the pre-polymerization mixture of a nicotinamide imprinted polymer. It was shown that the model works well for predicting the influence of different solvents on the retention and selectivity characteristics of the polymer, as long as the solvent itself is aprotic. A significant limitation of the PCM method is that not all solvents can be modelled adequately due to the inability of the PCM method to include the effect of hydrogen bonds to solvent molecules, which compete with the hydrogen bonds formed between the template and functional monomers. This was also exemplified by Liu et al. [48], who used a B3LYP/6-31+G(d,p) level of theory in which the solvation energies obtained using PCM were compared to the energies' template-solvent molecule interactions. An alternative strategy for using solvation energies obtained from B3LYP/6-31+G(d,p) including a PCM model, was demonstrated by Dong et al. [49]. Here, the solvation

energies of template and functional monomer molecules in various solvents were directly used as a measure of potential competition for interactions from the solvent.

The use of electronic structure methods in the evaluation of a given MIP has been demonstrated by Wang et al. [50]. Based on the optimized geometries and Mulliken charges calculated for a series of substrates using B3LYP/6-311G**, they were able to suggest a recognition mechanism explaining the selectivity of an *N*-(4-isopropylphenyl)-*N′*-butyleneurea imprinted polymer towards such compounds. Jacob et al. [51] were able to propose a model for the interaction between polymer and template using both ab initio and density functional theory (DFT) methods in combination with different basis sets. Similarly, by using PM3 calculations of template-monomer interactions, Wu and Li [52] could explain the failure of the imprinting of picolinamide in an MAA-based polymer. They subsequently developed a Cu(II) complex-based system that did show selectivity for the imprinted compound. The system has also been extended to the recognition of small organic acids [53].

Christoforidis et al. [54] investigated the mode of interaction of semiquinone radicals with an imprinted polymer that was elucidated using a series of B3LYP and MP2 calculations in connection with electron spin echo envelope modulation (ESEEM) spectroscopy. A detailed study on the mechanism of theophylline-polymer recognition was published by Che et al. [55], who had used B3LYP/6-31G (d,p) calculations in combination with 2D IR-spectroscopy.

Of potential importance for many of the new thin film- and surface-based applications of MIPs are computational studies describing adsorption to surfaces. For example, correlations have been found between the PM3-level calculated molecular volume and the adsorption coefficient of bile acids on a film of over-oxidized polypyrrole imprinted with sodium taurocholate [56]. In another study, Mukawa et al. [57] were able to explain the relative selectivities of a polymer synthesized using allyl phenyl disulfide towards phenol and the template analogue thiophenol. In this study, the different strengths of the hydrogen bonds being formed between polymer and ligand were calculated on the HF/6-31G* level of theory. A variation on this theme was used by Meng et al. [58] in the design of a MIP-based transesterification catalyst. Here, the calculation of the AM1 energies was used to examine the various functional monomers under study by probing their interaction with putative reaction intermediates.

To date, only one report has been published where modelling of the properties of an imprinted polymer has been undertaken using electronic structure calculations [59]. Here, the initial step involved PM3-based calculations to model the pre-polymerization complex of nicotinamide or *iso*–nicotinamide with MAA as functional monomer. In a second step, the spatial positions of the functional monomers were fixed and the template molecule removed from the system, thus creating a model for the binding site without the cross-linked polymeric backbone. Finally, a strong correlation with the experimental retention factors of the respective MIPs was observed upon comparison of the interaction energies calculated for a series of substrates with this binding site model.

A notable study is that of Tada et al. [60], who developed an Rh-amine complex imprinted silicate system that displayed shape-selectively in catalysis of hydrogenation reactions. PWC/DNP calculations were conducted on the complexation of the metal center and both the imprinted and catalytically active species were characterized by using these calculations in conjunction with a series of experimental studies.

In summary, recent years have seen an increase in the number of researchers using quantum chemical calculations to address various aspects of MIP science and technology. These approaches have been used primarily for studying interactions in the pre-polymerization mixture, even for explaining recognition phenomena in the finished polymer. Nonetheless, most studies have been focused on single aspects of the process of designing, synthesizing or testing of a system, and the impact on MIP research has so far been rather limited. With the development of refined computational techniques and improved availability of computational power, however, the impact of electronic structure-based calculations can be expected to increase.

3 Molecular Dynamics Simulations

Although there are now many reported protocols describing the successful development of selective MIPs, these protocols typically involve many variables and steps that ideally should be optimized in terms of MIP-template recognition characteristics when translating to other templates. Among these variables, it is generally accepted that the choice of the stoichiometry of polymer components as well as the temperature and pressure during synthesis are factors of major importance [61–63]. With this in mind, the use of in silico techniques for better understanding or optimizing these factors should afford savings in terms of time and cost for MIP production.

A rapidly emerging tool for this task is MD, a computational, force-field-based technique [64]—in particular, its use for simulating and allowing predictions of the nature of the ensemble of non-covalent complexes that are formed between polymer components in a MIP pre-polymerization mixture. Since the pioneering work of Alder and Wainwright in 1957 on the simulation of gaseous argon [65], simulations have progressed such that they nowadays allow for the study of multiple simultaneously interacting atoms. Among the great number of force-fields that exist and that are routinely being used for the study of biomolecules as well as small organic molecules are, for example, AMBER [66], GAFF [67], CHARMM [68], OPLS [69] and GROMOS [70, 71].

Owing to the accuracy of such force-fields, MD simulations have been used to study protein folding [72, 73], conformational changes of DNA [74, 75], orientation of phospholipids in bilayer membranes [76, 77], active transport of drug molecules across membranes [78], physical characteristics of solvents [79] and surfaces [80, 81], as well as biomolecular interactions [82–84].

It is today commonly accepted that the origin of the predetermined recognition in MIPs can be correlated back to the nature and strength of functional monomer-template complexes that are established at the pre-polymerization stage [1, 14, 85–87]. Accordingly, work over the years has been predominantly focused on the development of protocols that can suggest which functional monomer has the highest affinity for the template. The first MD-based protocol with the aim of selecting the best binding functional monomer(s) was reported in 2001 by Piletsky and colleagues [88]. Here, Piletsky and his group developed an approach that was based on a virtual library comprised of a total of 20 different monomers that were screened against one enantiomer of the template ephedrine. In a follow-up work by the group, in order to investigate how the choice of solvent (porogen) and monomers affects functional monomer-template complexation during the pre-polymerization stage, Piletsky and co-workers [88] used a simulated annealing approach to generate low-energy ensembles of ephedrine that was solvated with multiple copies of functional-, cross-linking monomers and explicit solvent molecules. Using this strategy, they later prepared MIPs that have been targeting a series of drugs and pharmaceutically interesting compounds such as simazine [89], cocaine, methadone and morphine [90, 91], creatinine [92], biotin [93], and the cyanobacterial toxin microcystin-LR [94, 95]. It is noteworthy that in the case of microcystin-LR, the use of their approach led to a MIP that demonstrated recognition characteristics similar to those demonstrated by antibodies.

Later, similar strategies utilizing virtual libraries of monomers have been developed by other researchers. Wei et al. [96] imprinted 17β-estradiol after simulating either a monomer-template pair or a single template molecule solvated with eight functional monomers to incorporate also the effect of monomer dimerization on the degree of template complexation. In both these cases, each 17β-estradiol was surrounded by explicit non-polar porogen molecules (acetone or chloroform). The selection of the "best binding" monomer here was made from a virtual library comprised of a total of nine different functional monomers. Here, the use of an MD-based computational screening approach to find the optimal functional monomer suggested that MAA, methacrylamide and 2-(diethylamino)ethyl methacrylate showed the strongest hydrogen bonding interactions to the selected template, with results in accordance with parallel experimental MIP-template batch rebinding studies.

To investigate the impact of the growing polymer chain during polymerization on the stability of functional monomer-template complexation, studies have been performed in which homo- and co-polymeric chains of functional monomers have been used in the search for the optimal monomer. Pavel and Lagowski [97, 98] reported on a strategy where they computed potential energy differences for a series of functional monomer-template complexes. The binding energies were calculated after simulating an ensemble of functional monomers in the absence or presence of the template. Secondly, the effect of polymer chain growth on complex stability was investigated instead, using linear homo- and co-polymer chains. In this, using the target theophylline and a series of structural analogues, they demonstrated that the use of itaconic acid or ethylene dimethacrylate (EDMA) resulted in the best binding

MIP. Later, Pavel and team [99] also reported on the successful virtual screening of a number of warfare agents. These studies were made in order to investigate the character of the non-covalent interactions dictating functional monomer-template complexation. Results from these investigations pointed to the importance of electrostatic interactions as well as the presence of carboxylic and vinyl groups on the functional monomers to drive template complexation.

To study the stability of the complex formed between the template, 2,4-dichlorophenoxyacetic acid and the functional monomer 4VP which is believed to be stoichiometric of type 1:1, Molinelli et al. [100] reported a series of studies inserting a pre-minimized complex that was explicitly solvated by either chloroform or water molecules. From using different starting geometries in the different solvents, hydrogen bond interaction in chloroform and π–π stacking interaction in water, the authors proposed mechanisms to explain the nature of the interactions involved during the pre-polymerization stage as well as during MIP rebinding in aqueous solution.

To develop this strategy further, Monti et al. [101] showed the great potential in using a combination of MD, molecular mechanics (MM), docking and site mapping for obtaining the best functional monomer binding to the template theophylline. Here, the authors demonstrated the presence of a "molecular memory" and a MIP-template selectivity in agreement with experimental data.

In order to investigate the selective adsorption properties of a dimethoate MIP, Lv et al. [102] used a series of simulations to predict the binding energies for a series of homo-polymers and the template. Results from these studies, later supported by chromatographic evaluations, suggested that a homo-polymer built up by butyl methacrylate demonstrated the most selective binding to the template.

Interestingly, MD has also been used to shed light on functional-monomer-template complex stabilities for MIPs prepared in formats other than bulk polymerization, the most commonly used strategy. To investigate the stability of functional monomer-template complexation during pre-polymerization in surface imprinting, Yoshida et al. [103] used simulations to make predictions regarding the stability of functional monomer-template complexation. The corresponding MIP was prepared to demonstrate chiral recognition for tryptophan methyl ester using phenyl phosphonic acid monododecyl ester (n-DDP) as recognition site-members in a water-in-oil emulsion. By studying the dynamics of a single complex (2:1 functional monomer:template stoichiometry), initially in vacuum and later in a toluene-water interface, the authors suggested that the imprinting effect in the prepared MIP was based on the stability of the n-DDP-tryptophan methyl ester complexes formed in the emulsion. In a further development in this field, Toorisaka and co-workers [104] reported on the stability of a complex formed at a water-toluene interface comprised of a cobalt ion, one molecule of alkyl imidazole, and a substrate analogue, *N*α-t-Boc-L-histidine, thus forming a key part in the active site in a catalytic MIP.

The large number of atoms typically present in a MIP pre-polymerization mixture often limits the use of quantum mechanics (QM) for the elucidation of monomer-template binding energies on account of the sheer amount of

computational time that would be required. However, some examples have appeared in the literature where QM has been integrated in the screening process, but with various simplifications being made. Dong et al. [40] reported an MD approach based on a combination of MM and QM for the virtual library screening of the best functional monomer to be used in the imprinting of the herbicide acetochlor. In their approach, the authors initially used a series of MD simulation steps representing a single functional monomer-template complex, surrounded by explicit porogen (either acetonitrile, chloroform or carbon tetrachloride). A measure of the stability of the complex was obtained through calculation of the potential energy for the formed complex using an MM force-field. Secondly, complex energies were computed using DFT and a 6-31G(d) basis set. The presence of an implicit solvent model was, however, computed using a polarizable continuum field. Based on the accuracy obtained from these computations, the top three functional monomers were selected and later used for the imprinting of acetochlor. Notably, this strategy for mixing MM/QM has been found to be successful and also used for the imprinting of rhodamine B [105] and sulfadimidine [106].

Importantly, as already discussed, the diverse nature of the non-covalent interactions that are formed at the pre-polymerization stage makes it necessary to account for all interactions, and not only those formed between functional monomer and the template, to make successful predictions on MIP-template recognition characteristics. To investigate the influence of template and monomer dimerization on final MIP-template recognition, studies on, for example, nicotine dimerization during the pre-polymerization stage helped to explain the unusual behavior observed in final MIP-template rebinding [107, 108]. Notably, in 1999, Katz and Davis [109] proposed that the binding capacity of a MIP that had been imprinted with phenylalanine anilide in either chloroform or acetonitrile originated from the strong degree of template dimerization occurring at the pre-polymerization stage. Recently, the basis of the formation and extent of phenylalanine anilide dimerization previously studied by Katz and Davis was further investigated by Olsson et al. [110] using MD.

To study the impact of functional monomer dimerization on MIP-ephedrine recognition, Ansell and co-workers demonstrated NMR-spectroscopic support for the importance of an all-component treatment of the pre-polymerization mixture [111–113].

To approach a more realistic representation of the “actual” pre-polymerization mixture, a series of efforts has been made towards mimicking the actual pre-polymerization mixture where large multiples of components are present in the stoichiometric ratios representative to the ones being used in typical MIP preparation protocols. O’Mahony et al. [44] used a number of MD simulations to study functional monomer-naproxen complexation and especially the effect of template dimerization on MIP performance. Although these mixtures did not include the initiator, extracted data from simulations suggested not only a high degree of 4VP-naproxen complexation, but also that the cross-linking agent EDMA was found to contribute to the high degree of selectivity demonstrated by the MIP. On the same

theme, the role of template dimerization on final MIP performance was also reported by O'Mahony et al. for imprinting of quercetin using 4VP as functional monomer [114]. In this example, results revealed the formation of sheet-like structures of quercetin-4VP complexes with stabilities typically independent of the concentration of EDMA used. Recently, O'Mahony and colleagues have developed a 4-VP-based MIP that was imprinted with hydroquinone and capable of extracting the endocrine disruptor Bisphenol-A from milk [115]. In this case, however, the group used a novel approach in which the template's capacity to dimerize (through hydrogen bonding) to later facilitate the formation of imprints for binding the target, Bisphenol-A, through a predicted 2:1 functional monomer-target complex.

By also including the initiator and multiple templates in correct stoichiometries to represent an actual pre-polymerization system, Karlsson et al. [45] were able to present a comprehensive investigation of all non-covalent interactions taking place in a bupivacaine imprinting procedure. Interestingly, the authors reported both a correlation between results obtained from a series of NMR spectroscopic studies on monomer-template complex stability and simulated data, and also the origin of the recognition-site heterogeneity frequently demonstrated in MIPs (see Fig. 1). This binding-site heterogeneity and possible consequences for polymer morphology and template rebinding in bupivacaine MIPs was later also investigated by Golker et al. [116, 117]. Here, the authors performed a large number of MD simulations and physical characterizations of polymer morphologies and template rebinding capacities using different polymer compositions (increasing molar fraction of the functional monomer MAA). Correlations between the nature and extent of the non-covalent interactions present at the pre-polymerization stage and the final polymer performance could be made. The success in using MD-based approaches for predicting MIP-template rebinding performance prompted a recently reported study to investigate the role of the cross-linking monomer (EDMA or TRIM) in (*S*)-propranolol MIPs [118]. This type of use of MD in the study of MIPS was further extended in an investigation of the role of π–π stacking interactions for establishing molecular memory in MIPs imprinted with polychlorinated benzenes such as 1,2,3-trichlorobenzene [119].

Up to this point in time, most MD-based studies aimed at predicting MIP recognition behavior have been focused on the interactions taking place during the pre-polymerization stage, i.e., prior to polymer formation. To eliminate the problems related to simulating the polymerization process, which requires a QM treatment of the simulated mixture, and the difficulties in obtaining information on polymer micro- and macrostructure due to heterogeneity, some interesting recent attempts have been made to model imprints in the final MIP through building rough models of chains of polymer.

To better understand the origin to the molecular memory in MIPs and to demonstrate the importance of pores on MIP-template recognition, Srebnik and colleagues [120–122] performed a series of MD studies to investigate the mechanisms to the imprinting effect. To shed light on the influence of pore formation, Youngermann and Srebnik [123] investigated factors contributing to binding-site imperfections

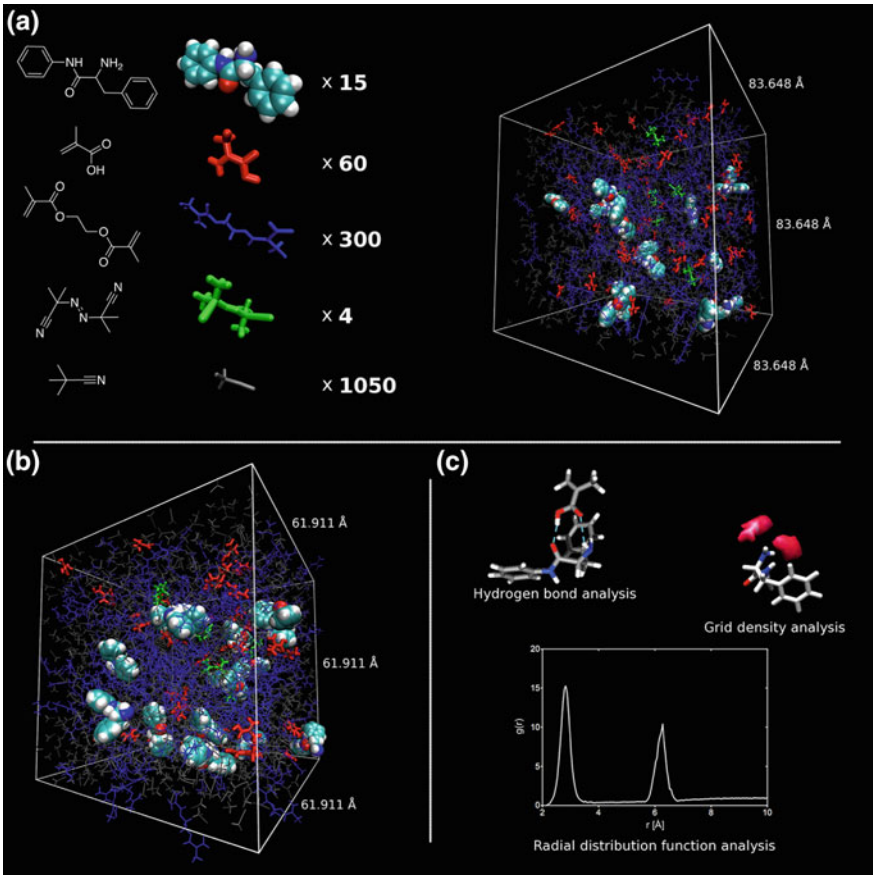

Fig. 1 The strategy used for all-component MD simulations, here for a bupivacaine MIP pre-polymerization mixture [115]. **a** The system is constructed using all the components used in the MIP synthesis and in the same stoichiometry as the synthesis. For small molecule templates, at least 10 template structures are generally used. Randomized initially packing geometries are used [110]. **b** After a series of energy minimization steps and equilibration, first at NVT and then at NPT, the collection of production-phase data is undertaken (for small organic templates, typically 5–10 ns production-phase at NVT, and generally >5 systems run in parallel). **c** Study of the interactions of the components in the pre-polymerization mixture is performed by examining the trajectories of all the components in the system over the production-phase, e.g., using radial distribution functions and hydrogen bond analyses. The prevalence of a given type of component around a particular element is illustrated using 3D grid density analyses

leading to the recognition-site heterogeneity using a series of coarse-grained MD simulations. Through topological analyses of a modelled cross-linked polymer network, before and after template removal, they suggested that the typically low yield of imprints (10–15 %) was a result of the quality of generated pores. They also proposed that when considering both the size and shape of the template, the best

performing MIP should have a high degree of cross-linkage (90 %) and that the low quality of the imprints induced by the templates resulted from the aggregation of template during the pre-polymerization stage.

Finally, to shed further light on the physical characteristics of the MIP matrix, MD simulations have also been used to study the role of the solvent during template rebinding as well as to simulate the dynamics of the final MIP. In a study by Zhao et al. [124], a cubic model of a MIP was built to represent a hydrogel network. This model polymer matrix was studied in the presence of the template, cholesterol, and the dynamics of this polymeric hydrogel as well as its interactions with explicit solvent molecules were evaluated. The authors modelled this highly cross-linked infinite polymer network based on a dummy cube inserting various numbers of single polymeric chains of poly-methacrylic acid. Results obtained from their simulations and subsequent analyses of the dynamics of the polymer and its interactions with surrounding water molecules revealed a highly ordered structure of water solvating the hydrogel. From these observations they concluded that by adjusting the amount of carboxyl groups incorporated in the polymer matrix, they could control the water structure and thereby the diffusion of water through the polymer. The authors found a good correlation between experimental template (cholesterol) diffusion data as compared with results obtained by simulation. In subsequent work by the same group, the effect of charge on the functional monomers positioned in a cubic methacrylate-based MIP model was investigated through artificially changing the charge of the carboxylic acid functionalities incorporated in the cubic lattice [125]. Results from these studies suggest that the diffusion of the target molecule cholesterol was not affected by the polymer network structure, and the authors notably concluded that the recognition process is solely governed by the mesh size of the network. Interestingly, the authors also suggested that the effect of increasing charge in the system resulted in an enhanced polymeric structure.

Xerogels have been the subject of another recent study, where the role of adding polyethylene glycol (PEG) for tuning the porosity of the final polymeric material was explored by Azeha et al. using MD simulations [126]. They also examined the sol-gel phase separation of the various components present in the damascenone imprinted xerogel pre-gelification stage. Results presented suggested that the presence of PEG in these mixtures had an adverse effect on template-functional monomer association and hence no improvement in the imprinting effect of damascenone was proposed—which was shown to be in accordance with experimental findings. Notably, the addition of PEG had no effect on the interactions related to the network structuring, and the authors proposed that the PEG molecules were pushed out into the aqueous-methanolic sol-phase when added to the pre-gelification mixture.

Taken together, the examples provided above clearly illustrate that MD-based studies can provide valuable insights into pre-polymerization systems in particular, but even into physical characteristics of the final MIP matrix.

4 Multivariate Statistical Analyses

The application of mathematical and statistical methods to chemical data is a discipline within computational science referred to as chemometrics [127–129]; its development has led to improved or simplified selection of optimal experimental parameters as well as the extraction of significant information generated from multivariate data analysis. It is important to note that in the field of chemometrics it is recommended to use an experimental design, in which the factors are systematically and simultaneously varied. Through experimental design, a minimal number of experiments can be used in order to extract a maximal amount of information. In essence, the concept involves changing all relevant factors simultaneously over a series of planned experiments and then interpreting the results using mathematical models. Traditionally, the different experimental design methods applied to the analysis of different aspects of MIP systems are considered to be fractional factorial [130–135], full factorial [136–140], central composite [134, 137, 138, 140, 141], Box-Behnken [142] and Doehlert [132, 133, 135, 139, 143]. The fundamental differences between these designs are that they differ in terms of how factors are varied and the number of experiments required. The experimental designs discussed above may be schematically illustrated, as shown in Fig. 2. There are no limitations, other than practical, in terms of the number of factors that can be used in an experimental design. Full and fractional designs are primarily used if the objective of the study is screening, and Box-Behnken and Doehlert are used for surface modelling while central composite design is an extension of the factorial designs intended for both optimization and surface modelling. The molecular imprinting literature includes a growing number of papers and even a range of different chemometric methods. We provide below a short description of the different uses to highlight the potential of these methods.

Within the field of molecular imprinting, the synthesis of MIPs, as well as rebinding of the template to the MIP, are good examples of experimental endeavors that may be addressed using chemometric approaches. Examples of factors that can be varied when working with MIPs include the types and amounts of monomer, template, cross-linker, porogen and initiator. Other factors that can be of relevance can include polymerization temperature, the ratio of the various reaction mixture components (stoichiometry), and the ligand recognition or rebinding environment. Chemometric strategies can be a powerful complement to traditional MIP analysis, which is generally univariate in nature, i.e., first one parameter is optimized and then that value is used to optimize the next parameter. By using the univariate approach, the optimum found could be false. Even so, only a few efforts have been reported on the use of chemometrics in the optimization of the MIP binding parameters [132–135, 139–142, 144–147], and in the optimization of polymer composition [130, 131, 136–138, 143, 148, 149].

A number of statistical methods are available for the analysis of experimental data. A quite common example is analysis of variance (ANOVA) that is used to analyze observations that depend on the variation of one or more factors. However,

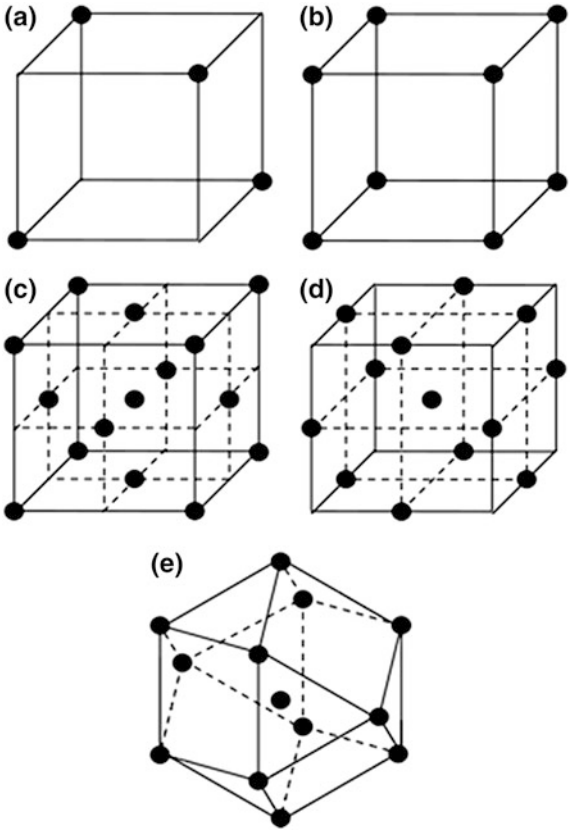

Fig. 2 Schematic illustration of the experimental designs used in the analysis of MIPs. The controlled variables in the studies are called factors and could be, for example, the amount of functional monomer, cross-linker and porogen. Points represent experimental runs of a three-factor **a** fractional factorial, **b** full factorial, **c** central composite, **d** Box-Behnken, and **e** Doehlert design

as ANOVA is a univariate method, it cannot take into account the covariance of different variables. Principal component analysis (PCA) is used in the classification of data. The principle by which PCA functions is to find the so-called principal components (PCs). The various PCs are graphically represented by vectors, where the first PC approximates the maximum variance direction in the data. The second PC is chosen so that it is orthogonal to the first PC and approximates the second maximum variance direction, and so forth. Through the identification of the PCs describing most of the variation, patterns in the data may be revealed as well as the factors that have the most influence on the variance. Different methods used in multivariate calibration of data include partial least squares regression (PLSR), principal component regression (PCR), and multiple linear regression (MLR) [127]. The major differences between these calibration methods are found in how they handle covariance. If the variables are independent, MLR is the preferred regression method, while PCR and PLSR handle covariance better.

Another method used to calibrate data is artificial neural network (ANN) construction [150]. The neural network is comprised of different layers and it functions as an associative memory by using experimental data to program itself. The input

layer receives input data, the hidden layer performs processing and transformation of the input data and the output layer processes the final results [17]. Numerical values, known as weights, are assigned to the connections between nodes of the various layers. These express the relative strength of the input data. The commonly used "back-propagation of error" algorithm is a supervised learning method used in ANN, meaning that it requires both the input and output to be known in advance. The weights are adjusted accordingly with respect to the error, which is calculated from the difference between the actual and predicted values.

The optimization of the composition of MIPs has been combined with different chemometric approaches in several papers. For example, PLSR was used to analyze a first order model for the composition of a bisphenol A-imprinted polymer [130]. By varying the amount of template, monomer (MAA or 4VP), cross-linker [EDMA or trimethylpropane trimethacrylate (TRIM)], initiator (2,2′-azobis(isobutyronitrile, AIBN), porogenic solvent (tetrahydrofuran, chloroform, toluene or acetonitrile) and the polymerization method (thermal or UV), mini-MIPs were prepared and evaluated through rebinding experiments in acetonitrile. After identification of the polymer composition that yielded the maximum specific binding, it was prepared on a larger scale in order to validate the prediction power of the model. It is important to note that validation is a critical step in the optimization process, although in this work it had its weakness in that only one part of the model (the optimum) was validated. The screening and evaluation of a small library of small-scale piroxicam-imprinted polymers was performed by Navarro-Villoslada and Takeuchi [131]. They did this by using a fractional factorial design for polymer compositions, and varying the amount of monomer (4VP), cross-linker (EDMA, TRIM, divinylbenzene or bisphenol A dimethacrylate), template (piroxicam), initiator (AIBN), porogenic solvent (acetonitrile), and polymerization method (thermal or UV). A first order calibration curve was used for the fitting of the experimental data and for cross-validation.

A central composite design was used by Kempe and Kempe [137] in another approach for the optimization of polymer composition—in this case for propranolol-imprinted polymer beads. They used the regression method MLR to analyze the variable factors: amount of monomer (MAA), cross-linker (TRIM), and porogenic solvent (acetonitrile). Propranolol rebinding was measured by a binding assay and the resulting quadratic model was validated. Davis et al. concluded in another paper that difficulties arise when using commonly used protocols when introducing new templates into molecular imprinting [136]. Consequently, they proposed a chemometric approach for the design of a polymer imprinted with sulfamethazine. They based their experimental study on an HPLC multi-analyte competition rebinding assay. A three-level full factorial design was used for the experimental setup, and a quadratic regression model containing squared terms was used for data fitting. Two factors [amount of monomer (MAA) and cross-linker (EDMA)] were considered. ANOVA was subsequently used for validating the model.

It is important to note that a chemometrics-based approach to polymer composition optimization provides no guarantee of finding the optimal MIP design. A general problem in this regard is evident in cases when the optimum is found in a

corner of the experimental region [130, 131, 136, 143, 148, 149]. In such cases, extension of the experimental region until a local optimum can clearly be seen as important in order to allow the drawing of more conclusions regarding MIP design.

Parameter analysis with respect to ligand rebinding to a MIP offers further opportunities for the optimization of molecular imprinting systems. One of the strengths of chemometrics is that the analysis methods can handle a great number of variables while also selecting the most important ones. Baggiani et al.used the semi-empirical quantum-chemical method AM1 for geometry optimization of the molecules studied and, on the basis of the optimized structures, molecular descriptors were calculated and used as variables in the chemometric methods [144]. The thermally polymerized pentachlorophenol MIP was comprised of 4VP as the functional monomer and EDMA as the cross-linking monomers, respectively. An analysis of the correlation of HPLC column selectivity with molecular descriptors was performed with PCA and PCR. The results obtained in this study showed that the pentachlorophenol-imprinted polymer demonstrates a pattern of selectivity towards several related phenols, and which steric and electronic molecular descriptors could be used to explain the selectivity. In another study, the binding of bupivacaine to imprinted polymers in different solvent mixtures and at various temperatures using equilibrium binding studies was investigated by Rosengren et al. [145]. By using PLSR, it was shown that binding could be described in terms of temperature and dielectric constant following a third-degree equation with cross-terms. The models developed in this work were validated using independent binding data obtained with a separate batch of polymers. Moreover, the complexity of the relationship highlighted the necessity for a robust validation process when building models.

The rebinding of chloroguaiacol to a MIP by utilizing a flow pre-concentration system coupled to amperometric detection was the subject of a study by Tarley et al. [132]. A fractional factorial design was initially used to establish an experiment for the study of the influence of the mobile phase physical properties (pH, flow rate, KCl concentration, elution flow rate and eluent volume). Analysis of these factors identified those most important with respect to rebinding. A Doehlert design yielded a quadratic model with cross terms and was used for the final optimization of the rebinding with the most important factors (pH and KCl concentration).

Nantasenamat et al. used literature data as the basis for a similar approach [146, 151]. They applied ANN to correlate imprinting factors from diverse published HPLC studies with molecular descriptors and mobile phase compositions [152]. The mobile phase descriptors were measured (pH and ionic strength) or taken from the literature (dielectric constant). Back-propagation of error algorithm was then used to calculate the model. The data-set was subsequently divided into two groups that were analyzed separately. Interestingly, one group consisted of data from uniformly sized MIPs and the other consisted of data from irregularly sized MIPs.

An interesting contribution to the literature involved the use of a stochastic simulation to examine the interaction between the components present in the pre-polymerization mixture [15]. Here, monomer-template binding affinities were used

in a stochastic algorithm [16] to position the monomer and template units in a lattice matrix. Subsequently, the cross-linker was added, the template removed, and the binding sites analyzed for heterogeneity. This modelling resulted in simulated MIPs that display the same trends as the MIPs formed under the corresponding imprinting conditions.

5 Conclusions and Future Perspectives

Recent years have witnessed exceptional growth in the number of studies using computational and theoretical techniques for describing, predicting and analyzing molecular imprinting systems. In many respects, the improvements in the accessibility of computational power and software have helped drive the development of MIP science and technology. As we can anticipate further improvements in computer hardware and software technologies, it is reasonable to assume that this trend will continue, and new, as well as barely addressed aspects of molecular imprinting, e.g., the investigation of relationships between morphology and polymer composition, may be studied, and steps taking us closer to truly rationally designed MIPs will be demonstrated.

References

1. Alexander C, Andersson HS, Andersson LI, Ansell RJ, Kirsch N, Nicholls IA, O'Mahony J, Whitcombe MJ (2006) Molecular imprinting science and technology: a survey of the literature for the years up to and including 2003. J Mol Recog 19:106–180
2. Wulff G (2002) Enzyme-like catalysis by molecularly imprinted polymers. Chem Rev 102: 1–27
3. Haupt K, Mosbach K (2000) Molecularly imprinted polymers and their use in biomimetic sensors. Chem Rev 100:2495–2504
4. Batra D, Shea KJ (2003) Combinatorial methods in molecular imprinting. Curr Opin Chem Biol 7:434–442
5. Sellergren B (ed) (2001) Molecularly imprinted polymers : man-made mimics of antibodies and their applications in analytical chemistry, vol 23. Elsevier, Amsterdam
6. Komiyama M, Takeuchi T, Mukawa T, Asanuma H (2002) Molecular imprinting: from fundamentals to applications. Wiley-VCH, Weinheim
7. Yan M, Ramström O (eds) (2005) Molecularly imprinted materials: science and technology. Marcel Dekker, New York
8. Piletsky SA, Turner APF (eds) (2006) Molecular imprinting of polymers. Landes Bioscience, Georgetown
9. Lei Y (2013) Molecular imprinting: principles and applications of micro- and nanostructured polymers. Pan Stanford Publishing, Singapore
10. Nicholls IA (1995) Thermodynamic considerations for the design of and ligand recognition by molecularly imprinted polymers. Chem Lett 24:1035–1036
11. Nicholls IA, Adbo K, Andersson HS, Andersson PO, Ankarloo J, Hedin-Dahlström J, Jokela P, Karlsson JG, Olofsson L, Rosengren J et al (2001) Can we rationally design molecularly imprinted polymers? Anal Chim Acta 435:9–18

12. Pande VS, Grosberg AY, Tanaka T (1997) How to create polymers with protein-like capabilities: a theoretical suggestion. Phys D 107:316–321
13. Nicholls IA (1998) Towards the rational design of molecularly imprinted polymers. J Mol Recognit 11:79–82
14. Piletsky SA, Panasyuk TL, Piletskaya EV, Nicholls IA, Ulbricht M (1999) Receptor and transport properties of imprinted polymer membranes—a review. J Membr Sci 157:263–278
15. Wu X, Carroll WR, Shimizu KD (2008) Stochastic lattice model simulations of molecularly imprinted polymers. Chem Mater 20:4335–4346
16. Veitl M, Schweiger U, Berger ML (1997) Stochastic simulation of ligand-receptor interaction. Comput Biomed Res 30:427–450
17. Nicholls IA, Andersson HS, Freebairn K, Henschel H, Karlsson BCG, Olsson GD, Rosengren AM, Shoravi S, Wiklander JG, Wikman S (2013) Rational molecularly imprinted polymer design: theoretical and computational strategies. In: Lei Y (ed) Molecular imprinting: principles and applications of micro- and nanostructured polymers. Pan Stanford Publishing, Singapore
18. Fu Q, Sanbe H, Kagawa C, Kunimoto KK, Haginaka J (2003) Uniformly sized molecularly Imprinted polymer for (S)-Nilvadipine. Comparison of chiral recognition ability with HPLC chiral stationary phases based on a protein. Anal Chem 75:191–198
19. Schwarz L, Holdsworth CI, McCluskey A, Bowyer MC (2004) Synthesis and evaluation of a molecularly imprinted polymer selective to 2,4,6-trichlorophenol. Aust J Chem 57:759–764
20. Li P, Rong F, Xie YB, Hu V, Yuan CW (2004) Study on the binding characteristic of s-naproxen imprinted polymer and the interactions between templates and monomers. J Anal Chem 59:939–944
21. Pietrzyk A, Kutner W, Chitta R, Zandler ME, D'Souza F, Sannicolo F, Mussini PR (2009) Melamine acoustic chemosensor based on molecularly imprinted polymer film. Anal Chem 81:10061–10070
22. Demircelik AH, Andac M, Andac CA, Say R, Denizli A (2009) Molecular recognition-based detoxification of aluminum in human plasma. J Biomater Sci Polym Ed 20:1235–1258
23. Riahi S, Edris-Tabrizi F, Javanbakht M, Ganjali MR, Norouzi P (2009) A computational approach to studying monomer selectivity towards the template in an imprinted polymer. J Mol Model 15:829–836
24. Holdsworth CI, Bowyer MC, Lennard C, McCluskey A (2005) Formulation of cocaine-imprinted polymers utilizing molecular modelling and NMR analysis. Aust J Chem 58: 315–320
25. Lulinski P, Maciejewska D, Bamburowicz-Klimkowska M, Szutowski M (2007) Dopamine-imprinted polymers: template-monomer interactions, analysis of template removal and application to solid phase extraction. Molecules 12:2434–2449
26. Baggiani C, Anfossi L, Baravalle P, Giovannoli C, Tozzi C (2005) Selectivity features of molecularly imprinted polymers recognising the carbamate group. Anal Chim Acta 531: 199–207
27. Dong WG, Yan M, Zhang ML, Liu Z, Li YM (2005) A computational and experimental Investigation of the interaction between the template molecule and the functional monomer used in the molecularly imprinted polymer. Anal Chim Acta 542:186–192
28. Gholivand MB, Khodadadian M, Ahmadi F (2010) Computer aided-molecular design and synthesis of a high selective molecularly imprinted polymer for solid-phase extraction of furosemide from human plasma. Anal Chim Acta 658:225–232
29. Alizadeh T (2008) Development of a molecularly imprinted polymer for pyridoxine using an ion-pair as template. Anal Chim Acta 623:101–108
30. Yao JH, Li X, Qin W (2008) Computational design and synthesis of molecular imprinted polymers with high selectivity for removal of aniline from contaminated water. Anal Chim Acta 610:282–288
31. Li Y, Li X, Dong CK, Li YQ, Jin PF, Qi JY (2009) Selective recognition and removal of chlorophenols from aqueous solution using molecularly imprinted polymer prepared by

reversible addition-fragmentation chain transfer polymerization. Biosens Bioelectron 25:306–312
32. Kowalska A, Stobiecka A, Wysocki S (2009) A computational investigation of the interactions between harmane and the functional monomers commonly used in molecular imprinting. J Mol Struct THEOCHEM 901:88–95
33. Del Sole R, Lazzoi MR, Arnone M, Della Sala F, Cannoletta D, Vasapollo G (2009) Experimental and computational studies on non-covalent imprinted microspheres as recognition system for nicotinamide molecules. Molecules 14:2632–2649
34. Azenha M, Kathirvel P, Nogueira P, Fernando-Silva A (2008) The requisite level of theory for the computational design of molecularly imprinted silica xerogels. Biosens Bioelectron 23:1843–1849
35. Ogawa T, Hoshina K, Haginaka J, Honda C, Moto TT, Uchida T (2005) Screening of bitterness-suppressing agents for quinine: the use of molecularly imprinted polymers. J Pharm Sci 94:353–362
36. Lai EPC, Feng SY (2003) Molecularly imprinted solid phase extraction for rapid screening of metformin. Microchem J 75:159–168
37. Wu LQ, Sun BW, Li YZ, Chang WB (2003) Study properties of molecular imprinting polymer using a computational approach. Analyst 128:944–949
38. Dineiro Y, Menendez MI, Blanco-Lopez MC, Lobo-Castanon MJ, Miranda-Ordieres AJ, Tunon-Blanco P (2005) Computational approach to the rational design of molecularly imprinted polymers for voltammetric sensing of homovanillic acid. Anal Chem 77: 6741–6746
39. Dineiro Y, Menendez MI, Blanco-Lopez MC, Lobo-Castanon MJ, Miranda-Ordieres AJ, Tunon-Blanco P (2006) Computational predictions and experimental affinity distributions for a homovanillic acid molecularly imprinted polymer. Biosens Bioelectron 22:364–371
40. Dong C, Li X, Guo Z, Qi J (2009) Development of a model for the rational design of molecular imprinted polymer: computational approach for combined molecular dynamics/ quantum mechanics calculations. Anal Chim Acta 647:117–124
41. Rathbone DL, Ali A, Antonaki P, Cheek S (2005) Towards a polymeric binding mimic for cytochrome CYP2D6. Biosens Bioelectron 20:2353–2363
42. Sagawa T, Togo K, Miyahara C, Ihara H, Ohkubo K (2004) Rate-enhancement of hydrolysis of long-chain amino acid ester by cross-linked polymers imprinted with a transition-State analogue: evaluation of imprinting effect in kinetic analysis. Anal Chim Acta 504:37–41
43. Voshell SM, Gagné MR (2005) Rigidified dendritic structures for imprinting chiral information. Organometallics 24:6338–6350
44. O'Mahony J, Karlsson BCG, Mizaikoff B, Nicholls IA (2007) Correlated theoretical, spectroscopic and x-ray crystallographic studies of a non-covalent molecularly Imprinted polymerisation system. Analyst 132:1161–1168
45. Karlsson BCG, O'Mahony J, Karlsson JG, Bengtsson H, Eriksson LA, Nicholls IA (2009) Structure and dynamics of monomer—template complexation: an Explanation for molecularly imprinted polymer recognition site heterogeneity. J Am Chem Soc 131:13297–13304
46. Miertuš S, Scrocco E, Tomasi J (1981) Electrostatic interaction of a solute with a continuum. A direct utilizaion of ab initio molecular potentials for the prevision of solvent effects. Chem Phys 55:117–129
47. Wu LQ, Zhu KC, Zhao WP, Li YZ (2005) Theoretical and experimental study of nicotinamide molecularly imprinted polymers with different porogens. Anal Chim Acta 549:39–44
48. Liu Y, Wang F, Tan TW, Lei M (2010) Rational design and study on recognition property of paracetamol-imprinted polymer. Appl Biochem Biotechnol 160:328–342
49. Dong WG, Yan M, Liu Z, Wu GS, Li YM (2007) Effects of solvents on the adsorption selectivity of molecularly imprinted polymers: molecular simulation and experimental validation. Sep Purif Technol 53:183–188

50. Wang JC, Guo RB, Chen JP, Zhang Q, Liang XM (2005) Phenylurea herbicides-selective polymer prepared by molecular imprinting using N-(4-isopropylphenyl)-N′-butyleneurea as dummy template. Anal Chim Acta 540:307–315
51. Jacob R, Tate M, Banti Y, Rix C, Mainwaring DE (2008) Synthesis, characterization, and ab Initio theoretical study of a molecularly imprinted polymer selective for biosensor materials. J Phys Chem A 112:322–331
52. Wu LQ, Li YZ (2003) Picolinamide-Cu(Ac)(2)-Imprinted polymer with high potential for recognition of picolinamide-copper acetate complex. Anal Chim Acta 482:175–181
53. Wu LQ, Li YZ (2004) Metal Ion-mediated molecular-imprinting polymer for indirect recognition of formate, acetate and propionate. Anal Chim Acta 517:145–151
54. Christoforidis KC, Louloudi M, Rutherford AW, Deligiannakis Y (2008) Semiquinone in molecularly imprinted hybrid amino acid-SiO2 biomimetic materials. An experimental and theoretical study. J Phys Chem C 112:12841–12852
55. Che AF, Wan LS, Ling J, Liu ZM, Xu ZK (2009) Recognition mechanism of theophylline-imprinted polymers: two-dimensional infrared analysis and density functional theory study. J Phys Chem B 113:7053–7058
56. Shiigi H, Kijima D, Ikenaga Y, Hori K, Fukazawa S, Nagaoka T (2005) Molecular recognition for bile acids using a molecularly imprinted overoxidized polypyrrole film. J Electrochem Soc 152:H129–H134
57. Mukawa T, Goto T, Nariai H, Aoki Y, Imamura A, Takeuchi T (2003) Novel strategy for molecular imprinting of phenolic compounds utilizing disulfide templates. J Pharm Biomed Anal 30:1943–1947
58. Meng ZH, Yamazaki T, Sode K (2004) A Molecularly imprinted catalyst designed by a computational approach in catalysing a transesterification process. Biosens Bioelectron 20:1068–1075
59. Wu LQ, Li YZ (2004) Study on the recognition of templates and their analogues on molecularly imprinted polymer using computational and conformational analysis approaches. J Mol Recognit 17:567–574
60. Tada M, Sasaki T, Iwasawa Y (2004) Design of a novel molecular-imprinted Rh-amine complex on SiO2 and its shape-selective catalysis for alpha-methylstyrene hydrogenation. J Phys Chem B 108:2918–2930
61. Piletsky SA, Piletska EV, Karim K, Freebairn KW, Legge CH, Turner APF (2002) Polymer cookery: influence of polymerization conditions on the performance of molecularly imprinted polymers. Macromolecules 35:7499–7504
62. Piletsky SA, Guerreiro A, Piletska EV, Chianella I, Karim K, Turner APF (2004) Polymer cookery. 2. Influence of polymerization pressure and polymer swelling on the performance of molecularly imprinted polymers. Macromolecules 37:5018–5022
63. Piletsky SA, Mijangos I, Guerreiro A, Piletska EV, Chianella I, Karim K, Turner APF (2005) Polymer cookery: influence of polymerization time and different initiation conditions on performance of molecularly imprinted polymers. Macromolecules 38:1410–1414
64. Leach AR (2001) Molecular dynamics simulation methods. In: Molecular modelling: principles and applications. Prentice Hall, Harlow, pp 353–409
65. Alder BJ, Wainwright TE (1957) Phase transition for a hard sphere system. J Chem Phys 27:1208–1209
66. Wang J, Cieplak P, Kollman PA (2000) How well does a restrained electrostatic potential (RESP) model perform in calculating conformational energies of organic and Biological molecules? J Comput Chem 21:1049–1074
67. Wang J, Wolf RM, Caldwell JW, Kollman PA, Case DA (2004) Development and testing of a general amber force field. J Comput Chem 25:1157–1174
68. Brooks BR, Bruccoleri RE, Olafson BD, States DJ, Swaminathan S, Karplus M (1983) CHARMM: a program for macromolecular energy, minimization, and dynamics calculations. J Comput Chem 4:187–217

69. Jorgensen WL, Maxwell DS, Tirado-Rives J (1996) Development and testing of the OPLS All-Atom Force Field on conformational energetics and properties of organic liquids. J Am Chem Soc 118:11225–11236
70. Berendsen HJC, van der Spoel D, van Drunen R (1995) GROMACS: a message-passing parallel molecular dynamics implementation. Comp Phys Commun 91:43–56
71. Scott WRP, Hunenberger PH, Tironi IG, Mark AE, Billeter SR, Fennen J, Torda AE, Huber T, Kruger P, van Gunsteren WF (1999) The GROMOS biomolecular simulation program package. J Phys Chem A 103:3596–3607
72. Duan Y, Kollman PA (1998) Pathways to a protein folding intermediate observed in a 1-microsecond simulation in aqueous solution. Science 282:740
73. Pervushin K, Riek R, Wider G, Wüthrich K (1997) Attenuated T2 Relaxation by mutual cancellation of dipole–dipole coupling and chemical shift anisotropy indicates an avenue to NMR structures of very large biological macromolecules in solution. Proc Natl Acad Sci USA 94:12366–12371
74. Cheatham TE (III), Kollman PA (1996) Observation of the A-DNA to B-DNA transition during unrestrained molecular dynamics in aqueous solution. J Mol Biol *259*:434–444
75. Cheatham TE (III), Miller JL, Fox T, Darden TA, Kollman PA (1995) Molecular dynamics simulations on solvated biomolecular systems: the particle mesh ewald method leads to Stable trajectories of DNA, RNA, and proteins. J Am Chem Soc 117:4193–4194
76. Berger O, Edholm O, Jahnig F (1997) Molecular dynamics simulations of a fluid bilayer of dipalmitoylphosphatidylcholine at full hydration, constant pressure, and constant temperature. Biophys J 72:2002–2013
77. Van der Ploeg P, Berendsen HJC (1982) Molecular dynamics simulation of a bilayer membrane. J Chem Phys 76:3271–3276
78. De Groot BL, Grubmuller H (2001) Water permeation across biological membranes: mechanism and dynamics of aquaporin-1 and GlpF. Science 294:2353–2357
79. Van Buuren AR, Marrink SJ, Berendsen HJC (1993) A molecular dynamics study of the Decane/water interface. J Phys Chem 97:9206–9212
80. Hsu QC, Wu CD, Fang TH (2005) Studies on nanoimprint process parameters of copper by molecular dynamics analysis. Comput Mat Sci 34:314–322
81. Garrison BJ, Delcorte A, Krantzman KD (2000) Molecule liftoff from surfaces. Acc Chem Res 33:69–77
82. Masukawa KM, Kollman PA, Kuntz ID (2003) Investigation of neuraminidase-substrate recognition using molecular dynamics and free energy calculations. J Med Chem 46: 5628–5637
83. Yang H, Elcock AH (2003) Association lifetimes of hydrophobic amino acid pairs measured directly from molecular dynamics simulations. J Am Chem Soc 125:13968–13969
84. Li X, Eriksson L (2005) Molecular dynamics study of lignin constituents in water. Holzforschung 59:253–262
85. Mayes AG, Whitcombe MJ (2005) Synthetic strategies for the generation of molecularly imprinted organic polymers. Adv Drug Del Rev 57:1742–1778
86. Karim K, Breton F, Rouillon R, Piletska EV, Guerreiro A, Chianella I, Piletsky SA (2005) How to find effective functional monomers for effective molecularly imprinted polymers? Adv Drug Del Rev 57:1795–1808
87. Wei S, Jakusch M, Mizaikoff B (2006) Capturing molecules with templated materials—analysis and rational design of molecularly imprinted polymers. Anal Chim Acta 578:50–58
88. Piletsky SA, Karim K, Piletska EV, Day CJ, Freebairn KW, Legge CH (2001) Recognition of ephedrine enantiomers by molecularly imprinted polymers designed using a computational approach. Analyst 126:1826–1830
89. Piletska EV, Turner NW, Turner APF, Piletsky SA (2005) Controlled release of the herbicide Simazine from computationally designed molecularly imprinted polymers. J Controlled Release 108:132–139

90. Piletska EV, Romero-Guerra M, Guerreiro AR, Karim K, Turner APF, Piletsky SA (2005) Adaptation of the molecular imprinted polymers towards polar environment. Anal Chim Acta 542:47–51
91. Piletska EV, Romero-Guerra M, Chianella I, Karim K, Turner AR, Piletsky SA (2005) Towards the development of multisensor for drugs of abuse based on molecular imprinted polymers. Anal Chim Acta 542:111–117
92. Subrahmanyam S, Piletsky SA, Piletska EV, Chen B, Karim K, Turner APF (2001) "Bite-and-Switch" approach using computationally designed molecularly imprinted polymers for sensing of creatinine. Biosens Bioelectron 16:631–637
93. Piletska EV, Piletsky SA, Karim K, Terpetschnig E, Turner APF (2004) Biotin-specific synthetic receptors prepared using molecular imprinting. Anal Chim Acta 504:179–183
94. Chianella I, Lotierzo M, Piletsky SA, Tothill IE, Chen B, Karim K, Turner APF (2002) Rational design of a polymer specific for Microcystin-LR using a computational approach. Anal Chem 74:1288–1293
95. Chianella I, Piletsky SA, Tothill IE, Chen B, Turner APF (2003) MIP-based solid phase extraction cartridges combined with MIP-based sensors for the detection of Microcystin-LR. Biosens Bioelectron 18:119–127
96. Wei S, Jakusch M, Mizaikoff B (2007) Investigating the mechanisms of 17β-estradiol imprinting by computational prediction and spectroscopic analysis. Anal Bioanal Chem 389:423–431
97. Pavel D, Lagowski J (2005) Computationally designed monomers and polymers for molecular imprinting of theophylline and its derivatives—Part I. Polymer 46:7528–7542
98. Pavel D, Lagowski J (2005) Computationally designed monomers and polymers for molecular Imprinting of theophylline—Part II. Polymer 46:7543–7556
99. Pavel D, Lagowski J, Lepage CJ (2006) Computationally designed monomers for molecular imprinting of chemical warfare agents—Part V. Polymer 47:8389–8399
100. Molinelli A, O'Mahony J, Nolan K, Smyth MR, Jakusch M, Mizaikoff B (2005) Analyzing the mechanisms of selectivity in biomimetic self-assemblies via IR and NMR spectroscopy of prepolymerization solutions and molecular dynamics simulations. Anal Chem 77:5196–5204
101. Monti S, Cappelli C, Bronco S, Giusti P, Ciardelli G (2006) Towards the design of highly selective recognition sites into molecular imprinting polymers: a computational approach. Biosens Bioelectron 22:153–163
102. Lv Y, Lin Z, Tan T, Feng W, Qin P, Li C (2008) Application of molecular dynamics modeling for the prediction of selective adsorption properties of dimethoate imprinting polymer. Sens Actuators, B 133:15–23
103. Yoshida M, Hatate Y, Uezu K, Goto M, Furusaki S (2000) Chiral-recognition polymer prepared by surface molecular imprinting technique. Colloids Surf A 169:259–269
104. Toorisaka E, Uezu K, Goto M, Furusaki S (2003) A molecularly imprinted polymer that shows enzymatic activity. Biochem Eng J 14:85–91
105. Liu R, Li X, Li Y, Jin P, Qin W, Qi J (2009) Effective removal of rhodamine B from contaminated water using non-covalent imprinted microspheres designed by computational approach. Biosens Bioelectron 25:629–634
106. Li Y, Li X, Li Y, Dong C, Jin P, Qi J (2009) Selective recognition of veterinary drugs residues by artificial antibodies designed using a computational approach. Biomaterials 30:3205–3211
107. Svenson J, Karlsson JG, Nicholls IA (2004) 1H nuclear magnetic resonance study of the molecular imprinting of (-)-nicotine: template self-association, a molecular basis for cooperative ligand binding. J Chromatogr A 1024:39–44
108. Andersson HS, Karlsson JG, Piletsky SA, Koch-Schmidt A-C, Mosbach K, Nicholls IA (1999) Study of the nature of recognition in molecularly imprinted polymers, II: influence of monomer-template ratio and sample load on retention and selectivity. J Chromatogr A 848 (1):39–49
109. Katz A, Davis ME (1999) Investigations into the mechanisms of molecular recognition with imprinted polymers. Macromolecules 32:4113–4121

110. Olsson GD, Karlsson BCG, Shoravi S, Wiklander JG, Nicholls IA (2012) Mechanisms underlying molecularly imprinted polymer molecular memory and the role of crosslinker: resolving debate on the nature of template recognition in phenylalanine anilide imprinted polymers. J Mol Recognit 25:69–73
111. Ansell RJ, Kuah KL (2005) Imprinted polymers for chiral resolution of (±)-ephedrine: understanding the pre-polymerisation equilibrium and the action of different mobile phase modifiers. Analyst 130:179–187
112. Ansell RJ, Wang D, Kuah JKL (2008) Imprinted polymers for chiral resolution of (±)-ephedrine. Part 2: probing pre-polymerisation equilibria in different solvents by NMR. Analyst 133:1673–1683
113. Ansell RJ, Wang DY (2009) Imprinted polymers for chiral resolution of (±)-ephedrine. Part 3: NMR predictions and HPLC results with alternative functional monomers. Analyst 134:564–576
114. O'Mahony J, Wei S, Molinelli A, Mizaikoff B (2006) Imprinted polymeric materials. Insight into the nature of prepolymerization complexes of quercetin imprinted polymers. Anal Chem 78:6187–6190
115. O'Mahony J, Moloney M, McCormack M, Nicholls IA, Mizaikoff B, Danaher M (2013) Design and implementation of an imprinted material for the exaction of the endocrine disruptor Bisphenol A from milk. J Chromatogr B 931:164–169
116. Golker K, Karlsson BCG, Olsson GD, Rosengren AM, Nicholls IA (2013) Influence of composition and morphology on template recognition in molecularly imprinted polymers. Macromolecules 46:1408–1414
117. Golker K, Karlsson BCG, Rosengren AM, Nicholls IA (2014) A functional monomer is not enough: principal component analysis of the influence of template complexation in pre-polymerization mixtures on imprinted polymer recognition and morphology. Int J Mol Sci 15:20572–20584
118. Shoravi S, Olsson GD, Karlsson BCG, Nicholls IA (2014) On the Influence of crosslinker on template complexation in molecularly imprinted polymers: a computational study of prepolymerization mixture events with correlations to template-polymer recognition behavior and NMR spectroscopic studies. Int J Mol Sci 15:10622–10634
119. Cleland D, Olsson GD, Karlsson BCG, Nicholls IA, McCluskey A (2014) Molecular dynamics approaches to the design and synthesis of PCB targeting molecularly imprinted polymers: interference to monomer-template interactions in imprinting of 1,2,3-trichlorobenzene. Org Biomol Chem 12:844–853
120. Srebnik S, Lev O, Avnir D (2001) Pore size distribution induced by microphase separation: effect of the leaving group during polycondensation. Chem Mater 13:811–816
121. Srebnik S, Lev O (2002) Toward establishing criteria for polymer imprinting using mean-field theory. J Chem Phys 116:10967–10972
122. Srebnik S (2004) Theoretical investigation of the imprinting efficiency of molecularly imprinted polymers. Chem Mater 16:883–888
123. Yungerman I, Srebnik S (2006) Factors contributing to binding-site imperfections in imprinted polymers. Chem Mater 18:657–663
124. Zhao Z-J, Wang Q, Zhang L, Wu T (2008) Structured water and water-polymer interactions in hydrogels of molecularly imprinted polymers. J Phys Chem B 112:7515–7521
125. Luo D, Zhao Z, Zhang L, Wang Q, Wang J (2014) On the structure of molecularly imprinted polymers by modifying charge on functional groups through molecular dynamics simulations. Mol Simul 40:431–438
126. Azenha M, Szefczyk B, Loureiro D, Kathirvel P, DS Cordeiro MN, Fernando-Silva A (2013) Computational and experimental study of the effect of PEG in the preparation of damascenone-imprinted xerogels. Langmuir 29:2024–2032
127. Esbensen KH (ed) (2002) Multivariate data analysis in practice, 5th edn. Camo Process AS, Oslo
128. Carlsson R (1992) Design and optimization in organic synthesis. Elsevier, Amsterdam

129. Eriksson L, Johansson E, Kettaneh-Wold N, Wold S (2001) Multi- and megavariate data analysis. Principles and application. Umetrics Academy, Umeå
130. Navarro-Villoslada F, Vicente BS, Moreno-Bondi MC (2004) Application of multivariate Analysis to the screening of molecularly imprinted polymers for bisphenol A. Anal Chim Acta 504:149–162
131. Navarro-Villoslada F, Takeuchi T (2005) Multivariate Analysis and Experimental Design in the Screening of Combinatorial Libraries of Molecular Imprinted Polymers. Bull Chem Soc Jpn 78:1354–1361
132. Tarley CRT, Segatelli MG, Kubota LT (2006) Amperometric determination of chloroguaiacol at submicromolar levels after on-line preconcentration with molecularly imprinted polymers. Talanta 69:259–266
133. Santos W.de JR, Lima PR, Tarley CRT, Kubota LT (2007) A Catalytically active molecularly imprinted polymer that mimics peroxidase based on hemin: application to the determination of p-aminophenol. Anal Bioanal Chem 389:1919–1929
134. Koohpaei AR, Shahtaheri SJ, Ganjali MR, Forushani AR, Golbabaei F (2008) Molecular imprinted solid phase extraction for determination of atrazine in environmental samples. Iran. J. Environ. Health. Sci. Eng. 5:283–296
135. Tarley CRT, Kubota LT (2005) Molecularly-imprinted solid phase extraction of catechol from aqueous effluents for its selective determination by differential pulse voltammetry. Anal Chim Acta 548:11–19
136. Davies MP, De Biasi V, Perrett D (2004) Approaches to the rational design of molecularly imprinted polymers. Anal Chim Acta 504:7–14
137. Kempe H, Kempe M (2004) Novel method for the synthesis of molecularly imprinted polymer bead libraries. Macromol Rapid Commun 25:315–320
138. Ceolin G, Navarro-Villoslada F, Moreno-Bondi MC, Horvai G, Horvath V (2009) Accelerated development procedure for molecularly imprinted polymers using membrane filterplates. J Comb Chem 11:645–652
139. Santos W de JR, Lima PR, Tarley CRT, Höehr NF, Kubota LT (2009) Synthesis and application of a peroxidase-like molecularly imprinted polymer based on hemin for selective determination of serotonin in blood serum. Anal Chim Acta 631:170–176
140. Koohpaei AR, Shahtaheri SJ, Ganjali MR, Forushani AR, Golbabaei F (2009) Optimization of solid-phase extraction using developed modern sorbent for trace determination of ametryn in environmental matrices. J Hazard Mater 170:1247–1255
141. Valero-Navarro A, Damiani PC, Fernández-Sánchez JF, Segura-Carretero A, Fernández-Gutiérrez A (2009) Chemometric-assisted MIP-optosensing system for the simultaneous determination of monoamine naphthalenes in drinking waters. Talanta 78:57–65
142. Alizadeh T, Ganjali MR, Nourozi P, Zare M (2009) Multivariate optimization of molecularly imprinted polymer solid-phase extraction applied to parathion determination in different water samples. Anal Chim Acta 638:154–161
143. Rossi C, Haupt K (2007) Application of the Doehlert experimental design to molecularly imprinted polymers: surface response optimization of specific template recognition as a function of the type and degree of cross-linking. Anal Bioanal Chem 389:455–460
144. Baggiani C, Anfossi L, Giovannoli C, Tozzi C (2004) Multivariate analysis of the selectivity for a pentachlorophenol-imprinted polymer. J Chromatogr B 804:31–41
145. Rosengren AM, Karlsson JG, Andersson PO, Nicholls IA (2005) Chemometric models of template-molecularly imprinted polymer binding. Anal Chem 77:5700–5705
146. Nantasenamat C, Naenna T, Isarankura-Na-Ayudhya C, Prachayasittikul V (2005) Quantitative prediction of imprinting factor of molecularly imprinted polymers by artificial neural network. J Comput-Aided Mol Des 19:509–524
147. Rosengren AM, Golker K, Karlsson JG, Nicholls IA (2009) Dielectric constants are not enough: principal component analysis of the influence of solvent properties on molecularly imprinted polymer-ligand rebinding. Biosens Bioelectron 25:553–557

148. Mijangos I, Navarro-Villoslada F, Guerreiro AR, Piletska EV, Chianella I, Karim K, Turner APF, Piletsky SA (2006) Influence of initiator and different polymerisation conditions on performance of molecularly imprinted polymers. Biosens Bioelectron 22:381–387
149. Koohpaei AR, Shahtaheri SJ, Ganjali MR, Forushani AR, Golbabaei F (2008) Application of multivariate analysis to the screening of molecularly imprinted polymers (MIPs) for ametryn. Talanta 75:978–986
150. Wythoff BJ (1993) Backpropagation neural networks—a tutorial. Chemom Intell Lab Syst 18:115–155
151. Nantasenamat C, Isarankura-Na-Ayudhya C, Naenna T, Prachayasittikul V (2007) Quantitative Structure-imprinting factor relationship of molecularly imprinted polymers. Biosens Bioelectron 22:3309–3317
152. Breneman CM, Thompson TR, Rhem M, Dung M (1995) Electron density modeling of large systems using the transferable atom equivalent method. Comput Chem 19:161–179

Adv Biochem Eng Biotechnol (2015) 150: 51–93
DOI 10.1007/10_2015_316

Published Online: 22 March 2015

Characterization of the Binding Properties of Molecularly Imprinted Polymers

Richard J. Ansell

Abstract The defining characteristic of the binding sites of any particular molecularly imprinted material is heterogeneity: that is, they are not all identical. Nonetheless, it is useful to study their fundamental binding properties, and to obtain average properties. In particular, it has been instructive to compare the binding properties of imprinted and non-imprinted materials. This chapter begins by considering the origins of this site heterogeneity. Next, the properties of interest of imprinted binding sites are described in brief: affinity, selectivity, and kinetics. The binding/adsorption isotherm, the graph of concentration of analyte bound to a MIP versus concentration of free analyte at equilibrium, over a range of total concentrations, is described in some detail. Following this, the techniques for studying the imprinted sites are described (batch-binding assays, radioligand binding assays, zonal chromatography, frontal chromatography, calorimetry, and others). Thereafter, the parameters that influence affinity, selectivity and kinetics are discussed (solvent, modifiers of organic solvents, pH of aqueous solvents, temperature). Finally, mathematical attempts to fit the adsorption isotherms for imprinted materials, so as to obtain information about the range of binding affinities characterizing the imprinted sites, are summarized.

Keywords Batch binding · Binding isotherms · Binding site heterogeneity · Chromatographic analysis · Selectivity

Contents

R.J. Ansell (✉)
School of Chemistry, University of Leeds, Leeds LS2 9JT, UK
e-mail: R.J.Ansell@leeds.ac.uk

1 Properties of Molecularly Imprinted Binding Sites

The defining characteristic of molecularly imprinted binding sites is heterogeneity: that is, they are not all identical (in the manner of monoclonal antibodies, or synthetic receptors such as crown ethers), but differ in the exact spatial arrangement of functional groups, the access to the site, the polarity of the immediate environment, etc. Thus, they are more analogous to polyclonal antibodies, where different sequences give different structures at the antigen binding sites. In the case of non-covalently imprinted materials, much of this heterogeneity arises from the fact that the monomer-template interactions are governed by equilibria such that a range of monomer-template complexes, along with free, uncomplexed monomers, are present in the pre-polymerization mixture (Fig. 1a), and this diversity is preserved in the macromolecular material after polymerization (Fig. 1b). Processing of the material (e.g., by grinding and sieving), removal of the template, and exchange of the polymerization solvent with a different solvent to study the binding properties, can all lead to further heterogeneity by damaging binding sites, sites collapsing on template removal, and locally variable swelling/collapse of the polymer in a different solvent (Fig. 1c).

The binding site heterogeneity is usually acknowledged, at least insofar as authors discuss “specific” and “non-specific” binding to imprinted materials. At the simplest level, we might consider sites arising from any form of monomer-template complex in the pre-polymerization mixture (i–vi in Fig. 1) to be “specific”: these are expected to have a higher affinity for the template (and similar structures), and to be more selective in not binding dissimilar ones (due to “the precise arrangement of the functional groups” and “shape selectivity”). Sites arising from free, non-complexed monomer in the pre-polymerization mixture (vii and viii in Fig. 1) are proposed to give “non-specific” sites: these are expected to have lower affinity for the template and to bind other species indiscriminately, just as a polymer with randomly arranged functional monomer (e.g., a non-imprinted polymer, prepared in the absence of template) would be expected to behave. However, while this

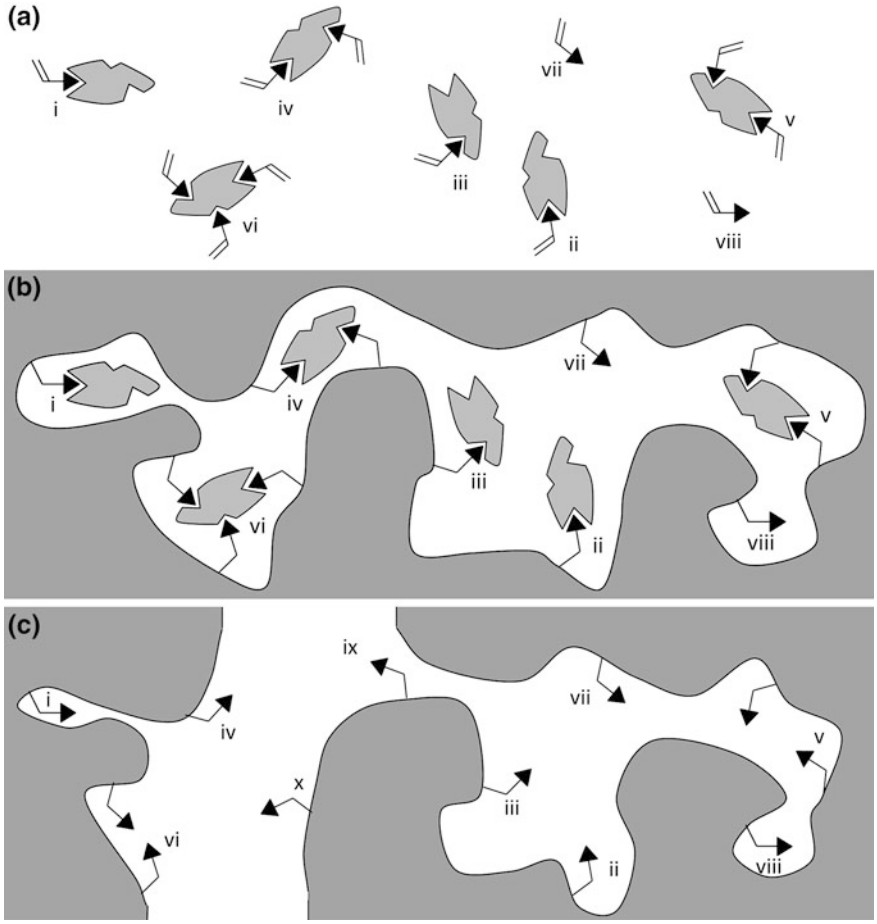

Fig. 1 Two-dimensional cartoon representation of the origins of heterogeneity in molecularly imprinted binding sites. **a** The species present in the pre-polymerization equilibria. *Gray shape* represents the template, *black triangles* represent monomer. Cross-linker not shown, for clarity. The template has three distinct sites to interact with monomer and a 2:1 ratio of monomer:template is shown. *i* and *ii* are 1:1 complexes, *iii* is a 1:1 complex but with a different form of monomer-template interaction, *iv* and *v* are 2:1 complexes, *vi* is a 3:1 complex, *vii* and *viii* are free uncomplexed monomer. **b** The structure post-polymerization. Previously equivalent structures *i* and *ii* have yielded different binding sites due to different outer-sphere interactions, i.e., different polymer backbone conformation, and different site accessibility. Likewise, *iv* and *v*, and *vii* and *viii*. **c** The structure after polymer processing, template removal, and solvent exchange. Site *i* has collapsed after template removal. Sites *iv* and *vi* have been damaged by polymer fracturing (and generated two new weak and non-selective sites: *ix* and *x*). All sites have been modified by the swelling of the polymer

simplistic dichotomy between "specific sites" and "non-specific sites" (or "imprinted sites" and "non-imprinted sites") can be useful, it certainly does not capture the full picture, which is of a continuous spectrum of sites from weaker binding, less selective, to stronger binding, more selective.

The diversity of species in the pre-polymerization mixture will be even greater than suggested in Fig. 1a if there is more than one type of monomer present, or if the monomer or the template are capable of interactions with the cross-linker, or if "clusters" of template are present [1–4]. The thesis that the pre-polymerization species (Fig. 1a) are precisely replicated in the polymerized material (Fig. 1b) is probably naïve, several studies having suggested that these structures change during the course of polymerization [5]; however, the broader principle that diversity is preserved or enhanced is certainly valid (e.g., due to the polymeric chains being folded in different ways around different sites, "outer sphere" interactions for each site will be different).

Although the model in Fig. 1 particularly illustrates the case for non-covalent imprinting of organic monomers, which polymerize into cross-linked chains, the principle is applicable to all forms of imprinting:

- *Stoichiometric non-covalent/covalent/semi-covalent/metal-mediated imprinting*. Although these strategies all involve entirely (or almost entirely) 1:1 complexes of monomer and template, such that there are (in theory) no free monomers, nor any 2:1 or higher complexes, diversity will still be generated due to the different "outer-sphere" interactions in the polymerized material, different site accessibility, plus changes due to site damage in polymer processing, site collapse, and swelling/collapse of the polymer after solvent exchange.
- *Sol–gel imprinting*. The monomeric species may form more than one covalent bond with the cross-linker, the cross-linker may be multivalent, and the polymerization ionic rather than free-radical, but the principles of Fig. 1 remain. The cross-linked gel is an amorphous material, even if it is inorganic, without crystalline form, so the structure is just as heterogeneous.
- *Surface imprinting*. The 2-dimensional nature of Fig. 1 demonstrates clearly how the same principles will apply in imprinting in 2-dimensions on a surface. When the monomer-template interaction is non-covalent, a range of monomer-template complexes will be present initially. If the imprinting is done on a homogeneous surface and the monomers form a monolayer, then the difference in "outer-sphere" environments of the binding sites will certainly be limited. However, even with stoichiometric monomer-template interactions and a monolayer approach, there will still be differences in the exact orientation of functional groups on the surface and defects in the structure.
- *Pre-polymer imprinting*. Polymer chains can be "fixed" in the presence of a template by phase-inversion precipitation [6] or solvent evaporation [7]; the chains are cross-linked physically, but not chemically. These approaches are closely related to "bioimprinting" in proteins whose structure is "frozen" by lyophilization or chemical cross-linking in the presence of a template [8]. A range of structures will be present initially as the template interacts with the linear polymer, and the heterogeneity of folded structures formed during precipitation will be no less than when the polymer chains cross-link covalently.

A great deal of effort has been invested in reducing the heterogeneity of the pre-polymerization mixture for non-covalent imprinting as represented in Fig. 1a, by

studying the monomer-template equilibria to optimize the monomer-template ratio [9], by choosing/creating new monomers such that the monomer-template interaction is as strong as possible [10–15], and at the simplest level by choosing a solvent in which the interactions are strongest. However, diversity in the binding sites cannot be avoided, for the same reasons that it is present even in covalent imprinting.

For some applications, some binding site diversity (for example, a range of different binding site affinities) may be useful [16]; however, in most applications it is considered a hindrance (e.g., in zonal chromatography, where it leads to the tailing of chromatographic peaks and consequently poor column efficiency and resolution), and it is perceived by the wider scientific community as a limitation. Certainly, in order to design imprinted materials for specific applications, it is essential to have an understanding of the binding site heterogeneity and how it arises.

When characterizing the binding properties, there are three properties of particular interest:

- *Binding site affinity*. The binding/unbinding of analyte to/from the imprinted binding sites can be represented as an equilibrium:

$$\text{free analyte} + \text{binding site} \overset{K_a}{\leftrightarrow} \text{bound analyte} \tag{1}$$

where K_a is the association constant (in mol^{-1} L), and if all sites are identical, then K_a might be expressed as

$$K_a = \frac{n_{\text{bound}}}{n_{\text{empty}} \times F} = \frac{1}{K_d} \tag{2}$$

where K_d is the dissociation constant (in mol L^{-1}), n_{bound} is the mols of bound analyte, F is the concentration of free analyte in solution (in mol L^{-1}) and n_{empty} is the mols of empty binding sites. Unfortunately, because the binding sites are not equivalent (as outlined above), each site (in the same material) will have a different K_a. The quotient ($n_{\text{bound}}/(n_{\text{empty}} \times F)$) will change even as the total amount of analyte changes. Moreover, the number of empty binding sites is not a parameter that can be readily measured, hence the calculation of association constants for a MIP polymer is not straightforward (see Sects. 2 and 5). Instead, the binding under a specified set of conditions is usually expressed simply as n_{bound}, or as % bound ($n_{\text{bound}}/n_{\text{analyte}} \times 100$ %, where n_{analyte} is the total mols of analyte present in the experiment), or as a distribution ratio D (in L g^{-1})

$$D = \frac{B}{F} = \frac{n_{\text{bound}}/M_{\text{MIP}}}{n_{\text{free}}/V} \tag{3}$$

where B is the concentration of bound analyte (in mol g^{-1}), M_{MIP} is the mass of MIP polymer (in g), V is the volume of solution in which the material is incubated and n_{free} is the amount of free analyte in solution (in mol) such that

$$n_{analyte} = n_{bound} + n_{free} \tag{4}$$

- *Binding site selectivity*. The presence of "imprinted sites" is usually verified by comparing an imprinted polymer with one made under the same conditions but in the absence of template (the non-imprinted polymer, NIP). One commonly calculated parameter is the *imprinting factor,* IF, best defined as the ratio of the distribution ratio for a particular analyte, under a particular set of conditions, on the imprinted polymer, to the distribution ratio for the same analyte, under identical conditions, on the NIP:

$$\text{IF} = \frac{D_{MIP}}{D_{NIP}} = \frac{B_{MIP}/F_{MIP}}{B_{NIP}/F_{NIP}} = \frac{n_{bound,MIP}/n_{free,MIP}}{n_{bound,NIP}/n_{free,NIP}} \tag{5}$$

where the volume V is the same for the MIP as for the NIP, and M_{MIP} is the same as M_{NIP}. The IF should have a value greater than 1; the higher the value, the greater the difference between the imprinted and non-imprinted case. It is important to bear in mind, however, that the NIP may bind less analyte than the MIP because monomer self-association occurs to a higher extent in the NIP and reduces the number of free functional groups. Moreover, Baggiani et al. [17] have suggested that when optimizing MIP composition, the MIP with the highest affinity and selectivity towards its template usually corresponds to a NIP that binds the template strongly too. Hence, a high IF may not be the best indicator of a useful MIP: comparing the binding of the template-analyte to a MIP with the binding of the template-analyte to a polymer imprinted with a different template may be a better measure of successful imprinting. Further, a high IF does not prove that the "imprinted sites" are selective. In order to demonstrate this, the rebinding of the template (or the target analyte, if different) to the MIP must be compared with the binding of a competitor, again under identical conditions:

$$\alpha_{competitor1} = \frac{D_{analyte,MIP}}{D_{competitor1,MIP}} = \frac{B_{analyte,MIP}/F_{analyte,MIP}}{B_{competitor1,MIP}/F_{competitor1,MIP}} \tag{6}$$

The *selectivity factor*, α, should have a value greater than 1, and high values of α for a range of competitors provide evidence of selectivity.

- *Binding/unbinding kinetics*. The binding/rebinding process can be represented as

$$\text{free analyte} + \text{binding site} \xrightarrow{k_1} \text{bound analyte} \tag{7}$$

where the rate constant k_1 (in mol^{-1} L s^{-1}) is such that

$$\frac{\mathrm{d}n_{\text{bound}}}{\mathrm{d}t} = k_1 \times n_{\text{empty}} \times F \tag{8}$$

The unbinding process is represented as

$$\text{bound analyte} \xrightarrow{k_{-1}} \text{free analyte} + \text{binding site} \tag{9}$$

where the rate constant k_{-1} (in s^{-1}) is such that

$$\frac{\mathrm{d}n_{\text{empty}}}{\mathrm{d}t} = -\frac{\mathrm{d}n_{\text{bound}}}{\mathrm{d}t} = k_{-1} \times n_{\text{bound}} \tag{10}$$

from which it follows that, under conditions of dynamic equilibrium

$$k_{-1} \times n_{\text{bound}} = k_1 \times n_{\text{empty}} \times F \tag{11}$$

and so

$$\frac{n_{\text{bound}}}{n_{\text{empty}} \times F} = \frac{k_1}{k_{-1}} = K_{\text{a}} = \frac{1}{K_{\text{d}}} \tag{12}$$

Unfortunately, just as every different site on the imprinted material has a different association constant K_{a}, so it will also have different on (k_1) and off (k_{-1}) rate constants. Nonetheless, under a specific set of conditions it is possible to measure *effective* constants, K_{a}', k_1' and k_{-1}'. The rate constants for binding and unbinding on a MIP may be considered to be governed by mass transfer—that is, the transfer between the solution phase and the solid phase. This can be quite slow, because of the need for analyte to diffuse through the (albeit usually porous) solid material. Kinetics are usually faster for surface-imprinted and thin-film-imprinted materials than for monolithic materials, or particles where the binding sites are in the interior.

2 The Binding/Adsorption Isotherm

2.1 Collecting Experimental Data

Although the binding of analyte is frequently reported as n_{bound}, % bound or D under a single set of conditions, this is a poor way to characterize MIP binding. Each of these values will vary, even for the same combination of polymer, analyte and solvent, if n_{analyte}, V or M_{MIP} are changed. This will effect both the binding to MIP and to a control polymer, and binding of competitors, such that IF and α will also change with n_{analyte}, V and M_{MIP} [18, 19]. Moreover, comparison between

different MIPs is extremely difficult if binding is only recorded under a single set of conditions. Both Allender et al. [20] and Horvai et al. [18, 19] have blamed the common use of single-point characterization for the confusion of many researchers from other fields when approaching the molecular imprinting literature.

According to both of these groups (and the current author), a far more useful way to characterize analyte binding is to measure/calculate values of the bound concentration B and free concentration F for a fixed amount of polymer and range of concentrations of added analyte: the graph of B versus F yields a *binding isotherm* as illustrated in Fig. 2. This can be achieved in various ways, the simplest being to vary n_{analyte} while V and M_{MIP} are kept constant; then, once equilibrium is achieved, measure F and calculate B. This method is commonly referred to as a *batch-binding* or *batch-rebinding* assay—it and other methods to derive the isotherm are discussed in Sect. 3. Using $B = n_{\text{bound}}/M_{\text{MIP}}$ and Eq. 4, B can be calculated from n_{analyte} and F:

$$B = \frac{n_{\text{analyte}} - n_{\text{free}}}{M_{\text{MIP}}} = \frac{n_{\text{analyte}}}{M_{\text{MIP}}} - \frac{V}{M_{\text{MIP}}} \times F \tag{13}$$

The data points may be connected by curves as shown in Fig. 2, either empirically or based on a particular model of the type of binding sites present, as discussed in Sect. 2.2. "Isotherm" refers to the temperature being kept constant: binding will change with temperature, so it is important that all measurements are made at a constant temperature (and that the temperature is reported), just as it is important that the solution conditions (solvent, buffer, pH, etc.) are also the same for all points on the experimental isotherm.

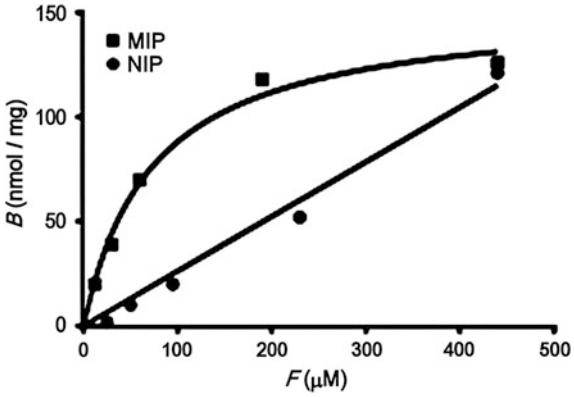

Fig. 2 A typical standard equilibrium bound (nmol/mg)/free (μM) isotherm for a molecularly imprinted polymer (*MIP*) and a control non-imprinted polymer (*NIP*). In this example, the data describe binding isotherms for a propranolol-imprinted poly(ethyleneglycoldimethacrylate-co-methacrylic acid) MIP and its corresponding NIP. Polymers were prepared by precipitation polymerization [21]. Figure reproduced with permission from [20]

The experimental isotherm should ideally be derived from as many measurements, covering as wide a range of $n_{analyte}$ as possible. The isotherm for a MIP is not expected to be linear; rather, it usually flattens off at high F, as in Fig. 2. This indicates saturation: all of the binding sites on the MIP are occupied so that B can increase no further, even if more analyte is added to the solution. The curvature of the binding isotherm can only be properly visualized if a wide enough range of concentration is studied.

Commonly, binding to a NIP (made under identical conditions and with identical constitution to the MIP except for the absence of the template molecule) is used as an indicator of non-specific binding (although this model is slightly naïve, as discussed in Sect. 1). The NIP is considered to possess functional groups randomly arranged on its surface, and these interact with the analyte and cause it to bind to some extent, although (hopefully) more weakly than it does to the MIP. The difference in binding to the MIP and the NIP is attributed to specific binding, i.e., the additional binding that occurs due to the presence of selective imprinted sites. For applications where selectivity for the analyte is important, efforts are usually made to maximize the specific binding, i.e., the difference between the MIP and the non-imprinted control.

For consistency and ease of comparison, it is important that the isotherm is indeed expressed as a plot of B versus F. Other representations (e.g., with % bound or n_{bound} on the y-axis, and/or with the total concentration of analyte $n_{analyte}/V$, or just n_{total} on the x-axis) are less useful for direct comparison, and unhelpful if parameters such as M_{MIP} or V are not given. Whereas F may indeed be similar to the total concentration of analyte when the % bound is very small (because binding is extremely weak and/or because M_{MIP} is small compared to the amount of analyte), these quantities will be different when % bound increases, and the visualization of B versus F is far more useful than B versus total concentration, as we shall see below.

One benefit of expressing the isotherm as B versus F and fitting data to an empirical curve is that we can draw, on the same graph, a straight line to represent the range of possible values for B and F, given particular values of $n_{analyte}$, V and M_{MIP} [20]. This "line of ligand conservation" is simply Eq. 13, and its y-intercept is the limiting value of B if all the analyte binds while its x-intercept is the limiting value of F if none of the analyte binds.

For example, Fig. 3 combines the isotherm with two straight lines representing different combinations of $n_{analyte}$, V and M_{MIP}. Where the straight line intersects, the empirical isotherm gives the expected values of B and F under these conditions. Under the theoretical conditions of Experiment 1, the MIP is expected to give $B \sim 92$ nmol mg^{-1} and $F \sim 110$ μmol dm^{-3} and the NIP $B \sim 52$ nmol g^{-1} and $F \sim 195$ μmol dm^{-3}. These values correspond to D for the MIP ~ 0.84 mL mg^{-1} and for the NIP ~ 0.27 mL mg^{-1}, giving an IF of ~ 3.1.

Under the theoretical conditions of Experiment 2 (in Fig. 3), where $n_{analyte}$ is much higher than in Experiment 1, the MIP is expected to give $B \sim 128$ nmol mg^{-1} and $F \sim 410$ μmol dm^{-3} and the NIP $B \sim 110$ nmol g^{-1} and $F \sim 420$ μmol dm^{-3}. These values correspond to D for the MIP ~ 0.31 mL mg^{-1} and for the NIP ~ 0.26 mL mg^{-1},

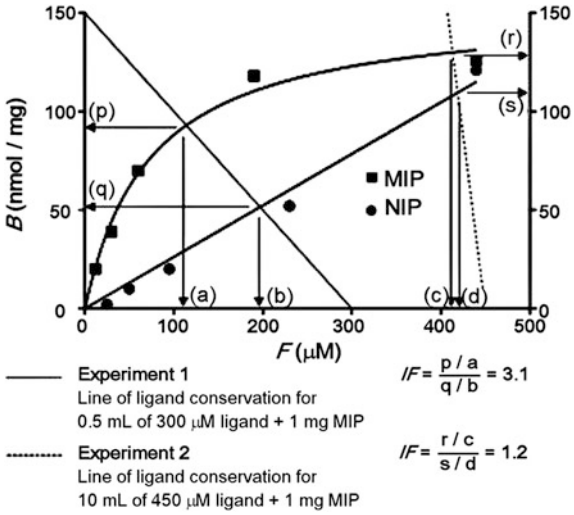

Fig. 3 An example of how distribution ratio (*D*) and imprinting factor (*IF*) are influenced by experimental parameters of ligand concentration, incubation volume, and polymer mass. In *Experiment 1*, 0.5 ml of 300 μM ligand and 1 mg of polymer results in an IF of 3.1, whereas in *Experiment 2*, for 1 mg of the same MIP and NIP, a larger volume (10 ml) of 450 μM ligand solution gives an IF of 1.2. Figure reproduced with permission from [20]

giving an imprinting factor of ~1.2. Thus, the model described in Fig. 3 helps illustrate and explain how, as n_{analyte} increases relative to M_{MIP}:

- n_{bound} increases, but due to the curvature of the MIP isotherm, not as rapidly as n_{analyte}. Hence
- D_{MIP}, falls, while
- D_{NIP} does not change so much, because the isotherm for the NIP is more linear. Hence
- IF decreases.

Therefore, to obtain a good IF in single-point experiments, measurements are usually made with a very low ratio of n_{analyte} to M_{MIP}. However, this may not reflect the conditions under which the MIP is intended to be used in a real application.

2.2 Fitting the Experimental Data to a Model

Where sufficient data points are collected and the errors are shown to be sufficiently low, data points on the binding isotherm may be fitted to a curve that can be either empirically based, or based on a theoretical model of the number of binding sites and their binding affinities. In Fig. 2, the isotherm is fitted to an arbitrary exponential function $B = 129.7(1 - e^{-0.01132F})$.

When the flattening of the curve at high values of F is clear, as it is in Fig. 2, it is possible to measure two empirical parameters B'_{max}, which is the value of B when all of the binding sites are occupied and must usually be extrapolated, and K'_d, which is the value of F (free analyte concentration) at which $B = 0.5 \times B'_{max}$. From Fig. 2, values are obtained of $B'_{max} = 130$ nmol mg^{-1} and $K'_d = 61$ μM. Allender et al. [20] have suggested that B'_{max} and K'_d should be used commonly as a measure of the affinity of a MIP, and they have conducted a meta-analysis of data on 47 MIPs from various publications between 2004 and 2008, which suggests that B'_{max} values commonly range between ~1 nmol and ~1 μmol per mg of polymer, while K'_d values commonly range between ~1 μM and 8 mM.

In order to understand the imprinting process better and improve the future design of MIPs, researchers have fitted MIP adsorption isotherms to various theoretical models of the number of binding sites and their binding affinities (for a review, see [22]). The features of the models used are summarized in Table 1.

The simplest (and most optimistic) model used has been the Langmuir isotherm, which assumes that all binding sites are identical, with a binding (association) constant K_a and dissociation constant $K_d = 1/K_a$. From the equation in Table 1, it may be seen that when $F = K_d$, then $B = 0.5 \times B_{max}$. Thus the empirical constants B'_{max} and K'_d described above are interpreted, in the Langmuir model, as the density of binding sites and the dissociation constant of those sites. Experimental values of B/F may be fitted to the isotherm using graph-fitting software; for example, Fig. 4 shows data for caffeine binding to a caffeine-imprinted polymer fitted to the Langmuir isotherm using OriginPro™. Values are obtained from the data fit of $B_{max} = (47 \pm 1)$ nmol mg^{-1} and $K_d = (2650 \pm 140)$ μM.

Prior to the availability of simple graph-fitting software, various approaches were used in which the Langmuir isotherm was linearized, to give a straight-line equation where y and x correspond to combinations of B and F. Best known of these

Table 1 Models used to fit experimental MIP adsorption isotherms

Model name	Equation	Classes of sites	Linearises	Saturates
Langmuir	$B = \frac{F \times B_{max}}{K_d + F}$	One, homogeneous	Yes	Yes
Bis-Langmuir	$B = \frac{F \times B_{max1}}{K_{d1} + F} + \frac{F \times B_{max2}}{K_{d2} + F}$	Two	No	Yes
Tri-Langmuir	$B = \frac{F \times B_{max1}}{K_{d1} + F} + \frac{F \times B_{max2}}{K_{d2} + F} + \frac{F \times B_{max3}}{K_{d3} + F}$	Three	No	Yes
Freundlich	$B = A \times F^m$	Continuous distribution—infinite number of v weak sites decaying to few v strong ones	Yes	No
Langmuir-Freundlich	$B = \frac{B_{max} \times a \times F^m}{1 + a \times F^m}$	Gaussian distribution with clear maximum	Yes, but requires estimation of B_{max}	Yes

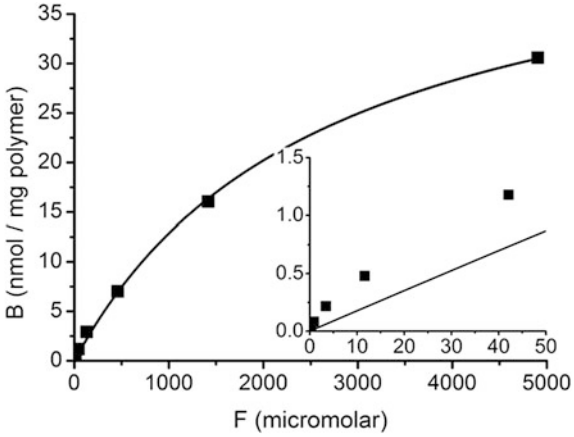

Fig. 4 Experimental *B–F* data for a caffeine-imprinted MIP determined by radioassay using the binding of ^{14}C-caffeine probe [23]. Assays performed in 1 mL volume of heptane/THF (3:1 v/v) using 8 mg of MIP and varying amounts of unlabelled caffeine. Data fitted to Langmuir isotherm using OriginPro™. Inset magnifies data at low *F*

is the Scatchard plot, where *B/F* is plotted against *B*. The Langmuir equation can be rearranged to show

$$\frac{B}{F} = -\frac{1}{K_d} \times B + \frac{B_{max}}{K_d} \tag{14}$$

Hence, a plot of *B/F* against *B* should be a straight line with gradient $-1/K_d$ and *y*-intercept B_{max}/K_d. Figure 5 shows the corresponding representation of the same data as in Fig. 4:

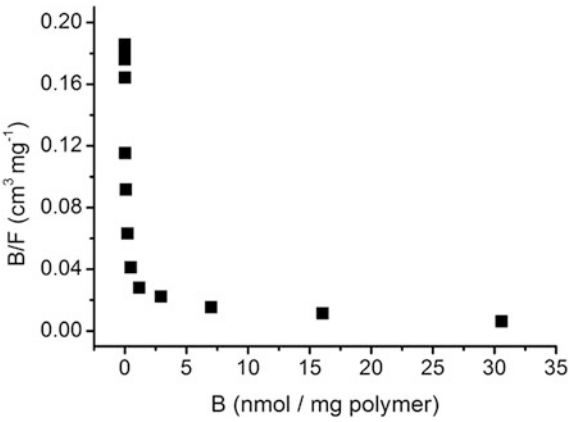

Fig. 5 Scatchard plot for binding data for a caffeine-imprinted MIP determined by radioassay using the binding of ^{14}C-caffeine probe, same conditions as Fig. 4 [23]

The data do not fit a straight line, confirming the inappropriateness of the Langmuir model in this case. However, it does appear (and is frequently observed with MIPs) that the Scatchard plot could be fitted with two separate straight lines—one line passing through the 7 points at lowest B values, and another through the 3 points at highest B values. This approach is often taken, with the gradients and intercepts of the two lines being used to derive two sets of B_{max} and K_d values—one attributed to "strong" binding sites and the other to "weak" binding sites. However, this yields poor estimates of the parameters (see Ref. [24]).

The bi-Langmuir isotherm (Table 1) is a model with two classes of binding sites (one with B_{max1} and K_{d1}, the other with B_{max2} and K_{d2}). This expression cannot be linearized in any combination of B and F, but non-linear graph-fitting software can be used to fit data. It was used initially by Mosbach et al. to fit isotherms obtained in MIP radioligand binding assays [25, 26] and has been very widely applied ever since (e.g., [27–30]). Figure 6 shows the same data as in Fig. 4, fitted to the bi-Langmuir isotherm: the fit is much better, particularly at low F values. The fitted parameters are B_{max1} = (1.09 ± 0.16) nmol mg^{-1} and K_{d1} = (30.4 ± 10.9) μM, B_{max2} = (48.8 ± 0.4) nmol mg^{-1} and K_{d2} = (3220 ± 90) μM.

The bi-Langmuir model is appealing, as it corresponds neatly to the simplistic picture of specific, imprinted sites (the stronger binding sites, of which there are but a few, in this case described by $B_{max1}$and K_{d1}), and the non-specific, non-imprinted sites (the weaker sites, of which there are relatively many, in this case described by $B_{max2}$and K_{d2}). Variations such as tri- (Table 1) and tetra-Langmuir isotherms can be created by adding third and fourth terms to the equation, describing additional classes of sites; however, it is important to acknowledge that adding additional parameters will inherently improve the fit between any model and data, and the inclusion of these additional parameters is only justified if the improvement in the fit is statistically significant as proven, for instance, by use of an F-test [22].

Models with two, three or even more classes of sites remain an oversimplification of the real situation in most cases, where there is likely to be a broad range of

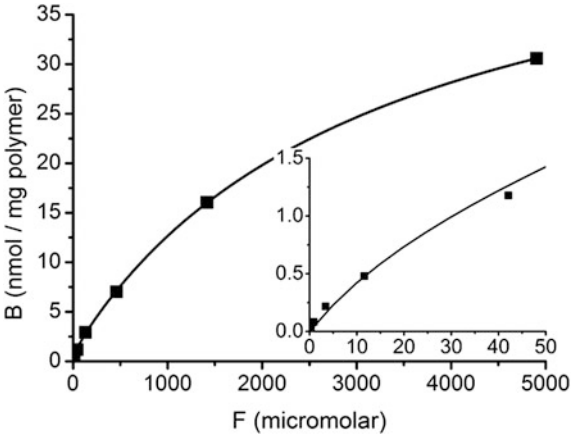

Fig. 6 Experimental B–F data for a caffeine-imprinted MIP as in Fig. 4 [23]. Data fitted to bi-Langmuir isotherm using OriginPro™. Inset magnifies data at low F

binding sites, each with slightly different conformations of functional groups and slightly different arrangements of polymeric chains, so that a more-or-less continuous range of binding sites with varying K_d values is more realistic.

An isotherm model that allows for a continuous range of binding sites with different affinities is the Freundlich isotherm (Table 1). A (cm^3 mg^{-1}) and m (dimensionless) are empirical constants. m can be interpreted as a measure of site heterogeneity (m = 1 corresponding to homogeneous sites), and both parameters may be related to the binding site densities and dissociation constants, but non-trivially (Sect. 5). In the case of the data from Fig. 4, the Freundlich isotherm fits rather poorly (Fig. 7), giving A = (0.19 ± 0.03) cm^3 mg^{-1} and m = 0.60 ± 0.02.

Although the Freundlich isotherm fits poorly in this case, it has been fitted more successfully to data from other MIPs, being used first by Guiochon et al. [29], and subsequently by the groups of Shimizu [31–33], Spivak [5] and many others. However, it does have some disadvantages, in comparison with other binding models [33]:

- It does not allow for binding saturation (that is, however much F is increased, the isotherm predicts that more analyte can bind to the polymer indefinitely); and
- the distribution of binding sites underlying the model is an exponentially decaying distribution that predicts an infinite number of binding sites with K_d = 0.

One advantage of the Freundlich isotherm is that it can be linearized, as in Eq. 15, such that the graph of log B versus log F has gradient m and intercept log A:

$$\log B = \log A + m \times \log F \tag{15}$$

When the data from Fig. 4 are transformed and plotted in this way (Fig. 8), the line of best fit yields A = (0.068 ± 0.005) cm^3 mg^{-1} and m = 0.762 ± 0.015. The

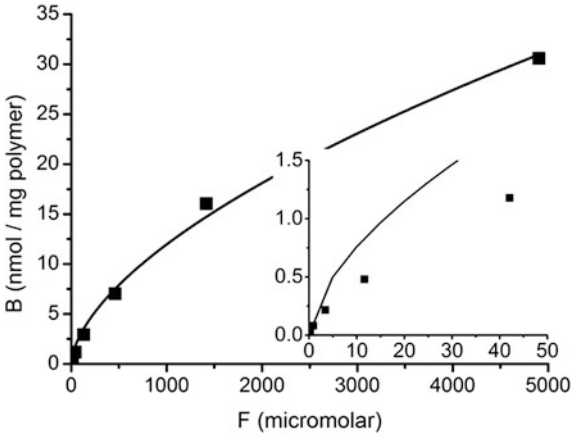

Fig. 7 Experimental B–F data for a caffeine-imprinted MIP as in Fig. 4 [23]. Data fitted to Freundlich isotherm using OriginPro™. Inset magnifies data at low F

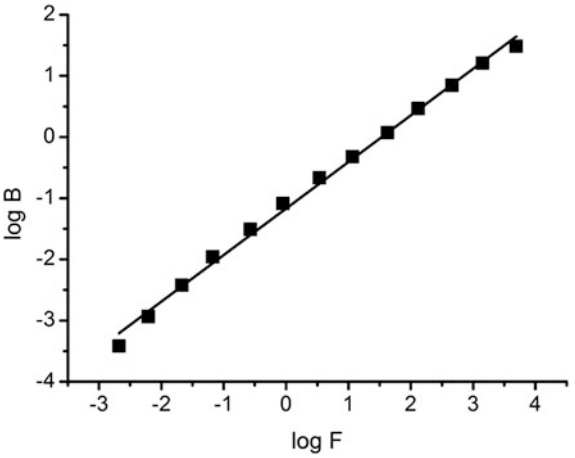

Fig. 8 Log-log plot of *B–F* data for a caffeine-imprinted MIP as in Fig. 4 [23]. Data fitted to *straight line* using OriginPro™

discrepancy between these values and those obtained above for non-linear fitting of the data in Fig. 7 directly reflects the fact that non-linear fitting of the raw data effectively weights the higher F data points more, while linear fitting of the log-log plot weights the lower F data points more.

The fourth commonly-applied model is the Langmuir-Freundlich isotherm (Table 1), which was first applied to MIP binding data by Shimizu et al. [34], and has since been used by the groups of Martin-Esteban [35–37], Tovar [27], Diaz-Garcia [38], and many others. As in the Freundlich isotherm, a (dm^3 μmol^{-1}) and m (dimensionless) are empirical constants, which may be related to the binding site densities and dissociation constants, but non-trivially (Sect. 5). When $m = 1$, the equation reduces to the Langmuir isotherm, while when F is extremely small, it reduces to the Freundlich isotherm (with $A = B_{max} \times a$). The equation is equivalent to the Hill Equation, used in biochemistry, in which the coefficient m indicates the co-operativity of binding ($m > 1$ indicates positive co-operativity, while $m < 1$ indicates negative co-operativity). The Langmuir-Freundlich isotherm does saturate, such that B_{max} is the maximum density of bound analyte at very high F. It can also be shown that the concentration of free ligand at which $B = 0.5 \times B_{max}$ is given by $K'_d = (a)^{-1/m}$.

Fitting the data from Fig. 4 to the Langmuir-Freundlich isotherm yields B_{max} (60.9 ± 3.2) nmol mg^{-1}, a = (7.69 ± 0.87) × 10^{-4} dm^3 μmol^{-1} and $m = 0.845 \pm 0.021$, hence $K'_d = 4840 \pm 570$ $\mu mol\ dm^{-3}$. The fit is better than for the Freundlich isotherm although not, in this case, as good as for the bi-Langmuir isotherm (Fig. 9). The Langmuir-Freundlich isotherm also has the advantage that it may be linearized in the form

$$\ln \frac{B}{B_{max} - B} = \ln a + m \times \ln F \tag{16}$$

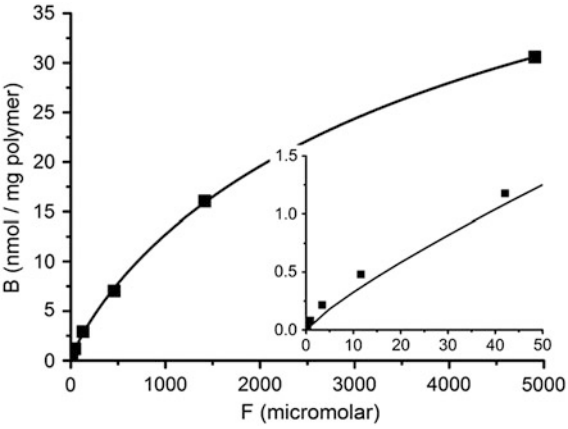

Fig. 9 Experimental *B–F* data for a caffeine-imprinted MIP as in Fig. 4 [23]. Data fitted to Langmuir-Freundlich isotherm using OriginPro™. Inset magnifies data at low *F*

Since B_{max} is unknown, it must be estimated from the *B–F* data and systematically optimized until the plot of $\ln(B/(B_{max} - B))$ versus $\ln F$ gives the best straight line possible.

3 Methods for the Characterization of Imprinted Binding Sites

3.1 Batch-Binding Studies

The simplest possible experiment to characterize the properties of an imprinted material involves incubating a known mass of material (M_{MIP}, in g) with a known quantity of analyte ($n_{analyte}$, in mol) in a known volume of solvent (V, in L or mL). Once equilibrium has been reached (minutes or hours, depending on the nature of the material), some will have bound to the material and some remains free in solution (Eq. 1). The material is separated from the solution and the free concentration F remaining in solution is measured. It is usually simpler (and more reliable) to measure F (from which n_{free} may be calculated) rather than B (which can then be calculated using Eq. 13).

In early research, Wulff et al. [39] performed batch-binding experiments, for example with racemic 4-nitrophenyl-mannopyranoside binding to a 4-nitrophenyl-α-D-mannopyranoside-imprinted vinylphenylboronic acid-co-DVB polymer. However, the batch-binding method was first applied to derive MIP adsorption isotherms by Shea et al. [40], but has subsequently been used in hundreds of publications, among others [27, 35, 38, 41–47].

The measurement of F must be as accurate and precise as possible, particularly if F is only slightly less than the total concentration, since B must be calculated from F as in Eq. 13. The experiment should be designed so as to minimize the error in the

measured F. Spectroscopic quantification—e.g., by absorbance at a single wavelength—may suffer from interferences, for example by any species released from the polymer. Since such a method is not selective, it is preferable to quantify F by a selective method such as HPLC. When the analyte is the same as the template molecule, bleeding of the template from the polymer will distort the results at low n_{analyte}; hence it is essential that the MIP be washed exhaustively before characterization. To check for the absence of error due to template bleeding, a control experiment where MIP is incubated in the assay solvent with $n_{\text{analyte}} = 0$ should be conducted. In all cases, experimental procedures should be thoroughly described and, where possible, uncertainties should be estimated and propagated in the calculation of B and F and shown as error bars on the isotherm.

Frequently, the isotherms on the MIP and an equivalent NIP are compared, as in Fig. 2. It was shown above that consideration of the MIP and NIP isotherm explains why IF is dependent on the ratio of analyte to polymer. Batch-binding experiments can also be applied to derive selectivity factors. The MIP is incubated together with the target analyte, and an equivalent experiment is set up with a competitor, under identical conditions. Measurement of the free concentrations of analyte, and of competitor, then allows calculation of the selectivity factor α via Eq. 6. Consideration of a wider range of data for a target analyte and a competitor, presented as binding isotherms as in Fig. 10, allows us to see why α is also dependent on n_{analyte}, and may increase for lower ratios of n_{analyte} to M_{MIP}.

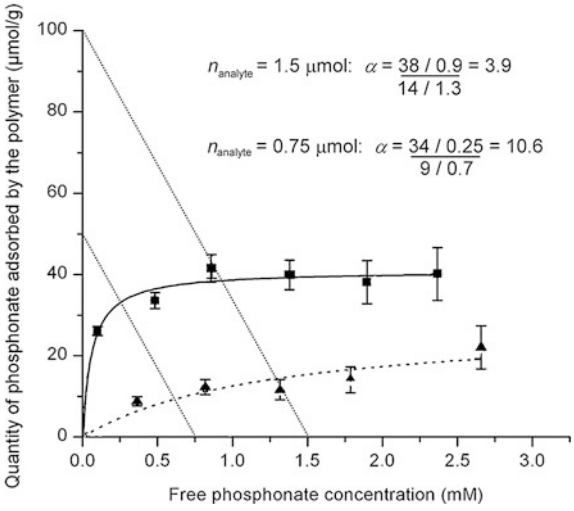

Fig. 10 An example of how distribution ratio (D) and selectivity factor (α) are influenced by ligand concentration. Data are for pinacolyl methylphosphonate (PMP, *squares*) and diphenylphosphinic acid (DPPA, *triangles*), incubated in 1 mL of toluene with 15 mg of PMP-imprinted MAA-co-DVB. Lines of ligand conservation drawn for $n_{\text{analyte}} = 1.5$ µmol and 0.75 µmol. For the higher n_{analyte}, $D_{\text{PMP}} = 42$ mL g^{-1} and $\alpha = 3.9$, while for the lower n_{analyte}, $D_{\text{PMP}} = 136$ mL g^{-1} and $\alpha = 10.6$. Figure adapted with permission from [47]

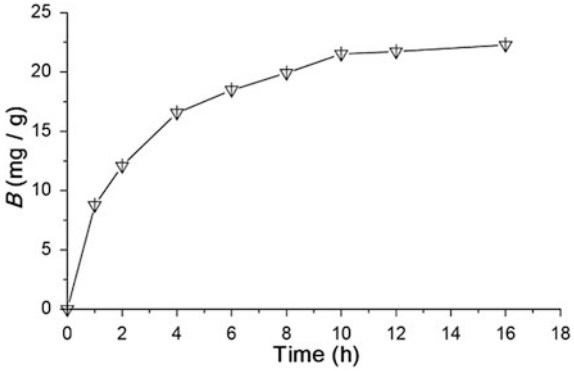

Fig. 11 Kinetic batch rebinding of hemoglobin (0.4 mg ml^{-1}) on hemoglobin-imprinted chitosan beads (0.5 g in 25 ml buffer). Concentration determined after sedimentation of beads by absorbance at 280 nm. Figure reproduced with permission from [41]

Batch-binding experiments can finally be applied to derive kinetic parameters. The MIP is incubated together with the target analyte, and after a specified time period the polymer is separated, the free analyte concentration F is measured, and the bound concentration B calculated using Eq. 13. This procedure is repeated at various time intervals, allowing a curve to be drawn as in Fig. 11.

The example in Fig. 11 is of extremely slow rebinding kinetics—attributable to the large size of the template (hemoglobin) which has been imprinted within large polymer particles. In contrast, kinetic batch-binding studies of a small molecule binding to a MIP can show much faster kinetics (for example, for chloramphenicol binding to a chloramphenicol-imprinted diethylaminoethylmethacrylate-co-EDMA polymer particles in THF, binding was observed to be essentially complete within 2 min [38]).

3.2 Radioligand Binding Studies

A variation on the batch-binding assay is where rather than incubating polymer and analyte in the assay solvent, a mixture of polymer, analyte and radiolabelled probe is incubated in the assay solvent. When the radiolabelled probe is simply an isotopic variant of the analyte, it may be assumed that the probe binding directly reflects the analyte binding (Eq. 17, where $n_{\text{free probe}}$ is the amount of free radiolabelled probe in mol, and n_{probe} is the total amount of radiolabelled probe in the assay, in mol).

$$\frac{n_{\text{free}}}{n_{\text{analyte}}} = \frac{n_{\text{free probe}}}{n_{\text{probe}}} \tag{17}$$

$n_{\text{free probe}}$ can be measured, after separation of the solution from the polymer, by scintillation counting, and n_{probe} can be quantified by a control with no polymer.

Thereafter, Eqs. 3 and 4 are used to derive B and F: the amount of probe is considered to be insignificant, such that the total amount of analyte, n_{analyte}, is just equal to the unlabeled amount. An advantage of this approach is that it is adaptable to a huge range of (unlabelled) analyte concentration: since n_{probe} is the same in every assay, the measurement of $n_{\text{free probe}}$ should not fall outside the instruments' linear range, even as n_{analyte} is varied over 5 or more orders of magnitude. Binding assays have been performed in this way by the Mosbach group [25, 26, 48] and others [49], and data obtained in this way are shown in Figs. 4, 6, 7 and 9. It must be stressed that this approach assumes the absence of any isotopic fractionation—i.e., the radiolabelled probe is assumed to bind in exactly the same way as the unlabeled analyte. If this condition is broken, Eq. 17 does not hold.

Selectivity can also be demonstrated using radioligand binding studies, where a mixture of polymer, analyte and radiolabelled probe in the assay solvent is compared with a mixture of polymer, competitor and radiolabelled probe. The ability of the analyte to displace the probe is compared with that of the competitor. The results may be plotted as $n_{\text{bound probe}}$ versus $[\text{ligand}]_{\text{total}}$ where $[\text{ligand}]_{\text{total}}$ is the initial, added concentration (not the free concentration) of either the target analyte or the competitor. This is the principle of the competitive binding assay, or molecular imprint sorbent assay (MIA) first demonstrated for MIPs in a seminal *Nature* paper by Mosbach et al. in 1993 [25]. For best results, n_{probe} is chosen to be as low as possible (subject to the need for the proportion free in solution to be measured accurately by scintillation counting); the solvent and amount of imprinted material are then chosen such that when there is no additional target analyte or competitor, $n_{\text{boundprobe}}/n_{\text{probe}}$ is in the range of 0.5–0.8. Results for caffeine and theophylline binding to a caffeine-imprinted polymer are shown in Fig. 12.

The increased displacement of the probe from the MIP as the total concentration of target analyte is increased may be understood in terms of the binding isotherm for

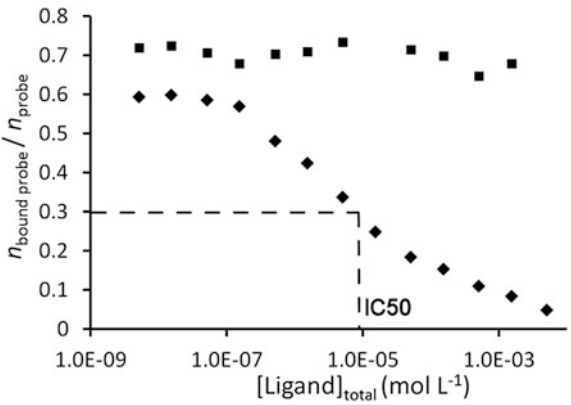

Fig. 12 Data for an MIA measuring the displacement of ^{14}C-caffeine probe from a caffeine-imprinted MIP by non-labelled caffeine (*diamonds*) and by theophylline (*squares*) [23]. Assays performed in 1 mL volume of heptane/THF (3:1 v/v) using 8 mg of MIP and varying amounts of unlabelled caffeine /theophylline

caffeine on this polymer, as shown in Fig. 6. At very low concentrations, the distribution ratio *B/F* takes a relatively high value (e.g., 0.004 nmol mg^{-1}/0.02 μM = 0.2 mL mg^{-1}, from which it may be calculated $n_{bound}/n_{analyte} \sim 0.6$, in agreement with Fig. 12). At high concentrations, *B/F* takes a lower value, due to the curvature of the isotherm data (e.g., 30 nmol mg^{-1}/5000 μM = 0.006 mL mg^{-1}, from which it may be calculated $n_{bound}/n_{analyte} \sim 0.04$, also in agreement). At about $F = 10$ μM, the experimental data suggest a B value of ~ 0.5 nmol mg^{-1}, giving $B/F = 0.05$ mL mg^{-1}, from which it may be calculated $n_{bound}/n_{analyte} \sim 0.3$. The intermediate value where $n_{boundprobe}/n_{probe}$ is exactly half the value it was in the absence of any non-labelled analyte, is known as the IC50. The relationship between the adsorption isotherm and the radioligand competition displacement curve is further discussed by Pap and Horvai [16].

Comparison of IC50 values for the target analyte and a particular competitor provides evidence for selectivity: If the sites that bind the probe are selective, then a competitor should be less effective at displacing the probe than the target analyte, and have a higher IC50. From Fig. 6 it may be seen that for this polymer, the IC50 for theophylline is in excess of 3 mM, and using Eq. 18, the MIA cross-reactivity is consequently ~0.3 %. However, while the IC50 for the analyte can be related to the isotherm, as outlined above, there is no such simple relationship between the isotherm for the competitor and the IC50 value of the competitor, and the MIA cross-reactivity cannot readily be related to the selectivity of a batch-binding experiment as described in Eq. 6.

$$\text{MIA cross-reactivity} = \frac{\text{IC50}_{\text{analyte}}}{\text{IC50}_{\text{competitor}}} \times 100\ \% \tag{18}$$

3.3 Zonal Chromatography

In many works, imprinted materials have been characterized by packing them into chromatography columns and measuring the retention times (t_R) of the analyte, and of competitors, when these are injected into a mobile phase flowing through the column. If the analyte exhibits a longer t_R than the competitor, this provides evidence for selectivity. This approach has been used in particular to demonstrate the separation of chiral mixtures, where one of the two enantiomers has been used as the template compound to generate an imprinted chiral stationary phase [50].

In conventional zonal chromatography under ideal, linear conditions, the retention time for an analyte should be related to its distribution ratio via Eqs. 19 and 20:

$$k'_{\text{analyte}} = \frac{t'_{\text{R,analyte}}}{t_0} = \frac{t_{\text{R,analyte}} - t_0}{t_0} \tag{19}$$

and

$$k'_{\text{analyte}} = D\frac{M_{\text{stationary phase}}}{V_{\text{mobile phase}}} \tag{20}$$

where t_0 is the void time (the retention time for a non-retained species), $t'_{\text{R,analyte}}$ is the corrected retention time ($=t_R - t_0$), k'_{analyte} is the capacity factor, $M_{\text{stationary phase}}$ is the mass of stationary phase (e.g., MIP or NIP, in g) and $V_{\text{mobile phase}}$ is the volume of mobile phase (in mL). In theory, then, measurement of t_R enables calculation of D.

This simple model has been extended by various authors to consider the effects of the concentration of a modifier (/strong eluent) in the (weak) eluent on k'_{analyte}, and, hence, to propose the stoichiometry and affinity of the modifier-analyte, analyte-binding site and modifier-binding site interactions [51–53].

If t_R is measured for a competitor, then

$$\alpha = \frac{D_{\text{analyte}}}{D_{\text{competitor}}} = \frac{k'_{\text{analyte}}}{k'_{\text{R,competitor}}} = \frac{t'_{\text{R,analyte}}}{t'_{\text{R,competitor}}} \tag{21}$$

In this way, selectivity factors are frequently calculated for the separation of peaks due to the imprinted and non-imprinted enantiomers on an imprinted chiral stationary phase (Fig. 13). However, this approach (like those in the previous paragraph) is based on the assumption that D is independent of the total amount of analyte injected, i.e., that the isotherm is linear, whereas in practice the isotherm is curved, so that D falls as the total amount of analyte increases (this can be seen from the chromatograms for increasing concentration of analyte in Fig. 14). Again, the highest values for α will usually be calculated when the ratio $n_{\text{analyte}}/M_{\text{MIP}}$ is as

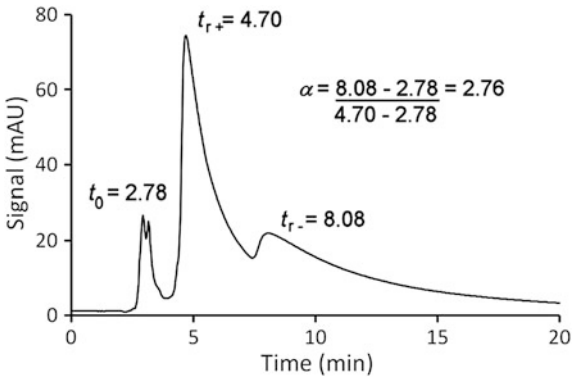

Fig. 13 Separation of enantiomers of ephedrine by zonal chromatography on a MIP stationary phase. (−)-ephedrine imprinted MAA-EDMA copolymer packed into 250 × 4.6 mm column. 200 μg (±)-ephedrine injected, chromatogram recorded at 254 nm using mobile phase of 20 % AcOH in DCM, at 1.0 mL min^{-1} and 30 ºC [54]

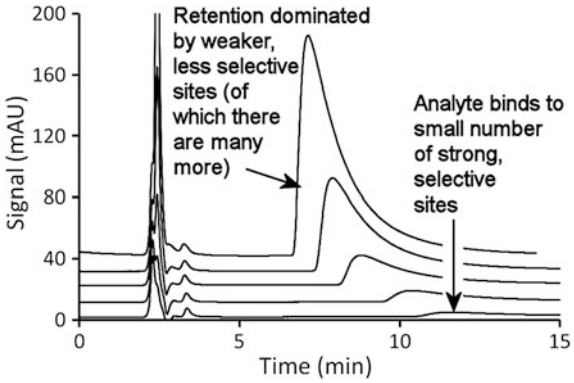

Fig. 14 Typical effect of increasing the amount of analyte injected on a MIP stationary phase in HPLC. MIP column is the same as for Fig. 13, chromatograms recorded at 254 nm using mobile phase of 5 % $BuNH_2$ in DCM, at 1.0 mL min^{-1} and 30 ºC. Injections of increasing amounts of (−)-ephedrine: 10 μg (*bottom*), 20, 40, 100, 200 μg (*top*). Peak at ∼3 min is the void peak due to the solvent in which analyte is injected [54]

small as possible, i.e., when the lowest detectable amounts of analyte and competitor are injected into the column (and when both the imprinted, and non-imprinted enantiomers will have longer retention times).

Three measures of the quality of a chromatographic separation that are commonly encountered are the plate number N (which describes the sharpness of a peak), the asymmetry A_s (which describes the tailing or fronting of a peak) and the resolution R_s (which is a ratio of the separation of two peaks over their width). In the ideal case, N and R_s are independent of the amount of analyte loaded, and $A_s = 1.0$. When these parameters are compared, MIPs usually appear inferior to conventional stationary phases such as octadecylsilica.

The extreme tailing of the peaks often observed for zonal chromatography of analytes on MIPs (in particular, for the imprinted molecule itself) is attributed to the inhomogeneity of the binding sites and to slow binding/unbinding kinetics (the shape of the peaks can usually be improved by increasing the temperature of the column, which speeds up the rates) [55]. In Fig. 14 one can imagine the peak for 10 μg of analyte representing the binding to the strongest binding sites on the polymer: When 20 μg are injected, there is too much analyte for the strongest binding sites, so that weaker sites are occupied too, giving a "front" to the 10 μg peak. Likewise, one can picture the peak for 40 μg of analyte building on the front of the 20 μg peak, that for 100 μg of analyte building on the front of the 40 μg peak etc., as the extra analyte may only be retained by occupying weaker and weaker sites.

More sophisticated models of chromatographic behavior incorporating non-ideality and/or non-linearity begin with the general rate model, in which the mass balance for an analyte at distance z along the column and time t after injection is given by:

$$\frac{\partial C}{\partial t} + \frac{u}{\varepsilon}\frac{\partial C}{\delta z} + \frac{(1-\varepsilon)}{\varepsilon}\frac{\delta C_p}{\delta t} = D_L \frac{\delta^2 C}{\delta z^2} \tag{22}$$

where C is the analyte concentration in the mobile phase (cf. F, mol L^{-1}), u is the linear flow rate (cm s^{-1}), ε is the porosity as a fraction of the column volume, C_p is the analyte concentration in the pores (such that $\varepsilon \times$ total volume $\times C_p = M \times B$) and D_L is the dispersion coefficient ($cm^2 s^{-1}$), which is largely due to axial diffusion. This equation cannot be solved analytically, but with various additional assumptions, non-ideal and non-linear behavior can be modelled and various predictions can be derived. Thus, Guiochon et al. [56–60] have used a model derived from Eq. 22, together with binding isotherms derived separately by frontal chromatography, to fit the peak shapes for (large volume and large concentration) injections of Fmoc-Trp enantiomers on an Fmoc-L-imprinted MIP, and derived kinetic parameters. Horvai et al. [18, 61] have shown that if ideal behavior (neglecting kinetic effects) is assumed, points on the trailing edge of a peak such as one of those in Fig. 14 can be related to points on the isotherm (the "elution by characteristic point" method). Seebach and Seidel-Morgenstern [62] used a similar relationship between the retention times for the peak maxima at a series of injected concentrations and B/F to derive an isotherm for Z-L-Phe binding to a Z-L-Phe MIP. Baggiani et al. [63] used a model derived from Eq. 22, but assuming a Langmuir-type isotherm to fit the complete peak shape for injections of pyrimethanil on pyrimethanil-imprinted MIPs, deriving apparent site densities and affinity constants as well as kinetic parameters. Lee et al. [64] have modelled the effect of sample concentration and affinity constant on the plate number and peak asymmetry.

3.4 Frontal Chromatography

In simple ("rectangular pulse") frontal chromatography, instead of injecting a short pulse of analyte, the mobile phase is altered to contain a specific concentration of analyte that is run continuously through the column [65–67]. Initially, as it first enters the column, the analyte binds to binding sites on the stationary phase; however, once the bound concentration of analyte reaches equilibrium with the concentration in the mobile phase over the whole of the column (as may be expressed via the distribution ratio for the analyte under those conditions), no more analyte can bind, and the analyte begins to elute from the column, the concentration in the eluent soon becoming the same as in the mobile phase that continues to be fed onto the column. The measured parameter is the breakthrough time, $t_{breakthrough}$ [or, frequently, the breakthrough volume, V_r in mL, which is just $t_{breakthrough} \times$ the volumetric flow rate (f, L min^{-1})], which is the interval from the point at which the mobile phase is changed, to the time when the analyte appears in the eluent.

The amount of analyte bound to the stationary phase is given by:

$$n_{\text{bound}} = f \times \left(t_{\text{breakthrough}} - t_0\right) \times [A] \tag{23}$$

where t_0 is the void time as before (and will correspond to $t_{\text{breakthrough}}$ if none of the analyte was to bind to the stationary phase), and $[A]$ is the concentration (mol L^{-1}) of analyte added to the mobile phase. The distribution ratio (Eq. 3) is given by:

$$D = \frac{B}{F} = \frac{f \times \left(t_{\text{breakthrough}} - t_0\right)}{M_{\text{MIP}}} \tag{24}$$

and hence the binding isotherm can be derived. Data obtained in this way can readily be fitted to a model assuming that all binding sites are equivalent (i.e., a Langmuir model). If this is the case, the total number of binding sites n_{total} is given by $n_{\text{total}} = n_{\text{empty}} + n_{\text{bound}}$ and (from Eq. 2)

$$K_{\text{d}} = \frac{n_{\text{empty}} \times F}{n_{\text{bound}}} = \frac{n_{\text{total}} \times F}{n_{\text{bound}}} - F \tag{25}$$

substituting $F = [A]$ and for n_{bound} as in Eq. 23 gives

$$K_{\text{d}} = \frac{n_{\text{total}}}{f \times \left(t_{\text{breakthrough}} - t_0\right)} - [A] \tag{26}$$

Thus, a series of experiments are performed, applying various concentrations of analyte in the mobile phase. $t_{\text{breakthrough}}$ is measured, then the column regenerated to remove all bound analyte and the experiment repeated using a different concentration. A plot of $1/([A] \times f \times (t_{\text{breakthrough}} - t_0))$ against $1/[A]$ should give a straight line with y-intercept $1/n_{\text{total}}$ and x-intercept $-1/K_{\text{d}}$.

Mosbach et al. [68, 69] were the first to apply this approach to MIPs, deriving apparent n_{total} values in the range 18–28 μmol g^{-1} of polymer, $K_{\text{d}}s$ in the range 1.6–8.1 mM, and showing that MIPs had lower K_{d} values (indicating stronger binding) for their template than its optical antipode, and lower K_{d}s than the corresponding NIPs, as expected. Andersson et al. [70] applied frontal chromatography to a model system of pyridines and bipyridines binding to 4,4′-bipyridyl-imprinted MAA-co-EDMA in order to demonstrate the increased strength of binding when more than one analyte-monomer interaction is present within the imprinted site. The approach has also been used extensively by Baggiani et al. [71, 72] and others [73, 74]. In one intriguing study, Baggiani's group compared the rebinding of 2,4,5-trichlorophenoxyacetic acid (2,4,5-T) to a conventional 2,4,5-T-imprinted 4-vinylpyridine-co-EDMA polymer and a polymer which, additionally, incorporated a covalently bound template analogue, and showed that the latter polymer had a lower binding capacity (lower n_{total}) but lower K_{d} (i.e., the covalently incorporated template analogue appeared to increase the strength of template re-binding) [3].

A variant of frontal chromatography is staircase frontal chromatography in which, once the detector signal has stabilized showing that the analyte is present in

the eluent at the same concentration as in the injected mobile phase, the mobile phase is altered to contain a higher concentration of the analyte, and the process repeated, giving a chromatogram with the appearance of a staircase, indicating a series of concentration steps. This approach was first applied to MIPs by Guiochon et al. [29]. On proceeding from step i to step $i + 1$, the additional amount of analyte bound to the stationary phase can be calculated as:

$$n_{\text{bound},i+1} - n_{\text{bound},i} = f \times \left(t_{\text{breakthrough}} - t_0\right) \times \left([A]_{i+1} - [A]_i\right) \tag{27}$$

from which the isotherm can be derived in a shorter time than would be required by the rectangular pulse method (where the column must be regenerated between each change in concentration). Figure 15 shows typical data.

The shape of the "front," or breakthrough curve, can also give information about the shape of the isotherm, as well as the kinetics of analyte binding to the stationary phase. For example, Fig. 16 shows a typical breakthrough curve obtained by Guiochon et al. $t_{\text{breakthrough}}$ is the time corresponding to half-height of the front, i.e., the center of mass of the concentration step—in this case 6.75 min. A classical transport model was applied to model the breakthrough curve, involving numerical solutions of an equation derived from Eq. 22. The modelled curves require as an input a relationship between B and F for any particular F at equilibrium (i.e., a theoretical isotherm—see Sect. 2), and an estimated value for the mass transfer rate coefficient k_f (in min^{-1}), which is related to, although not identical to, the forwards rate constant k_1 in Eqs. 7 and 8, and defined as:

$$\frac{\partial B}{\partial t} = k_f (B_{\text{eqm}} - B_t) \tag{28}$$

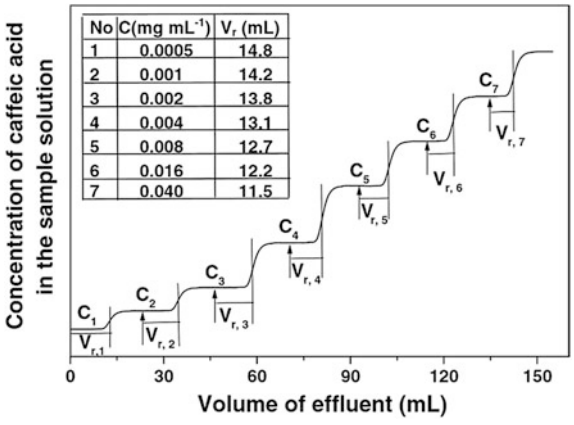

Fig. 15 Partial frontal chromatogram of caffeic acid on caffeic acid-imprinted MAA-co-EDMA monolith in a 200 × 4.6 mm column with THF mobile phase at 25 °C and 0.5 mL min^{-1}, monitored at 280 nm. Volume of effluent equals retention time multiplied by flow rate. *Arrows mark* introduction of sample solutions having the concentration indicated. Reproduced with permission from [28]

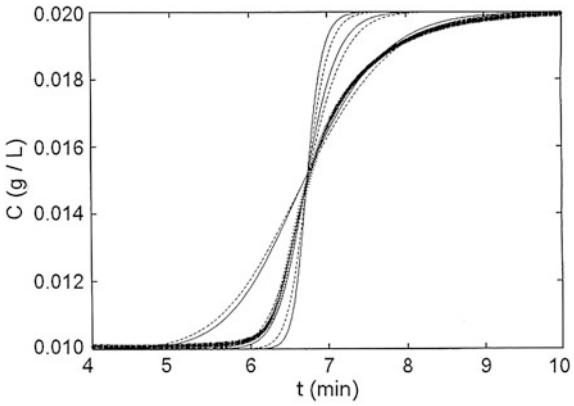

Fig. 16 Experimental breakthrough curve (*symbols*) and fitted curves (*lines*) for L-Phe-An applied to a L-Phe-An imprinted MAA-co-EDMA polymer, packed into a 100 × 4.6 mm column. Mobile phase of MeCN-0.05 M potassium phosphate (7:3 v/v) at 1.0 mL min^{-1} and 40 °C, monitored at 260 nm. The concentration step shown is from C_n = 0.01 to C_{n+1} = 0.02 g/l. Calculated breakthrough curves for k_f = 10 min^{-1}, k_f = 110 min^{-1} and for the rate coefficient that best fits the experimental data, k_f = 40 min^{-1} (the larger k_f, the steeper the curve). *Solid lines* Bi-Langmuir model. *Dashed lines* Freundlich model. Reproduced with permission from [29]

For the concentration step shown in Fig. 16, the classical transport model provides the best fit to the data when the isotherm is considered to be of the bis-Langmuir form and k_f is given the value 40 min^{-1}. For a sequence of concentration steps, k_f was found to increase with an increase in [*A*], to increase with temperature, and to be lower for the imprinted enantiomer than its optical antipode (particularly at lower concentrations). The latter effect may be rationalized by the strongest, most selective binding sites also being the less accessible, hence slower- binding ones [29]. The values of k_f found are low in comparison with other types of stationary phase, supporting the thesis that slow mass transfer contributes to the poor peak shapes seen in zonal chromatography, as well as binding site heterogeneity.

Staircase frontal chromatography was used further, in combination with models of non-ideal, non-linear chromatographic behavior, in a series of works by Guiochon et al. to show the effects of heat-treating the MIP [75, 76], the effects of the pH [77] and temperature [60] of the mobile phase, the effects of different organic mobile phases [78], of organic modifiers added to an acetonitrile mobile phase [79, 80], and of water in an organic-aqueous cosolvent mobile phase [58], to compare particulate and monolithic MIP stationary phases [81], to compare the retention of template analogues [82] and to deconvolute the effects of different kinetic processes in the lumped mass transfer rate coefficient k_f: It was shown that in some cases, diffusion within the pores of the MIP particles makes the largest contribution to the slow rate constants [83], and in other cases surface diffusion [56, 57].

3.5 Calorimetry

When the target analyte (or a competitor) binds to an imprinted binding site, there is expected to be a change in enthalpy H. If the binding process is thermodynamically favorable, then the change in Gibbs free energy, ΔG for the process must be negative, where ΔG is related to the changes in enthalpy and entropy, S:

$$\Delta G = \Delta H - T \times \Delta S \tag{29}$$

Hence a spontaneous (exergonic) process can be driven by a negative ΔH (exothermic) or by a positive ΔS (increase in entropy). Bond formation is usually exothermic.

Isothermal titration calorimetry (ITC) was first applied to imprinted materials by Chen et al. [84] and has subsequently been used by others [85–90], while batch calorimetry has also been used to study slow binding processes [88, 91, 92]. In batch calorimetry, two solutions are allowed to reach thermal equilibrium separately within the calorimeter, then mixed, and the heat produced Q is measured over time. ITC is similar, except that one solution—the titrant—is added via automated syringe in very small aliquots to the other, which is in a cell in the calorimeter. The heat is measured as the power (W, Js^{-1}) that is produced/taken in by the cell as a function of time, producing a spike on each injection (e.g., Fig. 17a), which can be integrated and divided by the amount of titrant added to give a decaying profile such as Fig. 17b.

The sample in the cell might be the imprinted material, with the target analyte added from the syringe, but in the experiment shown in Fig. 17, the set up was with the target analyte (Boc-Phe-An) in the cell and a suspension of imprinted nanoparticles in the syringe [90]. When the adsorption isotherm has been obtained independently, it may be possible to know exactly how much analyte binds to the imprinted polymer in each step ($n_{\text{bound after step}} - n_{\text{bound before step}}$), in which case:

$$Q_{\text{step}} = \Delta H \times \left(n_{\text{bound after step}} - n_{\text{bound before step}}\right) \tag{30}$$

If the binding isotherm is not known, the data can be converted to display $Q_{\text{cumulative}}$ against $[\text{titrant}]_{\text{total}}$ and fitted with a function assuming a single class of identical binding sites, derived from Eqs. 31–32:

$$Q_{\text{cumulative}} = \Delta H \times n_{\text{bound cumulative}} \tag{31}$$

$$n_{\text{bound}} = K_{\text{a}} \times (n_{\text{total}} - n_{\text{bound}}) \times \left([\text{analyte}]_{\text{total}} - n_{\text{bound}} \times M/V\right) \tag{32}$$

where M and V have their usual meaning. This yields n_{bound} as the root of a quadratic, and the function can be fit to yield ΔH, n_{total} and K_{a} (in the case of Weber et al. [90], n_{total} was estimated independently).

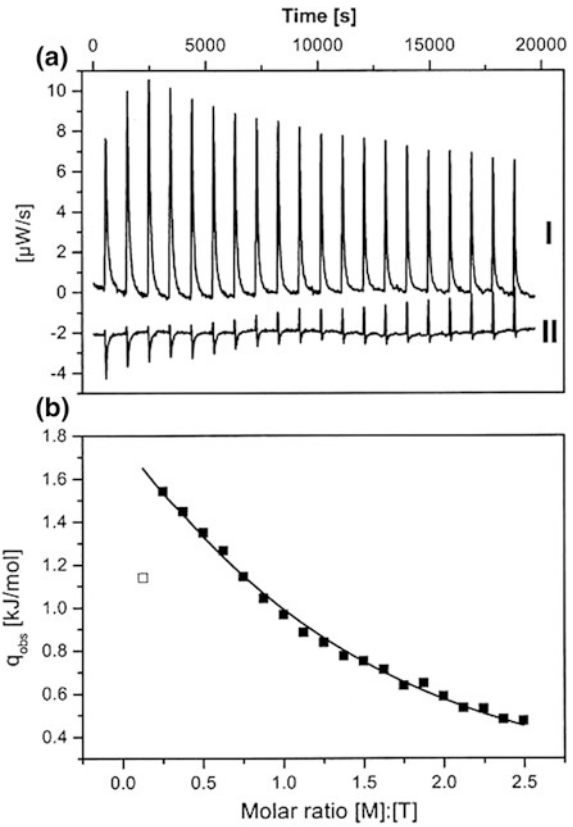

Fig. 17 **a** Experimental titration curves for the titration of Boc-L-Phe-An imprinted and extracted microgel A at 25 °C (*I*) and the corresponding control dilution experiment (*II*). Measured heat power versus time. A suspension of microgel in methanol/water (50:50 v/v) was titrated into Boc-L-Phe-An dissolved in the same solvent. **b** Observed titration heat Q_{step} versus molar ratio microgel to template (the first value was excluded from analysis). Reproduced with permission from [90]

In these or equivalent ways, quite varying values of ΔH have been obtained: +8 kJ mol^{-1} for 2,4-D binding to an imprinted VPy/EDMA polymer in aqueous buffer [84], +6.6 kJ mol^{-1} for phenyl mannopyranoside binding to a vinylphenylboronic acid/EDMA polymer in acetonitrile [88], −21 kJ mol^{-1} for Boc-L-Phe-An binding to the polymer shown in Fig. 17 [90], −8 kJ mol^{-1} for riboflavin binding to a 2,6-bis(acylamido)pyridine polymer in water/ethanol/formic acid (90.6:4.7:4.7 v/v/v).

In some cases, the further extension has been made that if the conditions can be approximated to standard conditions,

$$\Delta H = \Delta H^{\theta} = \Delta G^{\theta} + T \times \Delta S^{\theta} \tag{29}$$

and since

$$\Delta G^{\theta} = -RT\ln K_a \tag{30}$$

the entropy change on binding, *S* may also be estimated. There seem to be rather too many assumptions underlying quantitative estimates like this; however, it may

certainly be said that if the process is observed to be endothermic, as in Chen et al.'s study of 2,4-D binding to an imprinted VPy/EDMA polymer in aqueous buffer [84], then the binding must be driven instead by an increase in entropy. This makes sense in the case of binding in water, where hydrophobic interactions are well known to be entropically driven.

3.6 Other Methods

Since the application envisaged for many MIPs is in solid-phase extraction/sample clean-up of a dilute analyte in a complex matrix prior to quantitative analysis by HPLC, LC-MS or GC, Martin-Esteban et al. [35, 36, 93] have attempted to derive isotherms for analytes binding to MIPs under SPE-type conditions. In an experiment that is similar to a batch-binding experiment, analyte in binding solvent (1 mL, 0.05–500 mg L^{-1}) was loaded onto pre-conditioned MIP (100 mg) packed into an SPE cartridge. Some, but not all, of the analytes bound under these conditions. A washing solvent was applied, followed by the elution solvent (3–8 mL). The eluted fraction was concentrated, and analyzed by HPLC to determine n_{bound}. n_{free} was calculated as the difference between the amount loaded, n_{analyte}, and n_{bound}. Data were then fitted using Langmuir-Freundlich isotherms. Although the approach was certainly useful in characterizing MIPs for SPE, the validity of the isotherm fits is questionable because binding did not necessarily occur under equilibrium conditions, and there is no way of assessing the effect of kinetic limitations.

Spectroscopic interrogation of a MIP, in its clean state and after binding of analyte, forms the basis of many proposed applications of MIPs in chemical sensing. However, such an approach can also provide useful information about the nature of analyte-binding site interactions, including some indication of their strength. Hsu et al. [94] used infrared (IR) spectroscopy to monitor the binding of thymine to thymine-imprinted diacryloyl-2,6-diaminopyridine-co-tripropyleneglcol diacrylate polymer films in chloroform. Distinctive absorbances were observed due to the bound and non-bound thymine: by assuming the measured absorbances to be proportional to B and to F, apparent binding constants K'_a could be calculated. Resmini et al. [95] used a similar approach based on the quenching of the visible absorbance (435 nm) of a phosphate template when it rebinds to an arginine-containing MIP in DMSO, to calculate the binding site population (assuming a stoichiometric rebinding). Haupt et al. [96] used the Raman signal produced when propranolol was added to a propranolol-imprinted MIP and an NIP in MeCN to plot a form of isotherm and calculate apparent binding constants K'_a (their approach assumes that the free propranolol concentration is identical to the added concentration).

In each of these examples, the sensor response (change in absorbance of the polymer) is assumed to be proportional to B (or n_{bound}). This assumption was tested for two MIP systems by Ng and Narayanaswamy [97]. Cu^{2+} binding to copper-imprinted 4-vinylpyridine-co-hydroxyethylmethacrylate-co-EDMA polymer particles in water was measured both by batch-binding (supernatant added to eriochrome cyanine R and absorbance recorded at 568 nm) and by reflectance measurements at 750 nm on a layer of particles deposited on the tip of a fibre-optic bundle. *N*-phenyl-1-naphthylamine (NPN) binding to NPN-imprinted 2,4-diisocyanate cross-linked β-cyclodextrin particles in methanol was measured by batch-binding (direct measurement of supernatant absorbance at 340 nm) and fluorescence measurements (λ_{ex} = 365 nm, λ_{em} = 495 nm) on particles trapped in a fluorescence flow cell. The authors suggest a good correlation in each case, although a simple comparison of signal and B for differing F is not presented; more studies of this kind are needed in order to correlate sensor signals with binding isotherms.

Apparent isotherms can be recorded, and apparent affinity constants calculated, using other sensor techniques, such as surface plasmon resonance [98] and quartz crystal microbalance [99, 100]. Such analyses again rely on the assumption that the sensor response is proportional to B (or n_{bound}).

Another experimental measurement of analyte-MIP interactions that has been proposed is force measurements using AFM. In the first example of such work by Haupt et al. [101], the binding of cytochrome-C (immobilized on an AFM tip) to protein-imprinted acrylamide-co-bisacrylamide hydrogel films covalently coupled to glass slides was measured by force measurements. The interaction with imprinted films was stronger than with non-imprinted ones, and was correlated with the binding of fluorescein-labelled cytochrome-C from aqueous buffer. Recent work by Reddy et al. [102] yielded similar data for the binding of bovine hemoglobin (immobilized on an AFM tip) to protein-imprinted hydrogel particles.

In parallel with experimental studies, the interactions of analytes with MIPs have been modelled in silico [103]. Although there are fewer examples of computational studies on MIPs than on the pre-polymerization mixture (reflecting the greater complexity of the polymerized material), this is a field of increasing activity.

4 Parameters Influencing Rebinding

4.1 Polymer Design

MIP design cannot be dealt with in this chapter, but it should be emphasized that the binding properties of a MIP (and NIP) are inextricable from its composition and method of preparation. The major factors influencing the binding properties of the resulting polymer include the type of functional monomer and monomer:template ratio [1, 9, 104–106] and the porogenic solvent [105, 107].

4.2 Rebinding Solvent (Organic Solvents)

For MIPs prepared via non-covalent imprinting using hydrogen-bonding interactions (e.g., the vast majority of MIPs produced used MAA as functional monomer), a non-polar organic solvent is commonly used as a porogen (to promote the monomer-template interactions), and the strongest and most selective rebinding is also often observed in a non-polar organic solvent. Dogma suggests that for this class of MIPs, the rebinding will be strongest and most selective in the same solvent that was used as the porogen (because the swelling of the MIP is assumed to be different in different solvents, affecting the binding site integrity). This is frequently the case (e.g., 4-nitrophenol-imprinted 4-vinylpyridine-co-DVB particles gave the best separation between 4-nitrophenol and its isomers in zonal chromatography using a chloroform mobile phase if the porogen was chloroform, and using an MeCN mobile phase if the porogen was MeCN [107]), but not always (2-(morpholin-4-yl)ethyl (2-methoxyphenyl)carbamate-imprinted MAA-co-EDMA particles made with toluene porogen gave stronger binding of the template and its isomers in zonal chromatography using a toluene mobile phase than using MeOH, but the separation factors and IFs were higher using MeOH than using toluene [108]). Guiochon et al. [78] obtained isotherms for Fmoc-L-Trp on a Fmoc-L-Trp-imprinted 4-VPy-co-EDMA particles using staircase frontal analysis: the MIP was made with MeCN as porogen and exhibited higher affinity and selectivity for the template in MeCN than in DCM, chloroform, or THF. The isotherm in MeCN was well fitted to a tri-Langmuir model, but in the other solvents a bi-Langmuir model fit best, suggesting that the strongest adsorbing sites were absent. The influence of solvent dielectric constant and Snyder polarity index on rebinding of bupivacaine to a bupivacaine-imprinted MAA-co-EDMA in single-point experiments has been studied by Rosengren et al. [109].

Usually, a polar organic modifier is added to the organic solvent in which analyte binding to a MIP is being studied—the modifier serves to reduce the strength of binding. This is often desirable in order to promote selective binding, rather than non-selective—i.e., the modifier is thought to reduce binding to the weak, non-selective hydrogen bonding sites of the polymer more than it reduces binding to the strong, selective sites [9]. In MIA binding assays, in SPE, and in the use of MIPs as stationary phases in chromatography, the effect of increasing amounts of modifier on binding to the MIP and NIP is often compared, to find the modifier concentration at which the IF is maximized. The influence of type and concentration of modifiers on the binding of Fmoc-L-Trp to Fmoc-L-Trp-imprinted 4-VPy-co-EDMA particles was also studied in detail by Guiochon et al. [79, 80], using staircase frontal analysis. Isotherms were obtained and fitted to tri- or tetra-Langmuir models. Modifiers were found to reduce the density, B_{max} of the strongest binding sites more than the K_a, but reduce the K_a of the weak binding sites more than their B_{max}.

4.3 Rebinding pH and Cosolvent (Aqueous)

MIPs that are dependent on weak hydrogen bonds between the template and binding site do certainly work best in organic solvents, and furthermore the sugar-imprinted polymers studied by Wulff in the 1970s and 1980s (based on the covalent interactions between sugars and boronic acids) had a similar preference. This led to a prejudice among the wider scientific community that MIPs could not work in aqueous solvents. Nowadays there are numerous examples of MIPs both made in, and applied in, aqueous buffers or aqueous/organic cosolvent mixtures. MAA- or 4-VPy-based polymers can show good binding and selectivity in aqueous buffers if the analyte-polymer interaction is strong [110, 111].

Often for small molecules, an organic-aqueous cosolvent mixture is used. Pure aqueous conditions lead to significant hydrophobic interactions, which for MIPs made in organic solvents using DVB or EDMA as a cross-linker, lead to significant non-specific adsorption of the analyte, outside of the more selective sites. A certain amount of organic cosolvent can minimize these non-specific interactions, but must usually be carefully optimized. For example, Dong et al. [112] have optimized an organic-aqueous mobile phase for zonal chromatographic separation of the enantiomers of ephedrine on a (+)-ephedrine-imprinted MAA-co-EDMA polymer. Furthermore, the pH of the aqueous phase is usually critical when the analyte and/or functional groups of the MIP are ionizable. Sellergren and Shea [113] proposed a model for the influence of pH on retention and separation of the enantiomers of Phe-An on a Phe-L-An-imprinted MAA-co-EDMA polymer in zonal chromatography. At pH 4 and below, both the analyte and the carboxylate groups of the MIP are protonated, and the cationic analyte interacts only weakly with the neutral polymer. At pH 8 and above, both the analyte and the carboxylate groups of the MIP are deprotonated; the neutral analyte, however, interacts only weakly with the anionic polymer. In the intervening region, there is some overlap between the carboxylate groups being deprotonated and anionic and the analyte protonated and cationic—so binding is strongest. However, selectivity peaks at about pH 6, which was proposed to correlate with the carboxylate functions of the strongest, most selective sites having a lower average pK_a than the weaker, non-selective sites.

Guiochon et al have also studied the influence of the fraction and pH of aqueous cosolvent in an acetonitrile mobile phase on the isotherms for Phe-An [77] and Fmoc-Trp [58] enantiomers on their respective MIPs, obtained via staircase frontal analysis. In the former case, the isotherms supported the conclusions of Sellergren and Shea, with the number of weak binding sites increasing faster with pH than the number of strong binding sites. For Fmoc-Trp, the highest number of binding sites was calculated at pH 3.8, where both the analyte and polymer (4-VPy based) are neutral: this corresponded to zonal chromatography where the highest retention was at this pH. Selective binding in this case appears to be driven more by hydrophobic interactions and hydrogen bonds than by ion-pair formation.

4.4 Temperature

The first detailed study of the effect of temperature on MIP binding properties was reported by Sellergren and Shea [55]. The binding of the enantiomers of Phe-An to an L-Phe-An-imprinted MAA-co-EDMA polymer was studied in zonal chromatography using an MeCN-aqueous buffer mobile phase and an MeCN–AcOH mobile phase at temperatures between 20 and 80 ºC. For the aqueous mobile phase, increasing temperature led to a partial improvement in the peak shape (suggesting an acceleration of the kinetics), a decrease in the retention of both enantiomers (suggesting binding is an exothermic, enthalpy-driven process), and a decrease in separation (suggesting that binding of the imprinted enantiomer is more exothermic than that of its optical antipode). For the organic mobile phase, a partial improvement in the peak shape was again observed, but there was an increase in the retention of both enantiomers (suggesting that binding is an endothermic, entropy-driven process) and an increase in separation.

Hsu et al. [94] also studied the effect of temperature on the K'_a values obtained for thymine binding to their thymine-imprinted diacryloyl-2,6-diaminopyridine-co-tripropyleneglcol diacrylate polymer films in chloroform, observed using IR as described in Sect. 3.6. The apparent binding strength decreased with an increase in temperature, and an exothermic ΔH and corresponding ΔS were calculated.

Guiochon et al. [56, 57, 60] also studied the influence of the temperature on the isotherms for Fmoc-Trp enantiomers on the Fmoc-L-Trp-imprinted MIP, via staircase frontal analysis with an MeCN–AcOH (99:1 v/v) mobile phase. ΔH, ΔS and kinetic parameters were calculated for the various classes of sites that appeared to contribute to the isotherms fitted with bi- and tri-Langmuir models. While it was concluded that binding overall was enthalpy-driven, the dominant driving force for transfer of the imprinted enantiomer to the strongest, most selective sites was proposed to be entropic.

5 Binding Site Affinity Distributions

The number of binding sites and their binding affinities are parameters in the Langmuir, bi-, tri- and multi-Langmuir isotherms; hence, when an isotherm is fitted using these models, a simplistic picture of the classes of sites (each class having a unique K_a and B_{max}) is immediately available. In reality, however, as explained in the introduction, there will not be distinct classes of binding sites but rather a continuum, from strong and selective sites present in small numbers to weaker and less selective sites present at far greater densities. Both the Freundlich and Langmuir-Freundlich isotherms allow for such a distribution of sites, and the number of sites B_i with a particular affinity constant K_{ai} can be calculated from the isotherm fitting and displayed as an *affinity distribution* (Fig. 18). These models are restrictive, however, in that the shape of the distribution is fixed (for the Freundlich isotherm, it is an exponentially decaying distribution starting with an infinite

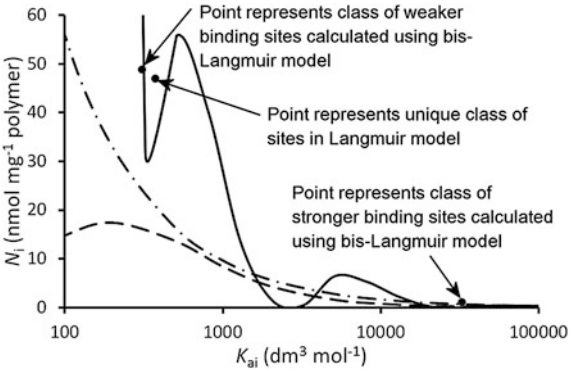

Fig. 18 Affinity distributions, calculated from *B–F* data for a caffeine-imprinted MIP as in Fig. 4 [23]. Curves for affinity distributions calculated using a numerical model without imposing an isotherm (*solid line*), or imposing Freundlich (*dot-dash*) and Langmuir-Freundlich (*dashed*) isotherms, all calculated and displayed using Microsoft Excel™. Step size $\ln K_{ai}$–$\ln K_{a(i-1)}$ for the Langmuir-Freundlich and numerical affinity spectra is 0.2

number of binding sites with $K_a = 0$; for Langmuir-Freundlich, it is a Gaussian distribution). An alternative approach involves converting the isotherm data directly to an affinity distribution without applying any fixed isotherm model; such an approach is valuable but depends on data of extremely high quality.

Shimizu et al. [114] were the first to calculate an affinity distribution from binding data for a MIP. The method is non-trivial. First, it is assumed that the concentration of bound ligand for a particular free ligand concentration is obtained by integration over all binding sites with differing affinities K_{ai} (Eq. 31):

$$B = \int_{-\infty}^{\infty} \frac{B_i \times F \times K_{ai}}{1 + K_{ai} \times F} d(\log K_{ai}) \tag{31}$$

This expression cannot be solved analytically for any particular set of B and F values. However, an approximate solution was developed by Hunston (Eqs. 32–36):

$$B_i = \left| \frac{B_1 - B_2}{2 \log \alpha} - \frac{\alpha \times ((B_3 - B_4) - 2(B_1 - B_2))}{2(\alpha - 1)^2 \times \log \alpha} \right| \tag{32}$$

Equation 32 gives the density of binding sites for a particular value of K_{ai} where

$$B_1 = B \quad \text{at } F = \frac{\alpha}{K_{ai}} \tag{33}$$

$$B_2 = B \quad \text{at } F = \frac{1}{\alpha \times K_{ai}} \tag{34}$$

$$B_3 = B \quad \text{at} \quad F = \frac{\alpha^2}{K_{\text{ai}}} \tag{35}$$

$$B_4 = B \quad \text{at } F = \frac{1}{\alpha^2 \times K_{\text{ai}}} \tag{36}$$

α is the step size [i.e., B_i is actually the density of binding sites with association constants in the interval B_i to $(B_i + \alpha)$]. The values B_1–B_4 must be interpolated from the calculated B–F data, and precise values are essential. To avoid imposing any model on the data, they are fitted using a smoothed spline. In this way, the values of B_i displayed in Fig. 18 are obtained. Note that the treatment has any validity only in the range $1/F_{\text{max}} \leq K_{\text{ai}} \leq 1/F_{\text{min}}$ where F_{max} and F_{min} are the highest and lowest values of F in the measured binding data. In this case, the numerical model interestingly produces a curve with two maxima, suggesting two broad site populations, which are not too different from the points corresponding to the two classes of binding sites calculated from the bis-Langmuir model.

An alternative method for solving Eq. 31 to produce an experimental affinity distribution without imposing any model on the B–F data has been described by Guiochon et al. [115].

More simply than the numerical methods, which make no assumptions of any particular isotherm, Eq. 31 can be solved analytically if a Freundlich isotherm is assumed [32], and while it cannot be solved analytically for the Langmuir-Freundlich isotherm, if B–F data are fitted to the Langmuir-Freundlich, then the fitted parameters can be used to calculate B_1–B_4 for differing values of K_{ai} in Eqs. 33–36 above [34] and

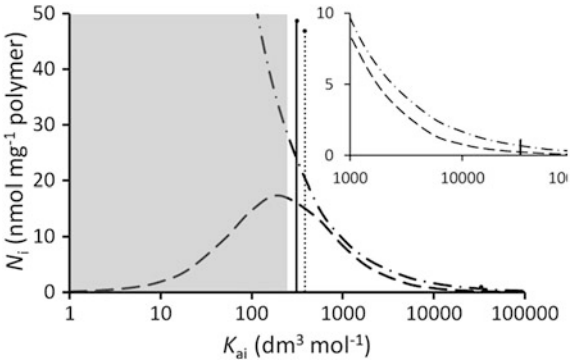

Fig. 19 Affinity distributions, calculated from B–F data for a caffeine-imprinted MIP as in Fig. 4 [23]. Curves for Freundlich (*dot-dash*) and Langmuir-Freundlich (*dashed*) isotherms calculated and displayed using Microsoft Excel™. *Dotted line* indicates the homogeneous binding site population predicted by the Langmuir isotherm, and *solid lines* the two homeogeneous populations predicted by the bi-Langmuir isotherm. *Inset* shows the values at high K_i, to emphasize the high-affinity sites in the bi-Langmuir approximation at $\sim$30,000 M^{-1}. Step size $\ln K_{\text{ai}}$–$\ln K_{\text{a}(i-1)}$ for the Langmuir-Freundlich isotherm is 0.2. The region where $K_{\text{ai}} < 1/F_{\text{min}}$, for which the fits are not really valid, is grayed out

hence the affinity distribution can be derived. These methods were used to derive the curves in Figs. 18 and 19. Clearly the Freundlich isotherm gives rise to an exponentially decaying distribution, while the Langmuir-Freundlich isotherm gives rise to a Gaussian distribution with a clear maximum. Of course, neither model is really valid in the range $K_{ai} < 1/F_{max}$ (in this case, $K_{ai} < 200\,M^{-1}$, the region grayed out in Fig. 11), and both models are in reasonable agreement at higher K_{ai}.

Batch rebinding data have been fitted to the Freundlich isotherm and converted to affinity distributions by Mizaikoff et al. [116], Diaz-Garcia et al. [38], and others. The alternative methods to derive affinity distributions have been reviewed by Shimizu et al. [30].

6 Conclusions

The binding properties of molecularly imprinted polymers have been reviewed, with particular emphasis on the binding/adsorption isotherm and on the methods used to characterize binding strength, selectivity and kinetics.

The defining characteristic of the binding sites in a MIP is heterogeneity, such that single-point measurements (i.e., studying binding using a unique concentration of analyte and amount of polymer) will always yield different values for the binding strength, selectivity and kinetics. Experimental capture of an isotherm is desirable, although it may not always be necessary if the MIP is being synthesized for a specific use and can easily be tested for efficacy in that application.

The detailed and extensive studies by Guiochon et al. have been exemplary in characterizing binding properties and their dependence on solvent composition and temperature. The simplistic model of one class of strong, selective sites and one of weak, non-selective sites has been shown to be a great simplification of the real situation, but remains a useful picture.

References

1. Andersson HS, Karlsson JG, Piletsky SA, Koch-Schmidt AC, Mosbach K, Nicholls IA (1999) Study of the nature of recognition in molecularly imprinted polymers, II 1—influence of monomer-template ratio and sample load on retention and selectivity. J Chromatogr A 848 (1–2):39–49. doi:10.1016/s0021-9673(99)00483-5
2. Katz A, Davis ME (1999) Investigations into the mechanisms of molecular recognition with imprinted polymers. Macromolecules 32(12):4113–4121. doi:10.1021/ma981445z
3. Baggiani C, Giraudi G, Giovannoli C, Tozzi C, Anfossi L (2004) Adsorption isotherms of a molecular imprinted polymer prepared in the presence of a polymerisable template—indirect evidence of the formation of template clusters in the binding site. Anal Chim Acta 504 (1):43–52. doi:10.1016/s0003-2670(03)00671-8
4. Lavignac N, Brain KR, Allender CJ (2006) Concentration dependent atrazine-atrazine complex formation promotes selectivity in atrazine imprinted polymers. Biosens Bioelectron 22(1):138–144. doi:10.1016/j.bios.2006.03.017

5. Kim H, Spivak DA (2003) New insight into modeling non-covalently imprinted polymers. J Am Chem Soc 125(37):11269–11275. doi:10.1021/ja0361502
6. Kobayashi T, Fukaya T, Abe M, Fujii N (2002) Phase inversion molecular imprinting by using template copolymers for high substrate recognition. Langmuir 18(7):2866–2872. doi:10.1021/la0106586
7. Yoshikawa M (2001) Molecularly imprinted polymeric membranes. Bioseparation 10 (6):277–286. doi:10.1023/a:1021537602663
8. Stahl M, Jeppssonwistrand U, Mansson MO, Mosbach K (1991) Induced stereo selectivity and substrate selectivity of bio-imprinted alpha-chymotrypsin in anhydrous organic media. J Am Chem Soc 113(24):9366–9368
9. Ansell RJ, Kuah KL (2005) Imprinted polymers for chiral resolution of (±)-ephedrine: understanding the pre-polymerisation equilibrium and the action of different mobile phase modifiers. Analyst 130(2):179–187. doi:10.1039/b408751h
10. Benito-Pena E, Urraca JL, Sellergren B, Cruz Moreno-Bondi M (2008) Solid-phase extraction of fluoroquinolones from aqueous samples using a water-compatible stochiometrically imprinted polymer. J Chromatogr A 1208(1–2):62–70. doi:10.1016/j.chroma.2008.08.109
11. Hall AJ, Manesiotis P, Emgenbroich M, Quaglia M, De Lorenzi E, Sellergren B (2005) Urea host monomers for stoichiometric molecular imprinting of oxyanions. J Org Chem 70 (5):1732–1736. doi:10.1021/jo048470p
12. Lubke C, Lubke M, Whitcombe MJ, Vulfson EN (2000) Imprinted polymers prepared with stoichiometric template-monomer complexes: efficient binding of ampicillin from aqueous solutions. Macromolecules 33(14):5098–5105. doi:10.1021/ma000467u
13. Manesiotis P, Osmani Q, McLoughlin P (2012) An enantio-selective chromatographic stationary phase for S-ibuprofen prepared by stoichiometric molecular imprinting. J Mater Chem 22(22):11201–11207. doi:10.1039/c2jm16659c
14. Urraca JL, Hall AJ, Moreno-Bondi MC, Sellergren B (2006) A stoichiometric molecularly imprinted polymer for the class-selective recognition of antibiotics in aqueous media. Angew Chem Int Ed 45(31):5158–5161. doi:10.1002/anie.200601636
15. Wulff G, Knorr K (2001) Stoichiometric noncovalent interaction in molecular imprinting. Bioseparation 10(6):257–276. doi:10.1023/a:1021585518592
16. Pap T, Horvai G (2004) Binding assays with molecularly imprinted polymers—why do they work? J Chromatogr B Anal Technol Biomed and Life Sci 804(1):167–172
17. Baggiani C, Giovannoli C, Anfossi L, Passini C, Baravalle P, Giraudi G (2012) A connection between the binding properties of imprinted and nonimprinted polymers: a change of perspective in molecular imprinting. J Am Chem Soc 134(3):1513–1518. doi:10.1021/ja205632t
18. Toth B, Pap T, Horvath V, Horvai G (2006) Nonlinear adsorption isotherm as a tool for understanding and characterizing molecularly imprinted polymers. J Chromatogr A 1119(1–2):29–33. doi:10.1016/j.chroma.2005.10.048
19. Toth B, Pap T, Horvath V, Horvai G (2007) Which molecularly imprinted polymer is better? Anal Chim Acta 591(1):17–21. doi:10.1016/j.aca.2007.01.016
20. Castell OK, Barrow DA, Kamarudin AR, Allender CJ (2011) Current practices for describing the performance of molecularly imprinted polymers can be misleading and may be hampering the development of the field. J Mol Recognit 24(6):1115–1122. doi:10.1002/jmr.1161
21. Castell OK, Allender CJ, Barrow DA (2006) Novel biphasic separations utilising highly selective molecularly imprinted polymers as biorecognition solvent extraction agents. Biosens Bioelectron 22(4):526–533. doi:10.1016/j.bios.2006.07.017
22. Garcia-Calzon JA, Diaz-Garcia ME (2007) Characterization of binding sites in molecularly imprinted polymers. Sens Actuators B Chem 123(2):1180–1194. doi:10.1016/j.snb.2006.10.068
23. Ansell RJ, Gamlien A, Berglund J, Mosbach K, Haupt K. Binding data for a caffeine-imprinted polymer obtained radioligand binding assay (Unpublished work)
24. Norby JG, Ottolenghi P, Jensen J (1980) Scatchard plot—common misinterpretation of binding experiments. Anal Biochem 102(2):318–320. doi:10.1016/0003-2697(80)90160-8

25. Vlatakis G, Andersson L, Müller R, Mosbach K (1993) Drug assay using antibody mimics made by molecular imprinting. Nature 361:645–647
26. Andersson LI, Muller R, Vlatakis G, Mosbach K (1995) Mimics of the binding sites of opioid receptors obtained by molecular imprinting of enkephalin and morphine. Proc Natl Acad Sci USA 92(11):4788–4792. doi:10.1073/pnas.92.11.4788
27. Lehmann M, Dettling M, Brunner H, Tovar GEM (2004) Affinity parameters of amino acid derivative binding to molecularly imprinted nanospheres consisting of poly (ethylene glycol dimethacrylate)-co-(methacrylic acid). J Chromatogr B Anal Technol Biomed Life Sci 808 (1):43–50. doi:10.1016/j.jchromb.2004.03.068
28. Li H, Nie LH, Yao SZ (2004) Adsorption isotherms and sites distribution of caffeic acid—imprinted polymer monolith from frontal analysis. Chromatographia 60(7–8):425–431. doi:10.1365/s10337-004-0403-9
29. Sajonz P, Kele M, Zhong G, Sellergren B, Guiochon G (1998) Study of the thermodynamics and mass transfer kinetics of two enantiomers on a polymeric imprinted stationary phase. J Chromatogr A 810(1–2):1–17
30. Umpleby RJ, Baxter SC, Rampey AM, Rushton GT, Chen YZ, Shimizu KD (2004) Characterization of the heterogeneous binding site affinity distributions in molecularly imprinted polymers. J Chromatogr B Anal Technol Biomed Life Sci 804(1):141–149. doi:10.1016/j.jchromb.2004.01.064
31. Umpleby RJ, Baxter SC, Bode M, Berch JK, Shah RN, Shimizu KD (2001) Application of the Freundlich adsorption isotherm in the characterization of molecularly imprinted polymers. Anal Chim Acta 435(1):35–42. doi:10.1016/s0003-2670(00)01211-3
32. Rampey AM, Umpleby RJ, Rushton GT, Iseman JC, Shah RN, Shimizu KD (2004) Characterization of the imprint effect and the influence of imprinting conditions on affinity, capacity, and heterogeneity in molecularly imprinted polymers using the Freundlich isotherm-affinity distribution analysis. Anal Chem 76(4):1123–1133. doi:10.1021/ac0345345
33. Rushton GT, Karns CL, Shimizu KD (2005) A critical examination of the use of the Freundlich isotherm in characterizing molecularly imprinted polymers (MLPs). Anal Chim Acta 528(1):107–113. doi:10.1016/j.aca.2004.07.048
34. Umpleby RJ, Baxter SC, Chen YZ, Shah RN, Shimizu KD (2001) Characterization of molecularly imprinted polymers with the Langmuir-Freundlich isotherm. Anal Chem 73 (19):4584–4591. doi:10.1021/ac0105686
35. Tamayo FG, Casillas JL, Martin-Esteban A (2003) Highly selective fenuron-imprinted polymer with a homogeneous binding site distribution prepared by precipitation polymerization and its application to the clean-up of fenuron in plant samples. Anal Chim Acta 482(2):165–173. doi:10.1016/s0003-2670(03)00213-7
36. Cacho C, Turiel E, Martin-Esteban A, Perez-Conde C, Camara C (2004) Characterisation and quality assessment of binding sites on a propazine-imprinted polymer prepared by precipitation polymerisation. J Chromatogr B Anal Technol Biomed Life Sci 802(2):347–353. doi:10.1016/j.jchromb.2003.12.018
37. Turiel E, Perez-Conde C, Martin-Esteban A (2003) Assessment of the cross-reactivity and binding sites characterisation of a propazine-imprinted polymer using the Langmuir-Freundlich isotherm. Analyst 128(2):137–141. doi:10.1039/b210712k
38. Corton E, Garcia-Calzon JA, Diaz-Garcia ME (2007) Kinetics and binding properties of cloramphenicol imprinted polymers. J Non Cryst Solids 353(8–10):974–980. doi:10.1016/j.jnoncrysol.2006.12.066
39. Wulff G, Grobeeinsler R, Vesper W, Sarhan A (1977) Enzyme-analogue built polymers, 5. Specificity distribution of chiral cavities prepared in synthetic polymers. Makromol Chem Macromol Chem Phys 178(10):2817–2825
40. Shea KJ, Spivak DA, Sellergren B (1993) Polymer complements to nucleotide bases—selective binding of adenine-derivatives to imprinted polymers. J Am Chem Soc 115 (8):3368–3369. doi:10.1021/ja00061a061

41. Guo TY, Xia YQ, Hao GJ, Song MD, Zhang BH (2004) Adsorptive separation of hemoglobin by molecularly imprinted chitosan beads. Biomaterials 25(27):5905–5912. doi:10.1016/j.biomaterials.2004.01.032
42. Ju JY, Shin CS, Whitcombe MJ, Vulfson EN (1999) Binding properties of an aminostyrene-based polymer imprinted with glutamylated monascus pigments. Biotechnol Tech 13 (10):665–669. doi:10.1023/a:1008955528251
43. Mathew J, Buchardt O (1995) Molecular imprinting approach for the recognition of adenine in aqueous medium and hydrolysis of adenosine 5′-triphosphate. Bioconjugate Chemistry 6 (5):524–528. doi:10.1021/bc00035a004
44. Milojkovic SS, Kostoski D, Comor JJ, Nedeljkovic JM (1997) Radiation induced synthesis of molecularly imprinted polymers. Polymer 38(11):2853–2855. doi:10.1016/s0032-3861(97)85624-8
45. Puzio K, Delepee R, Vidal R, Agrofoglio LA (2013) Combination of computational methods, adsorption isotherms and selectivity tests for the conception of a mixed non-covalent-semi-covalent molecularly imprinted polymer of vanillin. Anal Chim Acta 790:47–55. doi:10.1016/j.aca.2013.06.036
46. Song D, Zhang Y, Geer MF, Shimizu KD (2014) Characterization of molecularly imprinted polymers using a new polar solvent titration method. J Mol Recognit 27(7):448–457. doi:10.1002/jmr.2365
47. Malosse L, Palmas P, Buvat P, Adès D, Siove A (2008) Novel stoichiometric, noncovalent pinacolyl methylphosphonate imprinted polymers: a rational design by NMR spectroscopy. Macromolecules 41(21):7834–7842. doi:10.1021/ma801171g
48. Yilmaz E, Mosbach K, Haupt K (1999) Influence of functional and cross-linking monomers and the amount of template on the performance of molecularly imprinted polymers in binding assays. Anal Commun 36(5):167–170. doi:10.1039/a901339c
49. Wei ST, Molinelli A, Mizaikoff B (2006) Molecularly imprinted micro and nanospheres for the selective recognition of 17 beta-estradiol. Biosens Bioelectron 21(10):1943–1951. doi:10.1016/j.bios.2005.09.017
50. Sellergren B (2001) Imprinted chiral stationary phases in high-performance liquid chromatography. J Chromatogr A 906(1–2):227–252. doi:10.1016/s0021-9673(00)00929-8
51. Sellergren B, Lepisto M, Mosbach K (1988) Highly enantioselective and substrate-selective polymers obtained by molecular imprinting utilizing noncovalent interactions—NMR and chromatographic studies on the nature of recognition. J Am Chem Soc 110(17):5853–5860. doi:10.1021/ja00225a041
52. Lei JD, Tan TW (2002) Enantioselective separation of naproxen and investigation of affinity chromatography model using molecular imprinting. Biochem Eng J 11(2–3):175–179. doi:10.1016/s1369-703x(02)00022-0
53. Sun RF, Yu HM, Luo H, Shen ZY (2004) Construction and application of a stoichiometric displacement model for retention in chiral recognition of molecular imprinting. J Chromatogr A 1055(1–2):1–9. doi:10.1016/j.chroma.2004.08.161
54. Kuah KL, Ansell RJ. Zonal chromatography on a (-)-ephedrine imprinted chiral stationary phase (Unpublished work)
55. Sellergren B, Shea K (1995) Origin of peak asymmetry and the effect of temperature on solute retention in enantiomer separations on imprinted chiral stationary phases. J Chromatogr A 690:29–39
56. Kim H, Guiochon G (2005) Thermodynamic functions and intraparticle mass transfer kinetics of structural analogues of a template on molecularly imprinted polymers in liquid chromatography. J Chromatogr A 1097(1–2):84–97. doi:10.1016/j.chroma.2005.08.020
57. Kim H, Kaczmarski K, Guiochon G (2005) Mass transfer kinetics on the heterogeneous binding sites of molecularly imprinted polymers. Chem Eng Sci 60(20):5425–5444. doi:10.1016/j.ces.2005.04.057
58. Kim H, Kaczmarski K, Guiochon G (2006) Isotherm parameters and intraparticle mass transfer kinetics on molecularly imprinted polymers in acetonitrile/buffer mobile phases. Chem Eng Sci 61(16):5249–5267. doi:10.1016/j.ces.2006.03.043

59. Kim H, Kaczmarski K, Guiochon G (2006) Intraparticle mass transfer kinetics on molecularly imprinted polymers of structural analogues of a template. Chem Eng Sci 61 (4):1122–1137. doi:10.1016/j.ces.2005.08.012
60. Kim HJ, Kaczmarski K, Guiochon G (2006) Thermodynamic analysis of the heterogenous binding sites of molecularly imprinted polymers. J Chromatogr A 1101(1–2):136–152. doi:10.1016/j.chroma.2005.09.092
61. Toth B, Laszlo K, Horvai G (2005) Chromatographic behavior of silica-polymer composite molecularly imprinted materials. J Chromatogr A 1100(1):60–67. doi:10.1016/j.chroma.2005.09.015
62. Seebach A, Seidel-Morgenstern A (2007) Enantioseparation on molecularly imprinted monoliths—preparation and adsorption isotherms. Anal Chim Acta 591(1):57–62. doi:10.1016/j.aca.2007.02.059
63. Baggiani C, Baravalle P, Anfossi L, Tozzi C (2005) Comparison of pyrimethanil-imprinted beads and bulk polymer as stationary phase by non-linear chromatography. Anal Chim Acta 542(1):125–134. doi:10.1016/j.aca.2004.10.088
64. Lee W-C, Cheng C-H, Pan H-H, Chung T-H, Hwang C-C (2008) Chromatographic characterization of molecularly imprinted polymers. Anal Bioanal Chem 390(4):1101–1109. doi:10.1007/s00216-007-1765-2
65. Chaiken IM (1986) Analytical affinity chromatography in studies of molecular recognition in biology—a review. J Chromatogr 376:11–32. doi:10.1016/s0378-4347(00)80821-x
66. Kasai K, Oda Y, Nishikata M, Ishii S (1986) Frontal affinity chromatography—theory for its application to studies on specific interactions of biomolecules. J Chromatogr 376:33–47. doi:10.1016/s0378-4347(00)80822-1
67. Calleri E, Temporini C, Massolini G (2011) Frontal affinity chromatography in characterizing immobilized receptors. J Pharm Biomed Anal 54(5):911–925. doi:10.1016/j.jpba.2010.11.040
68. Ramstrom O, Nicholls IA, Mosbach K (1994) Synthetic peptide receptor mimics—highly stereoselective recognition in noncovalent molecularly imprinted polymers. Tetrahedron-Asymmetry 5(4):649–656. doi:10.1016/0957-4166(94)80027-8
69. Kempe M, Mosbach K (1991) Binding-studies on substrate- and enantio-selective molecularly imprinted polymers. Anal Lett 24(7):1137–1145
70. Andersson HS, KochSchmidt AC, Ohlson S, Mosbach K (1996) Study of the nature of recognition in molecularly imprinted polymers. J Mol Recognit 9(5–6):675–682. doi:10.1002/(sici)1099-1352(199634/12)9:5/6<675:AID-JMR320>3.0.CO;2-c
71. Baggiani C, Giovannoli C, Anfossi L, Tozzi C (2001) Molecularly imprinted solid-phase extraction sorbent for the clean-up of chlorinated phenoxyacids from aqueous samples. J Chromatogr A 938(1–2):35–44. doi:10.1016/s0021-9673(01)01126-8
72. Baggiani C, Trotta F, Giraudi G, Moraglio G, Vanni A (1997) Chromatographic characterization of a molecularly imprinted polymer binding theophylline in aqueous buffers. J Chromatogr A 786(1):23–29. doi:10.1016/s0021-9673(97)00537-2
73. Meng ZH, Zhou LM, Wang JF, Wang QH, Zhu DQ (1999) Molecule imprinting chiral stationary phase. Biomed Chromatogr 13(6):389–393. doi:10.1002/(sici)1099-0801(199910)13:6<389:AID-BMC897>3.3.CO;2-h
74. Liu HY, Yang GL, Liu SB, Wang MM, Chen Y (2005) Molecular recognition properties and adsorption isotherms of diniconaziole-imprinted polymers. J Liq Chromatogr Relat Technol 28(15):2315–2323. doi:10.1080/10826070500187509
75. Chen YB, Kele M, Sajonz P, Sellergren B, Guiochon G (1999) Influence of thermal annealing on the thermodynamic and mass transfer kinetic properties of D- and L-phenylalanine anilide on imprinted polymeric stationary phases. Anal Chem 71(5):928–938. doi:10.1021/ac981154o
76. Szabelski P, Kaczmarski K, Cavazzini A, Chen YB, Sellergren B, Guiochon G (2002) Energetic heterogeneity of the surface of a molecularly imprinted polymer studied by high-performance liquid chromatography. J Chromatogr A 964(1–2):99–111

77. Chen YB, Kele M, Quinones I, Sellergren B, Guiochon G (2001) Influence of the pH on the behavior of an imprinted polymeric stationary phase—supporting evidence for a binding site model. J Chromatogr A 927(1–2):1–17
78. Kim HJ, Guiochon G (2005) Thermodynamic studies of the solvent effects in chromatography on molecularly imprinted polymers, 3. Nature of the organic mobile phase. Anal Chem 77(8):2496–2504. doi:10.1021/ac040171c
79. Kim H, Guiochon G (2005) Thermodynamic studies on the solvent effects in chromatography on molecularly imprinted polymers, 1. Nature of the organic modifier. Anal Chem 77(6):1708–1717. doi:10.1021/ac040155f
80. Kim H, Guiochon G (2005) Thermodynamic studies on solvent effects in molecularly imprinted polymers, 2. Concentration of the organic modifier. Anal Chem 77(6):1718–1726. doi:10.1021/ac040164o
81. Kim HJ, Guiochon G (2005) Comparison of the thermodynamic properties of particulate and monolithic columns of molecularly imprinted copolymers. Anal Chem 77(1):93–102. doi:10.1021/ac0401218
82. Kim H, Guiochon G (2005) Adsorption on molecularly imprinted polymers of structural analogues of a template. Single-component adsorption isotherm data. Anal Chem 77 (19):6415–6425. doi:10.1021/ac050914+
83. Miyabe K, Guiochon G (2003) Measurement of the parameters of the mass transfer kinetics in high performance liquid chromatography. J Sep Sci 26(3–4):155–173. doi:10.1002/jssc.200390024
84. Chen WY, Chen CS, Lin FY (2001) Molecular recognition in imprinted polymers: thermodynamic investigation of analyte binding using microcalorimetry. J Chromatogr A 923(1–2):1–6. doi:10.1016/s0021-9673(01)00971-2
85. Dvorakova G, Haschick R, Chiad K, Klapper M, Muellen K, Biffis A (2010) Molecularly imprinted nanospheres by nonaqueous emulsion polymerization. Macromol Rapid Commun 31(23):2035–2040. doi:10.1002/marc.201000406
86. Hsu C-Y, Lin H-Y, Thomas JL, Wu B-T, Chou T-C (2006) Incorporation of styrene enhances recognition of ribonuclease A by molecularly imprinted polymers. Biosens Bioelectron 22(3):355–363. doi:10.1016/j.bios.2006.05.008
87. Kimhi O, Bianco-Peled H (2007) Study of the interactions between protein-imprinted hydrogels and their templates. Langmuir 23(11):6329–6335. doi:10.1021/la700248s
88. Kirchner R, Seidel J, Wolf G, Wulff G (2002) Calorimetric investigation of chiral recognition processes in a molecularly imprinted polymer. J Incl Phenom Macrocycl Chem 43(3–4):279–283. doi:10.1023/a:1021243826862
89. Manesiotis P, Hall AJ, Courtois J, Irgum K, Sellergren B (2005) An artificial riboflavin receptor prepared by a template analogue imprinting strategy. Angew Chem Int Ed 44 (25):3902–3906. doi:10.1002/anie.200500342
90. Weber A, Dettling M, Brunner H, Tovar GEM (2002) Isothermal titration calorimetry of molecularly imprinted polymer nanospheres. Macromol Rapid Commun 23(14):824–828. doi:10.1002/1521-3927(20021001)23:14<824:aid-marc824>3.0.co;2-p
91. Rick J, Chou TC (2005) Imprinting unique motifs formed from protein-protein associations. Anal Chim Acta 542(1):26–31. doi:10.1016/j.aca.2004.12.051
92. Rick J, Chou TC (2005) Enthalpy changes associated with protein binding to thin films. Biosens Bioelectron 20(9):1878–1883. doi:10.1016/j.bios.2004.11.015
93. Tamayo FG, Casillas JL, Martin-Esteban A (2005) Evaluation of new selective molecularly imprinted polymers prepared by precipitation polymerization for the extraction of phenylurea herbicides. J Chromatogr A 1069(2):173–181. doi:10.1016/j.chroma.2005.02.029
94. Duffy DJ, Das K, Hsu SL, Penelle J, Rotello VM, Stidham HD (2002) Binding efficiency and transport properties of molecularly imprinted polymer thin films. J Am Chem Soc 124 (28):8290–8296. doi:10.1021/ja0201146

95. Pasetto P, Flavin K, Resmini M (2009) Simple spectroscopic method for titration of binding sites in molecularly imprinted nanogels with hydrolase activity. Biosens Bioelectron 25(3): 572–578. doi:10.1016/j.bios.2009.03.042
96. Bompart M, Gheber LA, De Wilde Y, Haupt K (2009) Direct detection of analyte binding to single molecularly imprinted polymer particles by confocal Raman spectroscopy. Biosens Bioelectron 25(3):568–571. doi:10.1016/j.bios.2009.01.020
97. Muk NS, Narayanaswamy R (2011) Molecularly imprinted polymers as optical sensing receptors: correlation between analytical signals and binding isotherms. Anal Chim Acta 703 (2):226–233. doi:10.1016/j.aca.2011.07.032
98. Yoshikawa M, Guiver MD, Robertson GP (2008) Surface plasmon resonance studies on molecularly imprinted films. J Appl Polym Sci 110(5):2826–2832. doi:10.1002/app.28686
99. Diltemiz SE, Hur D, Ersoz A, Denizli A, Say R (2009) Designing of MIP based QCM sensor having thymine recognition sites based on biomimicking DNA approach. Biosens Bioelectron 25(3):599–603. doi:10.1016/j.bios.2009.01.032
100. Diltemiz SE, Hur D, Kecili R, Ersoz A, Say R (2013) New synthesis method for 4-MAPBA monomer and using for the recognition of IgM and mannose with MIP-based QCM sensors. Analyst 138(5):1558–1563. doi:10.1039/c2an36291k
101. El Kirat K, Bartkowski M, Haupt K (2009) Probing the recognition specificity of a protein molecularly imprinted polymer using force spectroscopy. Biosens Bioelectron 24(8):2618–2624. doi:10.1016/j.bios.2009.01.018
102. El-Sharif HF, Hawkins DM, Stevenson D, Reddy SM (2014) Determination of protein binding affinities within hydrogel-based molecularly imprinted polymers (HydroMIPs). Phys Chem Chem Phys 16(29):15483–15489. doi:10.1039/c4cp01798f
103. Levi L, Raim V, Srebnik S (2011) A brief review of coarse-grained and other computational studies of molecularly imprinted polymers. J Mol Recognit 24(6):883–891. doi:10.1002/jmr.1135
104. Ansell RJ, Wang D (2009) Imprinted polymers for chiral resolution of (±)-ephedrine. Part 3: NMR predictions and HPLC results with alternative functional monomers. Analyst 134 (3):564–576. doi:10.1039/b815145h
105. Ansell RJ, Wang D, Kuah JKL (2008) Imprinted polymers for chiral resolution of (±)-ephedrine. Part 2: probing pre-polymerization equilibria in different solvents by NMR. Analyst 133(12):1673–1683. doi:10.1039/b806376a
106. Schillinger E, Moeder M, Olsson GD, Nicholls IA, Sellergren B (2012) An artificial estrogen receptor through combinatorial imprinting. Chem Eur J 18(46):14773–14783. doi:10.1002/chem.201201428
107. Meier F, Schott B, Riedel D, Mizaikoff B (2012) Computational and experimental study on the influence of the porogen on the selectivity of 4-nitrophenol molecularly imprinted polymers. Anal Chim Acta 744:68–74. doi:10.1016/j.aca.2012.07.020
108. Denderz N, Lehotay J, Cizmarik J, Cibulkova Z, Simon P (2012) Thermodynamic study of molecularly imprinted polymer used as the stationary phase in high performance liquid chromatography. J Chromatogr A 1235:77–83. doi:10.1016/j.chroma.2012.02.051
109. Rosengren AM, Golker K, Karlsson JG, Nicholls IA (2009) Dielectric constants are not enough: principal component analysis of the influence of solvent properties on molecularly imprinted polymer-ligand rebinding. Biosens Bioelectron 25(3):553–557. doi:10.1016/j.bios.2009.06.042
110. Andersson LI (1996) Application of molecular imprinting to the development of aqueous buffer and organic solvent based radioligand binding assays for (S)-propranolol. Anal Chem 68(1):111–117. doi:10.1021/ac950668+
111. Haupt K, Mayes AG, Mosbach K (1998) Herbicide assay using an imprinted polymer based system analogous to competitive fluoroimmunoassays. Anal Chem 70(18):3936–3939. doi:10.1021/ac980175f
112. Dong XC, Sun H, Lu XY, Wang HB, Liu SX, Wang N (2002) Separation of ephedrine stereoisomers by molecularly imprinted polymers—influence of synthetic conditions and

mobile phase compositions on the chromatographic performance. Analyst 127(11):1427–1432. doi:10.1039/b202295h
113. Sellergren B, Shea KJ (1993) Chiral ion-exchange chromatography—correlation between solute retention and a theoretical ion-exchange model using imprinted polymers. J Chromatogr A 654(1):17–28. doi:10.1016/0021-9673(93)83061-v
114. Umpleby RJ, Bode M, Shimizu KD (2000) Measurement of the continuous distribution of binding sites in molecularly imprinted polymers. Analyst 125(7):1261–1265. doi:10.1039/b002354j
115. Stanley BJ, Szabelski P, Chen YB, Sellergren B, Guiochon G (2003) Affinity distributions of a molecularly imprinted polymer calculated numerically by the expectation-maximization method. Langmuir 19(3):772–778. doi:10.1021/la020747y
116. Wei S, Jakusch M, Mizaikoff B (2007) Investigating the mechanisms of 17 beta-estradiol imprinting by computational prediction and spectroscopic analysis. Anal Bioanal Chem 389 (2):423–431. doi:10.1007/s00216-007-1358-0

Adv Biochem Eng Biotechnol (2015) 150: 95–106
DOI 10.1007/10_2015_314

Published Online: 22 March 2015

Post-imprinting and In-Cavity Functionalization

Toshifumi Takeuchi, Hirobumi Sunayama, Eri Takano and Yukiya Kitayama

Abstract Molecularly imprinted polymers (MIPs) are artificial materials capable of molecular recognition for target molecules. Currently MIPs have been prepared without further modification after polymerization, and used for predetermined single purposes. Post-imprinting modifications (PIMs) presented here can provide site-specific modifications within the molecularly imprinted binding cavities after polymerization, enabling MIPs to become more complex functional materials as were the cases of naturally occurring conjugated proteins. We present an overview of the research on MIPs involving PIMs, including transformation of binding sites, on/off switching of binding activity, introduction of desirable functions such as fluorescent signalling functions, catalytic activity, and so on. The combination of PIMs with molecular imprinting appears to be a powerful tool for preparing a diverse range of biomimetic functional materials.

Keywords Artificial receptor · Molecularly imprinted polymer · Post-imprinting modification · Protein mimics · Reconstruction of binding cavity · Tunable binding sites

Contents

T. Takeuchi (✉) · H. Sunayama · E. Takano · Y. Kitayama
Graduate School of Engineering, Kobe University, 1-1 Rokkodai-cho, Nada-ku, Kobe 657-8501, Japan
e-mail: takeuchi@gold.kobe-u.ac.jp

1 Introduction

In nature, biomacromolecules, including enzymes and antibodies, perform a multitude of functions, and have attracted attention for their almost unlimited capability as bio-based functional materials. One of the unique features of biomacromolecules is that complicated biofunctions can be performed and/or are activated by conjugating nonprotein cofactors, including metal ions and small molecules, within or near their active sites [1]. For example, Zn^{2+} ions are bound by carbonic anhydrase to activate the catalytic function, and pyridoxal phosphate is bound by glycogen phosphorylase for activation. Such phenomena naturally occur in organisms under autonomous control to maintain necessary biological functions.

Molecularly imprinted polymers (MIPs) [2–6] have been prepared as monofunctioned materials for single-purpose use. Therefore, with post-polymerization modifications, MIPs could be exploited for use in more complex functional materials. Efforts have been made to develop post-imprinting modifications (PIMs), which are defined as site-specific modifications within the molecularly imprinted binding cavities after polymerization (Fig. 1). The technique is a powerful tool for

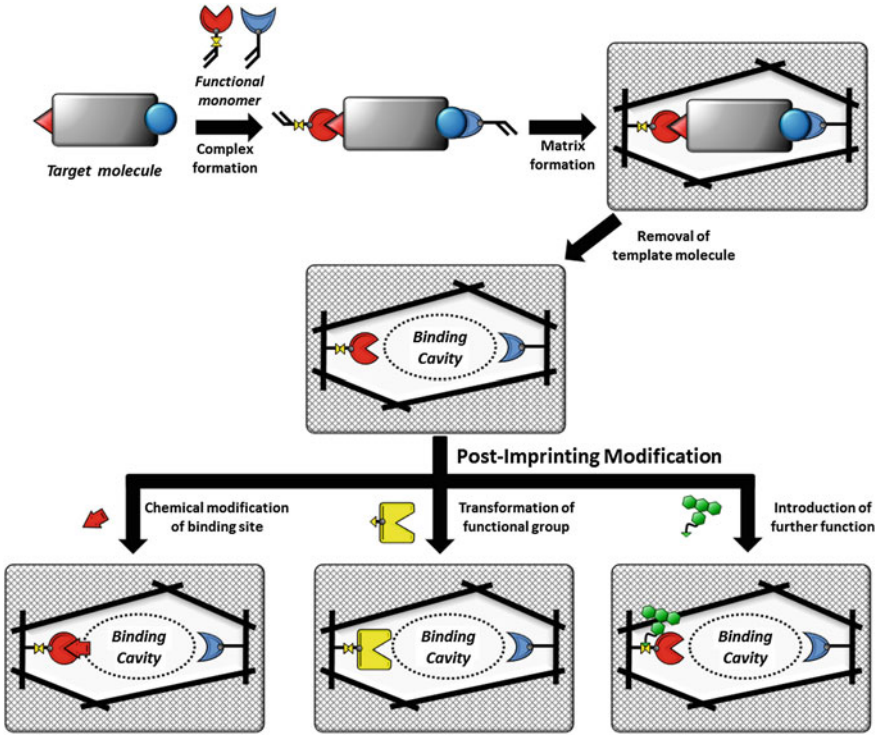

Fig. 1 Schematic illustration of MIPs and PIMs of the binding cavities of MIPs

realizing the preparation of mimics of biologically important functional macromolecules such as conjugated proteins.

In this chapter, we overview the research on MIPs involving PIMs, and provide several fascinating points of this technique, including transformation of binding sites in molecular recognition cavities, introduction of additional functions, and conjugated protein mimics. Early PIMs-related research published before 2001 has been reviewed elsewhere [7].

2 Transformation of Binding Sites in Molecular Recognition Cavities

The binding sites in molecularly imprinted cavities play a critical role in molecular recognition, because binding activity is strongly dependent upon the interaction between target molecules and the binding sites within the cavity. In this section, we overview important examples of PIMs that transform functional groups within molecular recognition cavities.

Takeuchi et al. [8] successfully produced dopamine recognition-MIPs bearing two-point binding sites in a cavity utilizing the designed dummy template molecule, (5-[2-(allyldithio)ethyl]-2-(4-vinylphenyl)benzo[1,3,2]dioxaborole) (Fig. 2), in which a disulfide and a phenylboronic acid cyclic diester were aligned, where the dummy template molecule is defined as a structurally related analogue of the target molecule. The dummy template molecule was copolymerized with styrene and divinylbenzene (DVB), and then the phenylboronic acid cyclic diester and the disulfide linkage were cleaved by hydrolysis and reduced to obtain binding cavities possessing both phenylboronic acid and thiol residues. Oxidative transformation of the thiol group into sulfonic acid was performed, yielding a site with strong interaction toward the amino

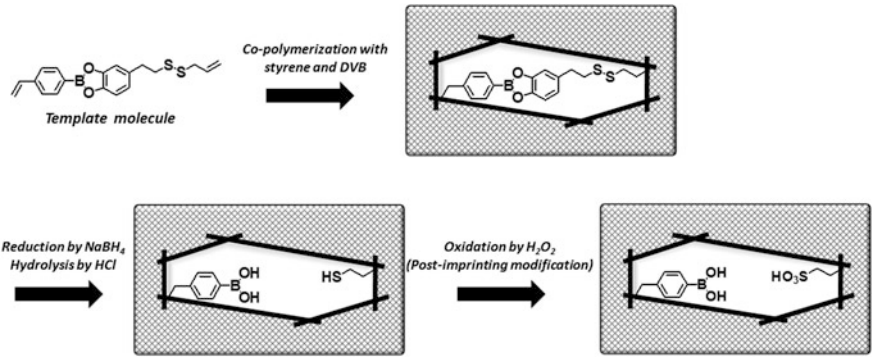

Fig. 2 Schematic illustration of preparation of MIPs for dopamine via PIMs

group of dopamine only inside the binding cavity, which synergistically facilitated dopamine binding with the phenylboronic acid residue, which was capable of cyclic diester formation with the catechol moiety of dopamine. In chromatographic analysis with MIPs as separation media, the dopamine retention factor dramatically increased, becoming 400 times greater than that of the MIP before oxidation. When selectivity was investigated using tyramine, catechol, 3,4-dihydroxyphenylacetic acid, homovanillic acid, epinephrine, and norepinephrin as reference compounds, dopamine was found to have the highest affinity. Thus, the activity of the MIP was significantly improved by employing the PIMs.

Binding site transformation in molecular recognition cavities by PIMs has also been applied to the preparation of molecularly imprinted catalysts (MICs). Yane et al. reported an acid MIC for methanolysis of atrazine, a triazine herbicide that is harmful to humans (Fig. 3) [9]. Methanolysis of atrazine transforms it into the less-toxic atraton by replacing the 6-position Cl with OCH_3. For this purpose, a dummy template molecule was designed with the following important properties: (i) creation of atrazine recognition cavities using a molecular imprinting process, and (ii) introduction of a catalytic site inside the imprinted cavity only, using PIMs, comprised of the atrazine structure and a styryl or an allyl group via a disulfide linker at the 6-position. The MIC was prepared using the following process. First, the designed template molecule, methacrylic acid, styrene, and DVB were copolymerized, and then the disulfide linker of the copolymerized template molecule residues was reduced with $NaBH_4$ to remove the atrazine moiety, yielding an

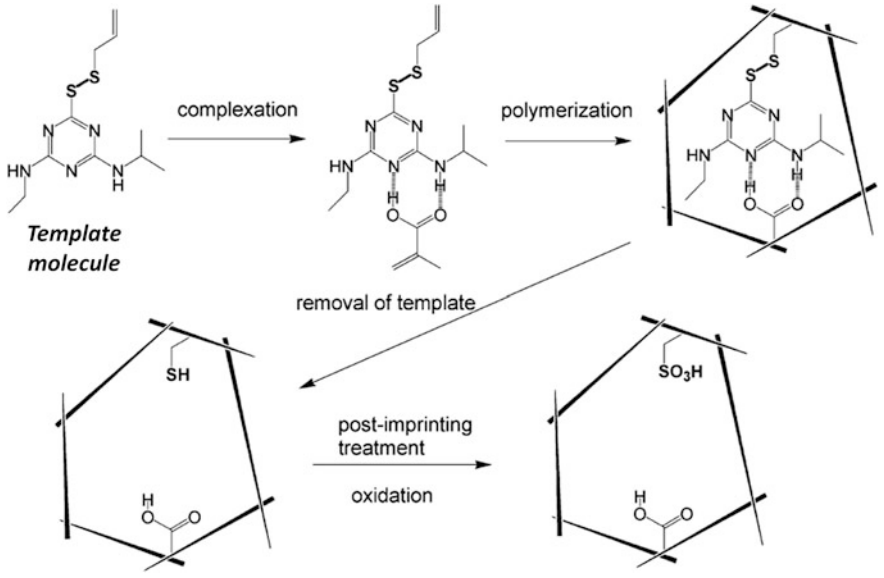

Fig. 3 Schematic illustration of the preparation of a molecularly imprinted catalyst (MIC) for atrazine transformation (reproduced from Ref. [9] with permission from The Royal Society of Chemistry)

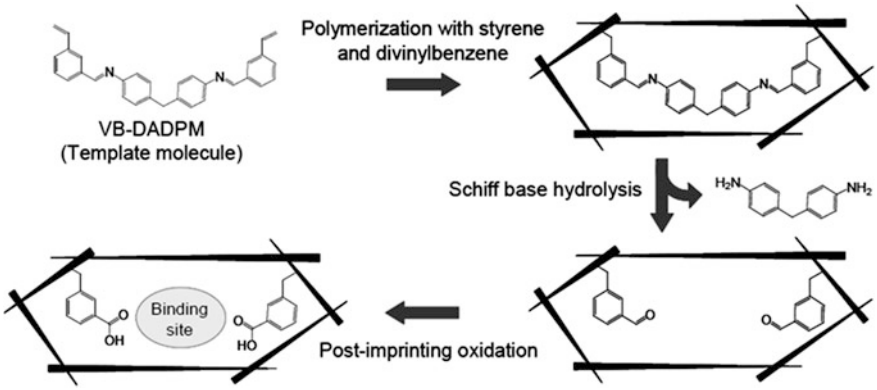

Fig. 4 Schematic illustration of preparation of a bisphenol A (BPA)-imprinted polymer using a dummy template (VB-DADPM) and post-imprinting oxidation to generate the interacting sites (reproduced from Ref. [10] with permission from Taylor & Francis)

atrazine-imprinted cavity. The following oxidation transformed the thiol residue into sulfonic acid via post-imprinting H_2O_2 treatment, in order to construct an acid catalytic site within the atrazine-binding cavity. The resulting MIC showed selective adsorption behavior for atrazine and other triazine herbicides compared to other types of pesticides, and catalytic activity for the methanolysis of atrazine with Michaelis–Menten kinetics-like behavior.

As another example of oxidative PIMs, Takano et al. reported MIPs for bisphenol A (BPA), a well-known endocrine disruptor, prepared using a dummy template containing Schiff base linkage (Fig. 4) [10]. A dummy template molecule, *N*,*N*′-bis(3-vinylbenzylidene)-4,4′-diaminodiphenylmethane (VB-DADPM), containing two Schiff bases comprised of 3-formyl styrenes and diaminophenylmethane was designed. After copolymerization with styrene and DVB, the Schiff bases were hydrolyzed, yielding two benzaldehyde residues in the imprinted cavity. Then an oxidative post-imprinting transformation from aldehyde to carboxylic acid was performed by H_2O_2 treatment to obtain a binding cavity in which two benzoic acid moieties were located at suitable positions for BPA binding. The post-imprinting transformed BPA-MIPs showed high affinity and selectivity toward BPA, and the binding constant was estimated to be $1.3 \times 10^6\ M^{-1}$ using a binding isotherm.

Using this strategy, Taguchi et al. [11] designed an optical sensing system for BPA, in which BPA-MIP nanoparticles (BPA-MIP NPs) were prepared and used as molecular recognition elements for BPA sensing, combined with a slab-type optical waveguide (s_OWG)-based microfluidic surface plasmon resonance (SPR) measurement system. The s_OWG-type SPR sensor was equipped with a high refractive index glass substrate with gold and silver thin-layer bands, which can detect changes in refractive index and permittivity near the surface of the gold/silver thin-layer band. BPA-MIP NPs were immobilized onto the BPA-grafted s_OWG

substrate via the interaction between the BPA-MIP NPs and the BPA immobilized on the substrate. BPA sensing was successfully demonstrated in a competitive binding manner, using BPA-modified gold NPs as competitors.

3 Conjugated Protein Mimics

In nature, proteins coupled with nonprotein prosthetic groups and cofactors, called conjugated proteins, are common; they display a diverse range of functions and play important roles in the activity of biosystems [1]. The routes by which these molecules are synthesized, involving post-translational modifications to obtain various functional proteins, [12] can be mimicked by molecular imprinting in conjunction with PIMs, producing more highly complex functional MIPs.

Murakami et al. synthesized cofactor-binding MIPs involving the subsequent post-imprinting introduction of a metalloporphyrin, which mimics hemoproteins and functions as an "on" switch for specific binding ability (Fig. 5) [13]. In this work, methacryloyl D-tyrosine anilide (D-TyrAN) was used as a template monomer, and Zn^{II}-5,10,15-tris(4-methacryloyloxyphenyl)-20-phyenylporphyrin (Zn-TMPP) was

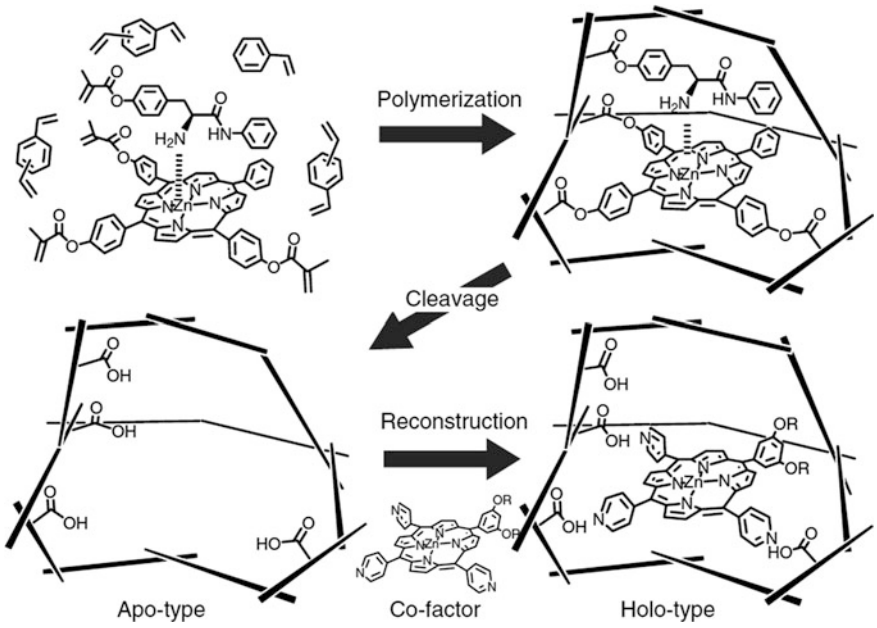

Fig. 5 Schematic illustration of preparation of a D-tyrosine anilide (D-TyrAN) imprinted polymer using methacryloyl D-tyrosine anilide as a template and Zn^{II}-5,10,15-tris(4-methacryloyloxyphenyl)-20-phyenylporphyrin (Zn-TMPP) as a functional monomer (reproduced from Ref. [13] with permission from The Chemical Society of Japan)

used as a functional monomer. After copolymerization with styrene and DVB, D-TyrAN and Zn-TMPP moieties were removed from the MIP by hydrolysis using KOH, resulting in an apo-type MIP lacking a cofactor. Zn^{II}-5-(3,5-dioctyloxyphenyl)-10,15,20-tri-4-pyridylporphyrin (Zn-TPyP), which is an analogue of Zn-TMPP that contains pyridyl groups instead of 4-methacryloyloxyphenyl groups, was added to reconstruct the binding field (holo-type MIP) via conjugation with Zn-TPyP, which is capable of complex formation with residual methacrylic acids within the apo-type MIP. The resulting holo-type MIP showed enantioselective binding activity for D-TyrAN, although the apo-type MIP did not show any enantioselectivity. This may be due to the synergetic activity of a methacrylic acid residue located on the upper portion of Zn-TPyP. Because reversed enantioselectivity was produced when the corresponding antipod, methacryloyl L-TyrAN, was used as the template molecule, precise reconstitution of the binding cavities was confirmed, recalling the structure of the template molecule, even after replacement of the original porphyrin by a structurally related cofactor.

The concept of conjugated protein mimics involving prosthetic groups and cofactors was expanded to the construction of MIPs tunable for binding activity toward bisphenol A (BPA). Takeda et al. synthesized template molecules containing two allyl(4-carboxyphenyl) disulfide groups linked with BPA (BPA-D), and MIPs were synthesized by copolymerizing BPA-D, styrene, and DVB (Fig. 6) [14]. The disulfide groups were then reduced with $LiAlH_4$, resulting in the formation of an apo-type MIP containing two SH groups in the cavity, which showed negligible

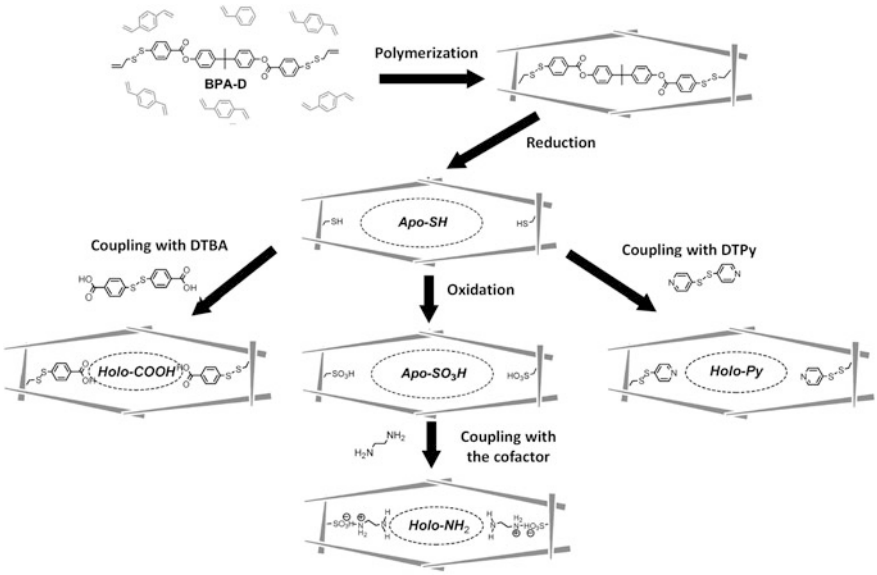

Fig. 6 Schematic illustration of the preparation of conjugated protein mimics involving prosthetic groups and cofactors (reprinted with permission from Ref. [14]. Copyright (2009) American Chemical Society)

binding activity toward BPA. The authors attempted to tune the binding properties of the MIP by covalent introduction of a prosthetic group of (i) benzoic acid or (ii) pyridine using a disulfide exchange reaction. Following the introduction of benzoic acid groups to transform the holo-type MIP (Holo-COOH), binding ability toward BPA was activated. A binding test for Holo-COOH indicated that BPA was selectively recognized by the Holo-COOH, except 4,4′-diaminophenylmethane, which contains two amino groups suitable for the benzoic acid residues in the cavity. This low selectivity was successfully improved by replacing the benzoic acid group with the basic pyridyl group, preventing the nonspecific binding caused by electrostatic interaction, where the pyridyl groups could be inserted at suitable positions for specific BPA binding, as the position of two hydroxyl groups on the BPA structure were memorized in the apo-type MIP.

Furthermore, a noncovalent-based cofactor was applied to the tuning of BPA binding affinity using oxidative PIMs. The thiol group in apo-type MIP was oxidized into sulfonic acid, and then 1,2-diaminoethane (DAE) was added to form sulfonate salt with sulfonic acid residues in the oxidative apo-type MIP cavity, resulting in the improvement of the binding properties of MIPs, due to the introduction of the space-filling interactive cofactor toward BPA. Notably, the binding properties were easily tuned using the DAE concentration, and the addition of competitive binding agents, such as mono- and diamines of various sizes, was effective for affinity control. Testing the control of binding properties in MIPs by introduction/removal of prosthetic groups/cofactors clearly showed the strong potential of PIM techniques for fine-tuning MIPs to mimic natural proteins.

4 Introduction of Desirable Functions

The detection of specific biomolecules related to diseases, health status, food quality, and environmental conditions is increasingly important. Antibodies have commonly been used as analytical tools for these purposes, but they have several drawbacks, including low stability, high production costs, and short shelf lives. Therefore, efforts have been made to develop substitutes for antibodies and other functional biomacromolecules. MIPs are excellent candidates for resolving these problematic issues, because signalling functions for the readout of binding events can easily be incorporated into MIPs through the design of template molecules and functional monomers prior to polymerization. Many researchers have investigated MIPs for proteins, [15, 16] and various detection techniques have been adopted including optical, electrical, and frequency signals. In particular, fluorescent sensing is a powerful tool for the detection and imaging of biologically relevant compounds.

Sunayama et al. [17] developed fluorescent MIPs for proteins prepared by specific post-imprinting introduction of fluorescent dye into the imprinted cavity (Fig. 7). In this study, a designed functional monomer, 4-[2-(N-methacrylamido) ethylaminomethyl]benzoic acid (MABA) bearing three components (a polymerizable methacryl group, a benzoic acid moiety to interact with template proteins, and

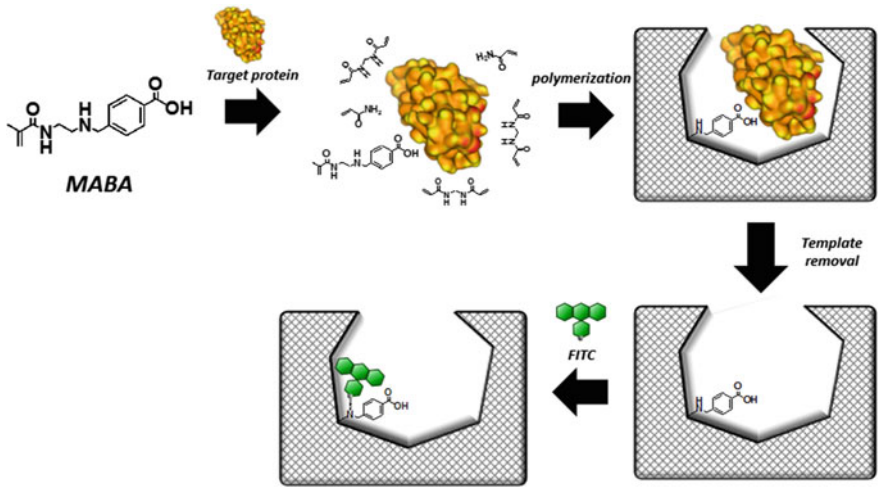

Fig. 7 Schematic illustration of preparation of a protein-imprinted polymer using MABA as a functional monomer and post-imprinting introduction of FITC as a fluorescent reporter dye within the binding cavity

a secondary amine for post-imprinting conjugation with a fluorescent reporter molecule) was synthesized and lysozyme-MIP thin films were prepared on a glass substrate by copolymerization of the designed functional monomer, acrylamide, and *N*,*N*′-methylenebisacrylamide in the presence of lysozyme. After removal of the lysozyme, fluorescein isothiocyanate (FITC) was conjugated with the secondary amino group of the functional monomer residues located within the binding cavity. The MIPs produced fluorescence at 520 nm (λ_{ex} 490 nm) derived from fluorescein, and the fluorescence intensity increased with lysozyme concentration; the magnitude of the relative change in fluorescence intensity ($\Delta I/I_0$) was greater than that of the nonimprinted polymer (NIP) film prepared without lysozyme.

These results indicate that the imprinted cavity was created via the imprinting process, and the fluorescence dye was successfully introduced into the lysozyme-imprinted cavity. The SPR response to lysozyme binding of NIPs prepared on gold-coated SPR sensor chips (in the same manner as the glass substrates) was found to be greater than the corresponding fluorescence response, because most of the SPR response from the NIP film may be caused by nonspecific binding to randomly located functional monomer residues and the polymer matrix; changes in fluorescence could be observed only when lysozyme was properly bound to the fluorophore-labelled imprinted cavity. These results imply that the present post-imprinting introduction of fluorescent dye provides a method to prepare fluorescent MIPs in which only specific binding events are transduced into changes in fluorescence, due to specific labelling of the functional monomer residues within the imprinted binding cavity.

Post-imprinting transformations were also performed using silica-based molecular imprinting as well as organic polymer-based molecular imprinting. Tao et al.

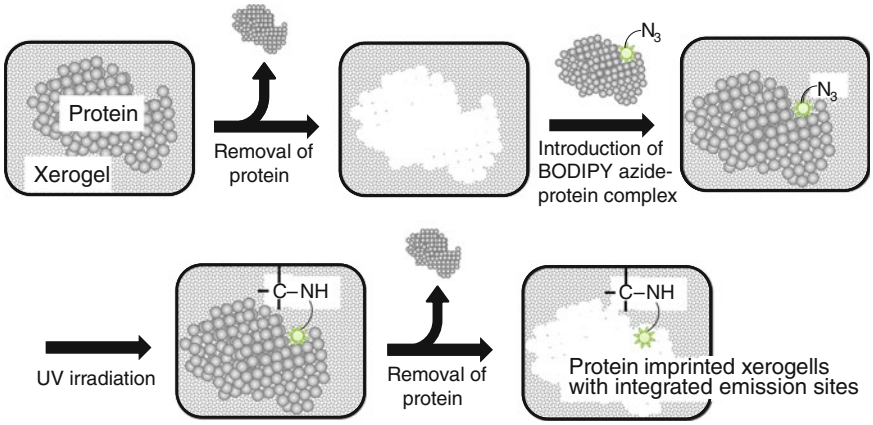

Fig. 8 Schematic illustration of the protein imprinted xerogel fabrication process

successfully applied molecularly imprinted xerogels for specific protein sensing, where the site-selective introduction of fluorescent molecules utilizing a PIM technique was performed for fluorescence detection of target proteins (Fig. 8) [18]. First, ovalbumin-imprinted xerogels were synthesized by sol-gel reactions with four types of monomers, including tetraethyl orthosilicate, 3-aminopropyltriethoxysilane, *n*-octyltrimethoxysilane, and bis(2-hydroxyethyl)aminopropyltriethoxysilane. The sol solution, including H_2O and HCl, was initially mixed with 10 mM phosphate buffer (pH 7.0), followed by the addition of ovalbumin dissolved in the same buffer. After the formation of xerogels, the ovalbumin was washed out with 5 M aqueous urea or dilute phosphoric acid, yielding ovalbumin-imprinted xerogels. The site-selective introduction of a fluorescent molecule, azidated BODIPY, was carried out using an ovalbumin-azidated BODIPY adduct as a labelling agent; ovalbumin played the role of carrier to deliver the azidated BODIPY to the binding cavities with ovalbumin affinity, followed by photoinitiated covalent bond formation between the xerogels and the BODIPY azide. A greater change in fluorescence intensity was observed as ovalbumin concentrations increased, and the xerogels recognized ovalbumin over human serum albumin and phenylsulfonamidated ovalbumin. Moreover, human interleukin-alpha (human IL-1a)-imprinted xerogels containing site-selectively introduced fluorescent molecules were prepared in a similar manner; these showed that the xerogels recognized human IL-1a over human IL-1b and porcine-1a, with an extremely low limit of detection of approximately 2 pg/mL.

5 Outlook

As described above, it has been clearly demonstrated that by using PIM-directed template molecules and functional monomers, site-specific labelling of reporter molecules that respond to binding events can be achieved, providing various MIPs with biologically relevant functions. The combination of PIMs with MIP synthesis is a powerful tool for the creation of a diverse range of advanced functional materials. In recent years, the number of reports on MIPs combined with PIMs has gradually increased, indicating that the focus of the MIPs field has gradually shifted to the synthesis of increasingly complicated and biomimetic receptors. We believe that PIMs would be of considerable interest to researchers in the fields of functional materials science, biomimetic chemistry, and even life science because of the enormous potential of the existing methods for the development of new classes of synthetic materials possessing a variety of posteriori functions, such as artificial enzymes, signalling plastic antibodies, drug-delivery systems, antidotes, restoration materials, stimuli-responsive materials, and tools for logic circuits. We hope this chapter will help readers to create more advanced materials.

References

1. Schulz GE, Scirmer RH (1979) Principles of protein structure. Springer, New York
2. Sellergren B (ed) (2001) Molecularly imprinted polymers: man-made mimics of antibodies and their applications in analytical chemistry. Elsevier, Amsterdam
3. Komiyama M, Takeuchi T, Mukawa T, Asanuma H (2003) Molecular imprinting: from fundamentals to applications. Wiely, Weinheim
4. Yan M, Ramstrom O (eds) (2005) Moleculary imprinted materials: science and technology. Marcel Dekker, New York
5. Haupt K (ed) (2012) Molecular imprinting. Springer, Berlin
6. Lee S-W, Kunitake T (eds) (2013) Handbook of molecular imprinting: advanced sensor applications. Pan Stanford Publishing, Singapore
7. Shimizu KD, Yan M, Ramstrom O (Eds) (2005) Post Modification of imprinted polymers, In: Molecularly imprinted materials: science and technology. Marcel Dekker, New York
8. Takeuchi T, Murase N, Maki H, Mukawa T, Shinmori H (2006) Dopamine selective molecularly imprinted polymers via post-imprinting modification. Org Bio Chem 4:565
9. Yane T, Shinmori H, Takeuchi T (2006) Atrazine transforming polymer prepared by molecular imprinting with post-imprinting process. Org Biomol Chem 4:4469
10. Takano E, Taguchi Y, Ooya T, Takeuchi T (2012) Dummy template-imprinted polymers for Bisphenol A prepared using a Schiff base-type template molecule with post-imprinting oxidation. Anal Lett 45:1204
11. Taguchi Y, Takano E, Ooya T, Takeuchi T (2012) SPR Sensing of bisphenol a using molecularly imprinted nanoparticles immobilized on slab optical waveguide with consecutive parallel Au and Ag deposition bands coexistent with bisphenol A-immobilized Au nanoparticles Langmuir 23:7083
12. Kannicht C (2008) Post-translational modifications of proteins. Springer, Berlin
13. Murakami S, Yamamoto K, Shinmori H, Takeuchi T (2008) A molecularly imprinted polymer for the reconstruction of a molecular recognition region. Chem Lett 37:1028

14. Takeda K, Kuwahara A, Ohmori K, Takeuchi T (2009) Molecularly imprinted tunable binding sites based on conjugated prosthetic groups and ion-paired cofactors. J Am Chem Soc 131:8833
15. Takeuchi T, Hishiya T (2008) Molecular imprinting of proteins emerging as a tool for protein recognition. Org Bio Chem 6:2459
16. Whitcombe MJ, Chianella I, Larcombe L, Piletsky SA, Noble J, Porter R, Horgan A (2011) The rational development of molecularly imprinted polymer-based sensors for protein detection. Chem Soc Rev 40:1547
17. Sunayama H, Ooya T, Takeuchi T (2010) Fluorescent protein recognition polymer thin films capable of selective signal transduction of target binding events prepared by molecular imprinting with a post-imprinting treatment. Biosens Bioelectron 26:458
18. Tao ZY, Tehan EC, Bukowski RM, Tang Y, Shughart EL, Holthoff WG, Cartwright AN, Titus AH, Bright FV (2006) Templated xerogels as platforms for biomolecule-less biomolecule sensor. Anal Chim Acta 564:59

Adv Biochem Eng Biotechnol (2015) 150: 107–129
DOI 10.1007/10_2015_319

Published Online: 19 March 2015

Molecularly Imprinted Polymers for Catalysis and Synthesis

Fosca Mirata and Marina Resmini

Abstract The area of biomimetic catalysis based on molecular imprinted polymers has progressed considerably over the last two decades, with research efforts focused on developing catalysts for challenging reactions and on understanding the key factors in template structure and polymer morphology that influence efficiency and selectivity. Recent advances and significant achievements in the field presented in this chapter are organized according to four topics: hydrolytic reactions of challenging substrates, oxidase mimics, metallo-enzyme mimics, and polymers that display unusual reactivity, such as in the case of reactions for which enzymes don't exist, such as Diels–Alder and Kemp elimination. For each theme, significant examples for recent literature are presented and discussed.

Keywords Biomimetic · Enzyme mimic · Imprinted polymers

Contents

Enzymes have been developed by nature to efficiently catalyze a large variety of chemical transformations, thanks to specific interactions in the active site between key amino acid residues and substrates and intermediates of the reaction [1]. The efficiency and specificity of these proteins can rarely be matched by synthetic mimics, but low stability in organic solvents, in extreme temperatures and pHs,

F. Mirata · M. Resmini (✉)
School of Biological and Chemical Sciences, Queen Mary University of London,
Mile End Road, London E1 4NS, UK
e-mail: m.resmini@qmul.ac.uk

significantly limits applications. For this reason researchers have investigated various approaches to develop artificial mimics, of which catalytic antibodies and molecularly imprinted polymers are two important examples. With both systems, catalysis of important reactions for which no enzyme exists, such as Diels–Alder [2] and hetero-Diels–Alder [3] have been achieved, together with examples of stereocontrolled chemical reactions [4], although in the case of catalytic antibodies, their protein structure still has the same limitations as enzymes.

The molecular imprinting technique uses a templating approach, where the target molecule forms a self-assembled complex with specific functional monomers and cross-linkers, which after polymerization and removal of the target leaves a macromolecular system with cavities that have specific molecular recognition characteristics. When the chemical structure of the template is designed to resemble the transition state or the intermediate of a reaction, the polymers display enzyme-like catalytic activity.

The late 1980s saw important developments in the field of catalytic-imprinted polymers with seminal papers by Neckers [5] and Shea [6] on the stereocontrol of chemical reactions, by Wulff [7] on enantioselective synthesis, and by Mosbach [8] on imprinting using substrate analogues. In 1989 Mosbach [9] also reported the first example of polymer imprinting using a transition state analogue (TSA) that lay the foundation for a flourishing field. A number of different systems for the formation of the target-functional monomer complex have been studied, such as the covalent approach used by Shea [10] and the stoichiometric non-covalent imprinting developed by Wulff [11], while a significant variety of chemical reactions, such as the dehydrofluorination [12], the β-elimination [13], the aldolase type II [14], the Diels–Alder cycloaddition [15], the phosphate hydrolysis [16], and the Suzuki cross-coupling [17] have been studied with varying results in terms of catalytic efficiency and substrate specificities.

After the initial proof of concept, research in the field of catalytic-imprinted polymers focused the efforts towards understanding the mechanisms that control catalytic efficiency and molecular recognition, with the aim of achieving catalytic activities much more similar to the ones obtained with enzymes [18–21].

This chapter will provide an overview of the most recent work done in the area of imprinted polymers used as catalysts and for synthetic purposes; the most significant findings are presented in four different groupings: hydrolysis reactions on challenging substrates, oxidase mimics, polymers mimicking metallo-enzymes, and polymers with unusual reactivity.

1 Hydrolytic Reactions on Challenging Substrates

In living organisms, hydrolytic reactions are constantly performed by various enzymes, e.g., hydrolases, esterases, and amidases, whose mechanisms of action have been studied in great detail [22], leading to the identification of important concepts such as the TSA [23]. For these very reasons, the hydrolysis of esters and

carbonates has been among the first types of reactions to be catalyzed by imprinted polymers [24].

In the last few years there has been a clear drive towards studying chemical reactions that are significantly more challenging from the point of view of energy, and among these organophosphates, hydrolysis has attracted considerable interest [25, 26]. Organophosphates are esters of phosphoric acid, and this class of compounds includes many important biomolecules such as DNA, RNA, and some cofactors, but also highly toxic organic pollutants such as pesticides, insecticides, and nerve gas agents. The latter are of particular concern, given their threat to human health, and therefore their detection, quantification, and especially decomposition into non-toxic products is a key priority. In the last few years, researchers have attempted to develop efficient catalysts for the hydrolysis of organophosphates by using novel approaches based on molecularly imprinted polymers. Prior to 2009, a few attempts in the synthesis of catalysts based on MIPs were made, but without achieving significant rate accelerations [27–29].

In 2013 Guo et al. [30] published an interesting work on the preparation of a dual-templated imprinted capsule that catalyzes the hydrolysis of organophosphate-based pesticides. The authors used an original approach, based on imprinting the substrate and the product at the same time. The aim was to obtain a material that can act as a catalyst with high efficiency and selectivity in the degradation of the pesticide target while simultaneously catalyzing an elimination reaction. The imprinted polymer was prepared as a hollow structure to minimize the degradation of the substrate and the product inhibition. Paraoxon was used as the model substrate; this is one of the most potent acetylcholinesterase-inhibiting insecticides currently available, and it is now rarely used due to the toxicity to humans and other animals. Zinc dimethacrylate (MAA-Zn) was used as a monomer, with divinylbenzene (DVB) as the cross-linker, while *p*-nitrophenol was used as the first template. Vinyl-bearing silica microspheres (v-SiO_2) were used as the seed around which the polymerization occurred. The core-shell microspheres were prepared first by precipitation polymerization; the copolymerization of MAA-Zn and DVB in the presence of paraoxon as the second template took place around the core-shell microsphere by precipitation polymerization. After removing the v-SiO_2, the dual-templated hollow microsphere was obtained (Fig. 1). The material was characterized by an paraoxon-imprinted outer shell, acting as the hydrolytic catalyst, and by a *p*-nitrophenol-imprinted inner shell, representing the adsorption layer. This layer acts as reservoir to enrich *p*-nitrophenol and to further promote hydrolysis of paraoxon by decreasing the concentration of the product in the medium.

Various polymers were prepared by using similar experiment conditions: non-imprinted polymer (NIP), MIP imprinted with the reactant, paraoxon (MIP-P), MIP imprinted both with paraoxon and *p*-nitrophenol, reactant and product (MIP-N/P), and H-MIP-N/P, obtained following the removal of the first seed. Results showed higher catalytic efficiency towards paraoxon when H-MIP-N/P is used; compared with MIP-N/P, it showed significant catalysis efficiency with a rate of 59.6×10^{-2} mM min^{-1}, which is 1.88-fold higher than that of MIP-N/P and 272-fold higher than that of paraoxon self-hydrolysis. This significant result is due to the synergistic

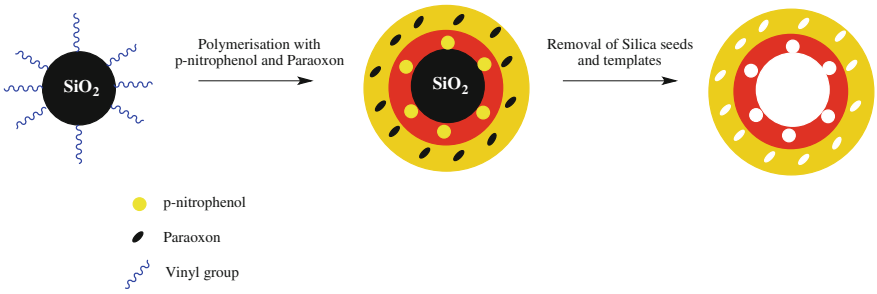

Fig. 1 Schematic representation of the synthesis of dual-templates imprinted capsule. First imprinting *p*-nitrophenol, then imprinting paraoxon, at the surface of vinyl-bearing silica seeds, followed by the removal of the silica seeds and templates [30]

effect of the two layers. Paraoxon-imprinted sites could catalyze the hydrolysis of paraoxon, which generates *p*-nitrophenol, which could be adsorbed in the *p*-nitrophenol-imprinted sites, resulting in the decrease of *p*-nitrophenol concentration. At the same time, besides showing higher catalysis efficiency towards paraoxon, H-MIP-N/P could also eliminate *p*-nitrophenol effectively. Moreover, the catalyst has an excellent catalytic efficacy; up to 80 % of the catalytic ability is indeed retained after three catalytic cycles using the same H-MIP-N/P. All the results prove that the catalyst has very good potential application in the environmental field, especially in the degradation of organophosphate-based toxic pollutants.

That same year, Carboni et al. [31] studied the hydrolysis of organophosphates by using an innovative strategy that involved the use of a complex between lanthanum and an organophosphate as template for molecular imprinted titanium-based mesoporous films. The metal was used because of its high affinity and strong interaction with organophosphates, acting as the catalytic center able to increase the reaction rate, while the mesoporous structure favors substrate binding and allows the easy removal of the template. The metal is integrated and dispersed in the matrix, giving rise to a mesoporous La-doped titanium film. Kinetic studies indicated that NIF provides a 17 % rate acceleration compared to the background, while MIF shows a 27 % increase in initial rate. This material was shown to have a very high number of active sites, and by using the density of active sites, the authors were able to determine also the catalytic loading corresponding to the area of the film used for the kinetics. These films have given promising results as catalysts, proving to be versatile tools for the degradation of organophosphate-based pollutants.

Another interesting study in the area of novel MIPs, catalyzing the hydrolysis of interesting substrates, was reported by Striegler and colleagues [32] (Fig. 2). Her work focused on the hydrolysis of glycoside by using catalytic microgels imprinted with carbonates. Glycosides are very important organic molecules in which a carbohydrate is bound to another functional group via a glycosidic bond on its anomeric carbon. In living organisms, the glycoside bond is cleaved by glycosidases, a family of enzymes that is able to hydrolyze the glycoside bonds. In organic

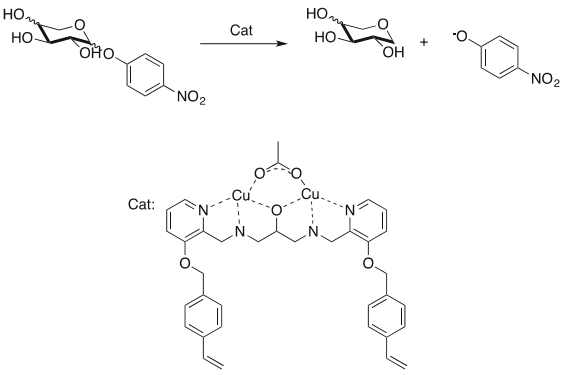

Fig. 2 Catalytic hydrolysis of *p*-nitrophenylglycopyranoside and structure of the catalyst used [32]

chemistry, glycosidase can be used as synthetic catalysts to form glycosidic bonds, through either reverse hydrolysis or by transglycosylation. The long-term goal of the authors is to use the developed catalyst to selectively form glycosidic bonds by transglycosylation. Data presented in a previous paper (published a year earlier [33]) showed that the hydrolysis of *p*-nitrophenyl-α-D-galactopyranoside can be accelerated 11,000 times over the background reaction when binuclear complex Cu_2(bpdpo)(OAc) is used as catalyst; however, despite the high rate of acceleration, significant product inhibition limits its application.

In order to increase the rate of the reaction even more and to avoid product inhibition, the metal complex was anchored on a polymeric matrix. The synthesized polymerizable ligand was immobilized in a co-polymer of styrene and butylacrylate in aqueous miniemulsion and activated by coordination of Cu(II) ions. Although the reaction catalyzed by the macromolecular catalyst showed an increased value of k_{cat}/k_{non} (from 11,000 to 100,000 M), the selectivity ability of the catalyst towards glycosidic bonds was very poor; indeed, neither the anomeric nor the epimeric form was discriminated. To overcome this limitation and supply the catalyst with higher selectivity, turnover rate, and catalytic efficiency, the imprinted approach was investigated and sugar-templated microgels were prepared. The miniemulsion was prepared in water from styrene, butyl acrylate and the carbohydrate metal complex by radical polymerization. The catalyst showed an increased catalytic efficiency ($k_{cat}/k_{non} = 6.6 \times 10^5$ M), as well as turnover (0.151 min^{-1}), that was 4 times higher than the value obtained for the macromolecular catalyst. These results, together with the enhanced selectivity of the catalyst towards the structure of the carbohydrates involved in the glycosidic bond (epimeric forms), provide evidence for the positive contribution of the template approach, even though the selectivity for the nature of the bond (anomeric forms) was not achieved.

Another interesting example of MIP catalyzing interesting reactions is the work of Abbate et al. [34] who in 2011 reported the first example of MIPs that shows catalytic activity on reactions involving silicon-based substrates. Hydrolysis and condensation reactions of alkoxysilane compounds were studied using trimethylethoxysilane (TMES) as a model molecule. The preparation of MIPs is based on

the non-covalent approach, which results in an easier and more efficient removal of the template from the MIP. Ethylene glycol dimethacrylate (EDGMA) and a-azo-iso-butyronitrile (AIBN) were used as cross-linker and initiator, respectively. Methacrylic acid (MAA) and diphenylsilanediol were used as functional monomer and template; the former was chosen due to its ability to form hydrogen bonds, while the latter, diphenylsilanediol, was used as a TSA. The polymerization, either thermal or photochemical, provided the polymer as a rigid monolith, which was manually ground and sieved to give particles ranging from 50 to 150 μm. The polymer was characterized in the solid state via FT-IR, solid-state NMR and SEM-EDS, the latter showing the polymer surface with high porosity and a sponge-like appearance. The porosity is believed to favor the fast exchange of substrates in and out of the polymer. Condensation of trimethylsilanol to hexamethyldisiloxane and hydrolysis of trimethylethoxysilane (TMES) to Me_3SiOH were conducted both with MIPs and NIPs (non-imprinted polymers), and the results showed that the MIP favors the condensation reaction, on the basis of the higher amount of HDMS product formed. Me_3SiOH, the hydrolysis product was, however, obtained in the same quantity with MIP- and NIP-catalyzed reactions, as a result of the non-specific catalysis mediated by randomly positioned functional monomers.

Good results were obtained in terms of reproducibility of the data. In the same study, the authors also presented MIPs able to catalyze the biomimetic synthesis of silica by hydrolysis and polycondensation of tetramethoxysilane (TMOS). The MIP was prepared by using the same experimental conditions using a pentacoordinate silicon compound as TSA-template and different functional monomers, either MAA or HEMA-VPY (2-hydroxyethyl methacrylate, HEMA, 4-vinylpyridine, VPY). The MIPs prepared in this way showed the ability to precipitate amorphous silica under ambient conditions.

As reactions with challenging substrates were investigated, there has also been a new drive towards studying more traditional reactions, such as the hydrolysis of esters and carbonates using novel polymeric formats. Li et al. [35] developed a new hydrolytic system designed to catalyze ester hydrolysis with an on-off switch. MIPs using NIPAM-based thermoresponsive polymers were prepared and used to catalyze hydrolysis of *p*-nitrophenylacetate. The innovation of this material lies on its temperature-dependent hydrophilicity/hydrophobicity, which gives a temperature-regulated catalysis; this is enhanced at a relatively low temperature (20 °C), thanks to its hydrophilic networks that enable access to the imprinted sites for analytes in water, whereas at a high temperature (40 °C), the hydrophobicity is increased and hence the polymer shows poor catalytic activity due to the reduced access to the imprinted matrix because the polymer has been shrunk. This characteristic is given by the presence of poly(N-isopropylacrylamide) (PNIPAm), which has a unique structure that changes hydrophilicity and hydrophobicity at its lower critical solution temperature (LCST).

Several studies have been conducted on this material, such as template-monomer interaction and stoichiometric amounts of monomer via UV spectra, FTIR spectra and SEM morphology, specific interactions between polymers and analyte via TPD (temperature-programmed desorption), thermosensitive hydrophilicity/

hydrophobicity via DLS (dynamic light scattering) analysis, and switchable binding behavior via DCV (dynamic desorbing cyclic voltammetry). The results and the number of advantages of the material-like stability, ease of preparation, and reusability, demonstrate the feasibility of the switchable catalysis by the clever and catalytic imprinted polymer obtained with this approach.

Two years later, the same group presented an original material, a nanoreactor based on molecularly imprinted polymer containing Ag nanoparticles [36]. The originality lies in the ability of the nanoreactor to catalyze cascade reactions—contrary to the conventional nanoreactors, which promote just one single reaction per time. Substrate recognition, catalytic selectivity—besides significantly decreasing the cost and number of steps—are just a few of the advantages of the new material. The model reaction used was the synthesis of aminophenol (AP). A common method for obtaining AP is based on the nitration of phenol, followed by catalytic reduction in the presence of an Ag, Au or Fe catalyst. This process is complicated and involves many separation steps; therefore, the proposed nanoreactor has a positive potential application.

The proposed reaction starts from the hydrolysis of 4-nitrophenyl acetate (NPA), followed by a further reduction (in which Ag is involved) of nitrophenol (NP) in order to obtain AP (Fig. 3). Since the nanoreactor catalyzes two consecutive reactions, it was imprinted with two molecular templates—NPA, and NP in the form of a complex with Ag. A classic molecular imprinting technology was used in the preparation of the nanoreactor. The templates, NPA and the AgNP complex, the functional monomer 1-vinylimidazole, the backbone monomer divinylbenzene, and the initiator AIBN were dissolved in a mixture of alcohol and dimethylsulfoxide. A photochemical polymerization was used; the system was irradiated with ultraviolet light (365 nm) overnight. Following removal of the templates, the nanoreactor (MIP–NPA–AgNP) was obtained. Two more control nanoreactors were prepared using the same experimental conditions, MIP–AgNP (without using NPA, NP and NPA), NIP–Ag (without using NP, NPA and Ag), and NIP. The catalytic activity of the nanoreactors was tested and compared in order to identify the cooperation between Ag nanoparticles and the imprinted polymers in relation to the sequence of reactions. The data demonstrate that successive-reaction catalysis can be realized by using this novel and unique imprinted nanoreactor, which opens up new opportunities for developing functional catalysts for complicated chemical processes.

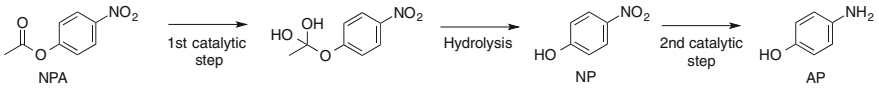

Fig. 3 Consecutive steps showing the conversion of 4-nitrophenyl acetate into 4-nitrophenol and subsequently into 4-aminophenol [35]

2 Oxidase Mimics

Another class of reaction largely studied, both in terms of bio-mimicking and catalytic effect of MIPs, is oxidation—in particular when applied to substrate of interest, such as phosphonate-based compounds and toxic environmental agents. Shiraishi et al. [37] in 2010 proposed a new way to degrade toxic pollutants using an oxidation reaction instead of hydrolysis. The innovative method was based on photooxidation, and chlorophenols (CPs) were used as the model. CPs are part of a class of organochloride of phenols that contains a covalently bonded chlorine atom. One molecule may contain one or more chlorine atoms up to five (pentachlorophenol), and monochlorophenol presents three isomers: 2-chlorophenol (2CP), 3-cholorophenol (3CP), 4-cholorophenol (4CP). These compounds are widely used in various industries as pesticides, herbicides and insecticides. Both the U.S. Environmental Protection Agency and the European Parliament and Council of the European Union listed the CPs as priority pollutants. However, CPs degrade slowly in the environment and can produce more complicated and toxic molecules, hence the need for a system that allows fast purification. A MIP containing Rose Bengal (RB), a photosensitizer able to selectively photooxidate CPs in water in the presence of O_2 by simple irradiation with visible light, was obtained. Radical thermal polymerization was used, and MAA, 4-chloromethylstyrene (CMS), EGDMA, AIBN and chlorophenol were used as functional and backbone monomer, cross-linker, initiator, and template, respectively. The RB was later added to the solution, followed by warming up and stirring together with the polymer. Three MIPs were prepared with each of the three isomers of chlorophenol as template substrate, obtaining IP-x with x = 2CP, 3CP, 4CP.

In order to test the selectivity and the photosensitization activity of the materials, photooxydation was evaluated by adding the respective IP-x in a sealed tube containing an aqueous solution of the substrates (2CP, 3CP, 4CP plus phenol) in which O_2 was bubbled; the tube was then photoirradiated with visible light at a wavelength greater than 530 nm. The same reaction was conducted with only unpolymerized RB as a sensitizer and with NIP (non-imprinted polymer), and the results were compared. With RB, no differences were observed in the conversion of all the substrates. IP-x shows specifically high conversion for the corresponding substrate used as templates for polymer synthesis, although the quantity of conversion of all substrates obtained with IP-x and NIP are lower than that obtained with RB. The selective activity of IP-x was therefore demonstrated and also confirmed by IR analysis and absorption experiments. The recognition site in the MIP selectively attracts the target CP via hydrogen bonding; the $^1O_2$ produced by energy transfer from RB can oxidize the substrate during diffusion within its lifetime. However, the efficiency of IP-x was found to be not very high due to the heterogeneous character of the energy transfer from exited RB units to O_2 and oxidation of substrates by $^1O_2$.

Oxydoreductases are some of the most important enzymes in living organisms due to their essential role in the respiratory processes. Jakubiak-Marcinkowska et al.

[38] reported a new MIP able to mimic oxygenases, enzymes part of the oxydoreductases family that catalyze insertion of oxygen atoms on substrates. These enzymes carry Cu(II) ions in the active centers, which are coordinated by histidine ligands—among others, amino acids residues, responsible for electron transfer and reagent binding. Unlike the other examples of catalytic MIPs, this material carries the recognition sites only on the inner surface of the polymer surface. This characteristic solves the diffusion issues and hence makes the transport of reagents in the medium easier. The surface imprinting technique was used in order to synthesize the MIPs; this is based on W/O emulsion on organic-aqueous interface, which is used as a recognition field for template molecules to assure correct orientation of the functional groups toward target molecules fixed at this interface.

The model reaction was the oxidation of hydroquinone (HQ) to quinine (Q) by H_2O_2. A complex of Cu(II) and 4-methoxybenzyl alcohol was used as template; this is a common strategy; indeed, other examples of metal complexes used as templates have already been studied within the hydrolysis catalysis section. 1-Vinylimadazole was used as functional monomer due to its similarity to the histydyl ligand present in the natural enzymes. The cross-linker, 1,1,1-tris (hydroxymethyl)propane trimethacrylate, gave a porous and rigid structure to the material (Fig. 4). Moreover, two more monomers were added to the monomer mixture during polymerization: acrylonitrile for the purpose of increasing the rigidity and porosity without using a high level of cross-linker, and 4-vynyloxybutylstearate, a surface active monomer, to improve the stability of water/oil emulsion, allowing an easier removal of metal ions.

Once the Cu(II)-complexes' templates were removed and the surface MIPs were obtained, they were further loaded with Cu(II) ions to prepare the catalysts with active centers. The Cu(II) ions interact with the imidazole nitrogen and with the carboxyl group formed by hydrolysis of the cross-linker during the polymerization. The catalyst was characterized by EPR, which highlighted the interactions taking place within the active center. In order to improve the catalytic efficiency of the materials, the authors modified the active center with ionic liquids (ILs) in a process that involves two steps, a first bromoalkylation and an ion-exchange of bromine. ILs are a salt-like material in the liquid state, and among their various properties, an excellent thermal and chemical stability, and miscibility with water and organic solvents stand out. Moreover, their high polarity, reactivity towards transition metal ions and ability to work in a two-phase system make these substances very useful

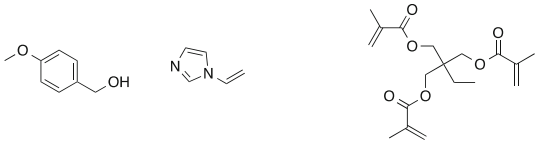

Fig. 4 From *right* to *left*: structures of template, functional monomer, and cross-linker [38]

for catalysis and polymer chemistry. Two series of surface MIPs were synthesized —a modified one and a non-modified one; EPR spectra were recorded and experimental spectra were computer simulated. Both results were compared, showing that protonation of the imidazole nitrogen and the introduction of groups with strong electrostatic properties in the cavities resulted in a clear increase in catalytic activity, with over a 50 % enhancement. These findings provide a very interesting example of how the addition of free active groups in a catalytic site can impact activity by making the metal loading less relevant for high efficiency.

Among biomimetic MIPs applied to catalyze oxidation reactions, there is an interesting study published by Diaz-Diaz et al. [39] in 2011 in which they developed MIPs with catalytic activity towards 2,4,6-trichlorophenol (TCP) mimicking the chloroperoxidase (CPO)s activity. CPO is a versatile heme-containing enzyme, where the heme group acts as the prostetic group, which is part of the family of oxidoreductases. Although the primary biological function of CPO is chlorination of organic compounds, CPO can also catalyze oxidative reactions, characteristic of other heme peroxidises. CPs, as mentioned earlier, are highly toxic pollutants that are persistent in the environment and are found in the ground and in wastewater. TCP especially is the most harmful of CPs due to the pulmonary lesions that it causes. Peroxidases have already been shown to degrade these pollutants, and therefore CPO was taken as a model system in order to catalyze the oxidative dehalogenation of TCP to 2,6-dichloro-1,4-benzoquinone (DCQ).

In this study, a general computational method for the rational design of an artificial oxidative hemeprotein was proposed. Density functional theory (DFT) calculations were applied in order to select the most suitable functional monomer that stabilizes both the pre-polymerization adduct and the intermediate in the catalytic reaction. Quantum chemical methods are very convenient due to their ability to ability to accurately predict the stabilization energies for the reactive complexes, which are then synthesized and analyzed. Four different functional monomers with different acid/base groups (trifloromethacrylic acid, TFMAA; methacrylic acid, MAA; methacrylamide, MA; and 4-vinylpyridine, VPY) and six solvents were screened. Methacrylamide (MA) and 4-vinylpyridine (VPY) gave the most stable interaction with the template in DMSO. MIPs were then synthesized by radical polymerization using AIBN and EGDMA with each of the four functional monomers and tested with DFT plus chlorohemin in the catalytic center, which is covalently included in the polymer backbone and which mimics the prostetic group of the natural CPO. SEM and TEM analysis were carried out; furthermore, the catalytic activity, the selectivity and the binding efficiency towards TCP were investigated on each prepared MIP. In accordance with the theoretical predictions, only TCP-imprinted polymers synthesized with MAA or VPY as functional monomers showed catalytic activity in oxidative dehalogenation of TCP. Moreover, the two catalysts produce regioselective transformation of the substrate, therefore acting as artificial mimics of CPO.

One year later, the same group published further findings on the synthesis of a new MIP containing both the neutral MAA and the 4-vinyl pyridine unit, mimicking the amino acid residues of CPO [40]. Different ratios of the two monomers

were screened to better understand their roles and to optimize the catalytic efficiency of the MIP. The polymers were prepared by radical polymerization using chlorohemin, TCP, MA-VPY in different ratios (3:1, 1:1, 9:1), EGDMA and AIBN; the polymers were characterized using ICP-MS to determine the amount of iron, SEM for the morphological characterization, as well as kinetics studies together with binding and selectivity experiments. Oxidative dehalogenation of TCP was carried out with both NIPs and MIPs as catalysts. The formation of the DCQ as the main oxidation product proves that the catalysts are regioselective. The highest catalytic efficiency was shown by the MIP with the lower VPY content (9:1 ratio), unlike the natural counterpart, which exhibits a 3:1 acid:base character in the catalytic center.

3 Polymers Mimicking Metallo-Enzymes

The use of metals in catalysis is widespread and these systems often suffer from a lack of substrate specificity; this is the reason that there has been considerable interest in coupling the metal containing centers with the imprinting approach.

Czulak, in collaboration with Jakubiak-Marcinkowska, prepared MIPs with catalytic centers containing transition metal ions in order to mimic the active sites of metalloenzymes, using the oxidation of hydroquinone by hydrogen peroxide as a model reaction [41]. The suspension polymerization technique was used in order to obtain two kinds of cavities: in the volume, and on the surface of the polymer matrix. Volume molecularly imprinted polymers were obtained from an organic phase that contained 4-vinylpyridine (VPY) and acrylonitrile (AN) as functional monomers; trimethylolpropane trimethacrylate (TMPMA) as a cross-linker; 4-methoxybenzyl alcohol (MBA) as template, with its structural similarity to the reagent, 2,2-azobisisobutyrronitrile (AIBN) as the initiator; and metal ions. VPY creates an acid-base interaction between imprinted metal ions and the pyridine nitrogen atom; a second functional monomer is used in order to facilitate the formation of porous structure. Surface molecularly imprinted polymers were obtained by adding aqueous phase containing metal ions solution to an organic phase containing the same functional monomers, cross-link agent, template and initiator seen above. In order to enhance the stability of the pre-polymerization emulsion, 4-vinyloxybutylstearate (VOBS) was added to the organic mixture. Characterization of the polymers was carried out by analyzing nitrogen content, surface area, porosity and sorption of metal ions. The authors synthesized nine polymers in total, using both volume and surface imprinting technique, using four transition metals: Cu(II), Co(II), Mn(II), and Zn(II). However the last two ions, Mn and Zn, were used only in volumetric imprinting due to their low stability and loading in the cavities.

The catalytic activity of the polymers was tested and compared. The highest and most efficient activity in the oxidation reaction of hydroquinone was showed by the MIP containing Cu(II), due to the formation of a stable complex between template,

metal ion and functional monomers during the polymerization step. In particular, the complex stability followed this series: Mn(II) < Fe(II) < Co(II) < Ni(II) < Cu (II) > Zn(II). Moreover, the surface imprinted polymers provided better results than the volumetric imprinted ones for the same metal ion and similar loading; in the latter, the substrate had to diffuse through the polymer matrix into the internal cavities while there was no requirement for diffusion surface cavities.

Another interesting and innovative investigation on catalytic Metals-based MIPs was reported by Yang et al. A molecularly imprinted Fe_3O_4/SiO_2 core-shell magnetic composites (Fe_3O_4/SiO_2-MIP) was prepared in order to selectively catalyze ozonation of *p*-nitrophenol (p-NP) (Fig. 5) [42].

Phenolic compounds are toxic and carcinogenic and very difficult to remove from the environment due to their stability and bioaccumulation. A possible approach involved the development of catalysts with high recognition and selectivity ability designed to remove these compounds from wastewater by ozonation processes; selectivity is crucial, given the large presence of other organic contaminants in polluted water. In order to synthesize the catalyst, Fe_3O_4 particles were prepared by precipitation, followed by Fe_3O_4/SiO_2 core-shell particles prepared by dispersing tetraethoxysilane (TEOS) in a Fe_3O_4 solution. Fe_3O_4/SiO_2-MIPs were further obtained by surface imprinting using Fe_3O_4/SiO_2 core-shell particles mixed together with 3-amynopropyltriethoxysilane, frequently used in functionalization of surfaces with alkoxysilane groups. The Fe_3O_4/SiO_2 particles with terminated amino groups obtained this way were vacuum dried and then dispersed in a solution containing the template *p*-NP, and the functional groups, o-phenylenediamine (OPDA) and ammonium persulfate.

The final polymer was isolated by magnetic separation and the template was removed. XRD, SEM and FT-IR were performed on the products. The adsorption ability of the catalyst was determined by calculating the organic mass balance

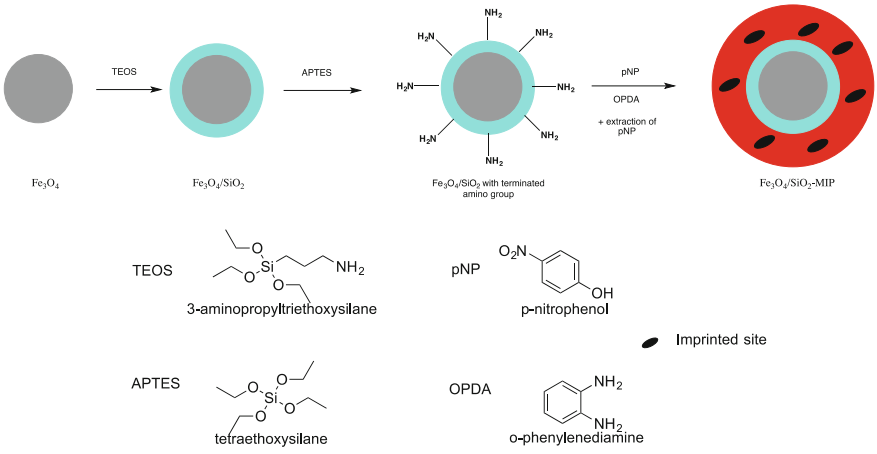

Fig. 5 Synthesis of molecularly imprinted Fe_3O_4/SiO_2 and structures of the used materials [42]

before and after the sorption; the conducted adsorption experiments showed that the adsorption ability of *p*-NP using Fe_3O_4/SiO_2-MIP was enhanced, compared to that of Fe_3O_4/SiO_2-NIP, synthesized in the absence of template. The reason for this enhanced ability of MIP could be due to the strong bonding between *p*-NP and the molecular imprinting layer. The catalytic ozonation activity was investigated by evaluating the degradation of *p*-NP. The degradation efficiency of *p*-NP using Fe_3O_4/SiO_2-MIP in the presence of O_3 reached approximately 75 % within 60 min, significantly higher than that using Fe_3O_4/SiO_2-MIP in the absence of O_3. The enhanced activity of catalytic ozonation using Fe_3O_4/SiO_2-MIP can be ascribed to the production of hydroxyl radicals in the catalytic ozonation process. The degradation efficiency of p-NP by catalytic ozonation using Fe_3O_4/SiO_2-MIP is much higher than that using Fe_3O_4/SiO_2-NIP, due to the binding between *p*-NP and the molecular imprinted layer on the MIP. Thus, Fe_3O_4/SiO_2-MIP demonstrated a preferential catalytic ozonation of *p*-NP by the recognition ability of the molecularly imprinted layer to the target *p*-NP molecules. Moreover, tests on the recognition ability and selectivity of Fe_3O_4/SiO_2-MIP to *p*-NP, when other organic contaminants (i.e., phenols) are present in the sample, were necessary. The degradation efficiency of *p*-NP and phenol by catalytic ozonation using Fe_3O_4/SiO_2-MIP in *p*-NP solution containing phenol is approximately 75 and 40 %, respectively, and the difference in the degradation efficiency between *p*-NP and phenol using Fe_3O_4/SiO_2-MIP is about 35 %. In contrast, the degradation efficiency of *p*-NP and phenol by catalytic ozonation using Fe_3O_4/SiO_2-NIP in *p*-NP solution containing phenol is about 39 and 31 %, respectively, and the difference in the degradation efficiency between *p*-NP and phenol is approximately 8 %. Thus, Fe_3O_4/SiO_2-MIP composites have higher recognition and selectivity to *p*-NP target compounds than phenol compounds in the catalytic ozonation process, even in the presence of coexistent non-target phenol. This material could hence be used in water purification.

Another interesting example of molecular surface-imprinted polymer was presented by Erdem et al. in 2010 [43]. Methacryloylhistidine-Co^{2+}, -Ni^{2+}, -Zn^{2+} (MAH-M^{2+}) monomers were used to synthesize MIPs in the form of beads (PIBs), which were used to hydrolyze paraoxon, the high toxic organophosphate used as pesticides. The technique used was suspension polymerization, which is carried out by stirring together the functional monomers, MAH-M^{2+}, and the template, paraoxon, the mixture to which the cross-linker, EDMA, is added, and then, the initiator, AIBN; the resulting solution is then transferred to the dispersion medium and heated. The precipitated PIBs are filtered off and washed in order to remove the template and leave the empty cavities. The polymers were characterized by UV-Vis, Zetasizer, surface area measurements, ICP-OES in order to calculate the amount of metals in the catalyst, and SEM. The hydrolytic catalytic activity was determined by monitoring the absorbance increase of 4-nitrophenoxide ions, the product of paraoxon hydrolysis. The rate of the paraoxon hydrolysis was enhanced both by PIBs and NIBs (non-imprinted beads), compared to the non-catalyzed reaction, although PIBs accelerate the hydrolysis more than NIBs due to their morphology, surface texture, and easy access and binding of paraoxon to the metal ions in

cavities that have the same shape and size of the analyte. The best results were obtained with MAH-Co^{2+}, which provided 365 times rate enhancement relative to the rate of non-catalyzed paraoxon hydrolysis. The effect of the temperature was also studied, and the initial rate was shown to increase as the temperature was raised.

4 Polymers with Unusual Reactivity

In this last section of the chapter, the focus will be on the preparation of MIPs that catalyze a variety of interesting chemical transformations, such as the asymmetric transfer hydrogenation, Weng et al. [44] presented the first example of a molecularly imprinted Ru-complex catalyst supported on an oxide surface for a catalytic reaction in water media. The immobilization of a metal-complex precursor on a support surface was already a well-known technique for the preparation of heterogeneous catalysts. In order to improve the characteristic of heterogeneous catalysts, a molecularly imprinted cavity was prepared close to the catalytically active sites, giving rise to a molecularly imprinted metal complex, thus enhancing the selectivity and efficiency.

The studied reaction was the asymmetric transfer hydrogenation (ATH) of o-fluoroacetophenone in water. The product of the reaction (R)-1-(o-fluorophenyl) ethanol was coordinated to a SiO_2-supported Ru-complex as template. Hydrophobic organic polymer matrices were stacked on the surface of SiO_2 by photopolymerization of ThreeBond 3026E (acrylate oligomer (65–75 %), 2-hydroxyethyl methacrylate (20–30 %), acrylic acid (1.4 %), and photoinitiator (1–5 %)). As a first step, the Ru-complex ([(p-cymene)Ru{(1R,2R)-$NH_2CH(Ph)CH(Ph)$-$NSO_2C_8H_7$} Cl]) was prepared; later on, *p*-styryl-functionalized SiO_2 was obtained by refluxing *p*-styryltrimethoxysilane with calcinated SiO_2 while the Ru-complex was attached to the surface by the two *p*-styryl moieties in the presence of AIBN, to give the supported catalyst. Subsequently, the salt of the template, (R)-1-(o-fluorophenyl) ethanol, was chemically coordinated to the supported Ru-complex and polymer-matrix overlayers were stacked on the surface of the SiO_2 surrounding the metal complex. The final MIP matrix was obtained following removal of the template. The stacking of polymer-matrix overlayers were conducted with four methods: photopolymerization of ThreeBond 3026E containing acrylate oligomer and 2-hydroxyethyl methacrylate (PH); vapor deposition polymerization of styrene and divinylbenzene (VPD); precipitation polymerization of methylmethacrylate and ethyleneglycol dimethacrylate (PP); and hydrolysis polymerization of Si(OCH3)4, (HP). The structure and the amount of stacked material were investigated by XPS, and results showed that the PH and VPD methods gave a better surface covering. Moreover, systematic investigation of the heights of polymer matrices revealed that the polymer matrices prepared by the PH method provided efficient reaction space on the active Ru-complex, with shape-selective and enantioselective behaviors for ATH. Solid-state NMR, DR-UV/vis, XPS, XRF, ICP, TGA, and SEM were used to

characterize the structures of the molecularly imprinted Ru-complex catalysts; the catalyst prepared in this way showed a high catalytic activity.

Li et al. [45] presented a substrate-selective nanoreactor based on the high selectivity and recognition ability of MIPs, and the model reaction studied was the reduction of 4-nitrophenol (NP). The catalyst was obtained by bulk polymerization using vinylpyridine, divinylbenzene and AIBN as functional monomer, cross-linker and initiator respectively, whereas a complex between NP and Ag^+ was used as template during the imprinting process; the Ag precursor was then reduced and the imprinted NP was washed away. Three more control MIPs were prepared using comparable conditions, MIP-Ag (MIP imprinted with only Ag nanoparticles), MIP-NP (MIP imprinted with only NP) and NIP (non-imprinted polymer). The polymers were characterized by FTIR, SEM, BET and SPR, and the imprinted nanoreactors showed a higher surface area and pore volumes compared with non-imprinted NIP, with the presence of Ag causing larger pore volumes and smaller surface areas. The catalytic specificity was investigated by testing the nanoreactors' activity towards two analogues of NP, 4-nitrophenyl acetate (NPA) and 2,6-dimethyl-4-nitrophenol (DNP). Specific interactions between the nanoreactors and the substrates were investigated by TPD profiles (temperature-programmed desorption). The NP-imprinted MIP-Ag-NP and MIP-NP demonstrated stronger interactions with NP than the non-NP-imprinted, MIP-Ag and NIP. Even though NPA and DNP are structurally similar to NP, MIP-Ag-NP and MIP-NP did not demonstrate any significant resolution for either of them. Moreover, the catalytic efficiency of the materials was tested and the results were compared with the four polymers prepared. Although the MIP-Ag-NP had the highest selectivity towards the substrate, it showed a lower catalytic activity compared to the MIP-Ag, which may be due to the larger pore volume of the latter, whereas the MIP-NP and NIP did not show significant catalysis. The substrate-selectivity was further demonstrated by preparing an additional nanoreactor MIP-Ag-DNP using DNP as template, and the catalyst showed a strong interaction and high selectivity towards the DNP.

The same group published two more papers in the following two years. In 2010 they presented an improvement of the Ag nanoparticles-based nanoreactor by making it temperature-responsive [46]. Two functional polymers, poly(acrylamide) (PAAm) and poly(2-acrylamide-2-methylpropanesulfonic acid) (PAMPS), were used together in order to supply a positive response to temperature. Both monomers are soluble in aqueous media and form strong electrostatic interactions. At a relatively low temperature (20 °C), an interpolymeric complexation between PAAm and PAMPS occurs, leading to a restricted access to the encapsulated Ag nanoparticles, therefore showing weak reactivity of the nanoreactor. At a relatively high temperature (40 °C) instead, the interpolmeric complexation is dissociated with a resulting simplified access of reactants to the Ag nanoparticles, increasing the catalytic activity of the nanoreactor. The nanoreactor was synthesized via a four-step process using a polystyrene core latex, prepared by emulsion polymerization, as a seed. MBA was the cross-linker used, while AMPS and AAm were used as functional monomers, in a stoichiometric amount in order to obtain the best thermosensitive responsiveness. The Ag^+ was then added to the shell network and

subsequently reduced in order to obtain the thermo-sensitive product. The morphology of the prepared nanoreactor was studied using TEM and SPR (surface plasma resonance), and results showed that it exihibited core-shell-type structures. Moreover, the interaction within the nanoreactors was investigated by DLS, which confirmed the expected behavior of the nanoreactor as a function of the temperature.

The following year Li et al. [47] presented another thermosensitive MIPs-based catalyst using the hydrolysis of 4-nitrophenyl acetate (NPA) as the model reaction. The idea behind the new catalyst was similar to what had already been published. The interpolimeric complexation between the functional polymers that occurs at low temperatures blocks the access to the active site inhibiting the catalysis; at high temperatures, the catalysis is increased due to the dissociation of the polymers, which facilitates the access to the active site. The thermosensitive monomers used were 2-trifluoromethylacrylic acid (TFMA) and poly(1-vinylimidazole) (VI) in stoichiometric amounts. Photopolymerization was used as the polymerization technique in order to obtain the catalyst; 4-nitrophenyl phosphate (NPP) was chosen as template since it is the TSA of NP. The morphology was investigated by SEM, and TPD analysis gave some information about the interaction between the polymers and the analyte, which was shown to be highly specific and selective. DLS was used to evaluate interpolymer interaction within the prepared polymers. The catalytic efficiency was also assessed, and at 40 °C, the MIP showed significant catalysis for the hydrolysis of NPA. However, at 20 °C, the catalytic activity resulted decreased. The study demonstrated that the prepared MIPs showed a thermo-switched catalytic mechanism.

Regarding MIPs-based stimuli-responsive catalysts, another interesting investigation was published in 2010 by Chen et al. [48]. Nanospheric imprinted hydrogels, shown to be pH-sensitive and water-soluble, were prepared in order to mimic the enzyme horseradish peroxidase (HRP).

The hydrogels were prepared by precipitation polymerization using four functional monomers: N-isopropylacrylamide (NIPAM), hemin, acrylamide (AAm), and 4-vinylpyridine (VP); ethylene glycol dimethacrylate (EDMA) was used as cross-linker and homovanillic acid (HVA) as template (Fig. 6). The analyzed reaction was the oxidation of HVA to a biphenyl dimer. The morphology of the material was evaluated by ESEM (environmental scanning electron microscopy), which showed that the polymers had a spherical shape. The pH is a factor that influences the catalytic activity of enzymes, and for natural HRP, the optimum pH is 8.5. The dependence of the catalytic rates of the prepared hydrogels as a function of pH were investigated; an increase of about tenfold of the catalytic rate was observed within the pH range of 7.5–9.5, with a maximum of 8.5, compared to a non-soluble MIP presented in a previous paper.

The results were correlated with the polymers' morphology, as ESEM analysis showed the polymers swollen under both acidic and basic conditions while having a compact state at pH 8.0. Moreover, the diameter of the imprinted nanospheres was investigated by DLS; the particles' size changed—depending on the value of the pH—due to the presence of specific groups in the network. At increasing pH values,

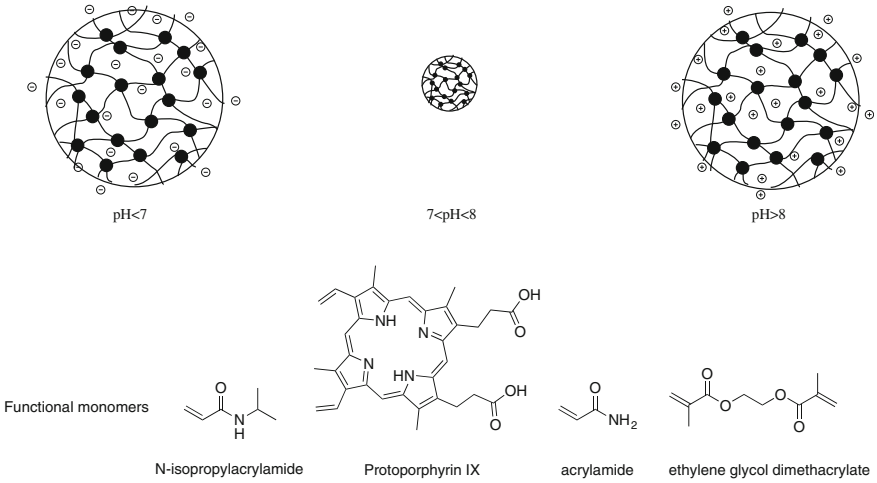

Fig. 6 Differences in size and charges expression of the hydrogels, depending on the pH. In acidic and basic conditions the hydrogel is swollen, while at pH between 7 and 8, it shrinks [48]

the carboxyl groups of hemin are deprotonated so that a negative electrostatic repulsion is created within the polymer, causing the gel network to swell. While under acidic conditions, the pyridine residues in the polymer are protonated and the positive repulsion forces increase so that the polymer gel also swells. In the pH 7–8 range, the negative and positive charges are balanced, so the gel particles turn to a compact hydrophobic spherical state. The decrease in the catalytic rate at higher or lower pH may result from a decrease in the hydrophobic affinity in the swollen gel for the substrate.

Kirsch et al. [49] presented a MIP able to catalyze Diels–Alder reactions. This is a cycloaddition reaction that is very useful in synthetic organic chemistry as a method for forming 6-membered systems with good control over regio- and stereochemical properties. The studied reaction was that of a 1-substituted diene and N,N-dimethylacrylamide, which affords a mixture of the endo- and exo-cycloaddition products. The starting material, the diene, as well as the endo- and exo-products and their TSAs, were synthesized and used as references. MIPs were prepared by photopolymerization using MAA as functional monomer, DVB (divinylbenzene) as cross-linker, and ACHN (azobis(cyclohexanecarbonitrile)) as a photoinitiator. The chosen templates were the TSA of the endo- and exo-products, thus obtaining the P_{ENDO} and P_{EXO} MIPs; a P_{REF} was furthermore prepared as a reference non-imprinted polymer. The three polymers were characterized by BET analysis and elemental analysis; batch-binding studies were also carried out, and good specific uptakes of the polymers were demonstrated.

Studies of the influence of the polymers on the reaction were performed in the presence (or absence) of the three polymers. The formation of the dominant Diels–Alder product (the endo- one), was used as a basis for monitoring the

reaction outcome. At room temperature, an increase up to 20-fold in the reaction rate relative to the non-catalyzed reaction, was observed when the three polymers were used. Although P_{ENDO} and P_{EXO} provided a slight increase in the rate over that of P_{REF}, no significant differences between the results for P_{ENDO} and P_{EXO} were evident—which indicates that there is no selectivity activity for the endo- and exo-TSAs in the active site of polymers. The same test carried out at 120 °C showed that the non-catalyzed reaction was faster than the reaction conducted with the three polymers. Moreover, the elemental composition of the polymers before and after the use as catalyst at room temperature did not change, whereas at high temperatures the elemental analysis of the recovered polymers revealed a difference in nitrogen content. These results suggested that at a high temperature, the polymers not only failed to exert an influence over the reaction outcome but seemed to inhibit the reaction.

Another experiment was carried out using TSAs as inhibitor of the catalysts, in order to prove the role of the TSA-selective sites on the reaction rate increase. The reactions were, therefore, performed in the presence of the endo-TSA at room temperature; this did not show any effect on the rate of the solution reaction, but a 30 % reduction in the performance of both P_{ENDO} and P_{EXO} were observed. Comparable results were obtained using the exo-TSA. The outcome implies that sites selective for the TSAs are responsible for the superior activity of both polymers. This indicates that approximately 30 % of the observed product arises from reactions that take place within the imprinted sites. The polymers were therefore found to enhance the rate of the reaction due to the presence of the selective sites, but only at room temperature; however, the prepared polymers showed no diastereoselective ability. The lack of discrimination between the reaction pathways leading to the two products may be due to physical closeness of the active sites that does not allow a sufficient difference in the corresponding polymers.

Two years later, the same group evaluated the influence of the cross-linker and temperature in the catalytic activity of the catalyst [50]. EGMA (ethylene glycol dimethacrylate) was used as cross-linker, while MAA, the two TSAs, and ACHN were kept in the polymerization mixture. P_{ENDO}, P_{EXO} and the P_{REF} were synthesized using the new cross-linker and tested as catalyst. The reaction carried out at room temperature in the presence of P_{ENDO} or P_{EXO} increased the rate of formation of the endo-product approximately sixfold, while the P_{REF} gave an increase of 4.5 times as compared to the solvent reaction. The only difference between the EGMA-based and DVB-based MIPs lies in the specific binding of the template to the MIP, which is higher in the former; however,the higher specific binding observed does not lead to a higher reaction rate as just seen. Although the rate of the reaction is increased when the catalyst is present, the catalysts are not diastereoselective; there is no observable difference in endo-product formation between the polymers imprinted with endo- and exo-TSAs.

The reaction was also carried out at 120 °C; at this temperature, the formation of the endo- product is slightly faster when the polymers are present in the reaction, but only during the first 20 h; after that, the non-catalyzed reaction is faster. In the case of the exo-product, the concentration in the presence of a polymer is at all

times lower than for the non-catalyzed reaction. As for the room temperature study, stereoselectivity in terms of products formed in the presence of different polymers could not be observed. Moreover, the reaction was carried out at 40 °C in order to further investigate the temperature dependence of the reaction. At this temperature, the formation of the endo-product is up to 9.5 times faster in the presence of polymer than in its absence, while a twofold enhancement of the reaction rate is obtained for the formation of the exo-product. No differences between imprinted and non-imprinted polymers were found in the formation of both products. In conclusion, the synthesized MIPs enhanced the rate of reaction only at room temperature, while at higher temperatures, the polymer participates in the reaction.

Regarding the application of MIPs as catalyst in specific classes of reactions for which no enzymes exists, as in the case of the Diels–Alder, Bonomi et al. [51] presented a nanogel able to catalyze the Kemp reaction. The Kemp elimination is a base-catalyzed ring opening of benzisoxazole. This reaction is an exothermic concerted reaction and involves an E2 mechanism; since it is not catalyzed by enzymes, various approaches were studied to develop novel catalysts. The authors studied several aspects that could influence the catalytic activity beside the morphology and the imprinting efficiency of the nanogels, such as the amount of the initiator used, the effect of the template/monomer ratio, and the molecular recognition and substrate selectivity. The studied reaction was the isomerization of 1,2-benzysoxazole resulting in the formation of 2-cyanophenol. The polymers were prepared by high dilution polymerization with AIBN as initiator, EGDMA as cross-linker and 4-vinylpyridine and indole as functional monomer and template respectively. Initiator content of 1, 2, and 3 % of the quantity of double bonds in the pre-polymerization mixture, were tested. Kinetic experiments using 1,2-benzysoxazole as substrate were carried out and the product formation was monitored by UV-Vis. The content of initiator has an effect on the catalytic properties of the nanogels, as the initiator is increased from 1 to 3 %; both the catalytic effect and the imprinting efficiency is reduced, even though a higher content of initiator leads to higher incorporation of functional monomer.

The effect of the change in template/monomer ratio was also investigated by synthesizing imprinted polymers with two and five equivalents of indole, compared with 4-vinylpyridine; the catalytic activity was compared with polymers prepared with a 1:1 ratio template/functional monomer. The resulting data showed that although the large amount of template does not affect the imprinting efficiency of the polymers, it does have a negative effect on the catalytic activity. The kinetic experiments showed, indeed, that the 1:1 ratio polymer has the highest catalytic activity. The large quantity of template involves a negative effect also in the selectivity and specificity of the polymers, leading to the generation of cavities with high heterogeneity and poor binding activity. On the other hand, similar experiments were carried out on imprinted polymers synthesized with an excess of the functional monomer (7 equivalents). Results showed a lower incorporation of functional monomer, thus a lower imprinting efficiency, even though it contained only 15 % more pyridine units compared to the polymers with a 1:1 ratio template/functional monomer. Both the imprinted and non-imprinted polymers, prepared under similar

conditions, showed some catalytic activity when compared with the background reaction, although there were no significant differences between the two polymers.

Important aspects in tailor-made catalysts are molecular recognition properties and substrate selectivity. These two features were studied by synthesizing a polymer imprinted with indole and by evaluating its catalytic activity for the Kemp elimination using a substrate analogue, 5-Cl-benzisoxazole. Moreover, new nanogels were synthesized, using 5-nitroindole as the template analogue, and the catalytic activity toward 1,2-benzisoxazole and the analogue 5-Cl-benzisoxazole was evaluated and compared. The reactions were all carried out under the same conditions, and experiments were conducted with both substrates in the presence and absence of nanogels in order to evaluate the non-catalyzed reaction rate. The kinetic data for the substrate analogue were compared with the ones for 1,2-benzisoxazole. The indole-imprinted nanogels were catalytically more efficient when working on the cognate substrate than when the analogue was present, with a k_{cat} 2.75 and 1.13 min^{-1} respectively; also, the imprinting factor in the presence of the cognate substrate was two times higher than with the analogue. The specificity and molecular recognition properties, coupled with specific catalytic activities of the indole-imprinted polymers were thus demonstrated.

Regarding the template analogue-imprinted polymer, kinetic studies on its catalytic activity with both substrates were carried out. The nanogel demonstrated catalytic activity for the reaction towards both the substrates, with k_{cat} 2.25 and 1.33 min^{-1} for the cognate and the analogue, respectively. The data indicate that the 1,2-benzisoxazole is a better substrate, giving rise to higher catalysis and imprinting efficiency. The affinity of the 5-nitroindole-shaped cavities for a smaller molecule, such as 1,2-benzisoxazole, is higher than in the case of a larger compound as 5-Cl-benzisoxazole. In conclusion, the size of the substrate seems to play an important role on its diffusion into the three-dimensional active sites of the nanogels and therefore moderate, to a certain extent, the imprinting process. Even though the template analogue-imprinted nanogel showed a higher activity towards the cognate substrate than the analogue, the activity of the indole-imprinted on the 1,2 benzisoxazole still remains the highest overall, although the imprinting efficiency remained fairly similar.

5 Conclusions

The efficiency and specificity of the enzyme active site is the outcome of specific interactions that have been optimized over time. The development of artificial mimics that can efficiently match and complement natural catalysts has considerably progressed over the past twenty years. The molecular imprinting approach has achieved significant results thanks to the sustained efforts focusing not only on the preparation of novel catalysts but also on understanding better the factors that influence the catalytic act and its detailed mechanism. Imprinted polymers have been shown to catalyze very challenging reactions such as phosphate hydrolysis,

Diels–Alder, and Kemp elimination. The efforts and future work will now need to focus on the polymeric matrix by developing novel formats and evaluating the additions of metals and ILs to enhance the activity. In addition, the ability to use materials that are stimuli responsive, for example to temperature, pH, and also UV light, will add a new dimension, and will offer new challenges and opportunities that are likely to lead to important applications.

References

1. Kirby AJ (1996) Enzyme mechanisms, models, and mimics. Angew Chem Int Ed 35:707–724
2. Hilvert D, Hill K, Nared K, Auditor M (1989) Antibody catalysis of a Diels–Alder reaction. J Am Chem Soc 111:9261–9262
3. Meekel AAP, Resmini M, Pandit UK (1996) Regioselectivity and enantioselectivity in an antibody catalysed hetero Diels–Alder reaction. Bioorg Med Chem 4:1051–1057
4. Zhang H, Piacham T, Drew M, Patek M, Mosbach K, Ye L (2006) Molecularly imprinted nanoreactors for regioselective huisgen 1,3-dipolar cycloaddition reaction. J Am Chem Soc 128:4178–4179
5. Damen J, Neckers D (1980) Stereoselective synthesis via a photochemical template effect. J Am Chem Soc 102:3265–3267
6. Shea K, Thompson E, Pandey S, Beauchamp P (1980) Template synthesis of macromolecules. Synthesis and chemistry of functionalised macroporous polydivinylbenzene. J Am Chem Soc 102:3149–3155
7. Wulff G, Vietmeier J (1989) Enzyme-analogue built polymers, 25. Synthesis of macroporous copolymers from a-amino-acid based vinyl compounds. J Macromol Chem Phys 190:1717–1726
8. Leonhardt A, Mosbach K (1987) Enzyme-mimicking polymers exhibiting specific substrate binding and catalytic functions. React Polym 6:285–290
9. Robinson DK, Mosbach K (1989) Molecular imprinting of a transition-state analog leads to a polymer exhibiting esterolytic activity. J Chem Soc Chem Commun 14:969–970
10. Sellergren B, Shea K (1994) Enantioselective ester hydrolysis catalyzed by imprinted polymers. Tetrahedron Asymmetry 5:1403–1406
11. Wulff G, Gross T, Schonfeld R (1997) Enzyme models based on molecularly imprinted polymers with strong esterase activity. Angew Chem Int Ed 36:1961–1964
12. Muller R, Andersson LI, Mosbach K (1993) Molecularly imprinted polymers facilitating a b-elimination reaction. Macromol Rapid Commun 14:637–641
13. Beach J, Shea K (1994) Designed catalysts—A synthetic network polymer that catalyzes the dehydrofluorination of 4-fluoro-4-(p-nitrophenyl)butan-2-one. J Am Chem Soc 116:379–380
14. Matsui J, Nicholls IA, Karube I, Mosbach K (1996) Carbon-carbon bond formation using substrate selective catalytic polymers prepared by molecular imprinting: An artificial class II aldolase. J Org Chem 61:5414–5417
15. Kirsch N, Hedin-Dahlstrom J, Henschel H, Whitcombe M, Wikman S, Nicholls I (2009) Molecularly imprinted polymer catalysis of a Diels–Alder reaction. J Mol Catal B Enzym 985 (58):110–117
16. Meng Z, Yamazaki T, Sode K (2003) Enhancement of the catalytic activity of an artificial phosphotriesterase using a molecular imprinting technique. Biotechnol Lett 25:1075–1080
17. Cammidge AN, Baines NJ, Bellingham RK (2001) Synthesis of heterogeneous palladium catalyst assemblies by molecular imprinting. Chem Commun 24:2588–2589

18. Alexander C, Andersson HS, Andersson LI, Ansell RJ, Kirsch N, Nicholls IA, O'Mahony J, Whitcombe MJ (2006) Molecular imprinting science and technology: a survey of the literature for the years up to and including 2003. J Mol Recognit 2:106–180
19. Flavin K, Resmini M (2009) Imprinted nanomaterials: a new class of synthetic receptors. Anal Bioan Chem 393:437–444
20. Resmini M (2012) Molecularly imprinted polymers as biomimetic catalysts. ABC 402 (10):3021–3026
21. Zhang JL, Zhang M, Tang KJ, Verpoort F, Sun TL (2014) Polymer-based stimuli-responsive recyclable catalytic systems for organic synthesis. Small 10:32–46
22. Fersht A (1999) Structure and Mechanism in Protein Science. Freeman, New York
23. Lienhard GE (1973) Enzymatic catalysis and transition-state theory. Science 180 (4082):149–154
24. Shokat KM, Ko MK, Scanlan TS, Kochersperger L, Yonkovich S, Thaisrivongs S, Schultz PG (1990) Catalytic Antibodies: a new class of transition-state analogues used to elicit hydrolytic antibodies. Angew Chem Int Ed Engl 29(11):1296–1303
25. Wulff G, Sarhan A (1972) The use of polymers with enzyme-analogous structures for the resolution of racemates. Angew Chem Int Ed 11:341
26. Wulff G (1995) Molecular imprinting in cross-linked materials with the aid of molecular templates—a way towards artificial antibodies. Angew Chem Int Ed Engl 34:1812–1832
27. Yamazaki T, Yilmaz E, Mosbach K, Sode K (2001) Towards the use of molecularly imprinted polymers containing imidazoles and bivalent metal complexes for the detection and degradation of organophosphotriester pesticides. Anal Chim Acta 435:209–214
28. Meng Z, Yamazaki T, Sode K (2003) Enhancement of the catalytic activity of an artificial phosphotriesterase using a molecular imprinting technique. Biotechnol Letters 25:1075–1080
29. Saya R, Erdema M, Ersoz A, Turka H, Denizli A (2005) Biomimetic catalysis of an organophosphate by molecularly surface imprinted polymers. Appl Catal A 286:221–225
30. Guo Y, Guo T (2013) A dual template imprinted capsule with remarkably enhanced catalytic activity for pesticide degradation and elimination simultaneously. Chem Commun 49:1073–1075
31. Carboni D, Malfatti L, Pinna A, Lasio B, Tokudome Y, Takahashi M, Innocenzi P (2013) Molecularly imprinted La-doped mesoporous titania film with hydrolytic properties toward organophosphates pesticide. New J Chem 37:2995–3002
32. Striegler S, Barnett JD, Dunaway NA (2012) Glycoside hydrolysis with sugar-templated microgel catalysts. ACS Catal 2:50–55
33. Striegler S, Dunaway NA, Gichinga MG, Barnett JD, Nelson AGD (2010) Evaluating binuclear copper(II) complexes for glycoside hydrolysis. Inorg Chem 49(6):2639–2648
34. Abbate V, Bassindale AR, Brandstadt KF, Taylor PG (2011) Biomimetic catalysis at silicon center using molecularly imprinted polymers. J Catal 284:68–76
35. Li S, Ge Y, Tiwari A, Wang S, Turner APF, Piletsky SA (2011) 'On/off'-switchable catalysis by a smart enzyme-like imprinted polymer. J Catal 278:173–180
36. Li S, Luo Y, Whitcombe MJ, Piletsky SA (2013) A successive-reaction nanoreactor made of active molecularly imprinted polymer containing Ag nanoparticles. J Mater Chem A 1:15102–15109
37. Shiraishi Y, Suzuki T, Hirai T (2010) Selective photooxidation of chlorophenols with molecularly imprinted polymers containing a photosensitizer. New J Chem 34:714–717
38. Jakubiak-Marcinkowska A, Legan M, Jezierska J (2013) Molecularly imprinted polymeric Cu (II) catalysts with modified active centres mimicking oxidation enzymes. J Polym Res 20:317
39. Díaz-Díaz G, Diñeiro Y, Menéndez MI, Blanco-López MC, Lobo-Castañón MJ, Miranda-Ordieres AJ, Tuñón-Blanco P (2011) Molecularly imprinted catalytic polymers with biomimetic chloroperoxidase activity. Polymer 52:2468–2473
40. Díaz-Díaz G, Blanco-López MC, Lobo-Castanón MJ, Miranda-Ordieres AJ, Tunón-Blanco P (2012) New materials for analytical biomimetic assays based on affinity and catalytic receptors prepared by molecular imprinting. J Mol Catal A: Chem 353–354:117–121

41. Czulak J, Jakubiak-Marcinkowska A, Trochimczuk A (2013) Polymer catalysts imprinted with metal ions as biomimics of metalloenzymes. Adv Mater Sci Eng 2013:9
42. Yang J, Li S, Gong Y, He C, Zhang Q, Wu J, Liao W, Shu D, Tian S (2014) Preferential catalytic ozonation of p-nitrophenol by molecularly imprinted Fe_3O_4/SiO_2 core-shell magnetic composites. Water Sci Technol 69(1):170–176
43. Erdem M, Say R, Ersöz A, Denizli A, Türk H (2010) Biomimicking, metal-chelating and surface-imprinted polymers for the degradation of pesticides. React Funct Polym 70:238–243
44. Weng Z, Muratsugu S, Ishiguro N, Ohkoshid S, Tada M (2011) Preparation of surface molecularly imprinted Ru-complex catalysts for asymmetric transfer hydrogenation in water media. Dalton Trans 40:2338–2347
45. Li S, Gong S (2009) A substrate-selective nanoreactor made of molecularly imprinted polymer containing catalytic silver nanoparticles. Adv Funct Mater 19:2601–2606
46. Li S, Ge Y, Tiwari A, Cao S (2010) A temperature-responsive nanoreactor. Small 6 (21):2453–2459
47. Li S, Ge Y, Turner APF (2011) A catalytic and positively thermosensitive molecularly imprinted polymer. Adv Funct Mater 21:1194–1200
48. Chen Z, Xu L, Liang Y, Zhao M (2010) pH-sensitive water-soluble nanospheric imprinted hydrogels prepared as horseradish peroxidase mimetic enzymes. Adv Mater 22:1488–1492
49. Kirscha N, Hedin-Dahlstroma J, Henschela H, Whitcombeb MJ, Wikmana S, Nicholls IA (2009) Molecularly imprinted polymer catalysis of a Diels–Alder reaction. J Mol Catal B Enzym 58:110–117
50. Henschela H, Kirscha N, Hedin-Dahlströma J, Whitcombeb MJ, Wikmana S, Nicholls IA (2011) Effect of the cross-linker on the general performance and temperature dependent behaviour of a molecularly imprinted polymer catalyst of a Diels–Alder reaction. J Mol Catal B Enzym 72:199–205
51. Bonomi P, Servant A, Resmini M (2012) Modulation of imprinting efficiency in nanogels with catalytic activity in the Kemp elimination. J Mol Recognit 25:352–360

Adv Biochem Eng Biotechnol (2015) 150: 131–166
DOI 10.1007/10_2015_317

Published Online: 22 March 2015

MIPs in Aqueous Environments

Ying-chun Wan, Hui-ting Ma and Bin Lu

Abstract When organic solvent-compatible molecularly imprinted polymers (MIPs) are used in aqueous environment, how to reduce nonspecific binding is a major challenge. By modifying the binding solvents and introducing appropriate washing and elution steps, even relatively hydrophobic MIPs can gain optimal rebinding selectivity in aqueous conditions. Furthermore, water-compatible MIPs that can be used to treat aqueous samples directly have been prepared. The use of hydrophilic co-monomers, the controlled surface modification through controlled radical polymerization, and the new interfacial molecular imprinting methods are different strategies to prepare water-compatible MIPs. By combining MIPs with other techniques, both organic solvent-compatible and water-compatible MIPs can display better functional performances in aqueous conditions. Intensive studies on MIPs in aqueous conditions can provide new MIPs with much-improved compatibilities that will lead to more interesting applications in biomedicine and biotechnology.

Keywords Aqueous conditions · Molecularly imprinted polymers · Preparation and application · Water-compatible · Organic solvent-compatible

Contents

Y. Wan · H. Ma · B. Lu (✉)
Institute of Environmental Medicine, School of Public Health, Tongji Medical College, Huazhong University of Science and Technology, #13 Hangkong Rd, Wuhan, China
e-mail: lubin@mails.tjmu.edu.cn

1 Introduction

Molecularly imprinted polymers (MIPs) are synthetic cross-linked polymers that possess specific cavities designed for a target molecule (template). MIPs are frequently named as artificial antibodies or plastic antibodies due to the fact that they can recognize and bind the target analytes selectively, as the antibody does. Compared to antibodies, MIPs are more stable to pH, temperature, and organic solvents, with high mechanical strength, low cost, reusability, and easy to make. MIPs have been widely used in separations, sensors, catalysis, and assays because they are very robust and can operate under largely different conditions.

MIPs are prepared by the cross-linking of functional monomers in the presence of a template molecule. Removal of the template from the polymer leaves cavities of complementary size, shape, and chemical functionality in the template. The selectivity of a MIP results from the presence of specific cavities designed for the target analytes. MIPs can be prepared by covalent [1], non-covalent [2, 3] and semi-covalent molecular imprinting [4]. Due to its simplicity and the easy access to numerous commercially available functional monomers, non-covalent imprinting has become the most widely used method to prepare MIPs for analytes present in the environment, ranging from pure organic solvents to biological fluids. In non-covalent imprinting, ligand-selective high-affinity binding sites in MIPs prepared in non-covalent polymerization are achieved through weak-to-medium non-covalent strength interactions (such as hydrogen bonding, electrostatic interactions, hydrophobic effect, metal–ion coordination, and Van der Waals force) between templates and functional monomers. Water can interfere with the hydrogen bonds between the template and the functional monomers, which will inevitably weaken the interactions formed between the template and the functional monomers. Furthermore, non-selective hydrophilic and metal–ion interaction between the sample matrix and functional monomers will increase in water. All these factors reduce binding selectivity of MIPs in aqueous conditions.

Because many target molecules of interest are present in aqueous media such as bodily fluids, foods, environmental samples, MIPs with satisfactory molecular recognition in aqueous media are greatly needed. Water generally destroys the polar interaction between the functional monomer and the template molecule. In order to retain selective molecular recognition in water, enhancing binding interactions

between the target molecule and the functional monomers while overcoming the non-specific binding induced by aqueous sample matrix are both needed. In this chapter, we focus on the preparation and application of MIPs in aqueous conditions.

2 Organic Solvent-Compatible MIPs in Aqueous Conditions

A large number of target molecules (templates) have been used in preparing MIPs over the past years. The majority of MIPs used in aqueous conditions are synthesized in aprotic or low polar organic solvents by the non-covalent method, especially for templates with low molecular weight. Although MIPs synthesized by this approach have exhibited recognition properties under non-aqueous and aqueous conditions, they offer the highest binding selectivity in porogens used in the polymerization process. Because water generally destroys the polar interaction between the functional monomer and the template molecule, binding selectivity of organic solvent compatible MIPs in water is generally reduced. Various approaches are used to improve molecular recognition of organic solvent-compatible MIPs in water.

2.1 Washing Solvents

In water, organic solvent-compatible MIPs behave like a reverse-phase sorbent. Therefore, a washing solvent able to remove interferences and to re-distribute nonspecifically bound analytes to the selective imprints, will enhance binding selectivity significantly. This approach is the most frequently used strategy in applications such as molecularly imprinted solid-phase extraction (MISPE), and HPLC with MIP column for analysis of complex samples.

Solid phase extraction based on MIPs, also named MISPE, is by far the most advanced application of MIPs. Typical MISPE procedures include conditioning, sample loading, washing and eluting, either in on-line or off-line MISPEs. Aqueous samples can be applied to MISPEs directly, or after sample pre-treatment such as liquid–liquid extraction. Optimizing washing conditions to remove non-selective binding but retain selective binding of target analytes with the functional monomer is critical for good MISPE effects. Most washing solvents are generally the same or close to the porogens with adding a small proportion of a polar modifier in order to limit the non-specific interactions of the target analytes with the functional monomer of the MIPs. The effects of washing solvents on the recovery of MISPEs after water samples loading are clearly illustrated in many recent reviews about MISPE [5–8].

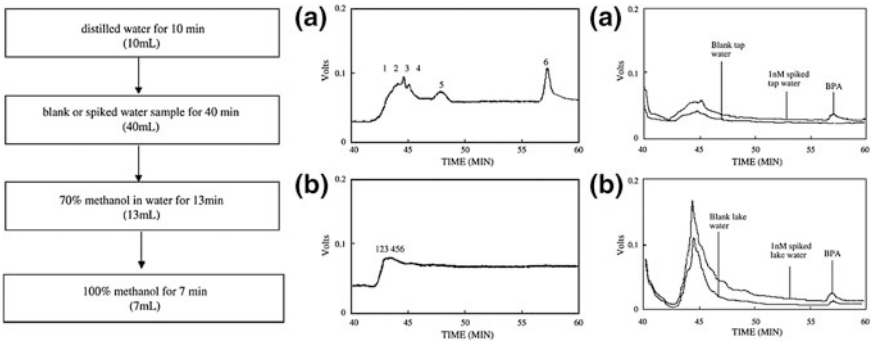

Fig. 1 *Left* The protocol for direct BPA analysis in water using MIP HPLC column. *Middle* Chromatograms obtained by direct analysis of standard solution of BPA and its analogues (10 nmol/L each) in **a** MIP column and **b** NIP column. *1* Phenol, *2* p-nitrophenol, *3* diethylstilbestrol, *4* hexoestrol, *5* Bisphenol C, and *6* Bisphenol A. *Right* Chromatograms obtained by direct analysis of BPA in **a** tap water and **b** lake water. HPLC conditions: flow rate: 1 mL/min; mobile phase: direct injecting water for 40 min, 70 % methanol in water for 13 min, then 100 % methanol for 7 min. From Ref. [9]

Organic solvent-compatible MIPs are also used as stationary phase for high-performance liquid chromatography (HPLC). When aqueous samples are loaded into MIP HPLC columns directly, washing solvents also needed to remove interferences rebind to MIPs through non-selective interactions. Results in Fig. 1 clearly indicate the effect of washing solvents for optimized HPLC detection. After water samples (40 mL) were injected into the MIP column, target analyte and interferences were retained on the column. Optimal washing solvents (70 % methanol in water for 13 min) could remove interferences effectively but retain the selective binding for the target analyte; then the target analyte can be quantified accurately in 100 % methanol. Trace BPA in lake and tap water can be simultaneously extracted, enriched, separated, determined and quantified in one analysis process using one MIPs column [9]. Recently, Liu et al. [10] reviewed the theoretical studies and application of using MIP monoliths as HPLC stationary phases.

2.2 Two-Step Extraction

Another practical strategy to solve the problem of non-selective adsorption of organic solvent-compatible MIPs in aqueous conditions is to use two-step extraction. Liquid–liquid extraction [11] or solid-phase extraction (SPE) are frequently applied as an additional extraction step to transfer analytes from aqueous media to organic phase prior to MISPE- or MIP-based solid-phase microextraction (MISPME). For example, different MIPs are used as clean-up sorbents for organic extracts obtained in a prior SPE procedure to avoid the disturbance from water [12]. But this approval is not convenient because two extraction steps are separated.

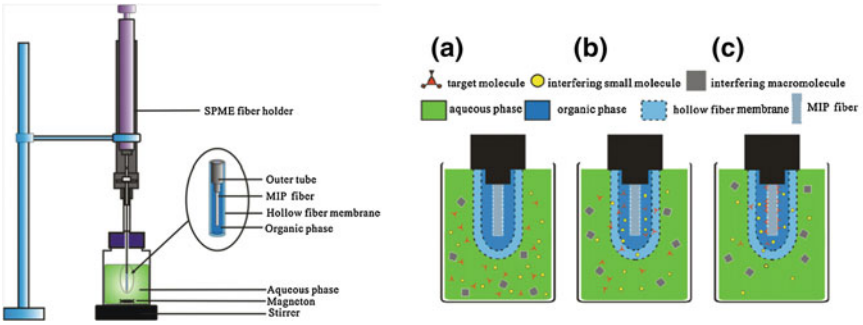

Fig. 2 *Left* Schematic of the LLSME device. *Right* Extraction process of the LLSME technique. **a** Before extraction, **b** during extraction and **c** after extraction. From Ref. [15]

Piletska et al. [13] simplified the two-step extraction by the combination of liquid–liquid extraction with MISPE in one step. By depositing a layer of mineral oil onto the surface of the polymer, a hydrophobic environment is created to improve the recognition properties of MIP in polar solvent. Following this concept, magnetic atrazine-imprinted MIP beads were applied to aqueous media with a small amount of *n*-hexane to form a co-extraction system. Compared with MIPs directly applied in aqueous samples, the binding selectivity to seven triazines increased 3.1–6.6 times in this dual-phase co-extraction system [14].

Two-step extraction is also used in microextraction. Hu et al. combined liquid–liquid extraction and MIP microextraction together (Fig. 2). A MIP-coated silica fiber was protected with a length of porous polypropylene hollow fiber membrane that was filled with water-immiscible organic phase. When immersed into an aqueous sample, target analytes were first extracted from the aqueous sample through organic phase residing in the pores and lumen of the membrane, and were then finally extracted onto the MIP fiber. This three-phase microextraction approach can effectively extract triazine herbicides in sludge water, watermelon, milk and urine samples [15].

2.3 Hydrophilic Layer

Coating a hydrophilic layer on the surface of organic solvent compatible MIPs is an effective method to improve the binding selectivity of MIPs in aqueous conditions. In order to reduce the nonspecific adsorption in water, Haginaka and co-workers coated a restricted-access hydrophilic external layer (a 1:1 mixture of glycerol monomethacrylate and glycerol dimethacrylate) on the MIPs. Selective chiral recognition sites of (S)-naproxen remained unchanged in the surface-modified MIPs [16]. In follow-up studies, the surface-modified MIPs could be applied to directly analyze (S)-naproxen and (S)-ibuprofen in serum [17] and β-blockers in biological fluids [18]. Furthermore, new restricted-access materials that combine MIPs with a

hydrophilic external layer (glycidil methacrylate) have been prepared to enable selective recognition of the corresponding templates including 5-fluorouracil [19, 20] in water.

Core–shell structure MIPs with a hydrophilic shell is another method to maintain target-specific binding in an aqueous solvent. Controlled radical polymerization (CRP) allows core–shell particles to be synthesized in one pot (Fig. 3). Hydrophilic shell layer made of acrylamide (AA) and methacrylic acid (MAA) provided good water compatibility, resulting in decreased nonspecific binding in water [21]. Other hydrophilic shells, such as dopamine, also provide good performances of MIPs achieved in aqueous conditions [22–25].

Surface-initiated reversible addition-fragmentation chain transfer (RAFT) polymerization is another method to graft hydrophilic monomers on the surface of organic solvent-compatible MIPs. As a living/control radical polymerization technique, RAFT polymerization is well under control in the presence of the RAFT agent. It has been used to prepare water-compatible MIPs with various applications including sensor and separation materials (Table 1).

RAFT precipitation polymerization mediated by hydrophilic macromolecular chain-transfer agents (macro-CTAs) were used to prepare water-compatible narrowly dispersed hydrophilic MIP nanoparticles in one-pot synthesis. The achieved MIPs can selectively rebind templates in a series of aqueous solutions (including river water, diluted and undiluted milk, and bovine serum) and prevent the accumulation of proteins on the nanoparticle surface. The chain length of the polymer brushes on the MIP nanoparticles had a significant influence on the compatibility of the nanoparticles with biological samples [26]. RAFT is also used to prepare fluorescent MIP sensors that can perform in aqueous conditions [27, 28].

Various hydrophilic chain-transfer agents used in RAFT provided different characters of the achieved MIPs [29–31]. Water-compatible and multiple stimuli-responsive MIP microspheres were prepared by grafting special hydrophilic (co) monomers such as poly(NIPAAm) (PNIPAAm), 4-((4-methacryloyloxy)-phenylazo) benzoic acid (MPABA) brushes onto the surface of MIP particles via successive

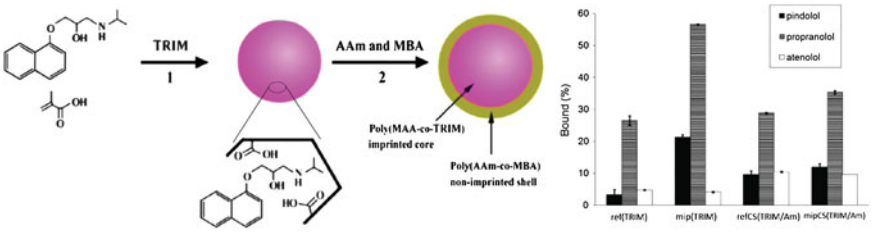

Fig. 3 *Left* One-pot synthesis of propranolol-imprinted core–shell nanoparticles. *Step 1* propranolol-imprinted sites are generated by cross-linking polymerization between MAA and TRIM in the presence of the molecular template. *Step 2* formation of hydrophilic shell by subsequent co-polymerization with AAm and MBA. *Right* Uptake of the three β-blockers by the TRIM-based nanoparticles in 25 mM citrate buffer (pH 6.0): acetonitrile (50:50). Initial concentration of each test compound: 34 μM; polymer concentration: 5 mg/mL. From Ref. [21]

Table 1 Preparation and application of water-compatible MIPs by RAFT polymerization

Ref.	Template	Monomer/ crosslinker/initiator	Chain transfer agent	Porogen	Rebinding solvent	Sample	Application
[26]	2,4-D	4-VP/EGDMA/AIBN	PHEMA/CDB	Ethanol/water	Water	Riverwater, milk, bovine serum	Sample pre-treatment
[27]	Pinacolyl methylphosphonate	MMA, styrene/ EGDMA, DVB/ Wako V-65	–	Toluene	Xylene	–	–
[28]	17β-estradiol	MAA/DVB/AIBN	Phenylmagnesium bromide	Anhydrous toluene	Ethanol	–	–
[29]	Theophylline	MAA/DVB/AIBN	–	Chloroform	Water	Human plasma serum	MISPE
[30]	2,4-dichlorophenol	MAA/DVB/AIBN	F-silica	Chloroform	Methanol–water	–	–
[31]	2,4-D	4-VP/EGDMA/AIBN	PHEMA	Methanol/water	Methanol–water	–	–
[32]	Propranolol	4-VP/EGDMA/AIBN	CS-MIP/CS-CP	DMF	ACN–water	–	–
[33]	Brucine	pGMMA/EGDMA/ AIBN	HEMA	DMF	Brucine solution	Sialic acid, galacturonic acid, ganglioside GM1	SPR sensor
[34]	2,4-D	4-VP/EGDMA/AIBN	CDB	Methanol: water (4:1)	Water	Milk, bovine serum	MISPE
[35]	Ofloxacin, pefloxacin, norfloxacin, ciprofloxacin, enrofloxacin	PVP, PAZ, MAA/ EGDMA/AIBN	CPA	Methanol, chloroform	Water	Egg	MISPE
[36]	Cholesterol	DMAAm/MBAAm/ AIBN	Sodium chloride	Toluene	Chloroform–ethanol–acetic acid	Human serum, milk, yolk, beef	MISPE
[37]	Pyrazosulfuron-ethyl	MAA/EGDMA/ AIBN	DBTTC/CDB	ACN, ACN/ toluene PEG/ acetonitrile	ACN	Dry soil	Online MISPE/ HPLC

(continued)

Table 1 (continued)

Ref.	Template	Monomer/ crosslinker/initiator	Chain transfer agent	Porogen	Rebinding solvent	Sample	Application
[38]	Carprofen	4-VP/EGDMA/AIBN	2-phenyl-2-propyl benzodithioate	DMF, DMSO, [BMIM]BF4	ACN	Milk	MISPE
[39]	Clenbuterol	pGMMA/EGDMA/ AIBN	DBTTC	Toluene/ dodecanol	MeOH–H_2O	Bovine serum albumin	Online MISPE–HPLC
[40]	Bisphenol A, propranolol	MAA/EGDMA/ AIBN	CDB	ACN/toluene	Methanol–water; ACN	–	–
[41]	Sudan I	MAA/TRIM/AIBN	Silica fibers	Acetone	Acetone	Chilli tomato sauce, chilli pepper	MIP–SPME
[42]	2,4-D	4-VP/EGDMA/AIBN	Macro-CTAs/CDB	Methanol/water	Methanol–water; water	–	–
[43]	Atrazine	MAA/EGDMA/ AIBN	CTA1/CTA2	ACN	ACN	Lettuce, corn samples	MISPE
[44]	Alkyne	MAA/DVB/AIBN	CPDB	Chloroform/ ACN	Chloroform	–	–
[45]	2,4-D	4-VP/EGDMA/AIBN	CDB	Methanol/water	Methanol–water	–	–

[BMIM]BF4 1-butyl-3-methylimidazolium tetrafluoroborate; *2,4-D* 2,4-dichlorophenoxyacetic acid; *4-VP* 4-vinylpyridine; *ACN* Acetonitrile; *AIBN* azobisisobutyronitrile; *CDB* cumyl dithiobenzoate; *CPA* Trithiocarbonate [3-(2-carboxyethylsulfanylthiocarbonyl-sulfanyl) propionic acid; *CPDB* 2-cyanoprop-2-y1-dithiobenzoate; *CS-MIP* core–shell MIP; *CS-CP* core–shell control polymer or NIP; *CTA* chain transfer agent; *DBTTC* dibenzyltrithiocarbonate; *DMAAm* dimethylacrylamide; *DMF* N,N-Dimethylformamide; *DMSO* Dimethyl sulfoxide; *DVB* divinyl benzene; *EGDMA* ethylene glycol dimethacrylate; *HPLC* High Performance Liquid Chromatography; *MAA* Methacrylic acid; *MBAAm* N,N′-methylene(bis)acrylamide; *MISPE* molecularly imprinted solid phase extraction; *PAZ* Pazufloxacin; *pGMMA* poly(glycerol mono-methacrylate); *PHEMA* hydrophilic poly(2-hydroxyethyl methacrylate); *PMP* pinacolyl methylphosphonate; *PVP* poly(vinyl pyrrolidone); *SPE* solid phase extraction; *SPR* Surface Plasmon Resonance; *STY* styrene; *TRIM* trimethylolpropane trimethacrylate; *wako V-65* 2,2′-Azobis(2,4-dimethylvaleronitrile)

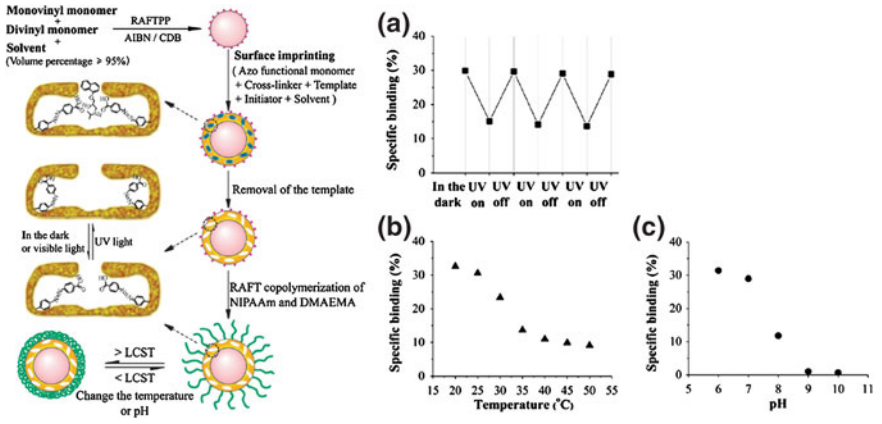

Fig. 4 *Left* Schematic protocol for the preparation of narrowly dispersed water-compatible MIP microspheres with photo-, thermos- and pH-responsive template binding properties by successive RAFT polymerization. *Right* Stimuli-responsive template bindings of the grafted CS-MIP microspheres in a propranolol solution (0.05 mM) under the photo switching conditions (i.e., UV light on for 6 h and off for 18 h alternately at 25 °C) in water (**a**), at different temperatures in water (**b**), and at different pH values at 40 °C in Britton–Robison buffer (**c**), respectively (polymer concentration: 1 mg mL^{-1}). From Ref. [32]

RAFT polymerization [32]. The achieved MIPs not only rebind templates selectively, either in water or in acentroline, but also react to various stimuli including photo, thermo and pH (Fig. 4).

Encapsulating organic solvent-compatible MIPs into water-compatible nanofibers is another method. Propranol-imprinted nanoparticles were encapsulated inside poly(ethylene terephthalate) nanofibers through electrospinning. The achieved imprinted membranes performed selective molecular adsorption either in organic or in aqueous (acetonitrile: 25 mM citrate buffer (pH 6.0), 50:50, v/v) solvents. The membranes were used as MISPE sorbents to extract propranol from water effectively [46]. Similarly, electrospun nanofiber membranes with multi-analyte selectivity were prepared by encapsulating two types of MIP nanoparticles into polyvinyl alcohol nanofibers (Fig. 5). The imprinted membranes maintained selective molecular recognition in water and can extract trace templates (bispheno A and tebuconazole) with opposite charges/polarities in vegetables and juices simultaneously with high recoveries [47].

3 Water-Compatible MIPs in Aqueous Conditions

The non-selective binding of organic solvent compatible MIPs in the pure aqueous system has limited their practical application. This drawback promotes the efforts toward the synthesis of water-compatible MIPs with reduced non-specific hydrophobic or ionic interactions. Many methods have been developed.

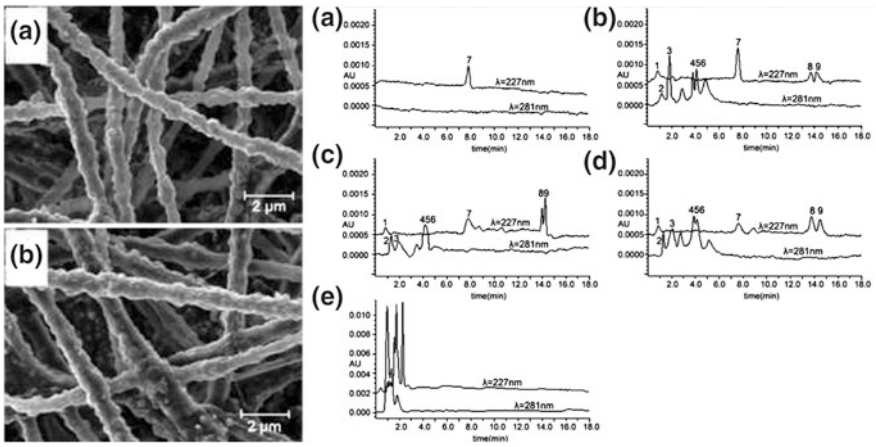

Fig. 5 *Left* SEM images of electrospun nanofiber membranes containing **a** 25 % of BPA-MIP and 25 % of TBZ-MIP nanoparticles together, **b** 50 % of non-imprinted nanoparticles. *Right* Chromatograms (HPLC) of cabbage detected at λ = 227 nm and λ = 281 nm: **a** blank cabbage after m-MISPE; **b** spiked cabbage after m-MISPE; **c** spiked cabbage after m-NISPE; **d** spiked cabbage after C18/SCX SPE; **e** spiked cabbage with direct injection. Peaks in the chromatograms relate to FTF (*1*), HQ (*2*), BPA (*3*), E2 (*4*), BPC (*5*), BPZ (*6*), TBZ (*7*), PNZ (*8*), HXZ (*9*). From Ref. [47]

3.1 Molecular Imprinting in Polar Porogens

When synthesizing MIPs, there is a strong correlation between porogen polarity, MIP microenvironment polarity and the imprinting effect. The combination of these parameters eventually determines the overall binding behavior of a MIP in a given solvent.

Water-compatible MIPs can be synthesized in a mixture of water and polar organic solvents such as methanol. Horemans et al. studied the correlation between porogen polarity, MIP microenvironment polarity and the imprinting effect. It was observed that the mixture of multiple porogens with varying polarities can lead to superior performance in aqueous environments [48]. When various ratios of water and organic solvents were used as porogens, the achieved MIPs showed higher selectivity in aqueous samples, including human urine and river water [49–54].

Suspension polymerization and emulsion polymerization were carried out in various oil/water systems. Mayers and Mosbach introduced suspension polymerization to prepare polar Boc-L-Phe imprinted microspheres using perfluorocarbon as the continuous phase. When used as a stationary phase for chromatography, small (5 μm) beaded packings gave low back pressure and rapid diffusion, giving good separation even at high flow rates [55].

Mono-dispersed MIPs were prepared by suspension polymerization using either aqueous or non-aqueous continuous phases. A stabilizer is normally used. Kempe and Kempe first introduced a stabilizer-free suspension polymerization method using acetonitrile as a pre-polymerization solvent and mineral oil as continuous

phase. The formation of stable suspension of acetonitrile microdroplets was achieved by vigorous agitation in mineral oil, followed by photoinduced free-radical polymerization [56]. Following this principle, chloroform was used as the pre-polymerization solvent and water as a continuous phase to prepare chiral selective MIPs with narrow size distribution. MIPs prepared by this approach rebind target analytes selectively in aqueous conditions [57].

Templates that are suitable for suspension polymerization include metal ions, and organic chemicals such as drugs and proteins. This heterogeneous polymerization method gives excellent heat dispersion and is easy to scale up, which makes it suitable for industrial production of MIPs (Table 2).

Emulsion polymerization is also a widely used surface imprinting method. Water-in-oil-in-water (W/O/W) multiple emulsion polymerization has been used to prepare surface-imprinted MIPs with good performance in water. A water-soluble surfactant is crucial to the stabilization of the spherical W/O/W emulsion. Morphologically well-defined imprinted spheres (sizes range from 10 to 100 μm) prepared through this approach displayed high binding selectivity in aqueous conditions (Table 3).

Mini-emulsion polymerization was used for the synthesis of molecularly imprinted nanoparticles (30–150 nm) with homogeneous binding sites (monoclonal MIP) [88]. By using a surfactant monomer sodium N-undecenoyl glycinate (SUG) and mini-emulsion polymerization, the achieved (S)-propranolol imprinted nanoparticles have a hydrophobic core region and a hydrophilic surface with size ranges from 30 to 120 nm. When used in partially filled capillary electrochromatography, there was no apparent tailing for the enantiomer peaks, and a baseline separation with 25,000–60,000 plate number was achieved in aqueous electrolytes (10 mM phosphate buffer containing 20 % acetonitrile solution at pH 7) (Fig. 6).

Nanoparticles tend to situate on water–oil interfaces to form stable nanoparticle-stabilized emulsions (Pickering emulsions). In Pickering emulsion polymerization, the monomer droplets are stabilized by nanoparticles instead of surfactants. Ye et al. first introduced a Pickering emulsion polymerization method by using template-modified nanoparticles as a stabilizer. The interfacial molecular imprinting was conducted in oil-in-water Pickering emulsions, where the molecular template was immobilized on the surface of SiO_2 nanoparticles during the polymerization. After removing the nanoparticles and the template, the MIP microspheres generated had a well-controlled hierarchical structure with easily accessible molecular binding sites and hydrophilic surface [90]. Binding capacity and water compatibility of MIP microspheres are enhanced by confining the actual molecular imprinting process in the interior of the monomer droplets in the oil-in-water Pickering emulsion (Fig. 7). Because of the special partitioning of MAA between the oil phase and the water phase, the obtained MIP particles had a high density of carboxyl groups on their surface, which allowed the hydrophilic MIP microspheres to display group selectivity toward a series of chemicals under purely aqueous conditions. Increasing the amount of porogen (toluene) can decrease the stability of the emulsion, as well as increase the surface area and the nonspecific binding of the MIP beads [91].

Table 2 Preparation and application of water-compatible MIPs synthesized by suspension polymerization

Ref.	Template	Monomer/crosslinker/initiator	Continuous phase	Stabiliser	Rebinding solvent	Sample	Application
[55]	Boc-D-Phe	MAA/EGDMA/AIBN	Perfluorocarbon liquid	PFPS	MeOH–acetic acid (9:1)	–	–
[56]	RS-propranolol	MAA/TRIM/AIBN	Mineral oil	–	ACN and water	Human serum	Sensor
[57]	CP, d-CP, BP, d-BP	MAA/TRIM/AIBN	Water	–	PBS and ACN	–	Chiral separation (HPLC column)
[58]	RS-propranolol	MAA/TRIM/DMPAP	Mineral oil, perfluorocarbon liquid	PFPS	SSC (25 mM, pH = 6.0)–ethanol (98:2)	–	–
[59]	Amobarbital	MAA/EGDMA/AIBN	Water	PVA	MeOH–water (55:45)	Human urine, medicines	MISPE
[60]	Chloro-Sudan	DMAEMA/EDMA/AIBN	Water	PVA	ACN–water	Food	MISPE
[61]	2-hydroxy-3-naphthoicacid,1-methylpiper-azine	MAA/EGDMA/AIBN	Water	PVP	0.02 M TBAB–MeOH–TFA (75:25:0.045)	Chicken muscle	MISPE
[62]	Indomethacin	MAA, AAM/EGDMA/AIBN	Water	PVA	ACN–0.2 % phosphoric acid (65:35)	Tap water, river water	MISPE
[63]	Metergoline	MAA/EGDMA/AIBN	Water	PVA	H_2O–NH_4HCO_3 buffer –MeOH	Barley	MISPE
[64]	R- or S-propranolol	MAA/EGDMA/AIBN	PMC	PPS	55 mM ammonium acetate buffer (pH = 4.0)	–	Drug delivery
[65]	Phenylephrine	MAA, 1-allyl-3-ethylimidazolium bromide/EGDMA/AIBN	Water	PVP	Water–ACN–TFA (76.5:23.5:0.001)	Urine	MISPE

(continued)

Table 2 (continued)

Ref.	Template	Monomer/crosslinker/initiator	Continuous phase	Stabiliser	Rebinding solvent	Sample	Application
[66]	Ractopamine	AAM/TRIM/AIBN	Water	PEG–Fe_3O_4	MeOH–phosphoric acid–water	Pork, pig liver	MISPE
[67]	Rhaponticin	AAM, styrene/EGDMA/AIBN	Water	PEG–Fe_3O_4	ACN–water	Patent medicines	SPE sorbents
[68]	Atrazine	MAA/EGDMA/AIBN	Water	PEG–Fe_3O_4	ACN–water (30:70)	Soybean, millet, lettuce, soil	Magnetic separation (MDE)
[69]	Cadmium nitrate	MAC, HEMA/EGDMA/BPO	Water	PVA	0.1 M acidic thiourea solution (pH 4.5)	Human plasma	Removal of Cd^{2+} (sorbents)
[70]	Aminoglutethimide	MAA/EGDMA/AIBN	Water	PVA	MeOH–acetic acid solution (9:1)	Human urine	MISPE
[71]	Chloramphenicol	DEAEM/EGDMA/AIBN	Water	PVA 1788	MeOH–water (40:60)	Milk, shrimp	MISPE
[72]	Bovine serum albumin	MAA/EGDMA/AIBN	Water	PVA	MeOH–acetic acid (9:1)	Milk	Sensor
[73]	Dibutyl phthalate (DBP)	MAA/EGDMA/AIBN	Water	PVA, Span 60	MeOH–water (10:90)	River and reservoir water	MISPE
[74]	Di(2-ethylhexyl) phthalate(DEHP)	MAA/MBAA/APS	Water	–	Dichloromethane	River water, waste water	MISPE
[75]	2,4-diamine-6-chlorine-1,3,5-triane	MAA/EGDMA/AIBN	Water	PVA	MeOH (50 mM pH = 3.0)–KH_2PO_4 (30:70)	Egg, milk	MISPE
[76]	Indole-3-acetic acid	4-VP, β-CD/EGDMA/AIBN	Water	PEG–Fe_3O_4	Acetic acid–water–MeOH	Pea, rice and wheat	Magnetic separation (MDE)
[77]	Naproxen	AAM/EGDMA/APS	Water	–	Britton–Robinson buffer (pH = 3)	Human urine	MISPE

(continued)

Table 2 (continued)

Ref.	Template	Monomer/crosslinker/initiator	Continuous phase	Stabiliser	Rebinding solvent	Sample	Application
[78]	3-hydroxy-2-naphthoic acid,1-methylpiperazine	MAA/EGDMA/AIBN	Water	PVP	Methanol–water–acetic acid (60:40:0.04)	Banana	MISPE
[79]	S-propranolol	MAA/EGDMA/AIBN	PMC	PFPS	PBS (pH = 7.4)	–	Drug delivery
[80]	Affeine	MAA/EGDMA/AIBN	Water	PVA	Ammonium formate–ACN–acetic acid (pH = 6)	Alexandrium tamarense	MISPE
[81]	RS-propranolol	MAA/TRIM/AIBN	Mineral oil	–	ACN	–	–
[82]	Benzo[a]pyrene	4-VP/EGDMA/AIBN	Water	PVA	ACN–DCM (80:20)	Water, coffee	MISPE
[83]	Trimethoprim	MAA/EGDMA/AIBN	Water	PVA	MeOH–water (80:20)	Human urine, pharmaceutical tablet	MISPE
[84]	Dibutylmelamine	MAA/EGDMA/ABVN	Water	PVA	ACN–ammonium acetate buffer (0.1 M, pH = 6.0) (47:53)	–	MISPE
[85]	Bisphenol A	4-VP/EGDMA/AIBN	Water	PVA	Water–ACN–acetic acid (65:35:0.0001)	River water	MISPE
[86]	Boc-L-Phe	MAA/TRIM/AIBN	Perfluorocarbon liquid	PFPS	DCM–acetic acid (99: l)	–	HPLC column
[87]	Matrine	MAA/EGDMA/AIBN	Water	PVA	MeOH–water (5:5)	S.flavescens extract	MISPE

AAM acrylamide; *ABVN* 2,2′-azobis(2,4-dimethylvarelonitrile); *ACN* acetonitrile; *AIBN* 2,2′-azobis-(2-methylpropionitrile); *APS* ammonium persulfate; *β-CD* β-cyclodextrin; *BIS* methylene bisacrylamide; *Boc-D-Phe* tert.-butyloxycarbonyl-D-phenylalanine; *Boc-L-Phe* tert.-butyloxycarbonyl-L-phenylalanine; *BP* brompheniramine; *BPO* enzoyl peroxide; *CP* chlorpheniramine; *chloro-Sudan* 1-(4-chlorophenyl)azonaphthalen-2-ol; *DCM* dichloromethane; *DEAEM* 2-(Diethylamino) ethyl methacrylate; *DMAEMA* N,N-dimethylaminoethyl methacrylate; *EGDMA* ethylene glycol dimethacrylate; *HEMA* hydroxyethyl methacrylate; *HPLC* high performance liquid chromatography; *MAA* methylacrylic acid; *MAC* N-Methacryloly-(l)-cysteinemethylester; *MBAA* N,N′-methylenebisacrylamide; *MeOH* methanol; *MISPE* molecularly imprinted solid phase extraction; *PBS* phosphate buffered saline; *PFPS* perfluorinated polymeric surfactants; *PPS* perfluoro polymeric surfactant; *PVA* polyvinyl alcohol; *PVP* polyvinylpyrrolidone; *Span 60* sorbitan monostearate; *SSC* sodium citrate buffer solution; *TEA* triethylamine; *TFA* trifluoroacetic acid; *TRIM* trimethylolpropane trimethacrylate; *4-VP* 4-vinylpyridine

Table 3 Preparation and application of water-compatible MIPs synthesized by emulsion polymerization

Ref.	Template	Monomer/cross linker/initiator	Oil phase/water phase	Stabilizer	Rebinding solvent	Sample	Application
[88]	S-propranolol	SUG monomer/EGDMA/AIBN	Hexadecane/water	SUG	10 mM PBS (pH = 7)–ACN (80:20)	–	Chiral separation (CEC column)
[89]	Atenolol	MAA/EGDMA/AIBN	–/water	Modified silica nanoparticles	Water	–	–
[90]	RS-propranolol	MMA/EGDMA/AIBN	Toluene/water	Silica nanoparticles, Triton X-100	Water and toluene	–	–
[91]	RS-propranolol	MAA/DVB/AIBN	ACN/water	MIP–NH_2 microspheres	25 mM SSC (pH = 6.0)–ACN (50:50)	–	Drug delivery
[92]	Lambdacyhalothrin	MAA/EGDMA/AAPD	Chloroform/water	Magnetic halloysite nanotubes	Ethanol–water (5:5)	–	–
[93]	Gatifloxacin	AAM, β-CD-A/MBAA/$K_2S_2O_3$	Cyclohexane/water	Span 60	MeOH–water (20:80)	–	–
[94]	Doxycycline	MAA/TRIM/AIBN	Oleic acid/water	Span 80	MeOH–ACN–10 mM oxalic acid solution (5:25:70)	Spiked milk	Magnetic separation (MDE)
[95]	RNase A	MMA/EGDMA/APS	Oleic acid/water	SDS	ACN–water–TFA (80:20:0.99)	–	–
[96]	Tratarzine	MAA, 1-MA-3MI-Br, 4-VP/TRIM/AIBN	Toluene/water	HEC, Span 80	MeOH–20 mM CH_3COONH_4 buffer (20:80)	River water, waste water	MISPE
[97]	Uranyl ions	HASS/DVB/KPS	Styrene/water	Triton X-100	0.1 M HNO_3 solution	–	–

(continued)

Table 3 (continued)

Ref.	Template	Monomer/cross linker/ initiator	Oil phase/ water phase	Stabilizer	Rebinding solvent	Sample	Application
[98]	Tetracycline	MMA/EGDMA/ PMDETA	–/water	Tween	Trichloroacetic acid solution	Pork	MISPE
[99]	Glycylglycine	UPTMOS/TMOS/NaOH (catalyst)	Hexane or cyclohexane/ water	Span 80	ACN-0.1 M CH_3COONa/CH_3COOH buffer (3:2)	–	MISPE
[100]	Propranolol	MMA/DVB/benzoyl peroxide	–/water	PVA	ACN–PBS (pH = 7.4)–triethylamine	–	–
[101]	Lysozyme	MAH/EGDMA/APS, $NaHSO_3$	–/water	PVA, SDS	PBS (100 mM, pH = 7.4)	Egg white	Sensor
[102]	Glucopyranoside	Phenylethylene/DVB/ AMBN	Hexadecane, styrene/water	SDS	ACN	–	–
[103]	Carbamazepine	MAA/EGDMA/AIBN	Hexadecane/ water	SDS	ACN–MeOH–water (20:38:42)	Human serum	Drug carriers
[104]	Bovine serum albumin	MMA/EGDMA/APS	Oleic acid/ water	SDS	ACN–water–TFA (80:20:0.09)	–	–
[105]	D,L-propranolol	MAA, MMA/EGDMA/ APS	–/water	SDS	25 mM SSC (pH = 4.2)–acetic acid–ethanol (98:0.005:2)	–	–
[106]	$CdCl_2$, $ZnCl_2$, sodium arsenate	Phenyl methacrylate, methyl methacrylate/ EDMA/AAPD	–/water	Brij-56	MeOH–water (4:1)	–	MISPE
[107]	Ferrocyanide	4-VP/DVB/V-50,V70	Styrene, *n*-butyl acrylate/ water	–	0.01 M potassium chloride solution	–	–

(continued)

Table 3 (continued)

Ref.	Template	Monomer/cross linker/ initiator	Oil phase/ water phase	Stabilizer	Rebinding solvent	Sample	Application
[108]	Hemoglobin	AAM, HMAAm, BIS/ TEOS/APS	Toluene, *n*-hexane/water	Hydrophobic SiO_2 nanoparticles	PBS (150 mM, pH = 7.4)	–	–
[109]	λ-cyhalothrin	MAA, 4-VP, styrene/–/ AIBME	Hexadecane/ water	Attapulgite particles	Ethanol–water (5:5)	–	–
[110]	λ-cyhalothrin	MAA/EGDMA/AIBME	–/water	Modified yeast particles	Ethanol–water (1:1)	–	–
[111]	Chlorogenic acid	MAA/TRIM/AIBN	Oleic acid, toluene/water	–	0.4 % phosphate solution —MeOH	Honey-suckle	Magnetic separation (MDE)

AAM acrylamide; *AAPD* 2,2-azobis(2-metbylpropionamidine) dihydrochloride; *ACN* acetonitrile; *AIBN* 2,2′-azobis-(2-methylpropionitrile); *AIBME* dimethyl 2,2′-azobis(2-methylpropionate); *AMBN* 2,2-azo(2-methylbutyronitrile); *APS* ammonium persulfate; *β-CD-A* acrylamide and acryloyl-β-CD; *BIS* methylene bisacrylamide; *CEC* capillary electrochromatography; *DVB* divinylbenzene; *EGDMA* ethylene glycol dimethacrylate; *HASS* salicyaldehyde-p-aminostyrene; *HEC* hydroxyethyl cellulose; *HMAAm* N-hydroxymethyl acrylamide; *HPLC* high performance liquid chromatography; *KPS* potassium persulfate; *MAA* methylacrylic acid; *MAH* N-methacryloyl-l-histidine methylester; *MBAA* N,N′-methylenebisacrylamide; *MeOH* methanol; *MISPE* molecularly imprinted solid phase extraction; *PBS* phosphate buffered saline; *PVA* polyvinyl alcohol; *PMDETA* 1,1,4,7,7-pentamethyl-diethylenetriamine; *SDS* sodium dodecyl sulfate; *Span 60* sorbitan monostearate; *Span 80* sorbitan monooleate; *SSC* sodium citrate buffer solution; *SUG* sodium N-undecenoyl glycinate; *TEOS* ethylsilicate; *TRIM* trimethylol-propane trimethacrylate; *UPTMOS* 1-[3-(trimethoxysilyl)propyl]urea; *V-50* 2,2′-Azobis(2-methylpropionamide)dihydrochloride; *V-70* 2,2′-Azobis(4-methoxy-2.4-dimethyl valeronitrile); *1-MA-3MI-Br* 1-(-methylacrylate)-3-methylimidazolium bromide; *4-VP* 4-vinylpyridine

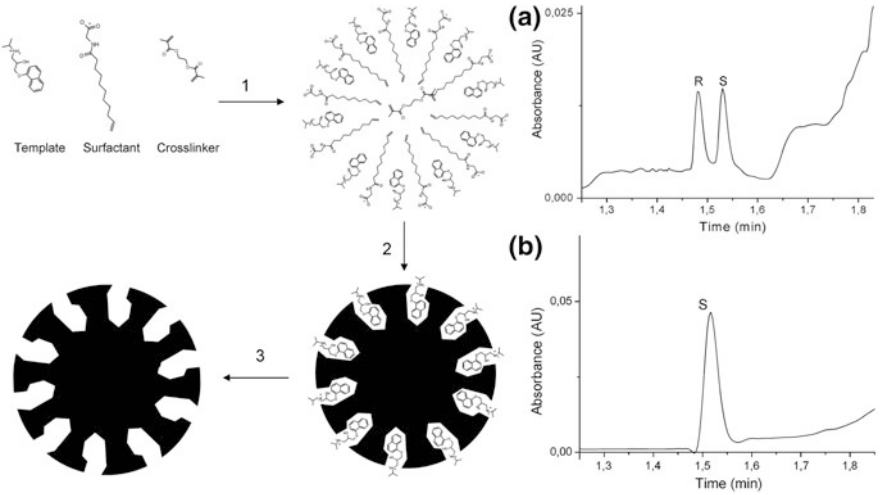

Fig. 6 *Left* Synthesis of imprinted nanoparticles by miniemulsion polymerization using a functional SUG surfactant: *1* pre-assembly of the imprinting complex; *2* cross-linking polymerization; *3* template removal. *Right* CEC analysis of *A* rac-propranolol and *B* (S)-propranolol (60 μM) demonstrating the imprinting effect and identifying the peaks. Nanoparticle hydrodynamic injection (10 mg/mL) 0.5 psi for 10 s, sample injection 3 s at 6 kV, electrolyte 10 mM phosphate/20 % (v/v) acetonitrile at pH 7, voltage of separation 16 kV, and temperature of the capillary 30 °C. From Ref. [88]

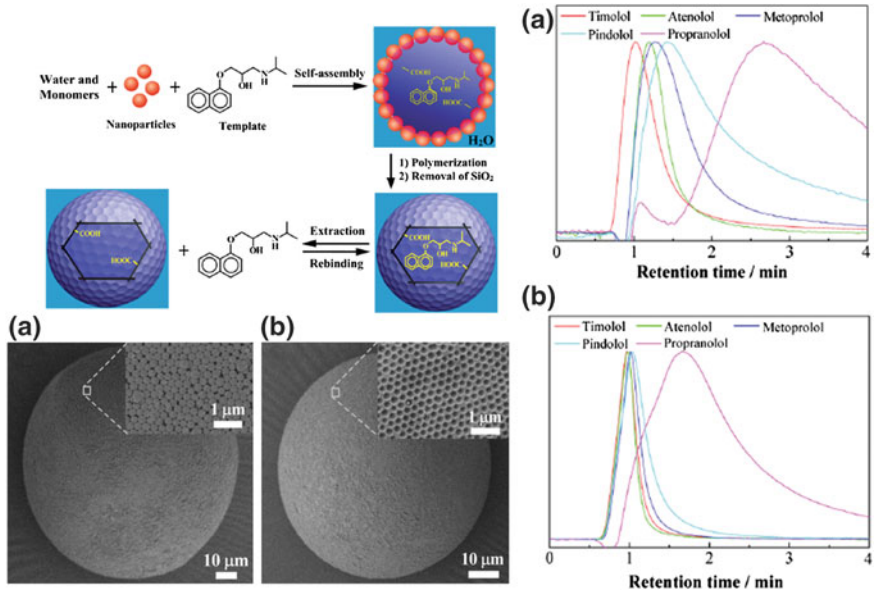

Fig. 7 *Top left* Schematic illustration for the synthesis of MIP microspheres via Pickering emulsion polymerization. *Bottom left* SEM images of the polymer microspheres before (**a**) and after (**b**) the silica particles have been removed. *Right* Chromatograms of propranolol and its analogues on **a** an MIP-P2 column and **b** an NIP-P2 column. MIP-P2 and NIP-P2 are polymer microspheres prepared by Pickering emulsion polymerization under optimized condition. From Ref. [90]

Except for template-modified nanoparticles, Janus particles [92] or magnetic halloysite nanotubes [93] were also used as stabilizers to prepare MIPs using Pickering emulsion polymerization. The achieved MIPs also have selectivity in aqueous conditions.

3.2 Using Hydrophilic Comonomer or Monomer

The incorporation of polar or nonpolar comonomers in the MIP matrix is another method for preparing water-compatible MIPs. Various hydrophilic monomers or comonomers and polymerization systems were reported. By using hydrophilic copolymers, MIPs can be wetted by water and exhibit low nonspecific adsorption in water (Table 4).

2-hydroxyethyl methacrylate (HEMA) and acrylamide are commonly used hydrophilic comonomers. Sellergren et al. [112] discovered that the water compatibility of achieved MIPs is affected by the added amount of the hydrophilic comonomer HEMA, the cross-linking ratio, and the porogen. MIPs prepared under optimal conditions showed high imprinting factors in water. Pure water-compatible MIPs have been successfully prepared by adding certain amounts of HEMA and acrylamide in the molecular imprinting processes, and their improved surface hydrophilicity proved to be responsible for the water-compatibility [112, 128, 130–140].

β-cyclodextrin (β-CD) is a series of cyclic oligosaccharides with a hydrophilic exterior and hydrophobic cavity. β-CD forms inclusion compounds with hydrophobic guests in water. MIPs prepared using functionalized silica gel bonded β-CD and acrylamide together. The material comprised a hydrophobic moiety [the selective recognition element (bonded β-CD)] and a hydrogen bond interaction functional monomer (acrylamide). The bonded β-CD and AA cooperating together improved the binding selectivity in water. The column packed with the MIPs could separate the template from its enantiomer in the aqueous mobile phase [123]. Other MIPs prepared using β-CD monomer have good binding selectivity in aqueous solutions [120–127].

Primary amines such as dopamine and o-phenylenediamine are also normally used hydrophilic monomers. By modification with primary amines in the polymer, the obtained MIPs can specifically recognize their targets and barely bind the nontargets in water. Incubation of a template in an alkaline dopamine solution resulted in oxidative polymerization of dopamine and formation of a heterogeneous imprinted polymer coating [22–25, 115–118]. This method combines the merits of surface-imprinting and self-polymerization together. Furthermore, hydrophilic macromolecules (such as chitosan [143]) and sugar moiety [144] have been directly introduced into the imprinted polymers, and the resulting MIPs could separate L-glutamic acid or phenobarbital from dilute aqueous solution.

Hydrogel, a colloidal gel using water as the dispersion medium, has been used in biomedical and applied biology, owing to its good water permeation characteristics. Molecularly imprinted hydrogels have highly ordered, three-dimensional (3-D)

Table 4 Preparation and application of water-compatible MIPs based on hydrophilic monomers/comonomers

Ref.	Template	Monomer/comonomer	Cross linker/ initiator	Porogen	Rebinding solvent	Sample	Application
[22]	Chlorpyrifos	Dopamine	/	Water	Water	Apples	SPR sensor
[23]	Bovine hemoglobin	Dopamine	/	Tris-HCl buffer	Water	Cattle whole blood	MISPE
[24]	Human serum albumin	Dopamine	/	PBS	PBS	–	HPLC column
[25]	Bovine hemoglobin	Dopamine	–/APS	PBS	10 mM PBS (pH 7.5) containing 0.01 % SDS	–	–
[112]	Bupivacaine	MAA/HEMA	EGDMA/ABDV	DCM, TCE, toluene, MTBE	Aqueous buffer	Blood plasma	MISPE
[113]	2-(4-methoxyphenyl) ethylamine	MAA, Acrylic acid; Trifluoromethacrylic acid; Itaconic acid; Acrylamide; 2-Phenylpropene; Allylamine	EGDMA/AIBN	Chloroform, toluene, methanol–toluene, methanol	Methanol–water (85:15 v/v)	–	–
[114]	Ascorbic acid	PPy	/	Ethanol–water	Water	–	–
[115]	Lysozyme	Dopamine	/	Tris-HCl buffer	Tris-HCl buffer	–	–
[116]	1,3,5-pentanetricarboxylic acid	Dopamine	/	Tris-HCl buffer	Methanol	Blue mussels	QCM sensor
[117]	Bovine hemoglobin	Dopamine	–/APS	PBS	PBS	–	–
[118]	Nicotine	Dopamine	/	PBS	PBS	Small aliquots of nicotine	MIPC sensor
[119]	Deltamethrin	BBA-β-CD, β-CD	TDI/65 °C	Distilled water	Water	River, lake, tap, pond water, drinking water	MISPE

(continued)

Table 4 (continued)

Ref.	Template	Monomer/comonomer	Cross linker/ initiator	Porogen	Rebinding solvent	Sample	Application
[120]	Gatifloxacin	Acryloyl-β-CD/AAM	MBAA/$K_2S_2O_3$	DMF	Water	–	–
[121]	Erythromycin	Acryloyl-β-CD/MAA	EGDMA/AIBN	ACN	CH_3Cl	Chicken muscle	MISPE
[122]	Indole-3-acetic acid	β-CD/4-VP	TRIM/AIBN	DMF	Methanol	Pea/rice/wheat	MISPE
[123]	Tryptophan, l-Trp	β-CD/acrylic acid	TEMED/APS	PBS	PBS	–	–
[124]	Bilirubin	β-CD	DICH/65 °C	DMSO	Methanol	Serum	Sample pretreatment (sorbent)
[125]	Norfloxacin	BMA-β-CD/DEAEM	EGDMA/AIBN	DMSO	H_2O–methanol	–	–
[126]	Creatinine	β-CD/4-VP	EPI-DVB/AIBN	DMSO	PBS	Human serum	Sample pretreatment (sorbent)
[127]	Creatinine	β-CD	Epichlorohydrin/ $NaBH_4$	NaOH solution	PBS	–	–
[128]	Myoglobin	HEMA-MATrp	EGDMA/AIBN	Dichloromethane	Isotonic solution	Human serum	SPR sensor
[129]	THC-OH	MAA, HEMA, 4-VP	EGDMA/AIBN	Methanol	Acetate buffer	urine	MISPE
[130]	17β-estradiol	HEMA	EGDMA/ TEMED	Toluene, ACN	Methanol–water	–	–
[131]	Cinchonidine	MAA/HEMA	DVB/AIBN	ACN–toluene	ACN	–	–
[132]	(-)-ephedrine	HEMA, TFMAA, IA	EGDMA, DVB/ AIBN	$CHCl_3$, MeCN, THF	DCM, DCM–$BuNH_2$, ACN–$BuNH_2$	–	HPLC column
[133]	Ofloxacin	HEMA	EGDMA/AIBN	Methanol–water	ACN	Milk	MISPE
[134]	CDHB, resorcinol, resorcylic acid	HEMA; 2-DAEM; 4-VP; 1-ALPP	TRIM/AIBN	ACN	ACN	–	–
[135]	Lysozyme	HEMA-MAH	MBAA/ TEMED-APS	Water	PBS	Chicken egg white	MISPE

(continued)

Table 4 (continued)

Ref.	Template	Monomer/comonomer	Cross linker/ initiator	Porogen	Rebinding solvent	Sample	Application
[136]	Al^{3+}	HEMA/acrylamide	EGDMA/AIBN	Methanol	PBS	–	–
[137]	Glucose, proxyphylline	HEMA	PEG600DMA/ Irgacure-184	Water	Water	–	MISPE
[138]	Propranolol, morphine	MAA, HEMA, AA, 2-VPy	EGDMA/ DMPAP	Ethanol	Ethanol	–	MISPE
[139]	Simazine	MAA, HEMA	EGDMA/AIBN	Water	Water	–	–
[140]	Ca^{2+}, Cd^{2+}	HEMA-MAC	EGDMA/ benzoyl peroxide	Toluene; benzoyl peroxide	Water	Cd^{2+}-overdosed human plasma	Sample pretreatment (sorbent)
[141]	Indole-3-acetic acid	HEMA, DMA	EGDMA/AIBN	Chloroform	Chloroform–acetic acid	–	–
[142]	p-Vinylbenzeneboronic acid ester, sialic acid	HEMA/N,N,N-trimethylaminoethyl methacrylate	EGDMA/AIBN	DMF	Tris-HCl buffer	Sialic acid, galacturonic acid, ganglioside GM1	SPR sensor

1-ALPP 1-allylpiperazine; *2-DAEM* 2-(diethylamino)ethyl methacrylate; *2-VP* 2-vinylpyridine; *4-VP* 4-vinylpyridine; *AAM* acrylamide; *ABDV* 2,2′-azobis(2,4-dimethyl-pentane nitrile); *ACN* Acetonitrile; *AIBN* azobisisobutyronitrile; *APS* ammonium persulfate; *BBA-β-CD* bis(-6-0-butanediacid monoester)-β-cyclodextrin(BBA-β-CD); *BHb* bovine hemoglobin; *BMA-β-CD* bismethacryloyl-beta-cyclodextrin; *CDHB* cyclododecyl 2,4-dihydroxybenzoate; *DCM* dichloromethane; *DEAEM* 2-(diethylamino) ethylmethacrylate; *DICH* 1,6-diisocyanatohexane; *DMA* N,N-dimethylaminoethyl methacrylate; *DMAEMA* N,N-dimethylaminoethyl methacrylate; *DMF* N,N-Dimethylformamide; *DMPAP* 2,2-dimethoxy-2-phenylacetophenone; *DMSO* dimethyl sulfoxide; *EGDMA* ethylene glycol dimethacrylate; *EPI-DVB* epichlorohydrin-divinylbenzene; *HEMA* 2-hydroxyethyl methacrylate; *HEMA-MATrp* hydroxyethyl methacrylate-N-methacryloyl-l-tryptophan methyl ester; *HSA* Human Serum Albumin; *IA* itaconic acid; *IAA* indole-3-acetic acid; *IgG* Immunoglobulin G; *Irgacure-184* (1-hydroxycyclohexyl)phenyl-methanon; *MAA* Methacrylic acid; *MAC* Nmethacryloly-(l)-cysteinemethylester; *MAH* N-Methacryloyl-(l)-histidinemethylester; *MBAA* N,N′-methylenebisacrylamide; *MISPE* molecularly imprinted solid phase extraction; *MTBE* methyltert-butylether; *PBS* phosphate buffer saline; *PEG600DMA* polyethyleneglycoldimethacrylate; *PPy* polypyrrole; *QCM* quartz crystal microbalance; *SDS* sodium dodecyl sulfate, sodium salt; *SPR* Surface Plasmon Resonance; *TCE* 1,1,1-Trichloroethane; *TDI* Toluene 2,4-diisocyante; *TEMED* N,N,N′,N′-tetramethylene diamine; *TFMAA* trifluoromethacrylic acid; *THF* Tetrahydrofuran; *TRIM* trimethylolpropane trimethacrylate; *β-CD* β-cyclodextrin

Table 5 Preparation and application of imprinted hydrogels

Ref.	Template	Monomer/cross-linker/initiator	Porogen	Rebinding solvent	Sample	Application
[145]	Bisphenol A	MAA/EGDMA/AIBN	Ethanol	Water		Sensor
[146]	17β-bestradiol	4-VP/EGDMA/AIBN	ACN	Water	Waste water	SPE
[147]	17β-bestradiol, atrazine, 4-nonylphenol	4-VP, DEAEM, MAA/EGDMA/AIBN	ACN, DMF/toluene	Water	–	Adsorbent
[148]	Arsenic	4-hydroxybiphenyl, 2-VP/EGDMA/60 °C	Water	Water	Waste water	–
[149]	Lysozyme, Bovine serum albumin	AM/BisAM/APS	Water	Water	Blood	HPLC column
[150]	Human serum albumin, Immunoglobulin G	AAm/EGDMA, DA, MBA/AIBN	Dimethylformamide	PBS	Human serum, fermentation broth	SPE
[151]	Theophylline	MAA/NIPA, HPC, MBA, DVS/APS	Water	Water	Theophylline	Sensor
[152]	6-phosphate monobarium salt	PAA·HCl/EPI/–	Water	BES buffer	–	–
[153]	Tobacco mosaic virus	PAA·HCl/EPI/–	Water	Water	–	–
[154]	Dexamethasone-21 phosphate disodium	HEMA, DEAEMA/EDGMA/UV	ACN, water	Water	–	Biosensors
[155]	Ketotifen fumarate	AA, AM, HEMA/NVP/AIBN	–	Water	Artificial lacrimal fluid	Therapeutic contact lenses
[156]	Imidacloprid	MAA/EGMDA/AIBN	MeOH	PBS	Apple, cabbage, cucumber, lettuce	Sensor

(continued)

Table 5 (continued)

Ref.	Template	Monomer/cross-linker/initiator	Porogen	Rebinding solvent	Sample	Application
[157]	Atropine	MAA/EGMDA/AIBN	MeOH	PBS	Urine	Chemosensor
[158]	Dibutyl phthalate (DBP)	MAA/EGMDA/AIBN	Chloroform	Ethanol	Juice drinks	Chemiluminescence sensor
[159]	Chrysoidine	MAA/EGMDA/AIBN	Ethanol	Water	Yellow croaker and yuba	Chemiluminescence sensor
[160]	Bovine serum albumin	NIPA, DMAPMA/BIS/UV	Tris-HCl buffer	Tris-HCl buffer	–	HPLC column
[161]	Apple stem pitting virus	AM, NIPAM/MBAA/APS, TEMED	PBS	–	Apple leaves	Sensor
[162]	Bovine serum albumin	AAm, 4-VP, NIPA/BIS/TEMED, APS	Tris-HCl buffer	Tris-HCl buffer	–	–
[163]	Hyaluronic acid	AM, DEAEM, NVP/–/photoinitator, (Irgacure 2959)	–	Acidic aqueous	–	Hydrogel contact lenses
[164]	Hemoglobin	AM/MBA/KPS	Na_2HPO_4 buffer	Sodium dihydrogen phosphate buffer	–	–
[165]	Bovine hemoglobin, trypsin	NiPAM, AA, NHMA/bis-acrylamide/TEMED	Water	Water	–	QCM sensor
[166]	Immunoglobulin G	AAm/MBAA/UV	Water	PBS	Human serum albumin	Gel permeation chromatograph
[167]	o-Xylene	Chitosan/genipin/–	Acetic acid	Water	–	

(continued)

Table 5 (continued)

Ref.	Template	Monomer/cross-linker/ initiator	Porogen	Rebinding solvent	Sample	Application
[168]	Tetracycline, oxytetracycline, chlortetracycline	AMD, AA/BIS/APS	Water	Buffer water	Milk and honey samples	Photonic polymer sensor
[169]	Bovine serum albumin	NIPAM, AAm/N-MACH/TEMED, APS	Tris-HCl buffer	Tris-HCl buffer	–	–
[170]	Bovine serum albumin	DMAPMA, NIPA, AAm/BIS/TEDED, APS	Tris-HCl buffer	Tris-HCl buffer	Bovine calf serum	MISPE
[171]	$PbCl_2$	MAA, IA/VSA/APS	Distilled water	Distilled water	–	–

AA Acrylic acid; *AAm, AM and AMD* acrylamide; *ACN* Acetonitrile; *AIBN* 2,2-azobis-(2-methylpropionitrile); *APS* Ammonium persulfate; *BES* N,N-bis [2-Hydroxyethyl]-2-aminoethanesulfonic acid; *BIS* Methylene bisacrylamide; *BisAM* N,N-methylenebisacrylamide; *DA* 3,4-dihydroxyphenethylamine; *DVS* Divinylsulfone; *DEAEM* 2-(diethylamino) ethyl methacrylate; *EPI* Epichlorohydrin; *DMAPMA* N-[3-(dimethylamino)propyl]-methacrylamide; *EGDMA* Ethylene glycol dimethacrylate; *KPS* Potassium persulfate; *HEMA* 2-hydroxyethyl methacrylate; *HPLC* High performance liquid chromatography; *IA* Italic acid; *MeOH* Methanol; *MAA* methylacrylic acid; *MBAA* N,N′-methylene bisacrylamide; *NVP* N-vinyl 2-pyrrolidone; *NHMA* Nhydroxymethylacrylamide; *PBS* Phosphate buffered saline; *NIPA and NiPAM* N-isopropylacrylamide; *PAA–HCl* poly (allylamine hydrochloride); *QCM* Quartz crystal microbalance; *SPE* Solid Phase Extraction; *VSA* Modified sodium alginate; *2-VP* 2-vinylpyridine; *4-VP* 4-vinylpyridine

structures that can re-bind target analytes selectively in aqueous conditions. Crystal 3-D structures of imprinted hydrogels also have optical-, thermal- and pH-sensitive response characters. For example, BPA-imprinted inverse opal hydrogel films provide BPA imprinted sites within the thin walls of 3D-ordered macroporous methacrylic acid-based inverse opal hydrogel. The resulting inverse opals were found to display large responses to external stimuli (pH or BPA) [145]. The film thickness was therefore shown to be a critical parameter for improving the sensing capacities of the imprinted inverse opal hydrogel films in water. Imprinted hydrogels have been widely used as sensors, selective adsorbents, drug release, water treatment, etc. (Table 5).

3.3 Ion-Mediated Imprinting

Preparation of ion-imprinted polymers comprises three steps: (1) complexation of an ion template to a polymerizable ligand; (2) polymerization of this complex; and (3) removal of the ion template after polymerization. There are already many reviews on ion imprinting. Recently, Mafu et al. [172] critically discussed the synthesis, characterization, and applications of ion-imprinted polymers for separating toxic metal ions (including arsenic, selenium, copper, nickel, cobalt, aluminum, and their complexes). Giakisikli et al. [173] reviewed recent developments on novel magnetic materials as sorbents for metal pre-concentration and determination as well as their implementation in sequential injection and microfluidic systems; therefore, we do not discuss ion imprinting in detail here.

4 Conclusions

The application of MIPs in aqueous environments faces a major challenge of increased nonspecific binding. The main problem is caused by the hydrophobic nature of most MIPs prepared in low polarity organic solvents. Various strategies have been developed to minimize the non-specific adsorption on MIPs. By modifying the binding solvents and introducing appropriate washing and elution steps, even relatively hydrophobic MIPs can be applied to treat water-based analytical samples to gain optimal results. More recently, the use of hydrophilic co-monomers, the controlled surface modification through controlled radical polymerization, and the new interfacial molecular imprinting methods have brought in truly water-compatible MIPs that can be used to treat aqueous samples directly. These intense studies provide more solutions to improve MIP performances in aqueous conditions. By combining MIPs with other techniques, both organic compatible and water compatible MIPs can display better functional performances in aqueous

conditions. We foresee that more and more new MIPs can lead to more interesting applications in biological and environmental analysis, and in more general biomedical and biotechnological applications.

References

1. Wulff G, Sarhan A (1972) The use of polymers with enzyme-analogous structures for the resolution of racemates. Angew Chem Int Ed 11:341
2. Arshady R, Mosbach K (1981) Synthesis of substrate-selective polymers by host-guest polymerization. Macromol Chem Phys 182:687–692
3. Vlatakis G, Andersson LI, Müller R, Mosbach K (1993) Drug assay using antibody mimics made by molecular imprinting. Nature 361:645–647
4. Whitcombe MJ, Rodriguez ME, Villar P, Vulfson EN (1995) A new method for the introduction of recognition site functionality into polymers prepared by molecular imprinting —synthesis and characterization of polymeric receptors for chloresterol. J Am Chem Soc 117:7105–7111
5. Turiel E, Martín-Esteban A (2010) Molecularly imprinted polymers for sample preparation: a review. Anal Chim Acta 668:87–99
6. Tse Sum Bui B, Haupt K (2010) Molecularly imprinted polymers: synthetic receptors in bioanalysis. Anal Bioanal Chem 398:2481–2492
7. Tamayo FG, Turiel E, Martín-Esteban A (2007) Molecularly imprinted polymers for solid-phase extraction and solid-phase microextraction: recent developments and future trends. J Chromatogr A 1152(1–2):32–40
8. Pichon V (2007) Selective sample treatment using molecularly imprinted polymers. J Chromatogr A 1152(1–2):41–53
9. Jiang M, Zhang JH, Mei SR, Shi Y, Zou LJ, Zhu YX, Dai K, Lu B (2006) Direct enrichment and high performance liquid chromatography analysis of ultra-trace bisphenol A in water samples with narrowly dispersible bisphenol A imprinted polymeric microspheres column. J Chromatogr A 1110(1–2):27–34
10. Zheng C, Huang YP, Liu ZS (2013) Synthesis and theoretical study of molecularly imprinted monoliths for HPLC. Anal Bioanal Chem 405:2147–2161
11. Martin PD, Jones GR, Stringer F, Wilson ID (2004) Comparison of extraction of a beta-blocker from plasma onto a molecularly imprinted polymer with liquid-liquid extraction and solid phase extraction methods. J Pharm Biomed Anal 35:1231–1239
12. Le Moullec S, Truong L, Montauban C, Begos A, Pichon V, Bellier B (2007) Extraction of alkyl methylphosphonic acids from aqueous samples using a conventional polymeric solid-phase extraction sorbent and a molecularly imprinted polymer. J Chromatogr A 1139:171–177
13. Piletska EV, Romero-Guerra M, Guerreiro AR, Karim K, Turner APF, Piletsky SA (2005) Adaptation of the molecular imprinted polymers towards polar environment. Anal Chim Acta 542:47–51
14. Hu Y, Liu R, Zhang Y, Li G (2009) Improvement of extraction capability of magnetic molecularly imprinted polymer beads in aqueous media via dual-phase solvent system. Talanta 79:576–582
15. Hu Y, Wang Y, Hu Y, Li G (2009) Liquid–liquid–solid microextraction based on membrane-protected molecularly imprinted polymer fiber for trace analysis of triazines in complex aqueous samples. J Chromatogr A 1216:8304–8311
16. Haginaka J, Takehira H, Hosoya K, Tanaka N, Haginaka J (1999) Uniform-sized molecularly imprinted polymer for (S)-naproxen selectively modified with hydrophilic external layer. J Chromatogr A 849:331–339

17. Haginaka J, Sanbe H (2000) Uniform-sized molecularly imprinted polymers for 2-arylpropionic acid derivatives selectively modified with hydrophilic external layer and their applications to direct serum injection analysis. Anal Chem 72:5206–5210
18. Sanbe H, Haginaka J (2003) Restricted access media-molecularly imprinted polymer for propranolol and its application to direct injection analysis of beta-blockers in biological fluids. Analyst 128:593–597
19. Puoci F, Iemma F, Cirillo G, Curcio M, Parisi OI, Spizzirri UG, Picci N (2009) New restricted access materials combined to molecularly imprinted polymers for selective recognition/release in water media. Eur Polym J 45:1634–1640
20. Parisi OI, Cirillo G, Curcio M, Puoci F, Iemma F, Spizzirri UG, Picci N (2010) Surface modifications of molecularly imprinted polymers for improved template recognition in water media. J Polym Res 17:355–362.)
21. Yang K, Berg MM, Zhao C, Ye L (2009) One-pot synthesis of hydrophilic molecularly imprinted nanoparticles. Macromolecules 42:8739–8746
22. Yao GH, Liang RP, Huang CF, Wang Y, Qiu JD (2013) Surface plasmon resonance sensor based on magnetic molecularly imprinted polymers amplification for pesticide recognition. Anal Chem 85:11944–11951
23. Xia Z, Lin Z, Xiao Y, Wang L, Zheng J, Yang H, Chen G (2013) Facile synthesis of polydopamine-coated molecularly imprinted silica nanoparticles for protein recognition and separation. Biosens Bioelectron 47:120–126
24. Nematollahzadeh A, Shojaei A, Abdekhodaie MJ, Sellergren B (2013) Molecularly imprinted polydopamine nano-layer on the pore surface of porous particles for protein capture in HPLC column. J Colloid Interface Sci 404:117–126
25. Jia X, Xu M, Wang Y, Ran D, Yang S, Zhang M (2013) Polydopamine-based molecular imprinting on silica-modified magnetic nanoparticles for recognition and separation of bovine hemoglobin. Analyst 138:651–658
26. Ma Y, Pan G, Zhang Y, Guo X, Zhang H (2013) Narrowly dispersed hydrophilic molecularly imprinted polymer nanoparticles for efficient molecular recognition in real aqueous samples including river water, milk, and bovine serum. Angew Chem Int Ed 52:1511–1514
27. Southard GE, Van Houten KA, Ott EW Jr, Murray GM (2007) Luminescent sensing of organophosphates using europium(III) containing imprinted polymers prepared by RAFT polymerization. Anal Chim Acta 581:202–207
28. Li Y, Dong C, Chu J, Qi J, Li X (2011) Surface molecular imprinting onto fluorescein-coated magnetic nanoparticles via reversible addition fragmentation chain transfer polymerization: a facile three-in-one system for recognition and separation of endocrine disrupting chemicals. Nanoscale 3:280–287
29. Li Y, Zhou WH, Yang HH, Wang XR (2009) Grafting of molecularly imprinted polymers from the surface of silica gel particles via reversible addition-fragmentation chain transfer polymerization: a selective sorbent for theophylline. Talanta 79:141–145
30. Li Y, Li X, Dong C, Li Y, Jin P, Qi J (2009) Selective recognition and removal of chlorophenols from aqueous solution using molecularly imprinted polymer prepared by reversible addition-fragmentation chain transfer polymerization. Biosens Bioelectron 25:306–312
31. Pan G, Ma Y, Zhang Y, Guo X, Li C, Zhang H (2011) Controlled synthesis of water-compatible molecularly imprinted polymer microspheres with ultra thin hydrophilic polymer shells via surface-initiated reversible addition-fragmentation chain transfer polymerization. Soft Matter 7:8428–8439
32. Ma Y, Zhang Y, Zhao M, Guo X, Zhang H (2012) Efficient synthesis of narrowly dispersed molecularly imprinted polymer microspheres with multiple stimuli-responsive template binding properties in aqueous media. Chem Commun 48:6217–6219
33. Kugimiya A, Takeuchi T (2001) Surface plasmon resonance sensor using molecularly imprinted polymer for detection of sialic acid. Biosens Bioelectron 16:1059–1062

34. Zhao M, Chen X, Zhang H, Yan H, Zhang H (2014) Well-defined hydrophilic molecularly imprinted polymer microspheres for efficient molecular recognition in real biological samples by facile RAFT coupling chemistry. Biomacromolecules 15:1663–1675
35. Liu S, Yan H, Wang M, Wang L (2013) Water-compatible molecularly imprinted microspheres in pipette tip solid-phase extraction for simultaneous determination of five fluoroquinolones in eggs. J Agric Food Chem 61:11974–11980
36. Zengin A, Yildirim E, Tamer U, Caykara T (2013) Molecularly imprinted superparamagnetic iron oxide nanoparticles for rapid enrichment and separation of cholesterol. Analyst 138:7238–7245
37. Yang M, Zhang Y, Lin S, Yang X, Fan Z, Yang L, Dong X (2013) Preparation of a bifunctional pyrazosulfuron-ethyl imprinted polymer with hydrophilic external layers by reversible addition-fragmentation chain transfer polymerization and its application in the sulfonylurea residue analysis. Talanta 114:143–151
38. Ban L, Han X, Wang XH, Huang YP, Liu ZS (2013) Carprofen-imprinted monolith prepared by reversible addition-fragmentation chain transfer polymerization in room temperature ionic liquids. Anal Bioanal Chem 405:8597–8605
39. Li X, Zhou M, Turson M, Lin S, Jiang P, Dong X (2013) Preparation of clenbuterol imprinted monolithic polymer with hydrophilic outer layers by reversible addition-fragmentation chain transfer radical polymerization and its application in the clenbuterol determination from human serum by on-line solid-phase extraction/HPLC analysis. Analyst 138:3066–3074
40. Ma Y, Pan G, Zhang Y, Guo X, Zhang H (2013) Comparative study of the molecularly imprinted polymers prepared by reversible addition-fragmentation chain transfer "bulk" polymerization and traditional radical "bulk" polymerization. J Mol Recogn 26:240–251
41. Hu X, Fan Y, Zhang Y, Dai G, Cai Q, Cao Y, Guo C (2012) Molecularly imprinted polymer coated solid-phase microextraction fiber prepared by surface reversible addition-fragmentation chain transfer polymerization for monitoring of Sudan dyes in chilli tomato sauce and chilli pepper samples. Anal Chim Acta 731:40–48
42. Pan G, Zhang Y, Ma Y, Li C, Zhang H (2011) Efficient one-pot synthesis of water-compatible molecularly imprinted polymer microspheres by facile RAFT precipitation polymerization. Angew Chem Int Ed Engl 50:11731–11734
43. Xu S, Li J, Chen L (2011) Molecularly imprinted polymers by reversible addition-fragmentation chain transfer precipitation polymerization for preconcentration of atrazine in food matrices. Talanta 85:282–289
44. Chang L, Li Y, Chu J, Qi J, Li X (2010) Preparation of core-shell molecularly imprinted polymer via the combination of reversible addition-fragmentation chain transfer polymerization and click reaction. Anal Chim Acta 680:65–71
45. Pan G, Zhang Y, Guo X, Li C, Zhang H (2010) An efficient approach to obtaining water-compatible and stimuli-responsive molecularly imprinted polymers by the facile surface-grafting of functional polymer brushes via RAFT polymerization. Biosens Bioelectron 26:976–982
46. Yoshimatsu K, Ye L, Lindberg J, Chronakis IS (2008) Selective molecular adsorption using electrospun nanofiber affinity membranes. Biosens Bioelectron 23:1208–1215
47. Wu Y, Zhang Y, Zhang M, Liu F, Wan Y, Huang Z, Ye L, Zhou Q, Shi Y, Lu B (2014) Selective and simultaneous determination of trace bisphenol A and tebuconazole in vegetable and juice samples by membrane-based molecularly imprinted solid-phase extraction and HPLC. Food Chem 164:527–535
48. Horemans F, Weustenraed A, Spivak D, Cleij TJ (2012) Towards water compatible MIPs for sensing in aqueous media. J Mol Recogn 25:344–351
49. Xu L, Hu Y, Shen F, Li Q, Ren X (2013) Specific recognition of tyrosine-phosphorylated peptides by epitope imprinting of phenylphosphonic acid. J Chromatogr A 1293:85–91
50. Caro E, Marcé RM, Cormack PA, Sherrington DC, Borrull F (2004) Molecularly imprinted solid-phase extraction of naphthalene sulfonates from water. J Chromatogr A 1047:175–180

51. Baggiani C, Giovannoli C, Anfossi L, Tozzi C (2001) Molecularly imprinted solid-phase extraction sorbent for the clean-up of chlorinated phenoxyacids from aqueous samples. J Chromatogr A 938(1–2):35–44
52. Suedee R, Seechamnanturakit V, Suksuwan A, Canyuk B (2008) Recognition properties and competitive assays of a dual dopamine/serotonin selective molecularly imprinted polymer. Int J Mol Sci 9:2333–2356
53. Scorrano S, Longo L, Vasapollo G (2010) Molecularly imprinted polymers for solid-phase extraction of 1-methyladenosine from human urine. Anal Chim Acta 659:167–171
54. Pakade V, Lindahl S, Chimuka L, Turner C (2012) Molecularly imprinted polymers targeting quercetin in high-temperature aqueous solutions. J Chromatogr A 1230:15–23
55. Mayes AG, Mosbach K (1996) Molecularly imprinted polymer beads: suspension polymerization using a liquid perfluorocarbon as the dispersing phase. Anal Chem 68:3769–3774
56. Kempe H, Kempe M (2006) Development and evaluation of spherical molecularly imprinted polymer beads. Anal Chem 78:3659–3666
57. Walsh R, Osmani Q, Hughes H, Duggan P, McLoughlin P (2011) Synthesis of imprinted beads by aqueous suspension polymerisation for chiral recognition of antihistamines. J Chromatogr B Anal Technol Biomed Life Sci 879:3523–3530
58. Zourob M, Mohr S, Mayes AG, Macaskill A, Pérez-Moral N, Fielden PR, Goddard NJ (2006) A micro-reactor for preparing uniform molecularly imprinted polymer beads. Lab Chip 6:296–301
59. Hu SG, Wang SW, He XW (2003) An amobarbital molecularly imprinted microsphere for selective solid-phase extraction of phenobarbital from human urine and medicines and their determination by high-performance liquid chromatography. Analyst 128:1485–1489
60. Baggiani C, Anfossi L, Baravalle P, Giovannoli C, Giraudi G, Barolo C, Viscardi G (2009) Determination of banned Sudan dyes in food samples by molecularly imprinted solid phase extraction-high performance liquid chromatography. J Sep Sci 32:3292–3300
61. Qiao J, Yan H, Wang H, Lv Y (2011) Determination of ofloxacin and lomefloxacin in chicken muscle using molecularly imprinted solid-phase extraction coupled with liquid chromatography. J Sep Sci 34:2668–2673
62. Yang T, Li YH, Wei S, Li Y, Deng A (2008) Development of a selective molecularly imprinted polymer-based solid-phase extraction for indomethacin from water samples. Anal Bioanal Chem 391:2905–2914
63. Lenain P, Diana Di Mavungu J, Dubruel P, Robbens J, De Saeger S (2012) Development of suspension polymerized molecularly imprinted beads with metergoline as template and application in a solid-phase extraction procedure toward ergot alkaloids. Anal Chem 84:10411–10418
64. Suedee R, Srichana T, Martin GP (2000) Evaluation of matrices containing molecularly imprinted polymers in the enantioselective-controlled delivery of β-blockers. J Controlled Release 66:135–147
65. Yan H, Liu S, Gao M, Sun N (2013) Ionic liquids modified dummy molecularly imprinted microspheres as solid phase extraction materials for the determination of clenbuterol and clorprenaline in urine. J Chromatogr A 1294:10–16
66. Hu Y, Li Y, Liu R, Tan W, Li G (2011) Magnetic molecularly imprinted polymer beads prepared by microwave heating for selective enrichment of β-agonists in pork and pig liver samples. Talanta 84:462–470
67. Chen FF, Xie XY, Shi YP (2012) Magnetic molecularly imprinted polymer for the detection of rhaponticin in Chinese patent medicines. J Chromatogr A 1252:8–14
68. Zhang Y, Liu R, Hu Y, Li G (2009) Microwave heating in preparation of magnetic molecularly imprinted polymer beads for trace triazines analysis in complicated samples. Anal Chem 81:967–976
69. Andaç M, Say R, Denizli A (2004) Molecular recognition based cadmium removal from human plasma. J Chromatogr B Anal Technol Biomed Life Sci 811:119–126

70. Lai JP, Chen F, Sun H, Fan L, Liu GL (2014) Molecularly imprinted microspheres for the anticancer drug aminoglutethimide: synthesis, characterization, and solid-phase extraction applications in human urine samples. J Sep Sci 37:1170–1176
71. Shi X, Wu A, Zheng S, Li R, Zhang D (2007) Molecularly imprinted polymer microspheres for solid-phase extraction of chloramphenicol residues in foods. J Chromatogr B Anal Technol Biomed Life Sci 850:24–30
72. Yu J, Wan F, Zhang C, Yan M, Zhang X, Wang S (2010) Molecularly imprinted polymeric microspheres for determination of bovine serum albumin based on flow injection chemiluminescence sensor. Biosens Bioelectron 26:632–637
73. He J, Lv R, Cheng J, Li Y, Xue J, Lu K, Wang F (2010) Preparation and characterization of molecularly imprinted microspheres for dibutyl phthalate recognition in aqueous environment. J Sep Sci 33:3409–3414
74. Shaikh H, Memon N, Khan H, Bhanger M, Nizamani S (2012) Preparation and characterization of molecularly imprinted polymer for di (2-ethylhexyl) phthalate: Application to sample clean-up prior to gas chromatographic determination. J Chromatogr A 1247:125–133
75. Wang X, Fang Q, Liu S, Chen L (2012) Preparation of a magnetic molecularly imprinted polymer with pseudo template for rapid simultaneous determination of cyromazine and melamine in bio-matrix samples. Anal Bioanal Chem 404:1555–1564
76. Zhang Y, Li Y, Hu Y, Li G, Chen Y (2010) Preparation of magnetic indole-3-acetic acid imprinted polymer beads with 4-vinylpyridine and β-cyclodextrin as binary monomer via microwave heating initiated polymerization and their application to trace analysis of auxins in plant tissues. J Chromatogr A 1217:7337–7344
77. Madrakian T, Ahmadi M, Afkhami A, Soleimani M (2013) Selective solid-phase extraction of naproxen drug from human urine samples using molecularly imprinted polymer-coated magnetic multi-walled carbon nanotubes prior to its spectrofluorometric determination. Analyst 138:4542–4549
78. Yan H, Wang F, Han D, Yang G (2012) Simultaneous determination of four plant hormones in bananas by molecularly imprinted solid-phase extraction coupled with high performance liquid chromatography. Analyst 137:2884–2890
79. Jantarat C, Tangthong N, Songkro S, Martin GP, Suedee R (2008) S-propranolol imprinted polymer nanoparticle-on-microsphere composite porous cellulose membrane for the enantioselectively controlled delivery of racemic propranolol. Int J Pharm 349:212–225
80. Lian ZR, Wang JT (2013) Study of molecularly imprinted solid-phase extraction of gonyautoxins 2,3 in the cultured dinoflagellate Alexandrium tamarense by high-performance liquid chromatography with fluorescence detection. Environ Pollut 182:385–391
81. Kempe H, Kempe M (2004) Novel method for the synthesis of molecularly imprinted polymer bead libraries. Macromol Rapid Commun 25:315–320
82. Lai JP, Niessner R, Knopp D (2004) Benzo [a] pyrene imprinted polymers: synthesis, characterization and SPE application in water and coffee samples. Anal Chim Acta 522:137–144
83. Hu SG, Li L, He XW (2005) Comparison of trimethoprim molecularly imprinted polymers in bulk and in sphere as the sorbent for solid-phase extraction and extraction of trimethoprim from human urine and pharmaceutical tablet and their determination by high-performance liquid chromatography. Anal Chim Acta 537:215–222
84. Matsui J, Fujiwara K, Ugata S, Takeuchi T (2000) Solid-phase extraction with a dibutylmelamine-imprinted polymer as triazine herbicide-selective sorbent. J Chromatogr A 889:25–31
85. Kawaguchi M, Hayatsu Y, Nakata H, Ishii Y, Ito R, Saito K, Nakazawa H (2005) Molecularly imprinted solid phase extraction using stable isotope labeled compounds as template and liquid chromatography–mass spectrometry for trace analysis of bisphenol A in water sample. Anal Chim Acta 539:83–89

86. Ansell RJ, Mosbach K (1997) Molecularly imprinted polymers by suspension polymerisation in perfluorocarbon liquids, with emphasis on the influence of the porogenic solvent. J Chromatogr A 787:55–66
87. Lai JP, He XW, Jiang Y, Chen F (2003) Preparative separation and determination of matrine from the Chinese medicinal plant Sophora flavescens Ait by molecularly imprinted solid-phase extraction. Anal Bioanal Chem 375:264–269
88. Priego-Capote F, Ye L, Shakil S, Shamsi SA, Nilsson S (2008) Monoclonal behavior of molecularly imprinted polymer nanoparticles in capillary electrochromatography. Anal Chem 80:2881–2887
89. Shen X, Ye L (2011) Interfacial molecular imprinting in nanoparticle-stabilized emulsions. Macromolecules 44:5631–5637
90. Shen X, Ye L (2011) Molecular imprinting in Pickering emulsions: a new insight into molecular recognition in water. Chem Commun 47:10359–10361
91. Huang C, Shen X (2014) Janus molecularly imprinted polymer particles. Chem Commun 50:2646–2649
92. Hang H, Li C, Pan J, Li L, Dai J, Dai X, Yu P, Feng Y (2013) Selective separation of lambdacyhalothrin by porous/magnetic molecularly imprinted polymers prepared by Pickering emulsion polymerization. J Sep Sci 36:3285–3294
93. Zhang H, Dramou P, He H, Tan S, Pham-Huy C, Pan H (2012) Molecularly imprinted stationary phase prepared by reverse micro-emulsion polymerization for selective recognition of gatifloxacin in aqueous media. J Chromatogr Sci 50:499–508
94. Lv YK, Zhao CX, Li P, He YD, Yang ZR, Sun HW (2013) Preparation of doxycycline-imprinted magnetic microspheres by inverse-emulsion suspension polymerization for magnetic dispersion extraction of tetracyclines from milk samples. J Sep Sci 36:2656–2663
95. Tan CJ, Tong YW (2007) Preparation of superparamagnetic ribonuclease A surface-imprinted submicrometer particles for protein recognition in aqueous media. Anal Chem 79:299–306
96. Luo X, Zhan Y, Huang Y, Yang L, Tu X, Luo S (2011) Removal of water-soluble acid dyes from water environment using a novel magnetic molecularly imprinted polymer. J Hazard Mater 187:274–282
97. Monier M, Elsayed NH (2014) Selective extraction of uranyl ions using ion-imprinted chelating microspheres. J Colloid Interface Sci 423:113–122
98. Dai J, Pan J, Xu L, Li X, Zhou Z, Zhang R, Yan Y (2012) Preparation of molecularly imprinted nanoparticles with superparamagnetic susceptibility through atom transfer radical emulsion polymerization for the selective recognition of tetracycline from aqueous medium. J Hazard Mater 205–206:179–188
99. Ornelas M, Loureiro D, Araujo MJ, Marques E, Dias-Cabral C, Azenha M, Silva F (2013) Synthesis of glycylglycine-imprinted silica microspheres through different water-in-oil emulsion techniques. J Chromatogr A 1297:138–145
100. Tonglairoum P, Chaijaroenluk W, Rojanarata T, Ngawhirunpat T, Akkaramongkolporn P, Opanasopit P (2013) Development and characterization of propranolol selective molecular imprinted polymer composite electrospun nanofiber membrane. AAPS Pharm Sci Tech 14:838–846
101. Sener G, Ozgur E, Yilmaz E, Uzun L, Say R, Denizli A (2010) Quartz crystal microbalance based nanosensor for lysozyme detection with lysozyme imprinted nanoparticles. Biosens Bioelectron 26:815–821
102. Curcio P, Zandanel C, Wagner A, Mioskowski C, Baati R (2009) Semi-covalent surface molecular imprinting of polymers by one-stage mini-emulsion polymerization: glucopyranoside as a model analyte. Macromol Biosci 9:596–604
103. Esfandyari-Manesh M, Javanbakht M, Dinarvand R, Atyabi F (2012) Molecularly imprinted nanoparticles prepared by miniemulsion polymerization as selective receptors and new carriers for the sustained release of carbamazepine. J Mater Sci Mater Med 23:963–972

104. Tan CJ, Chua HG, Ker KH, Tong YW (2008) Preparation of bovine serum albumin surface-imprinted submicrometer particles with magnetic susceptibility through core-shell miniemulsion polymerization. Anal Chem 80:683–692
105. Perez-Moral N, Mayes AG (2004) Noncovalent imprinting in the shell of core-shell nanoparticles. Langmuir 20:3775–3779
106. Ashraf S, Cluley A, Mercado C, Mueller A (2011) Imprinted polymers for the removal of heavy metal ions from water. Water Sci Technol 64:1325–1332
107. Fujiwara I, Maeda M, Takagi M (2003) Preparation of ferrocyanide-imprinted pyridine-carrying microspheres by surface imprinting polymerization. Anal Sci 19:617–620
108. Shen X, Zhou T, Ye L (2012) Molecular imprinting of protein in Pickering emulsion. Chem Commun 48:8198–8200
109. Pan J, Li L, Hang H, Wu R, Dai X, Shi W, Yan Y (2013) Fabrication and evaluation of magnetic/hollow double-shelled imprinted sorbents formed by Pickering emulsion polymerization. Langmuir 29:8170–8178
110. Zhu W, Ma W, Li C, Pan J, Dai X, Gan M, Qu Q, Zhang Y (2014) Magnetic molecularly imprinted microspheres via yeast stabilized Pickering emulsion polymerization for selective recognition of λ-cyhalothrin. Colloids Surf A 453:27–36
111. Gu XH, Xu R, Yuan GL, Lu H, Gu BR, Xie HP (2010) Preparation of chlorogenic acid surface-imprinted magnetic nanoparticles and their usage in separation of traditional Chinese medicine. Anal Chim Acta 675:64–70
112. Dirion B, Cobb Z, Schillinger E, Andersson LI, Sellergren B (2003) Water-compatible molecularly imprinted polymers obtained via high-throughput synthesis and experimental design. J Am Chem Soc 125:15101–15109
113. Lulinski P, Maciejewska D (2013) Effect of functional monomers and porogens on morphology, structure and recognition properties of 2-(4-methoxyphenyl)ethylamine imprinted polymers. Mater Sci Eng C Mater Biol Appl 33:1162–1169
114. Mehdinia A, Aziz-Zanjani MO, Ahmadifar M, Jabbari A (2013) Design and synthesis of molecularly imprinted polypyrrole based on nanoreactor SBA-15 for recognition of ascorbic acid. Biosens Bioelectron 39:88–93
115. Zhang M, Zhang X, He X, Chen L, Zhang Y (2012) A self-assembled polydopamine film on the surface of magnetic nanoparticles for specific capture of protein. Nanoscale 4:3141–3147
116. Zhou WH, Tang SF, Yao QH, Chen FR, Yang HH, Wang XR (2010) A quartz crystal microbalance sensor based on mussel-inspired molecularly imprinted polymer. Biosens Bioelectron 26:585–589
117. Ouyang R, Lei J, Ju H (2010) Artificial receptor-functionalized nanoshell: facile preparation, fast separation and specific protein recognition. Nanotechnology 21:185502
118. Liu K, Wei WZ, Zeng JX, Liu XY, Gao YP (2006) Application of a novel electrosynthesized polydopamine-imprinted film to the capacitive sensing of nicotine. Anal Bioanal Chem 385:724–729
119. Xu ZF, Wen G, Kuang DZ, Zhang FX, Tang SP (2013) Selective separation of deltamethrin by molecularly imprinted polymers using a beta-cyclodextrin derivative as the functional monomer. J Environ Sci Health B 48:336–343
120. Zhang H, Dramou P, He H, Tan S, Pham-Huy C, Pan H (2012) Molecularly imprinted stationary phase prepared by reverse micro-emulsion polymerization for selective recognition of gatifloxacin in aqueous media. J Chromatogr Sci 50:499–508
121. Zhang Z, Yang X, Zhang H, Zhang M, Luo L, Hu Y, Yao S (2011) Novel molecularly imprinted polymers based on multi-walled carbon nanotubes with binary functional monomer for the solid-phase extraction of erythromycin from chicken muscle. J Chromatogr B Anal Technol Biomed Life Sci 879:1617–1624
122. Zhang Y, Li Y, Hu Y, Li G, Chen Y (2010) Preparation of magnetic indole-3-acetic acid imprinted polymer beads with 4-vinylpyridine and beta-cyclodextrin as binary monomer via microwave heating initiated polymerization and their application to trace analysis of auxins in plant tissues. J Chromatogr A 1217:7337–7344

123. Qin L, He XW, Li WY, Zhang YK (2008) Molecularly imprinted polymer prepared with bonded beta-cyclodextrin and acrylamide on functionalized silica gel for selective recognition of tryptophan in aqueous media. J Chromatogr A 1187(1–2):94–102
124. Yang Y, Long Y, Cao Q, Li K, Liu F (2008) Molecularly imprinted polymer using beta-cyclodextrin as functional monomer for the efficient recognition of bilirubin. Anal Chim Acta 606:92–97
125. Xu Z, Kuang D, Liu L, Deng Q (2007) Selective adsorption of norfloxacin in aqueous media by an imprinted polymer based on hydrophobic and electrostatic interactions. J Pharm Biomed Anal 45:54–61
126. Hsieh RY, Tsai HA, Syu MJ (2006) Designing a molecularly imprinted polymer as an artificial receptor for the specific recognition of creatinine in serums. Biomaterials 27:2083–2089
127. Tsai HA, Syu MJ (2005) Synthesis of creatinine-imprinted poly(beta-cyclodextrin) for the specific binding of creatinine. Biomaterials 26:2759–2766
128. Osman B, Uzun L, Besirli N, Denizli A (2013) Microcontact imprinted surface plasmon resonance sensor for myoglobin detection. Mater Sci Eng C Mater Biol Appl 33:3609–3614
129. Nestic M, Babic S, Pavlovic DM, Sutlovic D (2013) Molecularly imprinted solid phase extraction for simultaneous determination of Delta9-tetrahydrocannabinol and its main metabolites by gas chromatography-mass spectrometry in urine samples. Forensic Sci Int 231:317–324
130. Koc I, Baydemir G, Bayram E, Yavuz H, Denizli A (2011) Selective removal of 17beta-estradiol with molecularly imprinted particle-embedded cryogel systems. J Hazard Mater 192:1819–1826
131. Liu Y, Hoshina K, Haginaka J (2010) Monodispersed, molecularly imprinted polymers for cinchonidine by precipitation polymerization. Talanta 80:1713–1718
132. Ansell RJ, Wang D (2009) Imprinted polymers for chiral resolution of (±)-ephedrine. Part 3: NMR predictions and HPLC results with alternative functional monomers. Analyst 134:564–576
133. Yan H, Tian M, Row KH (2008) Determination of enrofloxacin and ciprofloxacin in milk using molecularly imprinted solid-phase extraction. J Sep Sci 31:3015–3020
134. Urraca JL, Carbajo MC, Torralvo MJ, Gonzalez-Vazquez J, Orellana G, Moreno-Bondi MC (2008) Effect of the template and functional monomer on the textural properties of molecularly imprinted polymers. Biosens Bioelectron 24:155–161
135. Bereli N, Andac M, Baydemir G, Say R, Galaev IY, Denizli A (2008) Protein recognition via ion-coordinated molecularly imprinted supermacroporous cryogels. J Chromatogr A 1190:18–26
136. Ng SM, Narayanaswamy R (2006) Fluorescence sensor using a molecularly imprinted polymer as a recognition receptor for the detection of aluminium ions in aqueous media. Anal Bioanal Chem 386:1235–1244
137. Oral E, Peppas NA (2006) Hydrophilic molecularly imprinted poly(hydroxyethyl-methacrylate) polymers. J Biomed Mater Res A 78:205–210
138. Perez-Moral N, Mayes AG (2006) Direct rapid synthesis of MIP beads in SPE cartridges. Biosens Bioelectron 21:1798–1803
139. Piletska EV, Turner NW, Turner AP, Piletsky SA (2005) Controlled release of the herbicide simazine from computationally designed molecularly imprinted polymers. J Controlled Release 108:132–139
140. Andac M, Say R, Denizli A (2004) Molecular recognition based cadmium removal from human plasma. J Chromatogr B Anal Technol Biomed Life Sci 811:119–126
141. Kugimiya A, Takeuchi T (2002) Molecular recognition by indoleacetic acid-imprinted polymers—effects of 2-hydroxyethyl methacrylate content. Anal Bioanal Chem 372:305–307
142. Kugimiya A, Takeuchi T (2001) Surface plasmon resonance sensor using molecularly imprinted polymer for detection of sialic acid. Biosens Bioelectron 16:1059–1062

143. Monier M, El-Sokkary AMA (2010) Preparation of molecularly imprinted cross-linked chitosan/glutaraldehyde resin for enantioselective separation of L-glutamic acid. Int J Biol Macromol 47:207–213
144. Hua K, Zhang L, Zhang Z, Guo Y, Guo T (2011) Surface hydrophilic modification with a sugar moiety for a uniform-sized polymer molecularly imprinted for phenobarbital in serum. Acta Biomater 7:3086–3093
145. Griffete N, Frederich H, Maître A, Ravaine S, Chehimi MM, Mangeney C (2012) Inverse opals of molecularly imprinted hydrogels for the detection of bisphenol A and pH sensing. Langmuir 28:1005–1012
146. Le Noir M, Plieva FM, Hey T, Guieysse B, Mattiasson B (2007) Macroporous molecularly imprinted polymer/cryogel composite systems for the removal of endocrine disrupting trace contaminants. J Chromatogr A 1154:158–164
147. Le Noir M, Plieva FM, Mattiasson B (2009) Removal of endocrine disrupting compounds from water using macroporous molecularly imprinted cryogels in a moving-bed reactor. J Sep Sci 32:1471–1479
148. Önnby L, Pakade V, Mattiasson B, Kirsebom H (2012) Polymer composite adsorbents using particles of molecularly imprinted polymers or aluminium oxide nanoparticles for treatment of arsenic contaminated waters. Water Res 46:4111–4120
149. Lin Z, Yang F, He X, Zhao X, Zhang Y (2009) Preparation and evaluation of a macroporous molecularly imprinted hybrid silica monolithic column for recognition of proteins by high performance liquid chromatography. J Chromatogr A 1216:8612–8622
150. Nematollahzadeh A, Lindemann P, Sun W, Stute J, Lutkemeyer D, Sellergren B (2014) Robust and selective nano cavities for protein separation: an interpenetrating polymer network modified hierarchically protein imprinted hydrogel. J Chromatogr A 1345:154–163
151. Troiani D, Dion JR, Burns DH (2011) Ultrasonic quantification using smart hydrogel sensors. Talanta 83:1371–1375
152. Parmpi P, Kofinas P (2004) Biomimetic glucose recognition using molecularly imprinted polymer hydrogels. Biomaterials 25:1969–1973
153. Bolisay LD, Culver JN, Kofinas P (2006) Molecularly imprinted polymers for tobacco mosaic virus recognition. Biomaterials 27:4165–4168
154. Wang C, Javadi A, Ghaffari M, Gong S (2010) A pH-sensitive molecularly imprinted nanospheres/hydrogel composite as a coating for implantable biosensors. Biomaterials 31:4944–4951
155. Ali M, Horikawa S, Venkatesh S, Saha J, Hong JW, Byrne ME (2007) Zero-order therapeutic release from imprinted hydrogel contact lenses within in vitro physiological ocular tear flow. J Controlled Release 124:154–162
156. Wang X, Mu Z, Liu R, Pu Y, Yin L (2013) Molecular imprinted photonic crystal hydrogels for the rapid and label-free detection of imidacloprid. Food Chem 141:3947–3953
157. Meng L, Meng P, Tang B, Zhang Q, Wang Y (2013) Molecularly imprinted photonic hydrogels for fast screening of atropine in biological samples with high sensitivity. Forensic Sci Int 231:6–12
158. Qiu H, Fan L, Li X, Li L, Sun M, Luo C (2013) A microflow chemiluminescence sensor for indirect determination of dibutyl phthalate by hydrolyzing based on biological recognition materials. J Pharm Biomed Anal 75:123–129
159. Lu F, Sun M, Fan L, Qiu H, Li X, Luo C (2012) Flow injection chemiluminescence sensor based on core–shell magnetic molecularly imprinted nanoparticles for determination of chrysoidine in food samples. Sens Actuators B 173:591–598
160. Hua Z, Zhou S, Zhao M (2009) Fabrication of a surface imprinted hydrogel shell over silica microspheres using bovine serum albumin as a model protein template. Biosens Bioelectron 25:615–622
161. Bai W, Spivak DA (2014) A double-imprinted diffraction-grating sensor based on a virus-responsive super-aptamer hydrogel derived from an impure extract. Angew Chem Int Ed Engl 53:2095–2098

162. Li SH, Wang J, Zhao MP (2009) Cupric ion enhanced molecular imprinting of bovine serum albumin in hydrogel. J Sep Sci 32:3359–3363
163. Ali M, Byrne ME (2009) Controlled release of high molecular weight hyaluronic acid from molecularly imprinted hydrogel contact lenses. Pharm Res 26:714–726
164. Xia YQ, Guo TY, Song MD, Zhang BH, Zhang BL (2005) Hemoglobin recognition by imprinting in semi-interpenetrating polymer network hydrogel based on polyacrylamide and chitosan. Biomacromolecules 6:2601–2606
165. Reddy SM, Phan QT, El-Sharif H, Govada L, Stevenson D, Chayen NE (2012) Protein crystallization and biosensor applications of hydrogel-based molecularly imprinted polymers. Biomacromolecules 13:3959–3965
166. Yin D, Ulbricht M (2013) Antibody-imprinted membrane adsorber via two-step surface grafting. Biomacromolecules 14:4489–4496
167. Espinosa-Garcia BM, Arguelles-Monal WM, Hernandez J, Felix-Valenzuela L, Acosta N, Goycoolea FM (2007) Molecularly imprinted chitosan-genipin hydrogels with recognition capacity toward o-xylene. Biomacromolecules 8:3355–3364
168. Wang LQ, Lin FY, Yu LP (2012) A molecularly imprinted photonic polymer sensor with high selectivity for tetracyclines analysis in food. Analyst 137:3502–3509
169. Zhang C, Jia X, Wang Y, Zhang M, Yang S, Guo J (2014) Thermosensitive molecularly imprinted hydrogel cross-linked with N-malely chitosan for the recognition and separation of BSA. J Sep Sci 37:419–426
170. Hua Z, Chen Z, Li Y, Zhao M (2008) Thermosensitive and salt-sensitive molecularly imprinted hydrogel for bovine serum albumin. Langmuir 24:5773–5780
171. Wang W, Zong L, Wang A (2013) A nanoporous hydrogel based on vinyl-functionalized alginate for efficient absorption and removal of Pb^{2+} ions. Int J Biol Macromol 62:225–231
172. Mafu LD, Msagati TAM, Mamba BB (2013) Ion-imprinted polymers for environmental monitoring of inorganic pollutants: synthesis, characterization, and applications. Environ Sci Pollut Res 20:790–802
173. Giakisikli G, Anthemidis AN (2013) Magnetic materials as sorbents for metal/metalloid preconcentration and/or separation. A review. Anal Chim Acta 789:1–16

Adv Biochem Eng Biotechnol (2015) 150: 167–182
DOI 10.1007/10_2015_312

Published Online: 12 March 2015

Utilizing the Cross-Reactivity of MIPs

Ecevit Yilmaz, Johan Billing, Carina Nilsson, Brian Boyd, Rüstem Kecili, David Nivhede, Sara Axelsson and Anthony Rees

Abstract The crossreactivity of molecularly imprinted polymers (MIPs) and its practical implications are discussed. Screening of MIP libraries is presented as a fasttrack route to discovery of resins selective towards new targets, exploiting the fact that MIPs imprinted with one type of template molecule also show recognition to related and sometimes also to apparently unrelated molecules. Several examples from our own and others' studies are presented that illustrate this crossreactivity and the pattern of recognition is discussed for selected examples.

Keywords Commercial MIP products · Crossreactivity · Molecularly imprinted polymers

Contents

E. Yilmaz (✉) · J. Billing · C. Nilsson · A. Rees
MIP Technologies AB (a Wholly Owned Subsidiary of Biotage AB), Box 737, 220 07 Lund, Sweden
e-mail: Ecevit.Yilmaz@Biotage.com

A. Rees
Rees Consulting AB, 75591 Uppsala, Sweden

B. Boyd
Straumann, 205 12 Malmö, Sweden

D. Nivhede
Gambro Lundia AB, 226 43 Lund, Sweden

S. Axelsson
Sigma Aldrich, 135 70 Stockholm, Sweden

R. Kecili
Anadolu University, Plant, Drug and Scientific Research Center, 26470 Eskisehir, Turkey

1 Introduction

The technology of molecular imprinting dates back to Polyakov [1] but the foundations of modern molecular imprinting were laid by Wulff [2] (covalent imprinting) and Mosbach [3] (noncovalent imprinting). In its most widely used form, a molecularly imprinted polymer (MIP) is a highly crosslinked organic polymer that is prepared using functional and crosslinking monomers that are polymerized in the presence of a template molecule. The template (or imprint) molecule is typically preassociated with appropriate functional monomer(s) to form a covalent or noncovalent complex prior to initiation of the polymerization. A commonly held view in the literature is that this imprinting process results in the formation of a cavity wherein the template molecule is surrounded by both functional and crosslinking monomers that together form a specific binding site. Within this site the functional monomers are postulated to be more or less precisely positioned to form complementary interactions (H-bond, ionic, hydrophobic, etc.), with functional groups present in the template molecule.

A well-known example exploring the notion that MIP binding sites were analogous to biological receptors (or antibodies) was published in 1993 by Mosbach's group. In this work, a theophylline-imprinted polymer that could distinguish between theophylline and the very similar molecules caffeine and theobromine were described [4]. In a direct comparison with a natural receptor, the relative binding selectivity obtained with the MIP showed good correspondence, contributing to the view expressed by many authors that MIPs are "highly selective." This view has prevailed and is still commonly stated in the literature [5].

2 Crossreactivity of MIPs

When MIPs are prepared using the target compound as template, leakage of trace amounts of the template molecule (so-called bleeding) from the MIP may occur under harsh conditions. This leakage has been considered to be one of the main reasons why MIPs cannot be reliably employed in the accurate quantification of

trace levels of analytes [6]. Hence, when MIP development is aimed at trace compound analysis, it is not advisable to use the target molecule as the template. In such applications, an elegant solution has been developed that utilizes the cross-reactivity of MIPs through using a similar compound as a "dummy template" in the imprinting process instead of the target compound. An early example where the bleeding problem was successfully circumvented by using a related drug derivative as the template was presented by Andersson, Paprica, and Arvidsson for the target pharmaceutical compound sameridine [7]. The utilization of the inherent crossreactivity of MIPs and their ability to recognize molecules that share common features with the template molecule was reported in that work and binding site cavities with a sufficiently high fidelity were obtained. Figure 1 displays the slight but decisive difference of the template molecule used and the target compound sameridine. The mere difference lies in the replacement of a methyl group to an ethyl group. After MIP preparation, trace analysis of sameridine was then possible without the potential contamination of the template arising from the slight bleeding that plagued the early MIP synthesis methods.

For use of MIPs in analytical applications, we have previously recommended a "rule of six," one of whose requirements is obligatory avoidance of the use of the target analyte as a template during MIP formation [8].

In an extension of the template analogue approach, Takeuchi and coworkers showed that the use of trialkylmelamines as template molecules led to well-functioning, class-selective MIPs [9]. In this study it was shown that the use of a nonherbicide with a sufficiently similar structure to the target herbicides was close enough in structural agreement with the target to lead to MIPs with a selectivity towards a whole range of triazine herbicides (Fig. 2).

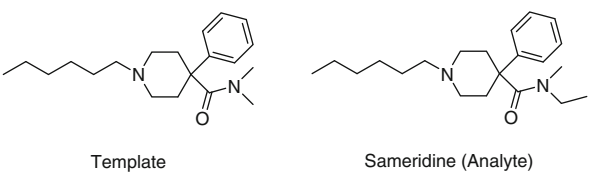

Fig. 1 Structure of the used template and the trace analyte sameridine

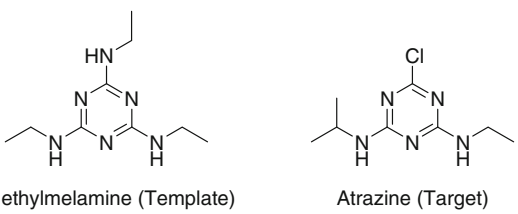

Fig. 2 Structures of the trialkylmelamine dummy template and a triazine herbicide

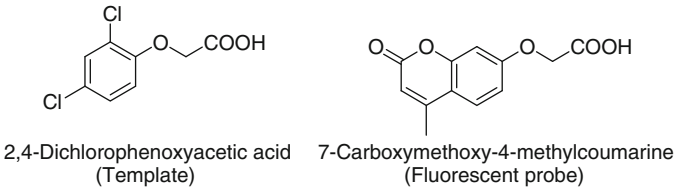

Fig. 3 Structures of the template and the fluorescent probe

A noteworthy study of chiral MIPs and an investigation on their crossreactivity was presented by Ramström et al. where an ephedrine-imprinted polymer as an artificial adrenergic receptor was described. The MIP was able to both recognize different alpha and beta adrenergic compounds and furthermore, the chirally imprinted polymer could separate both alpha and beta adrenergic enantiomers. Apparently, the chiral site created by (+)-ephedrine could harbor other similar small compounds in the chiral cavity, even though alpha and beta adrenergic compounds differ slightly in their molecular structure [10].

As another example on this theme, Haupt, Mayes, and Mosbach described a 2,4-dichlorophenoxyacetic acid imprinted polymer that displayed an extended crossreactivity profile. In these experiments, the group showed that other compounds with the phenoxyacetic acid moiety, such as the fluorescent compound 7-carboxymethoxy-4-methylcoumarine, could compete well with the binding of the target (Fig. 3). As a consequence, the resulting MIPs could be utilized in selective displacement assays [11].

MIPs have also been found in some cases to recognize molecules that are, at first sight, not obviously related to the template molecule. When Martin, Wilson, and Wilson imprinted the beta antagonist propranolol, they found that this MIP also displayed selectivity and an imprinting effect towards tamoxifen, a compound used in the treatment of breast cancer. Incidentally, this example was one of the first that described a somewhat unexpected crossreactivity between a studied analyte and the template molecule [12]. Nevertheless, upon a more detailed analysis of the molecular substructures it can be seen that both molecules contain related functional groups, that is, the O–C-C–N motif (Fig. 4).

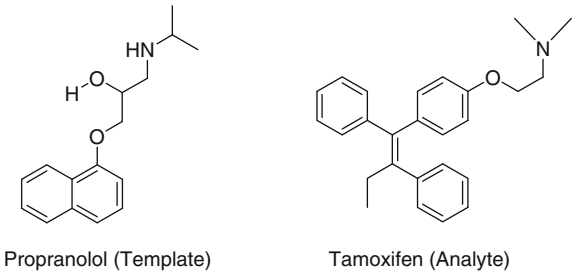

Fig. 4 Structures of the propranonol (template molecule) and the rebinding molecule tamoxifen

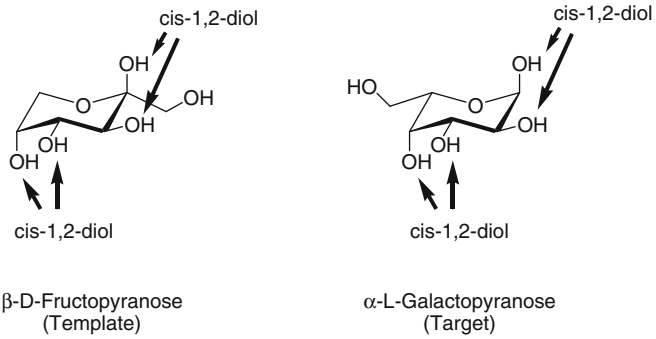

Fig. 5 Structures of the D-fructopyranose (template molecule) and the rebinding molecule L-galactopyranose

Already very early on, Wulff and Schauhoff [13] observed a somewhat unexpected crossreactivity in a covalently imprinted polymer. In their efforts to design and synthesize a chiral MIP, the sugar D-fructose was covalently imprinted using a boronic acid monomer. After workup, the imprinted polymer was very well able to distinguish D-fructose over L-fructose. However, in further evaluations with other sugars and their chiral enantiomers it was found that the chiral MIPs would also show an inverse chiral selectivity towards L-galactose over D-galactose. When inspecting the spatial orientation of the hydroxyl groups involved in the imprinting process, it became evident that L-galactose might offer the same functional groups to the chiral binding site of the cavity as those offered by D-fructose (Fig. 5).

There are more publications presented in the recent past that underline the utility of the crossreactivity potential of MIPs and we expect more reports on this theme to be published in the future [14–17].

3 Commercial Product Development Utilizing the Crossreactivity of MIPs

Although clearly of practical utility, the dummy template approach was in a sense a slight contradiction to the notion that MIPs were highly selective and could distinguish molecules that differed only slightly in structure (e.g., by a methyl group). A cautionary note that should be sounded is that this may be the exception rather than the rule. As is well known, there is no such thing as "absolute specificity" in chemistry or in biology. In the work described here we explore the crossreactivity in a more systematic manner and demonstrate that target analyte molecules can bind selectively to MIPs prepared with templates that superficially appear to be dissimilar and may even be of different "scaffold classes" but which exhibit sufficient substructural similarity to be able to drive recognition. This phenomenon,

well known in pharmaceutical discovery, greatly enhances the landscape of template–analyte crossreactivity and speeds the discovery of new artificial receptors based on molecular imprinting.

3.1 Development of a MIP Selective Towards Chloramphenicol

During our own efforts to develop a MIP towards the antibiotic compound chloramphenicol (CAP) we surmised that screening MIPs containing monomers able to bind diols may be a fruitful approach. In the screening (not shown), we discovered that a MIP imprinted with an unrelated diol-containing template using 4-vinylbenzeneboronic acid as the functional monomer [18] displayed a relatively strong imprinting effect, as shown in Fig. 6 where the imprinted polymer (MIP) retained the target compound chloramphenicol considerably stronger than the NIP (imprinting factor: k′MIP/k′NIP = 1.7).

Very similar imprinting factors were also determined for the related compound thiamphenicol, which is the methyl-sulfonyl analogue of chloramphenicol having

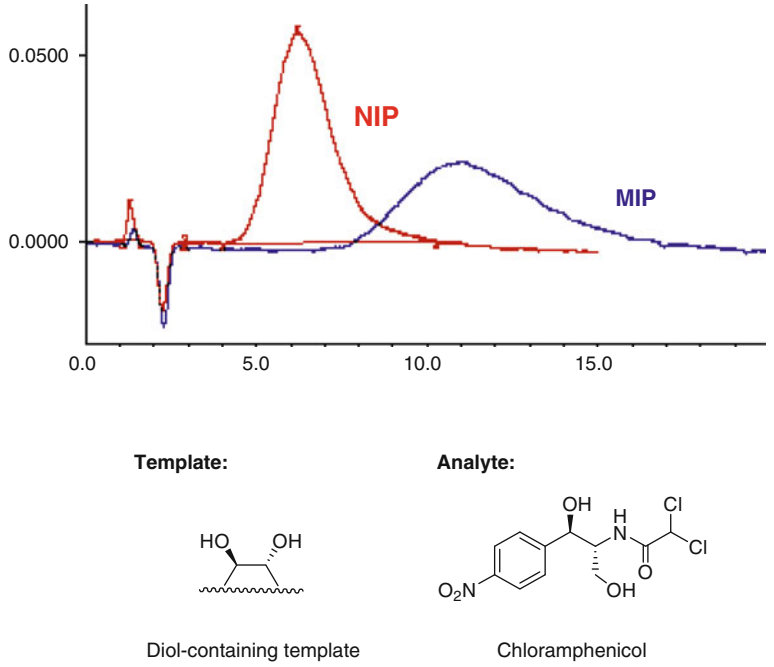

Fig. 6 Imprinting effect for chloramphenicol on a MIP imprinted with a diol-template. MIP and NIP packed in 200 × 4.6-mm stainless steel columns, mobile phase 36 % acetonitrile in 1 % ammonium hydroxide, flow rate 1 mL/min, detection wavelength 215 nm

the same diol substructure. Solid phase extraction (SPE) protocols were developed that allowed use of this MIP for the selective extraction of CAP from milk, honey, urine, and plasma [19, 20]. In this protocol, the signal-to-noise ratio was 3.7 times higher than that obtained with the conventional LLE–SPE method allowing the detection of chloramphenicol down to 0.03 μg/kg (30 parts per trillion), ten times lower than the European Union minimum required performance limit [20]. These results demonstrate that effective SPE can be carried out using MIPs based on the crossreactivity principle.

3.2 Development of a MIP Selective Towards Genotoxic Compounds

In our laboratories, we recently utilized the crossreactivity and screening concept to shortcut the discovery of a desired MIP selectivity. The target was to obtain a sufficiently selective material that displayed recognition of particular genotoxic compounds [21]. Genotoxic compounds are a collection of different compound classes that may be present in pharmaceutical APIs. The group of molecules studied here were 5 different members of the class of aminopyridines, used for example as building blocks of the pharmaceutical compounds piroxicam and tenoxicam. A first screening with a broad variety of resin chemistries was conducted to determine the type of MIPs that would be feasible for effective aminopyridine retention. In this first screening, it was found that resins with weak cation exchange functionality in the form of surface carboxylic acid moieties were most retentive. In the subsequent screening, a broad collection of carboxylic acid containing MIPs and NIPs was evaluated. The study showed that one MIP was outstanding in both binding and imprinting effect. This so-called hit-MIP was a polymer imprinted with nornicotine. This MIP displayed an unexpectedly high selectivity as well as a good imprinting effect towards several of the aminopyridines. Looking at the template molecule of the hit-MIP, the similarity of nornicotine and aminopyridines is of course striking (Fig. 7).

Subsequent purification studies showed that the nornicotine-imprinted polymer was able to remove aminopyridines from their respective API effectively with virtually no loss of API. Although this was a proof-of-concept study, from a practical utility point of view it can be anticipated that this selective resin would be an effective adsorbent for removal of this type of genotoxic candidate in the presence of the relevant API with broad applicability in the pharmaceutical industry.

3.3 Development of a MIP Selective Towards Beta-Blockers

To further utilize this discovery approach, a series of chemically related MIPs, all prepared using methacrylic acid as the functional monomer but with widely

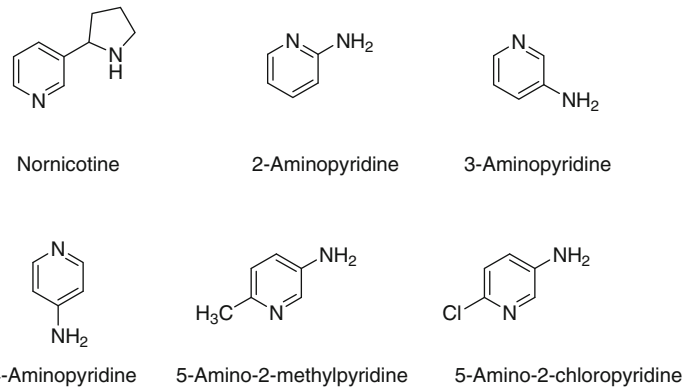

Fig. 7 Structure of MIP template nornicotine and aminopyridines

differing templates and varied backbone monomers, were screened for their ability to recognize the beta-blocker metoprolol. This simple one-step screening experiment resulted in two candidate MIPs for metoprolol, EA009 and EA011 (Fig. 8).

Both candidate MIPs had been prepared with templates containing related chemical functionality to metoprolol. This somewhat expected crossreactivity was a validation of the screening approach to resin discovery. Sample preparation protocols using EA009 for the analysis of beta-blockers in water and urine samples have now been developed with excellent results [22, 23].

3.4 Development of a MIP Selective Towards Fluoroquinolones

In a further example, an extended version of the same library was screened for MIPs that bind fluoroquinolones, a class of antibiotics that are sometimes present in trace amounts in foodstuffs, such as meat and honey, and which are tightly controlled by regulatory bodies in both the European Union and the United States.

To find a MIP candidate for this class of compound, the MIP library was screened using the fluoroquinolone antibiotic ciprofloxacin. In Fig. 9, four candidate MIPs with a significant MIP–NIP difference were identified, EA009, EA011, EA033, and EA023.

To distinguish these four candidate MIPs from each other, a new experiment with a more gradual gradient of acetic acid was carried out and the template T-imprinted MIP EA023 was found to have the most pronounced difference between the MIP and the corresponding NIP (Fig. 10). Although it had been prepared using a template with no obvious relation to ciprofloxacin it still displayed a high imprinting effect and the resin also recognized other fluoroquinolones (Fig. 11).

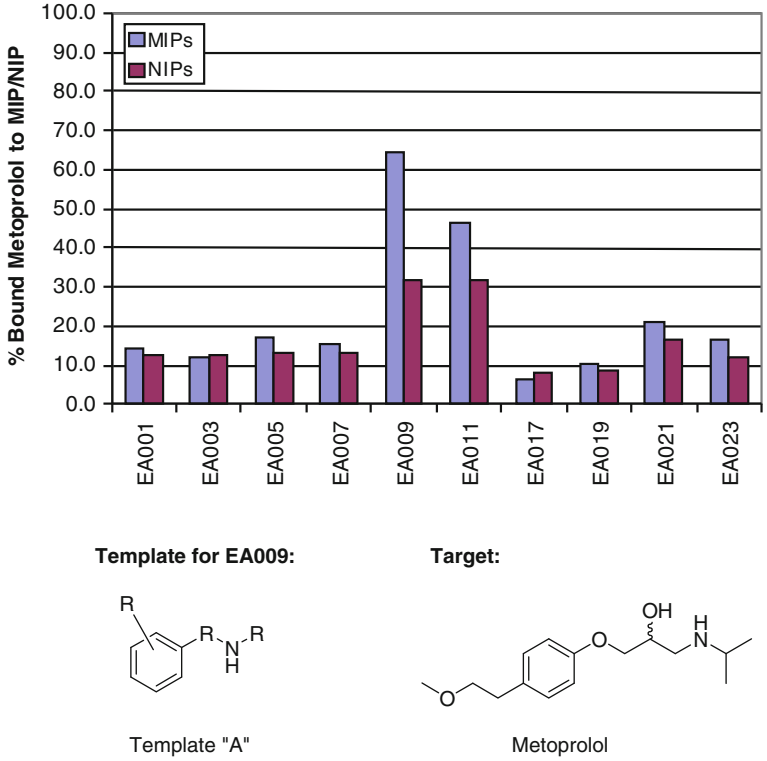

Fig. 8 Results from the screening experiment with metoprolol. In the experiment, 25 mg of each MIP and the corresponding NIP were packed in duplicate in 2-mL SPE cartridges and first conditioned with 1 mL MeOH and 1 mL acetonitrile. Then 1 mL of a solution containing 5 µg/mL metoprolol in acetonitrile was passed through each cartridge. After this step, the amount of nonbound metoprolol was quantified using HPLC-UV and the corresponding amount of bound metoprolol was calculated. Comparison of the chemical structure of metoprolol with the template used to prepare MIP EA009

On the basis of the performance of this MIP, commercially relevant sample preparation methods were developed for trace analysis of different fluoroquinolones from various biological matrices such as bovine kidney and honey [24]. Compared to conventional analytical workup methods, the current MIP-based fluoroquinolone cleanup accomplishes the pretreatment in only one step, whereas previous methods require a large number of laborious workup steps.

4 The Molecular Basis of Crossreactivity

A summary of the compounds recognized by EA009 and EA023 in these experiments and additional examples from other screening experiments are shown in Figs. 12 and 13.

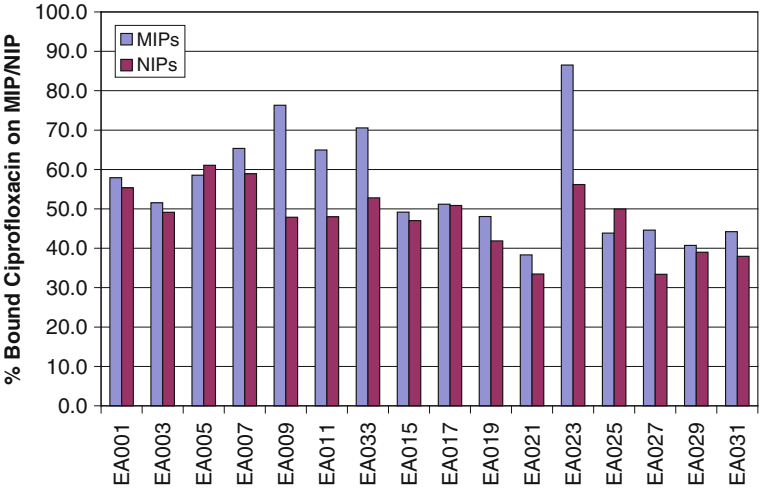

Fig. 9 Results from the screening experiment with ciprofloxacin. 1 mL 100 ng/mL ciprofloxacin in water was loaded onto the conditioned MIP and NIP columns which were then washed sequentially with 1 mL 0.5 % and 1 mL 3 % acetic acid in acetonitrile. After each step the amount of eluted ciprofloxacin was quantified by HPLC-MS and the amount of ciprofloxacin still bound to the resins after the last step was calculated and plotted

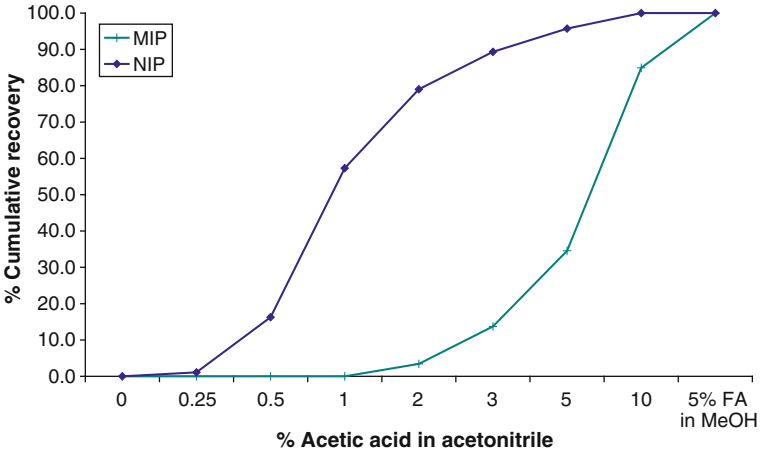

Fig. 10 Normalized cumulative recovery of ciprofloxacin loaded onto 2-mL SPE cartridges containing 25 mg of EA023 or the corresponding NIP. Elution steps: 1 mL each of 0, 0.25, 0.5, 1, 2, 3, 5, and 10 % acetic acid in acetonitrile and 5 % formic acid in MeOH

In explaining the observed crossreactivity of particular polymers, we have assumed that the "similarity" principle applies which, in its simplest form states "similar chemical structures will have similar properties." Typically, similarities

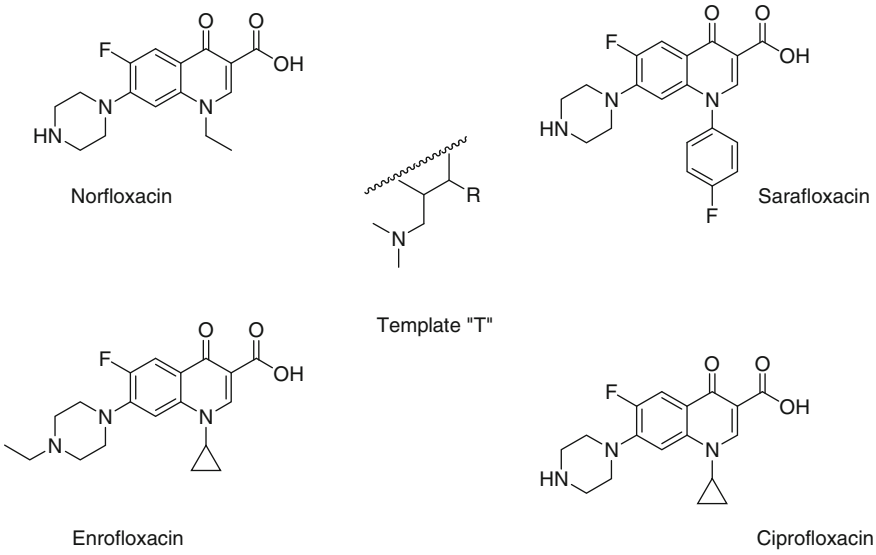

Fig. 11 Relevant substructure of the template "T" and fluoroquinolone structures that are recognized by EA023

may be measured by generating 2D chemical fingerprints of the target molecule and then searching a database of molecules for overlapping substructure features.

The hit molecules obtained are then weighted by any of a number of analysis schemes to generate a valid hit group [25]. The second aspect that should be revealed by such searching is that there should be a landscape of molecules that do not bind or that bind very weakly, molecules that are dissimilar. In the small datasets described here it is not instructive to carry out an exhaustive similarity–dissimilarity analysis. Similarity assessment is an uncertain process and may not always generate explanations for the observed chemical compound behavior. Where the chemical compound motifs important for the interaction with the MIP binding site are unknown or uncertain, quantitating substructure properties between molecules to arrive at similarity scores may not be productive.

In a more qualitative approach, one can make a simpler substructure analysis. For template "A"-templated MIP EA009, metoprolol, clenbuterol, naphazoline, methamphetamine, fluoxetine, tramadol, and methadone all show a substructural pattern of the following form: Aryl-(3 bonds)-N(R1,R2) or Aryl-(4 bonds)-N(R1, R2). For those not exhibiting an exact match to any of these substructures, nicotine has the aryl but a shorter side chain (one carbon) linked to a cyclic NH; ergocornine contains the embedded substructure but the multiplicity of functional groups makes this crossreactivity difficult to interpret; cocaine is only a weak binder and may bind through a different mechanism.

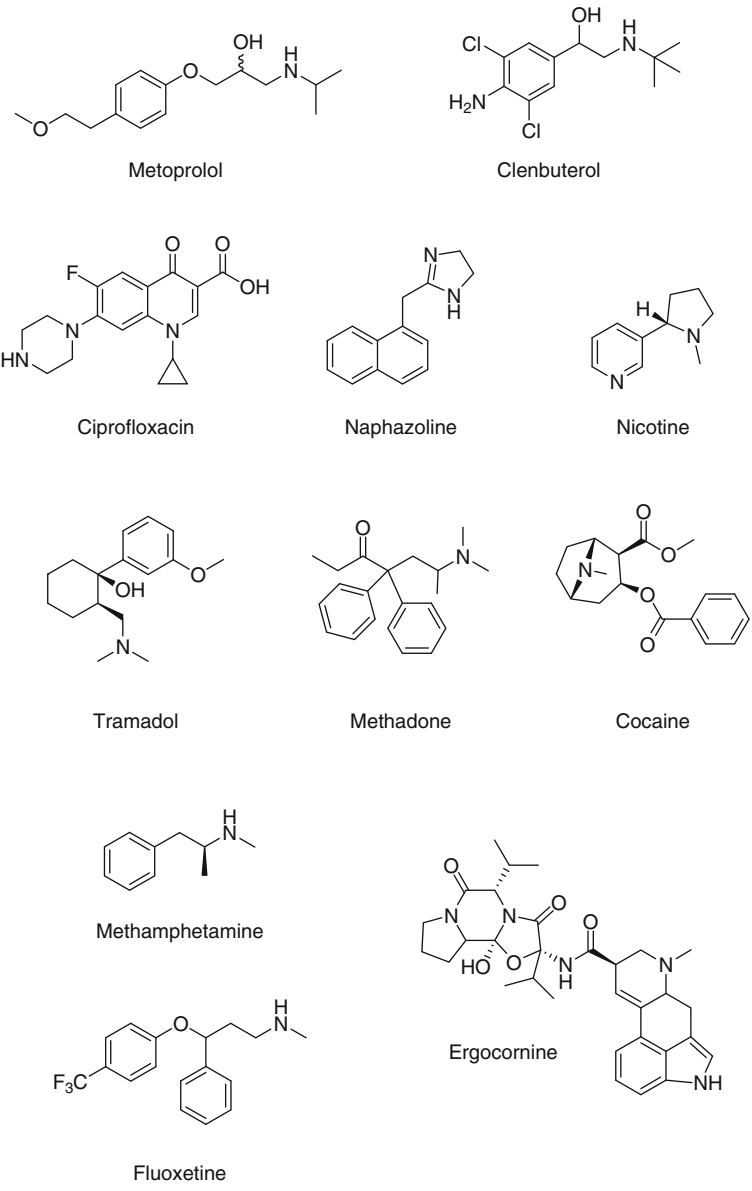

Fig. 12 Compounds recognized by MIP EA009

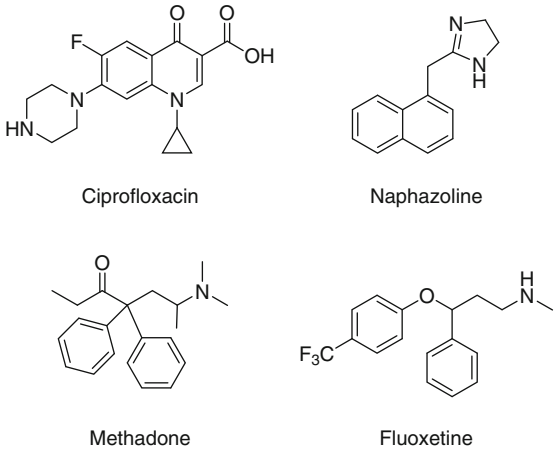

Fig. 13 Other compounds recognized by template T-imprinted MIP EA023

4.1 Template T-Templated MIP EA023

This template has a more bulky structure than template "A" but with some substructural similarities. Of the subset of the four molecules binding this MIP strongly, methadone, fluoxetine, and ciprofloxacin contain the motif Aryl-(4 bonds linear or cyclic)-N(R1,R2). The outsider, naphazoline, instead has the Aryl-(3 bonds)-N(R1,R2) motif.

The above two comparisons, albeit rather qualitative, suggest a structure-binding profile that can be explained by a process similar to that of crude pharmacophore matching. To continue the analysis, we compared those molecules tested against these MIPs that were not recognized by any of the two MIPs discussed above (Fig. 14). Inspection of the dataset suggests an explanation for the absence of binding inasmuch as most of the molecules do not contain the motifs contained in template "A" or template "T".

In compounds where substructures appear related to appropriate binding motifs such as bupivacaine, the spacer between the aryl ring and the amine is rigid and these may be prevented from binding by geometrical constraints. It must also be said that this screening was not comprehensive and we cannot rule out that other molecules lacking these motifs may also show binding.

It has to be emphasized and repeated, that MIPs were successfully synthesized towards a number of the structures in Fig. 14 and mentioned in this chapter such as theophylline [4] and atrazine [9].

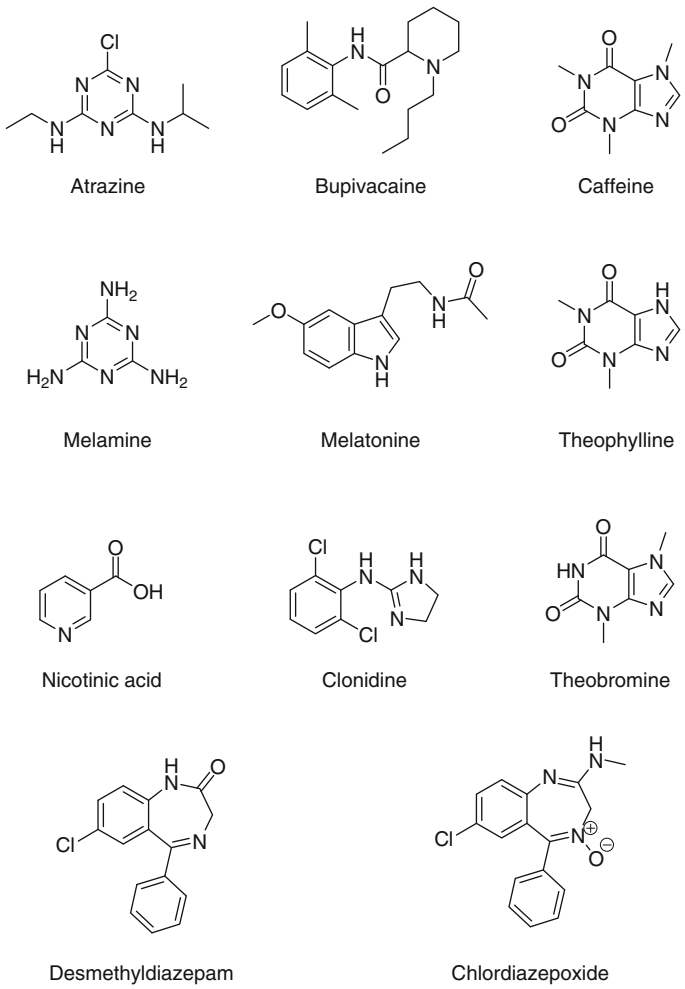

Fig. 14 Compounds not recognized by MIP EA009 or MIP EA023

5 Conclusions

Taken at face value the data we have presented in this chapter suggest a number of revisions to the MIP specificity concept. We list these below as a set of postulates for stimulating further discussion.

1. MIPs do not generally show absolute specificity however strong a template–monomer interaction is.
2. A MIP prepared with a particular template can exhibit crossreactivity with molecules from other chemical scaffold families provided those molecules contain the relevant substructures.

3. Templated MIPs can exhibit chemical crossreactivity by fortuitous interactions that cannot be explained by substructure similarity.

Postulate 1 merely suggests that there is no absolute specificity and that specificity in MIPs can be similar to that of antigen-specific antibodies. Postulate 2 is not a new concept but here we state that it is a property of probably all MIPs prepared by both covalent and noncovalent templating. Postulate 3 is different from nonspecific binding which is typically low affinity and high capacity whereas this "fortuitous crossreactivity" may be quite strong. We hope that the studies described in this chapter stimulate further evaluation of MIPs as surrogate receptors in pharmacological research as well as separation materials in analytical and process scale separations. As a consequence of the above postulations, we would wish to see that the evaluations of MIP studies done will include a much broader selection of molecules to cover the aspects of apparent crossreactivity and also unexpected interactions. In our view, testing only a few molecules in binding or recognition studies is not sufficient to reveal the potentially extensive recognition pattern of MIPs and thus its full potential. From our view this attribute, in contrast to "highly selective," is probably the more correct and factual description of the majority of MIPs. Although those new findings and the present discussions may be somewhat deviant, they are appealing for many applications and should thus not be overlooked.

References

1. Polyakov M (1931) Adsorption properties and structure of silica gel. Zhur Fiz Khim 2: 799–805
2. Wulff G, Sarhan A (1972) Über die Anwendung von enzymanalog gebauten Polymeren zur Racemattrennung. Angew Chem 84:364–369
3. Arshady R, Mosbach K (1981) Synthesis of substrate-selective polymers by host-guest polymerization. Makromol Chem 182:687–692
4. Vlatakis G, Andersson LI, Müller R, Mosbach K (1993) Drug assay using antibody mimics made by molecular imprinting. Nature 361:645–647
5. Alexander C, Andersson HS, Andersson LI, Ansell RJ, Kirsch N, Nicholls IA, O'Mahony J, Whitcombe MJ (2006) Molecular imprinting science and technology: a survey of the literature for the years up to and including 2003. J Molec Recog 19:106–180
6. Ellwanger A, Karlsson L, Owens PK, Berggren C, Crecenzi C, Ensing K, Bayoudh S, Cormack P, Sherrington D, Sellergren B (2001) Evaluation of methods aimed at complete removal of template from molecularly imprinted polymers. Analyst 126:784–792
7. Andersson LI, Paprica A, Arvidsson T (1997) A highly selective solid phase extraction sorbent for pre-concentration of sameridine made by molecular imprinting. Chromatographia 46(1/2):57–62
8. Widstrand C, Yilmaz E, Boyd B, Billing J, Rees A (2006) Molecularly imprinted polymers: a new generation of affinity matrices. American Laboratory News, Oct 2006
9. Matsui J, Fujiwara K, Takeuchi T (2000) Atrazine-selective polymers prepared by molecular imprinting of trialkylmelamines as dummy template species of atrazine. Anal Chem 72:1810–1813
10. Ramström O, Cong Y, Mosbach K (1996) Chiral recognition in adrenergic receptor binding mimics prepared by molecular imprinting. J Mol Recog 9:691–696

11. Haupt K, Mayes AG, Mosbach K (1998) Herbicide assay using an imprinted polymer-based system analogous to competitive fluoroimmunoassays. Anal Chem 70:3936–3939
12. Martin PD, Wilson TD, Wilson ID, Jones GR (2001) An unexpected selectivity of a propranolol-derived molecular imprint for tamoxifen. Analyst 126:757–759
13. Wulff G, Schauhoff S (1991) Racemic resolution of free sugars with macroporous polymers prepared by molecular imprinting. Selectivity dependence on the arrangement of functional groups versus spatial requirements. J Org Chem 56:395–400
14. Sabourin L, Ansell RJ, Mosbach K, Nicholls IA (1998) Molecularly imprinted polymer combinatorial libraries for multiple simultaneous chiral separations. Anal Commun 35: 285–287
15. Spivak D, Campbell J (2001) Systematic study of steric and spatial contributions to molecular recognition by non-covalent imprinted polymers. Analyst 126:793–797
16. Allender CJ, Brain KR, Ballatore C, Cahard D, Siddiqui A, McGuigan C (2001) Separation of individual antiviral nucleotide prodrugs from synthetic mixtures using cross-reactivity of a molecularly imprinted stationary phase. Analytica Chim. Acta 435:107–113
17. Turiel E, Perez-Conde C, Martin-Esteban A (2003) Assessment of the cross-reactivity and binding sites characterization of a propazine-imprinted polymer using the Langmuir-Freundlich isotherm. Analyst 128:137–141
18. Boyd B, Björk H, Billing J, Shimelis O, Axelsson S, Leonora M, Yilmaz E (2007) Development of an improved method for trace analysis of chloramphenicol using molecularly imprinted polymers. J Chromatogr A 1174:63–71
19. Mohamed R, Richoz-Payot J, Gremaud E, Mottier P, Yilmaz E, Tabet JC, Guy PA (2007) Advantages of molecularly imprinted polymers LC-ESI-MS/MS for the selective extraction and quantification of chloramphenicol in milk-based matrixes. Comparison with a classical sample preparation. Anal Chem 79:9557–9565
20. Shimelis O, Trinh A, Brandes H (2007) The selective extraction of chloramphenicol using molecularly imprinted polymer SPE. Supelco Reporter (US Edition), vol 25.1, pp 9–11
21. Kecili R, Billing J, Nivhede D, Sellergren B, Rees A, Yilmaz E (2014) Fast identification of selective resins for removal of genotoxic aminopyridine impurities via screening of molecularly imprinted polymer libraries. J Chrom A 1339:65–72
22. Gros M, Pizzolato TM, Petrovic M, López de Alda MJ, Barceló D (2008) Trace level determination of beta-blockers in waste waters by highly selective molecularly imprinted polymers extraction followed by liquid chromatography-quadrupole-linear ion trap mass spectrometry. J Chrom A 1189:374–384
23. Kronauer S, Wihlborg AK, Trinh A (2007) The class selective extraction of beta-agonists and antagonists using molecularly imprinted polymer SPE. Supelco Reporter (US Edition), vol 25.4, pp 13–15
24. Wihlborg AK, Shimelis O, Trinh A (2009) The selective extraction of fluoroquinolones in veterinary samples using molecularly imprinted polymer SPE. Supelco Technical Report, T408177
25. Willett P (2011) Similarity searching using 2D structural fingerprints. Methods Mol Biol 672:133–158

Adv Biochem Eng Biotechnol (2015) 150: 183–205
DOI 10.1007/10_2015_311

Published Online: 22 March 2015

MIPs as Tools in Environmental Biotechnology

Bo Mattiasson

Abstract Molecular imprints are potentially fantastic constructions. They are selective, robust, and nonbiodegradable if produced from stable polymers. A range of different applications has been presented, everything from separation of enantiomers, via adsorbents for sample preparation before analysis to applications in wastewater treatment. This chapter deals with molecularly imprinted polymers (MIPs) as tools in environmental biotechnology, a field that has the potential to become very important in the future.

Keywords Cryogels · Endocrine disruptors · Wastewater treatment

Abbreviations

AAm	Acrylamide
E2	Estradiol
HRT	Hydralic retention time
MG	Macroporous gel
MGP	Macroporous gel particle
NIP	Nonimprinted polymer
PVA	Poly (vinylalcohol)

Contents

B. Mattiasson (✉)
Department of Biotechnology, Lund University, P.O. Box 124, 221 00 Lund, Sweden
e-mail: Bo.Mattiasson@biotek.lu.se

B. Mattiasson
Indienz AB, Annebergs Gård PL 5520, 268 73 Billeberga, Sweden

1 Introduction

Molecular imprinting is a technology to make affinity adsorbents that are chemically and potentially also mechanically stable. Such adsorbents may find applications in many areas, but of special interest are those where conventional adsorbents are not sufficient. One good example is in environmental technology for remediation of water. Here, unpredictable mixtures of chemicals may appear together with microbial cells and other suspended material. The development in this area is rather slow, and the first efforts to integrate molecularly imprinted polymers (MIPs) in environmental technology were within analysis.

Cleaning of polluted water is by far the largest biotechnological process in society today. Technology development in the wastewater treatment area has to a large extent been focused on municipal wastewater and in recent years on treatment of industrial waters. A reason for these priorities has been the obvious results of water pollution. Municipal wastewater released without proper cleaning caused massive death of fish and other water-living organisms due to consumption of oxygen in the water. The introduction of the concept of biological oxygen demand (BOD) when characterizing a wastewater helped to set limits for what was allowed to be released to recipients, and what needed more treatment before it could be released.

Industrial wastewaters are of different characters. From industries processing biomass, pulp and paper industries, food industries, and the like, BOD is one important characteristic for defining purity. However, in many cases this is not enough. Process industries, in addition to biomass, use chemicals in the processes and these chemicals or their reaction products are released. These emissions often do not have the same instant effect on the recipient water as observed when high BODs were released. It often took a longer time before effects were observed, and in some cases one needed to follow the effects up the food/feed chain before dramatic effects were observed. Because of the slow response to the pollution, it took time before proper water treatment technology was developed and

implemented in society. Today, the situation is relatively good in those countries where an environmental protection policy has been decided on and implemented. In several places, however, there are laws, but they are not properly implemented. The reasons may be lack of competence or lack of suitable equipment to monitor pollution, and therefore also to put pressure on the pollution agencies. Still another factor is corruption that in many cases causes lack of implementation of environmental laws.

In addition to biological oxygen-demanding pollution and industrial releases there is a "new" category of pollutants to handle. Many compounds are spread in society and appear in wastewater at low concentrations. These compounds are often poorly degraded but at the same time they may be potent physiologically.

Examples of these "emerging" pollutants are hormone-active compounds, flame-retardants, pharmaceuticals, and pesticides [1]. In this group can also be included some heavy metal ions, even if they are not new as polluters, but they may be present at similar low concentrations as those of the new pollutants. This group of polluting compounds is poorly degraded in the treatment processes used today and there is room for new developments (metal ions are of course not degraded, but they may get immobilized). The limiting factor is the very low concentrations, within the range of 1 μg/L–1 ng/L. To remove such compounds using precipitation is unrealistic, and using microbes is not an alternative because the microbes will not handle compounds as substrates at such low concentration levels. Advanced oxidation processes have been developed and they may be efficient, but expensive. Adsorption or extraction might be possible modes of operation to remove/enrich pollutants, and after such a process take care of the pollutants separately. There are very few cases where MIPs have been used for treating wastewater as a remediation step, but on the other side there are many examples of MIPs in sample pretreatment for analysis of pollutants in wastewater (Table 1). These sample pretreatment examples will give guidance towards what is to be expected on the day when proper technology is available for utilizing MIPs in water treatment processes.

To utilize adsorbents capable of enriching compounds present in low concentrations raises demands on the quality of the binding sites of the adsorbents. There are several examples of immunoaffinity from pharmaceutical biotechnology that in

Table 1 Environmental pollutants in water enriched with MIPs

Target pollutant	Template	Matrix	References
Bisphenol A	Bisphenol A	Tap water	[2]
Bisphenol A	Bisphenol A-d16	Surface water	[3]
Carbamazepine	Carbamazepine	Wastewater	[4, 5]
17 β-estradiol	17 β-estradiol	Wastewater	[6, 7]
Microcystin-LR	Microcystin-LR	Drinking water	[8]
Triazines	Terbutylazine	Surface water	[9]
Pb^{2+}	Pb^{2+}	Surface water	[10]
Domoic acid	Domoic acid	Sea water	[11]

theory would be possible to use. However, wastewater is not a sterile milieu and one can expect any protein-based affinity ligand to be quickly degraded. Therefore, one needs to investigate possible ligands of synthetic nature that will not be degraded in an open system such as that represented by wastewater. MIPs have certain advantages making them attractive for this application [12–17]. Their binding strength has been demonstrated to be almost that of antibodies [18]; their robustness may be high provided suitable polymers are used.

1.1 Adsorbents for Enrichment as a Pretreatment Step to Analysis

Solid phase extraction is well developed in the medicinal–pharmacokinetic area. A range of studies has been conducted where environmental pollutants have been efficiently enriched on MIPs. Some of these are listed in Table 1.

A characteristic of these systems is the use of small MIP particles in small columns through which water samples are passed. Then the captured material is released and analyzed, often with mass spectrometry. In many cases, the removal efficiency of the compounds is high, and provided a more suitable physical appearance of the adsorbent is available, use of MIPs seems attractive. A drawback of MIPs has been that they are used as small particles and when packed in columns, represent massive backpressure and therefore low flow rates. What is needed is larger particles such that the pressure drop is lower, and robustness so that the adsorbent can stand the often harsh conditions present in wastewater.

Wastewater usually comprises large volumes and thus high flow rate is a prerequisite for any treatment method to become a realistic alternative. By inserting MIPs into larger polymer structures it may be possible to improve the flow properties with retained binding properties. This was done using supermacroporous gels, so-called cryogels, and one could see good flow properties and efficient enrichment of the polluting molecules. Still another method would be to aggregate the small particles in order to form larger structures with good flow properties. The potential of this technology has been demonstrated when developing some macroporous adsorbents [19]. A combination of the two mentioned strategies, the composite approach in supermacroporous gels and the aggregation method is represented by supermacroporous cryogels built from aggregated nanoparticles [20].

Many of the “emerging” pollutants are present at very low concentrations, but because they are physiologically potent, one needs to remove them. For this study it was decided to work with estrogen-like compounds, that is, estrogen and any compound that will bind to the estrogen receptor.

2 Production of MIPs and Evaluation of Their Performance for Cleaning Water

MIPs were synthesized according to a protocol by Rachkov et al. [21].

Estradiol was dissolved in chloroform in a 30-mL tube to which was added the functional monomers, the crosslinker, and initiator. The mixture was gently mixed for 5 min and then cooled on ice and purged with nitrogen for 5 min before the test tube was sealed and the mixture was heated to 65 °C for 20 h. The polymer monolith formed was smashed and the pieces obtained were ground. Particles passing through a 25-μm test sieve were collected and washed with methanol. This washing was repeated several times in order to secure that no print molecules were left that could subsequently be leaking from the MIP. Then the methanol was allowed to evaporate. The dry MIPs were washed 6 times with a mixture of methanol and acetic acid (4:1 v/v) and then dried in a desiccator for 24 h.

In parallel to the MIP preparation, nonimprinted polymer was also produced. Here all reagents were the same, except for the print molecule. The nonimprinted polymers were later called NIP.

The binding of estradiol to the MIPs was evaluated using radiolabelled estradiol. After proper equilibration, aliquots were taken from the supernatant and the radioactivity was measured. The amount bound was obtained after subtracting the amount present in the supernatant from the total amount added.

2.1 Extraction of Estradiol at 1 ppb Level

A comparative study was performed using a MIP-column, a NIP-column, a C18-column, and an activated carbon column; see Fig. 1. Two liters of an aqueous solution of estradiol at 1 ppb was then passed through each column by applying a weak vacuum (0.5 bar). Elution was done twice with a methanol–acetic acid mixture (4:1 v/v) and the content of estradiol was quantified. The experiments were carried out in duplicate or triplicate. The studies were then repeated with aqueous solutions of 0.1 ppb of estradiol.

Assuming that elution removed the entire fraction extracted, the concentrations of estradiol in the treated samples were below 0.02 ppb for the MIP compared to 0.1 ppb for the NIP and 0.2 ppb for C18 and the activated carbon phase.

Studies on interference by different aromatic substances such as phenol, 2-chlorophenol, 4-chlorophenol, and 2,6-dichlorophenol revealed that these compounds bound, but less strongly and they could then be more easily eluted from the adsorbent.

As stated above, flow properties are not good when using small MIP particles, and therefore supermacroporous gels were introduced. The MIP particles were either entrapped or covalently bound to the porous material. The gels that were used are called cryogels.

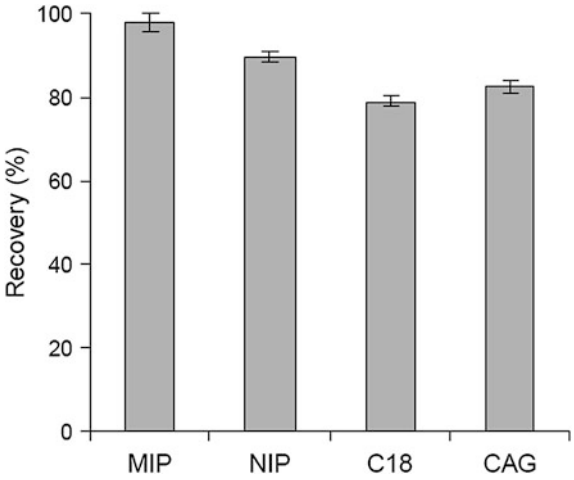

Fig. 1 Amount of estradiol recovered from the extraction of 2 L of aqueous solution containing 1 ppb of estradiol by MIP (100 mg), NIP (100 mg), C18 phase (200 mg), or granulated activated carbon (100 mg) and after elution by 4 mL of MeOH:acetic acid (4:1 v/v). No estradiol was found in the second eluate. *Vertical bars* represent the standard deviation in triplicate (MIP) or duplicate (other adsorbents) (reproduced with permission from Le Noir et al. [22])

2.2 Cryogels

These gels are prepared at subzero temperatures, having highly interconnected pores up to 100 μm in size. Cryogels can be produced as monoliths, sheets, or beads. The present study was focused on the use of monoliths. When the gel is to be in contact with wastewater it is preferable to use material that will not be degraded by microorganisms. The gels were therefore produced in crosslinked polyacrylamide. The monomers, acrylamide, and the crosslinker N,N-methylenebis(acrylamide) were mixed with the MIP-particles, the catalyst, and initiator system. After mixing, the solution was placed at −12 °C and left overnight to polymerize. During the freezing process, ice crystals are formed and the monomers and the particulate matter are found in the interstitial space. It is in this space that polymerization proceeds. Upon thawing of the gel, the melted ice left behind a network of interconnected pores. Cryogels were also produced using polyvinyl alcohol or chitosan. The former polymer forms a gel upon freezing and the polymer chains are held together via hydrogen bonds. The chitosan-derived structures need crosslinking, and glutaraldehyde was added to a precooled mixture before the freezing period.

A first study with the composite cryogels involved enrichment of estrogen-active components in wastewater. It is clear that not only estrogen itself, but also a whole range of compounds have estrogen-like activity. This means that they interact with the estrogen receptor. Therefore, organisms will react as if there were estrogen in the water. A total of more than 100 different substances have estrogenic activity [23].

Because this activity is expressed by the ability to bind to the estrogen receptor, it seems logical to use such receptors to capture the molecules. However, in addition to the risks of proteolytic degradation, such receptors are labile and would not survive even the immobilization procedure. Therefore it was logical to evaluate MIPs [23].

From Table 2 it can be seen that using MIP-cryogel composites was advantageous with regard both to efficiency in removing estrogen-active compounds from the water phase and to the flow rate that could be applied. Also PVA-composites turned out to be efficient. Figure 2 shows that efficient removal of E2 was observed, also upon repeated extractions.

Mechanical stresses on cryogels when exposing them to turbulent wastewater MIP-cryogel composites are obviously good for capturing target molecules from water. One problem remained after this demonstration. The macroscopic properties of the gel would rapidly degrade. In order to reduce the deterioration of the gel structure, cryogel composites were prepared within plastic housings such that the gel was protected from mechanical attrition, but at the same time could bind target molecules from the water. The plastic housings were of the AnoxKaldnes-type which are used for cultivation of microorganisms in wastewater treatment plants [24, 25]. Examples of such protected gels are shown in Fig. 3.

Table 2 Application of wastewater through the MIP, PVA, and composite MIP/PVA monolith columns

Material	MIP	PVA	MIP/PVA
Applied wastewater (mL)	55	200	200
Flow rate of wastewater applied (mL/min)	1[a]	50	50
Recovery (%)[b]	10	100	100

[a] After passing wastewater effluent for 180 min, the MIP column was completely clogged
[b] Recovery (%) was estimated as $(A_1/A_0) \times 100$, where A_1 and A_0 represent the absorbance of wastewater effluent at 420 nm after and before passing the column, respectively

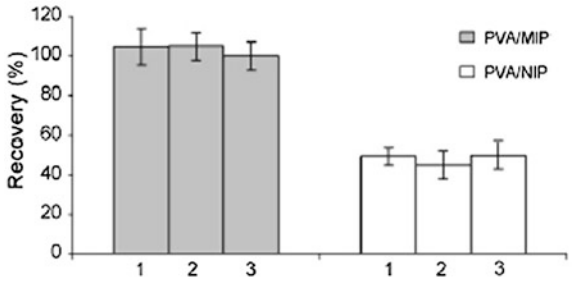

Fig. 2 Repetitive extractions of estrogen from PVA/MIP and PVA/NIP composite columns. Experimental conditions: in each cycle (*1*, *2*, and *3*), 2 L of an aqueous solution containing 2 mg/L of 17β-estradiol was applied to PVA/MIP (*grey bars*) and PVA/NIP (*white bars*) at a flow of 50 mL/min. Extraction was performed with methanol:acetic acid (4:1 v/v) solution. *Vertical bars* represent the standard deviation on duplicate (reproduced with permission from Le Noir et al. [6])

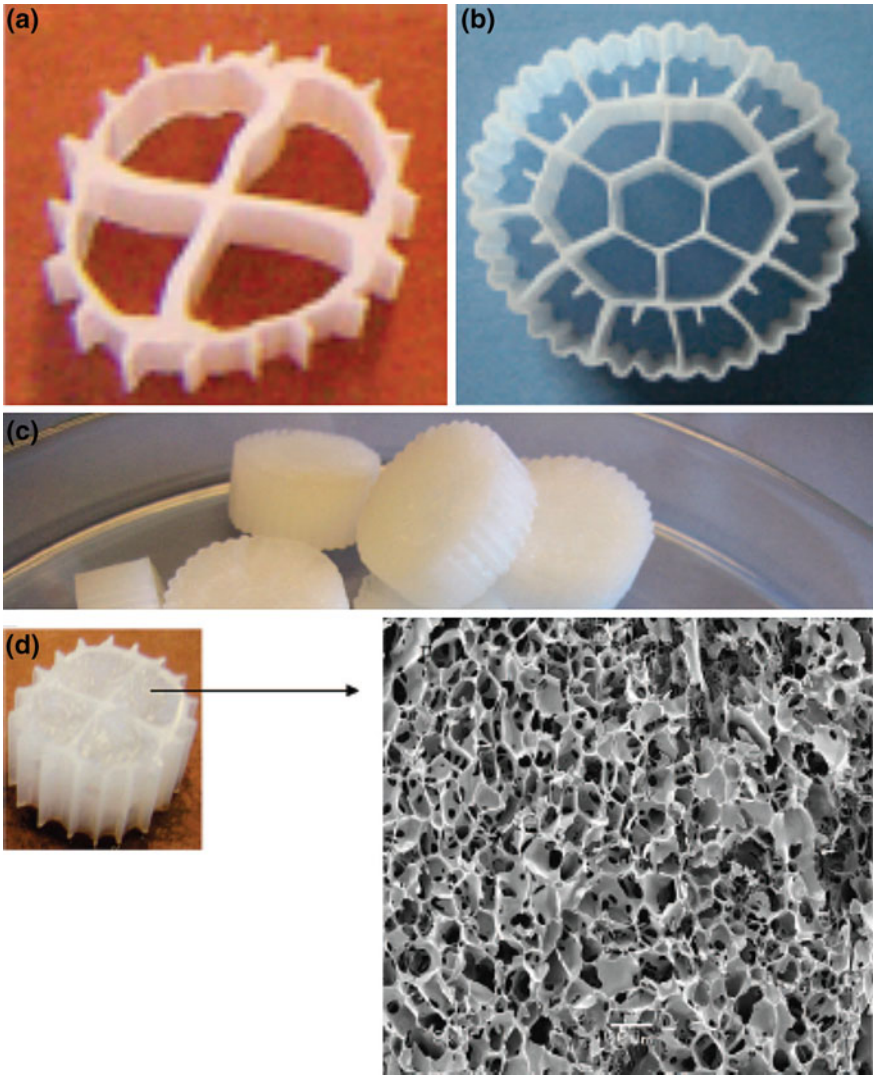

Fig. 3 **a**, **b** Picture of the plastic carriers of different types present an inert supporting medium for the formation of soft and highly elastic hydrophilic materials inside; **c** macroporous gels bearing different functionalities formed inside the carriers; **d** SEM image of polyacrylamide-based macroporous gel formed inside the Kaldnes carrier (reproduced with permission from Plieva and Mattiasson [26])

The attrition was tested by keeping the protected gels in a vigorously stirred aqueous solution (400 rpm) and then monitoring the attrition effects. Cryogel monoliths were converted into a suspension of small gel particles within a short time. As seen in Fig. 4 [26] there was an initial attrition so that 10–20 % of the gel

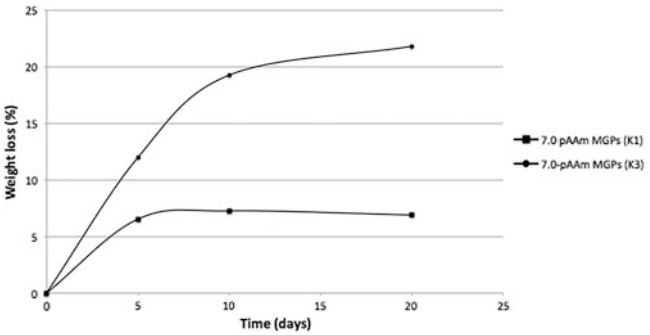

Fig. 4 Weight loss of 7.0 %-pAAm MGs prepared inside K1-carriers (*closed diamonds*) and prepared inside K3-carriers (*open squares*) after being stirred at 400 rpm for 20 days (reproduced with permission from Plieva and Mattiasson [26])

material was removed, but after that the MGPs were stable. The mixing intensity will be less dramatic in wastewater processing which would lead to an extended period during which the particles would be "polished" to their final shape.

From this study is it clear that placing MIPs in a cryogel thereby forming a composite generates an adsorbent that is easy to handle and still efficient in binding the target molecules. The cryogel with the MIP particles was formed within plastic housings as illustrated in Fig. 3. The cryogel is an open structure with pores in the range 1–100 μm (see Fig. 5). When forming composites, the MIPs are distributed within the polymer walls of the cryogel (Fig. 6). Because the pores form an interconnected network, transport of liquid within the gel-plug is relatively efficient. Efforts have also been made to covalently couple MIP particles to the pore walls of cryogels. In this case, the particles were in the submicron range (Fig. 7).

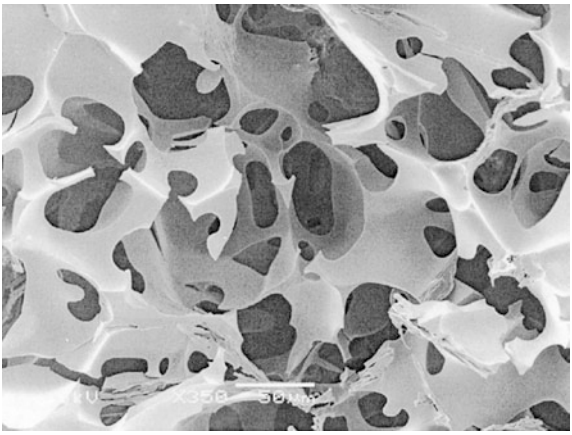

Fig. 5 A scanning electron microscope (SEM) photograph of the monolith matrix (reproduced with permission from Persson et al. [27])

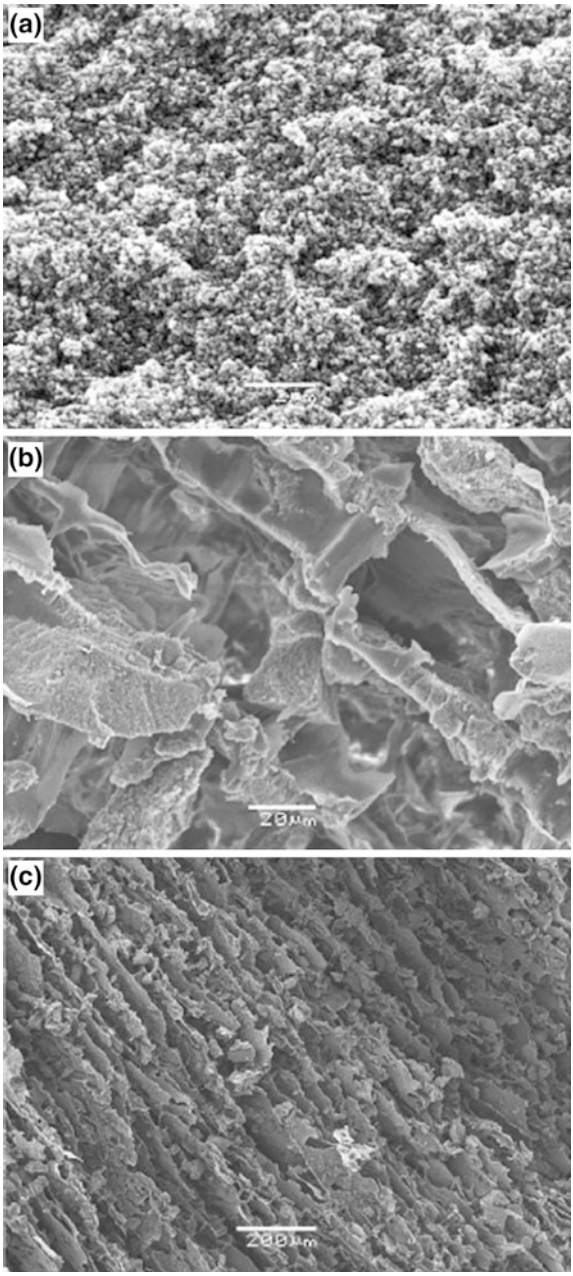

Fig. 6 SEM images of MIP (**a**) and PVA/MIP at different magnifications (**b**, **c**) (reproduced with permission from Le Noir et al. [6])

The macroporous gel particles formed with an outer plastic protecting shell and an inner macroporous polymer structure in this chapter are called MGPs (macroporous gel particles).

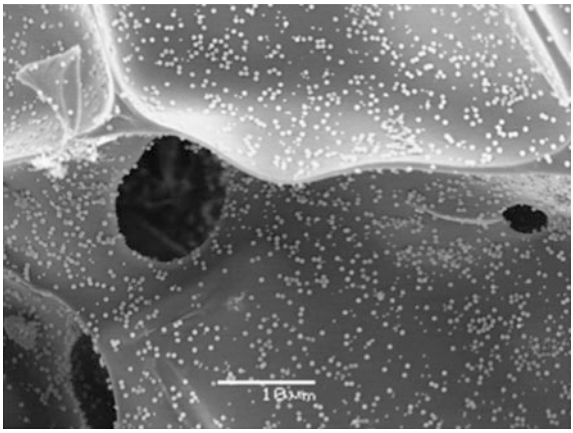

Fig. 7 SEM images of epoxy particles after immobilization for 24 h on AAm–AMPA cryogels with AAm:AMPA molar ratio 2:1. Scale bar: 10 mm (reproduced with permission from Hajizadeh et al. [28])

After enriching environmental pollutants from a water phase and eluting them in a concentrated form, it is important to take care of them in an efficient mode. Eluted estradiol was degraded by *Pseudomonas veronii*. In Fig. 8 it can be seen that oxygen was consumed and carbon dioxide was produced upon this exposure. In the control with no estradiol, there were no changes in oxygen or carbon dioxide concentrations.

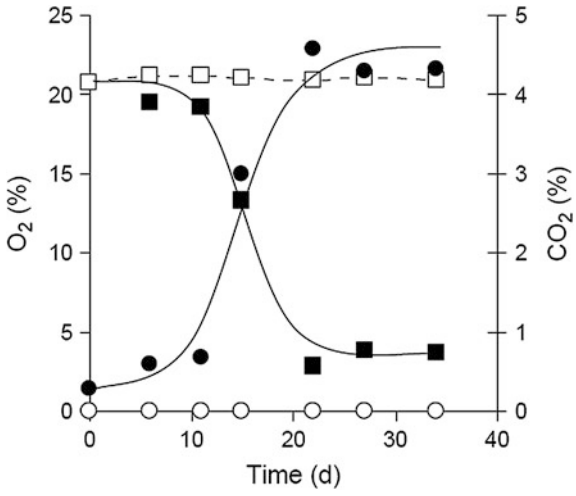

Fig. 8 Change in the levels of O_2 (*squares*) and CO_2 (*circles*) in a serum flask amended with estradiol as the sole source of carbon and energy and inoculated with a nonylphenol degrading *Pseudomonas veronii* (*filled symbols*) or in the controls inoculated and incubated under the same conditions but not supplied with estradiol (*open symbols*). *Vertical bars* show the standard deviation on triplicates (reproduced with permission from Le Noir et al. [22])

The same preparation of MIPs was utilized in competitive binding studies. 17β-estradiol was mixed with fluoxetine and acenaphtene and the capacity of the MIPs was evaluated with regard to adsorption of one single substance and also from mixtures. When 17β-estradiol was used in a solution of 2 mg/L, then 100 ± 0.6 % was captured by 100 mg MIP when passing 2 L of solution. NIP has 77 ± 4 % capture and C18 has 87 % whereas granulated activated carbon only captured 19 ± 8 %. MIPs are in this case superior to the other studied systems. In competitive binding studies, the efficiency of MIP only dropped marginally when fluoxetine and acenaphtene were present at the same concentrations as that of 17β-estradiol. The recovery was 96 ± 4 % whereas that for NIP decreased to 55 ± 9 %. The other more nonspecific adsorbents also showed marked decreases in binding efficiency (Fig. 9).

When treating water that had been processed in the municipal wastewater treatment plant in Lund, Sweden and that was about to be released to the recipient, it became clear that MIPs have an interesting potential in wastewater treatment. After passage of the processed wastewater through a bed of MIPs, bound material was eluted and exposed to a yeast with a cloned receptor for estrogen. This receptor will bind many different compounds, and in this study it was only interesting to evaluate the total burden of estrogen-like compounds. The yeast cells, when stimulated by estrogen activity, start to produce β-galactosidase that when exposed to a proper substrate produces a blue color which can be used to quantify the level of estrogen activity in the sample. The more estrogen activity, the more intense is the color. It was found that the treated water held a concentration of estrogen active compounds corresponding to 22 ± 4 ng estrogen per L of water. Such a concentration is sufficient to induce harmful effects on fish [29]; Fig. 10).

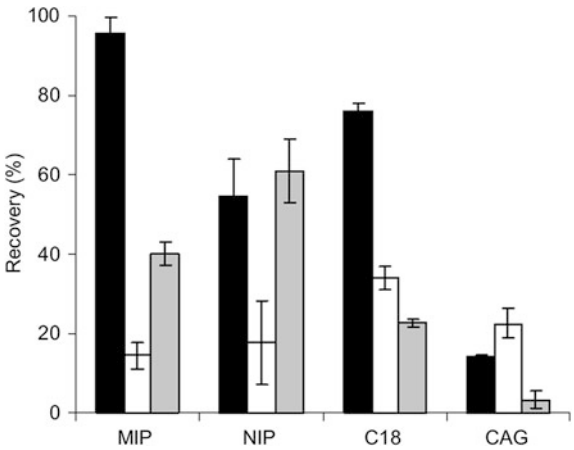

Fig. 9 Amount of E2 (*black bars*), fluoxetine (*white bars*), and acenaphtene (*grey bars*) recovered from the extracts of SPE columns packed with MIP (100 mg), NIP (100 mg), C18 (200 mg), and GAC (200 mg), and percolated with 2 L of an aqueous solution of 2 μg/L of each pollutant. The polymers were extracted three times with 4 mL of methanol:acetic acid (4:1 v/v) (MeOH:Aa). No pollutant was found in the third extract and the values shown represent the average total amount of pollutant recovered from the first two extracts ± standard deviation (reproduced with permission from Le Noir et al. [6])

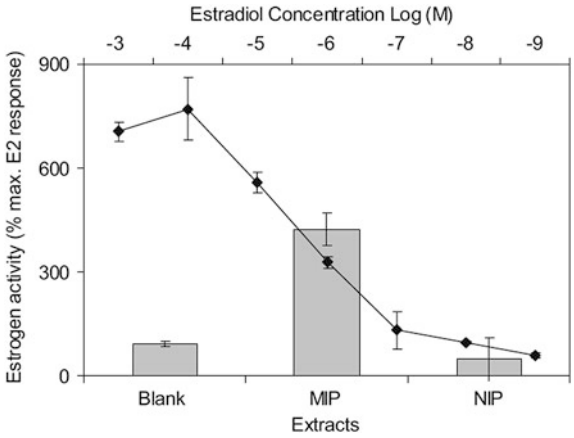

Fig. 10 β-Galactosidase activities in transformed *Saccharomyces cerevisiae* cultures [30] exposed to E2 concentrations of 1×10^{-3} to 1×10^{-9} M in MeOH/Aa (*diamond*) compared to clean MeOH (*blank*) or extracts from SPE columns packed with 100 mg MIP and NIP and percolated with 100 mL of a wastewater sample (*bars*). The polymers were extracted with 4 mL of MeOH:Aa and the values shown represent the average yeast activity (normalized to 100 mL of wastewater) ± standard deviation. No activity was found in the extracts (4 mL MeOH:Aa) of SPE packed with clean MIP and NIP (100 mg). β-Galactosidase activity is calculated as $1000 \times OD_{420}/(t \times V \times OD_{660})$ where OD_{420} is the final absorbance at 420 nm, t is the time of reaction of the mixture (41 min), V is the volume of the culture used in the assay, and OD_{660} is the absorbance of the diluted yeast inoculum (reproduced with permission from Le Noir et al. [6])

From Table 2 it can be seen that using MIP–cryogel composites was advantageous with regard both to efficiency in removing estrogen-active compounds from the water phase and to the flow rate that could be applied. Also PVA composites turned out to be efficient. Figure 2 shows that efficient removal of E2 was observed, also upon repeated extractions.

The MGPs were used in expanded bed configuration as shown schematically in Fig. 11. The experimental setup allows far better flow rates than what was possible for the small MIP particles. As is seen in Fig. 12 there was a high efficiency in removing 17β-estradiol at flow rates of 4 and 8 mL/min and there was no change when increasing the flow rate up to 120 mL/min. The AnoxKaldnes-type carriers are often used in wastewater treatment plants for microorganisms to grow on, and then they are exposed to the water in a stirred/mixed batch process configuration. Such an alternative for removing environmental pollutants seems realistic for a future scaleup.

2.3 Atrazine

In the studies on removal of endocrine disruptors, the herbicide atrazine was also studied. This compound is also said to have hormone activity [23]. Several

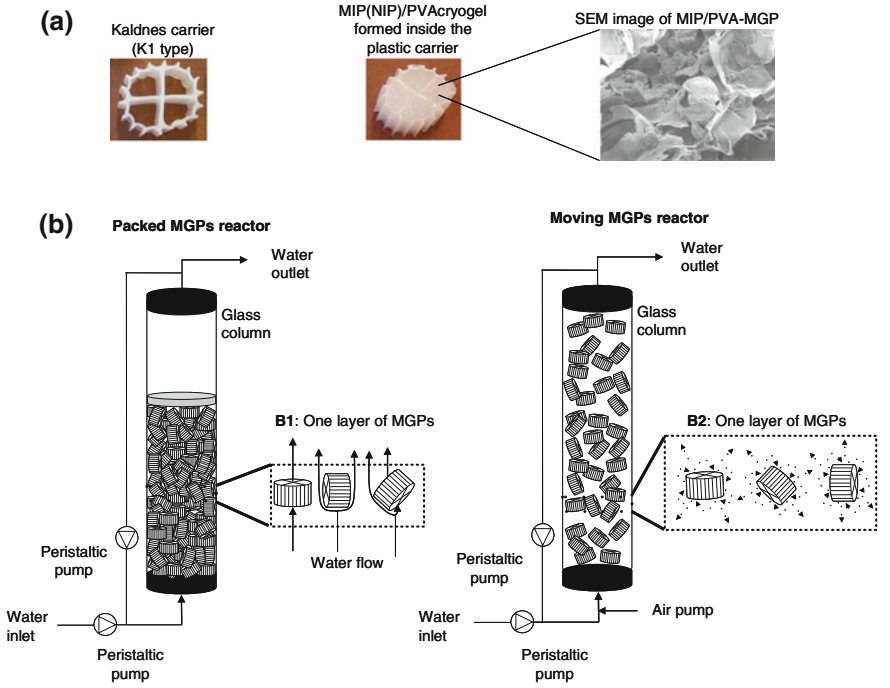

Fig. 11 **a** Appearance of an empty Kaldnes carrier and MIP/PVA-MGs formed inside the plastic carrier (called MGPs). The SEM image represents the MIP/PVA-MGs formed inside the Kaldness plastic carrier. **b** Schematic representation of a packed MGP reactor (*left*) and a moving MGP reactor (*right*). B1: schematic representation of one layer of MGPs in a packed MGPs reactor. The *arrows* show the water flow routes in the column. B2: schematic representation of one layer of MGPs in moving MGP reactor. The *arrows* show the perpetual motion of the MGPs in the column (reproduced with permission from Le Noir et al. [31])

preparations of cryogel–MIP composites were prepared. It was clearly shown that atrazine was captured, but to a lower extent than seen for estrogen with an estrogen-selective MIP. It was observed that an almost constant level of removal took place when the flow rate was varied as given for the estradiol capturing process.

2.4 Beta-Blockers and Other Pharmaceuticals

A group of emerging environmental pollutants is that of pharmaceuticals [20, 32–33]. The problem has been present for several decades, but it is only recently that it has attracted interest. Many of the pharmaceuticals are recalcitrant. Pharmaceutical producers had to a large extent neglected the problem, but when active substances started to appear in groundwater from where water for human consumption was taken, it became obvious that something needed to be done.

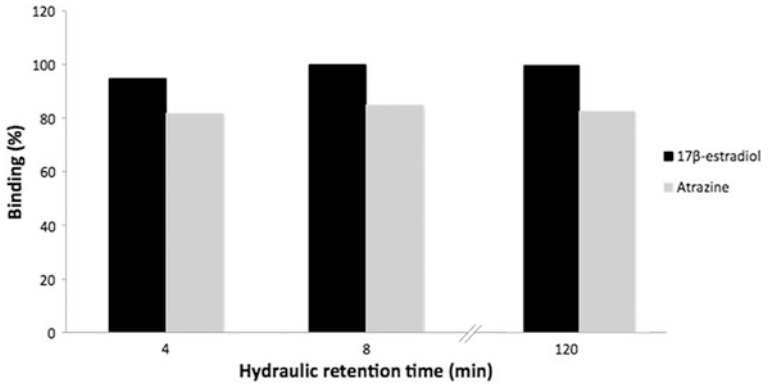

Fig. 12 Amount of 17β-estradiol and atrazine bound to E2-MIP/PVA-MGPs and atrazine MIP/PVA-MGPs, respectively, using different hydraulic retention times of a solution of 1 mg/L 17β-estradiol or atrazine in a moving-bed MGP reactor. Samples (1 mL) were taken every 200, 60, and 30 min at HRTs of 120, 8, and 4 min, respectively. The values given in this figure are based on the amounts recorded when no further adsorption was observed. The concentrations of the contaminants were quantified using HPLC

Many studies have been carried out concerning analysis of environmental samples in order to document the magnitude of the problem [33, 34].

With the technology used today wastewater treatment plants are usually inefficient in treating this kind of pollution. There are methods that should be useful, but economic constraints have hampered their application. Among these methods are ozonation, advanced oxidation, and photocatalysis [35].

Adsorption seems to be a useful method. When treating wastewater, there may be many different compounds that might bind to an adsorbent, some of which are environmental pollutants and others are less harmful. Using nonspecific adsorbents results in the capacity often being utilized less effectively due to nonspecific adsorption.

2.5 Heavy Metal Ions

It seems to be problematic to form MIPs against small ions. However, there are examples of successful experiments, for example, Zhu et al. [10] who produced a MIP selective against Pb^{2+}. The MIP was produced from silica that was first activated by refluxing silica in 6 M HCl for 8 h. After washing, the gel was modified by trimethylaminopropylsilane (APS) in the presence of $Pb(NO_3)_2$. The lead salt was first equilibrated with APS before the silica was added. After reaction and washing the MIP was ready for evaluation. The capacity of the MIP to bind Pb^{2+} was 19.7 mg/g MIP and 6.2 mg/g of NIP. It was further shown that the binding of lead was more efficient than the binding of cadmium with a selectivity coefficient of 450. The MIP produced was used for sample preparation before analysis.

2.6 Arsenic Contamination

A MIP was prepared using a poly(acrylamide) basis. $AsCl_3$ was dissolved in methanol and mixed with 4-hydroxybiphenyl and 2-vinylpyridine, and after equilibration ethylene glycol dimethacrylate was added [36]. Polymerization produced a block that afterwards was crushed. Particles <38 μm were collected after sieving the material, and these particles were then entrapped in a poly(acrylamide) cryogel (Fig. 13). In comparison with NIP, it turned out that the MIP was more efficient in binding arsenic (V) than the corresponding NIP (Fig. 14).

2.7 Bromate

When using ozone to disinfect water there are high risks of forming bromate, provided bromide is initially present in the water. Bromate is a risk chemical whereof WHO recommends concentrations shall not be higher than 10 μg/L in drinking water. Efficient technology to remove bromate is lacking. Using ion

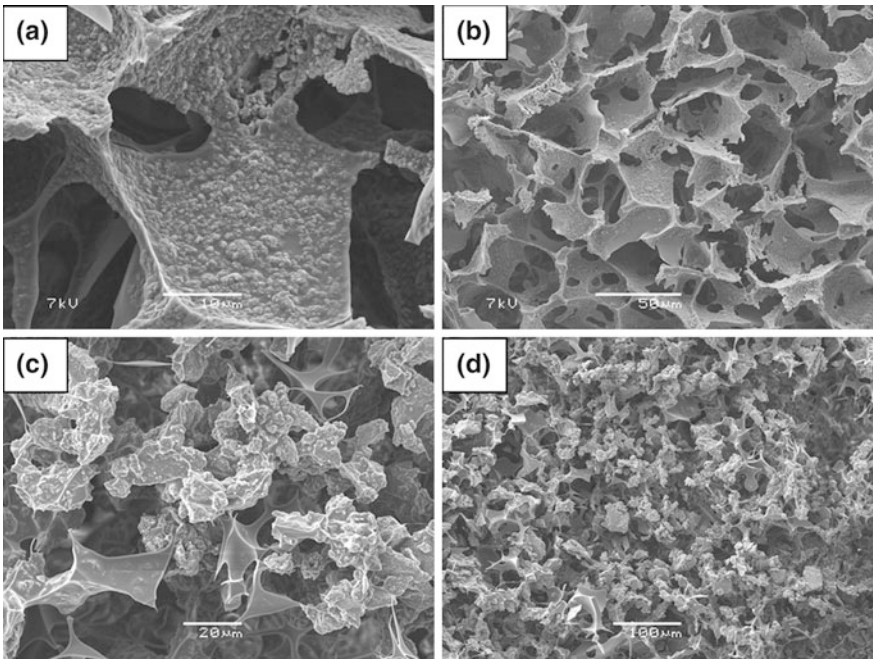

Fig. 13 **a–d** Scanning electron microscope images of composite materials, Alu-cryo presented at a scale of 10 and 50 μm (**a**, **b**) and MIP-cryo at a scale of 20 and 100 μm (**c**, **d**) (reproduced with permission from Hajizadeh et al. [37])

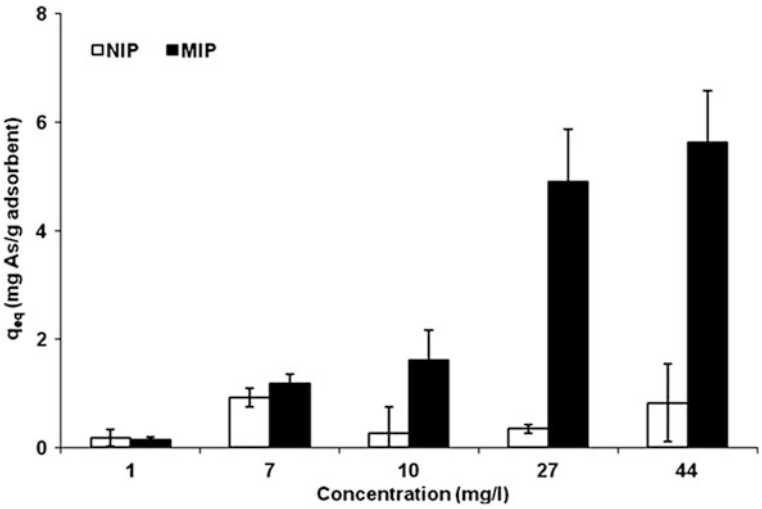

Fig. 14 Adsorption capacities of arsenic (V) for MIP and the control (NIP) at different initial concentrations (reproduced with permission from Onnby et al. [36])

exchangers is of course a possibility, but a range of other ions will interact and reduce the capacity. Common competitors are nitrate and sulphate [37].

In an effort to develop a MIP against bromate several strategies were evaluated. A molecularly imprinted chitosan, and as a reference a sol-gel inorganic adsorbent made of double hydrous oxide (Fe_2O_3, Al_2O_3 xH_2O) were produced. The chitosan-based MIP had better selectivity for bromate, whereas the inorganic adsorbent had a much higher total capacity. Furthermore, the adsorptive capacity for the MIP was strongly pH-dependent, and the inorganic adsorbent had almost the same capacity over a broad pH range.

When making a comparison on the adsorption behavior at different concentrations of bromate and nitrate for three different adsorbents, the chitosan MIP, the inorganic adsorbent, and DEAE-Sepharose, it became clear that the selectivity for bromate was highest for the MIP. In addition to studying suspended adsorbent particles, they were also entrapped in cryogels placed in plastic housings, and again the same adsorption pattern was seen there (Fig. 15).

3 Elution

A crucial step in MIP-mediated removal of environmental pollutants from wastewater is the elution of the bound material needed to regenerate the MIP composite for recycling. The firmer the target binds, the more difficult it is to elute the bound material. Elution is often carried out by treatment with organic solvents [38, 39]. This is a less attractive mode of operation for a large-scale process. Furthermore,

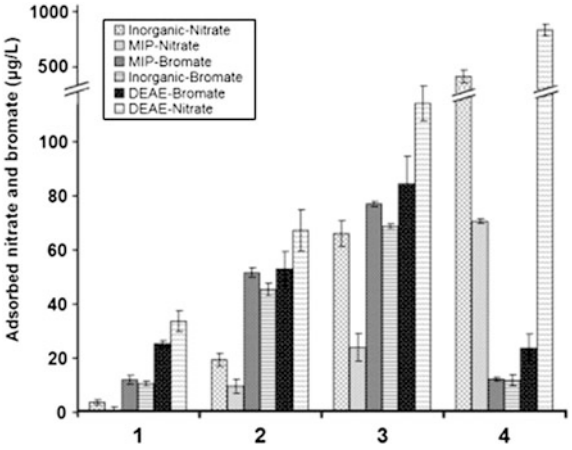

Fig. 15 Adsorption of nitrate and bromate by DEAE-Sepharose and by MIP or inorganic adsorbents. Experimental conditions: (1) 30 mg/L bromate and 30 mg/L nitrate; (2) 60 mg/L bromate and 60 mg/L nitrate; (3) 100 mg/L bromate and 100 mg/L nitrate; and (4) 30 mg/L bromate and 1 mg/L nitrate, 22 °C for 12 h. Adsorption is presented as the concentration of bromate and nitrate removed by the adsorbent from solution, respectively (reproduced with permission from Hajizadeh et al. [37])

such treatment will influence the structure and thereby also the stability of the macroporous gel in which the MIP particles are embedded. The firmer the binding is, the more harsh elution conditions must be used.

This leads to a conclusion that it might be advantageous not to use as efficient binders as possible, but rather to search for a compromise between efficient removal of the pollutant and a facilitated elution of bound material. One such example of a successful optimization is shown in Fig. 16 illustrating the binding of metergoline to a capacitive biosensor [40]. The sensitivity was in the micromolar range, but in this case regeneration took place spontaneously when the loaded MIP was exposed to plain water. Furthermore, weak binding to a receptor can be counteracted by high density of binding sites thereby creating efficient depletion of target molecules from the medium. Elution from such structures with high-density binding sites may be slower than what could be expected from separated binding sites.

Still another alternative is to design a system that binds the target to the MIP and on the same solid phase also introduce functionality to degrade captured material.

3.1 Catalysis: MIP on Surface of Titanium Oxide for Photocatalysis

Catalytically active MIPs have been discussed for a long time [41]. There are some efforts in this direction, but initially some substrates were used where it was

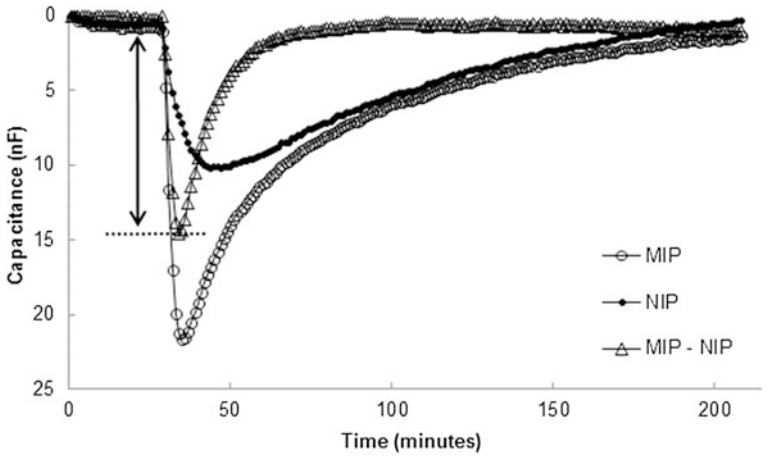

Fig. 16 Capacitive response (nF) plotted towards time (min); each measurement was obtained with a 1 min interval. The capacitance values of an (*empty circle*) MIP and (*filled circle*) NIP functionalized electrode, and (*triangle*) the difference between both, were normalized for the baseline values (set equal to 0 nF) of each curve. The *arrow* indicates the specific binding of metergoline (reproduced with permission from Lenain et al. [40])

relatively easy to catalyze their conversion [41]. The turnover numbers were also small. Later on more developed transition-state analogues were used, and the catalytic unit could be combined with an affinity pocket (also MIP) where the product could be trapped [42]. Even if much progress has been reported in recent years, there is still a relatively long way to go using the classical way of making imprints towards transition-state analogues of the substrate to be converted.

An alternative route has been taken by coimmobilizing the MIP and a photocatalytically active unit, for example, titanium dioxide [43, 44].

3.2 Macromolecular and Particulate Structures

There is a lack of good examples on preparative applications of MIPs capable of capturing macromolecular structures of particulate matter from environmental samples. However, within the analytical area there are good examples which may very well also be implemented as preparative steps when treating water (Table 1).

3.3 Toxins from Cyanobacteria and Algae

Freshwater cyanobacteria produce a family of microcystins, toxins that cause liver failure and in severe cases may induce liver cancer. It is therefore of interest to first

of all keep control over the levels of microcystins in freshwater from where drinking water is taken and then also be prepared to treat the water to remove the toxins. So far, focus has been on analysis, but the technology used for recognition could in the future also be applied in treatment. A piezoelectric sensor for quantification of microcystins was constructed based on a MIP made against microcystins as print molecules [8]. The MIPs were constructed based on computational design and the polymer was produced by mixing in DMSO equimolar concentrations of microcystin-LR (one of the many variants of microcystins) with 2-Acrylamido-2-methyl-1-propanesulfonic acid, 6 times surplus of urocanic acid ethyl ester, and 1.5 times surplus of the crosslinker ethylene glycol dimethacrylate and as initiator 1.1-azobis(cyclohexane-carbonitrile). After polymerization and proper washing, the MIP was ready for evaluation on the sensor. A MIP was used for preconcentrating the analyte prior to test with the biosensor. Crossreactivity against other microcystins was relatively low (20–30 %). This means that the MIP was too selective to be used as a general recognition element for all microcystins.

In another study, microcontact imprinting was used for the fabrication of a selective biosensor against microcystins [45]. The technique was a development of a method for imprinting selectivity in a sensor chip as presented by Ertürk et al. [46]. In both these cases, the microcontact imprinting resulted in sensor chips with a higher selectivity than that found when using antibodies as capturing structures.

In seawater there are toxins produced by red algae. Some of these toxins cause problems for fish farming and here it is also important first to analyze and then to apply treatment methods to protect the farmed fish from overly high concentrations of toxins. A MIP was produced with domoic acid as the print molecule and it was later shown that this MIP was suitable for quantifying domoic acid [11]. After the assay, the captured target molecules were removed and the sensor was reused. It turned out that the strategy was successful and the sensor could be used repeatedly over at least 2 months.

Inasmuch as it was possible to produce MIPs with suitable selectivity, then it would also be possible in the future to design adsorbents to capture the same target molecules.

3.4 Viruses and Microorganisms

These two groups of organisms represent species that can cause diseases and it is therefore of interest to remove them from the environment. Waterborne diseases are spread quickly and are therefore of special interest to combat. The new development concerning microcontact imprinting seems to hold interesting potential for future applications of MIP technology in water processing.

4 Concluding Remarks

For many years MIPs have been evaluated for high resolving separations such as the resolution of racemic mixtures. The nature of MIPs, being made from recalcitrant polymers, having good binding capacities, and being resistant to both mechanical and microbial degradation makes them very attractive reagents to use in environmental technology when conditions are variable and sterile conditions are not possible. MIPs for affinity binding as well as catalytically active MIPs may have a great future in environmental technology.

Acknowledgments Part of this work was supported by the Swedish Research Council.

References

1. Environmental Protection Agency: Contaminants of emerging concern. http://water.epa.gov/scitech/cec/
2. Jiang X, Tian W, Zhao C, Zhang H, Liu M (2007) A novel sol-gel-material prepared by surface imprinting technique for the selective solid-phase extraction of Bisphenol A. Talanta 72:119–125
3. Kawaguchi M, Hayatsu Y, Nakata H, Ishii Y, Ito R, Saito K, Nakazawa H (2005) Molecularly imprinted solid phase extraction using stable isotope labeled compounds as template and liquid chromatography–mass spectrometry for trace analysis of bisphenol A in water sample. Anal Chim Acta 539:83
4. Beltran A, Caro E, Marce RM, Cormac PAG, Sherrington DC, Borrull F (2007) Synthesis and application of a carbamazepin-imprinted polymer for solid phase extraction from urine and wastewater. Anal Chim Acta 597:6–11
5. Dai C, Geissen S-U, Zhang Y-l, Zhang Y-j, Zhou X-f (2010) Performance of evaluation and application of molecularly imprinted polymer for separation of carbamazepine in aqueous solution. J Hazard Mater 184:156–163
6. Le Noir M, Lepeuple AS, Guieysse B, Mattiasson B (2007) Selective removal of 17β–estradiol at trace concentration using a molecularly imprinted polymer. Water Res 41:2825–2831
7. Le Noir M, Plieva F, Hey T, Guieysse B, Mattiasson B (2007) Macroporous molecularly imprinted polymer/cryogel composite systems for the removal of endocrine disrupting trace contaminants. J Chromatogr A 1154:158–164
8. Chianella I, Piletsky SA, Tothill IE, Chen B, Turner APF (2003) Selection of imprinted nanoparticles by affinity chromatography. Biosens Bioelectron 18:2740–2743
9. Koeber R, Fleischer C, Lanza F, Boos K-S, Sellergren B, Barcelo D (2001) Evaluation of a multidimensional solid-phase extraction platform for highly selective on-line cleanup and high-throughput LC-MS analysis of triazines in river water samples using molecularly imprinted polymers. Anal Chem 73:2437–2444
10. Zhu X, Cui Y, Chang X, Zou X, Li Z (2008) Selective solid-phase extraction of lead(II) from biological and natural water samples using surface-grafted lead(II)-imprinted polymers. Microchim Acta. doi:10.1007/s00604-008-0045-y
11. Lotierzo M, Henry OYF, Piletsky S, Tothill I, Cullen D, Kania M, Hock B, Turner APF (2004) Surface plasmon resonance sensor for domic acid based on grafted imprinted polymer. Biosens Bioelectron 20:145–152

12. Ferrer I, Lanza F, Tolokan A, Horvath V, Sellergren B, Horvai G, Barcelo D (2000) Selective trace enrichment of chlorotriazine pesticides from natural waters and sediment samples using terbuthylazine molecularly imprinted polymers. Anal Chem 72:3934–3941
13. Jenkins AL, Yin R, Jensen JL (2001) Molecularly imprinted polymer sensors for pesticide and insecticide detection in water. Analyst 126:798–802
14. Kandimalla VB, Ju H (2004) Molecular imprinting: a dynamic technique for diverse applications in analytical chemistry. Anal Bioanal Chem 380:587–605
15. Lin Y, Shi Y, Jin Y, Peng Y, Lu B, Dai K (2008) Removal of phenolic estrogen pollutants from different sources of water using molecularly imprinted polymeric microspheres. Environ Pollut 153:483–491
16. Pichon V, Chapuis-Hugon F (2008) Role of molecularly imprinted polymers for selective determination of environmental pollutants—a review. Anal Chim Acta 622:48–61
17. Zhongbo Z, Hu J (2008) Selective removal of estrogenic compounds by molecular imprinted polymer (MIP). Water Res 42:4101–4108
18. Vlatakis G, Andersson LI, Muller R, Mosbach K (1993) Drug assay using antibody mimics made by molecular imprinting. Nature 361:645–647
19. Afeyan NB, Fulton SP (1991) Perfusion chromatography packing material for proteins and peptides. J Chromatogr A 544:267–279
20. Hajizadeh S, Xu C, Kirsebom H, Lei Y, Mattiasson B (2013) Cryogelation of molecularly imprinted nanoparticles: a macroporous structure as affinity chromatography column for removal of beta-blockers from complex samples. J Chromatogr A 1274:6–12
21. Rachkov AE, Cheong S-H, El′skaya AV, Yano K, Karube I (1998) Molecular imprinted polymers as artificial steroid receptors. Polym Adv Technol 9:511–519
22. Le Noir M, Guieysse B, Mattiasson B (2006) Removal of trace contaminants using molecularly imprinted polymers. Water Sci Technol 53:205–212
23. Le Noir M (2007) Removal of endocrine-disrupting compounds from wastewater using molecular imprinting. PhD-thesis Lund University. ISBN 978-91-869627-55-0
24. Dahlentoft E, Thulin P (1997) The use of the Kaldnes suspended carrier process in treatment of wastewaters from the forest industry. Water Sci Technol 35:123–130
25. Odegaard H, Gisvold B, Strickland J (2000) The influence of carrier size and shape in the moving bed biofilm process. Water Sci Technol 41:383–391
26. Plieva FM, Mattiasson B (2008) Macroporous gel particles as novel sorbent materials: rational design. Ind Eng Chem Res 47:4131–4141
27. Persson P, Beybak O, Plieva F, Galaev IYu, Mattiasson B, Nilsson B, Axelsson A (2004) Characterization of a continuous supermacroporous monolithic matrix for chromatographic separation of large bioparticles. Biotechnol Bioeng 88:224–236
28. Hajizadeh S, Mattiasson B, Kirsebom H (2014) Flow-through-mediated surface immobilization of sub-micrometre particles in monolithic cryogels. Macromol Materials Eng 299:631–638
29. Auriol M, Filali-Meknassi Y, Tyagi RD, Adams CD, Surampali RY (2006) Endocrine disrupting compounds removal from wastewater, a new challenge. Process Biochem 41:525–539
30. Gaido KW, Leonar LS, Lovell S, Gould JC, Dabai D, Portier CJ, McDonnell DP (1997) Evaluation of chemicals with endocrine modulating activity in a yeast-based steroid hormone receptor gene transcription assay. Toxicol Appl Pharmacol 143:205–212
31. Le Noir M, Plieva F, Mattiasson B (2009) Removal of endocrine-disrupting compounds from water using macroporous molecularly imprinted cryogels in a moving-bed reactor. J Sep Sci 32:1471–1479
32. C Dai, Geissen S-U, Y-l Zhang, Y-j Zhang, X-f Zhou (2011) Selective removal of diclofenac from contaminated water using molecularly imprinted polymer microspheres. Environ Pollut 159:1660–1666
33. Alvarez ABC, Diaper C, Parsons SA (2001) Partial oxidation by ozone to remove recalcitrance from wastewater—a review. Environ Technol 22:409–427

34. Ulson de Souza G, Santos Bonilla KA, Ulson de Souza AA (2010) Removal of COD and color from hydrolyzed textile azo dye by combined ozonation and biological treatment. J Hazard Mater 179:35–42
35. Azbar N, Yonar T, Kestioglu K (2004) Comparison of various advanced oxidation processes and chemical treatment methods for COD and colour removal from polyester and acetate fiber dying effluent. Chemosphere 55:35–43
36. Onnby L, Pakade V, Mattiasson B, Kirsebom H (2012) Polymer composite adsorbents using particles of molecularly imprinted polymers of aluminium oxide nanoparticles for treatment of arsenic contaminated waters. Water Res 46:4111–4120
37. Hajizadeh S, Kirsebom H, Galaev IY, Mattiasson B (2010) Evaluation of selective composite cryogel for bromate removal from drinking water. J Sep Sci 33:1752–1759
38. Prasad BB, Tiwari K, Singh M, Sharma PS, Patel AM, Srivastava S (2008) Molecularly imprinted polymer-based solid-phase microextraction fiber coupled with molecularly imprinted polymer-based sensor for ultratrace analysis of ascorbic acid. J Chromatogr A 1198–1199:59–66
39. Suna Z, Schüsslerb W, Senglb M, Niessnera R, Knopp D (2008) Selective trace analysis of diclofenac in surface and wastewater samples using solid-phase extraction with a new molecularly imprinted polymer. Anal Chim Acta 620:73–81
40. Lenain P, De Saeger S, Hedström M, Mattiasson B (2015) Affinity sensor based on immobilized molecular imprinted synthetic ligands. Biosens Bioelectron 69:34–39
41. Wulff G, Sarhan A, Zabrocki K (1973) Enzyme-analogue built polymers and their use for resolution of racemates. Tetrahedron Lett 14(44):4239–4332
42. Alexander C, Davison L, Hayes W (2003) Imprinted polymers: artificial molecular recognition materials with applications in synthesis and catalysis. Tetrahedron 59:2025–2057
43. Shen X, Zhu L, Liu G, Yu H, Tang H (2008) Enhanced photocatalytic degradation and selective removal of nitrophenols by using surface molecular imprinted titania. Environ Sci Technol 42:1687–1692
44. Shen X, Zhu L, Huang C, Tang H, Yu Z, Deng F (2009) J Mater Chem 19:4843–4851
45. Lebogang L (2014) Biosensor-based methods for detection of microcystins as early warning systems. PhD-thesis, Lund University. ISBN 978-91-76623-082-4
46. Ertürk G, Berillo D, Hedström M, Mattiasson B (2014) Microcontact BSA-imprinted capacitive biosensor for real time, sensitive and selective detection of BSA. Biotechnol Reports 3:65–72

Adv Biochem Eng Biotechnol (2015) 150: 207–226
DOI 10.1007/10_2015_315

Published Online: 17 March 2015

Molecularly Imprinted Polymers as Tools for Bioassays and Biotransformation

Yibin Liu, Shan Huang, Zhuo Li and Meiping Zhao

Abstract In the past five years, significant progress has been made in preparation of various molecularly imprinted polymer (MIP)-based materials for applications in bioassays and biotransformation. This chapter reviews the important advances in these two fields. The first part mainly focuses on the development of various MIP-based bioassays that convert the rebinding of template to the imprinted cavities into measurable luminescent signals, including fluorescence, phosphorescence, Raman scattering, diffraction, and the like. In addition, MIP-based bioassays that are measured by surface plasmon resonance or quartz crystal microbalance are also discussed. In the following part, representative biotransformation reactions that make use of MIPs are summarized. In the last part of this chapter, some remaining challenges are briefly discussed for further development of the two fields.

Keywords Bioassay · Biotransformation · Luminescent detection · Molecularly imprinted polymer · Quartz crystal microbalance · Surface plasmon resonance

Abbreviations

3D	Three-dimensional
AAI	Affinity adsorption imprinting
AbAP	Goat antihuman AP antibody
AgNPs	Silver nanoparticles
AP	Alkaline phosphatase
ASPV	Apple stem pitting virus
BPDE	Benzo[a]pyrenediol epoxide
CCA	Colloidal crystal array
CD	Carbon dot

Y. Liu · S. Huang · Z. Li · M. Zhao (✉)
Beijing National Laboratory for Molecular Sciences, MOE Key Laboratory of Bioorganic Chemistry and Molecular Engineering, College of Chemistry and Molecular Engineering, Peking University, Beijing 100871, China
e-mail: mpzhao@pku.edu.cn

CK-MB	Creatine kinase-MB
cm	Centimeter
Da	Dalton
dBSA	Denatured bovine serum albumin
DGs	Diffraction gratings
DNA	Deoxyribonucleic acid
DOPC	Determined osteogenic precursor cell
ELISA	Enzyme-linked immunoasssay
ENRO	Enrofloxacin
FIPCIA	Fluorescently imaged particle counting immunoassay
FQ	Fluoroquinolone
GO	Graphene oxide
HSA	Human serum albumin
IgG	Human immunoglobulin G
IgM	Immunoglobulin M
LCST	Lower critical solution temperature
LOD	Limit of detection
l-Pga	L-pyroglutamic acid
MAA	Methyl acrylic acid
MAGA	Methacryloylamidoglutamic acid
MAH	Methacryloylamido histidine
MAPBA	Methacryloylamidophenylboronic acid
MASE	Methacryloylamido serine
MG	Malachite green
MIP	Molecularly imprinted polymer
MIPC	Molecularly imprinted photonic crystal
MIP-GLaDiS	Molecularly imprinted polymer gel laser diffraction sensor
mM	Millimole per liter
μM	Micromole per liter
MPA	Methyl phosphonic acid
MRL	Maximum residue limit
NGAL	Neutrophil gelatinase-associated lipocalin
nm	Nanometer
nM	Nanomole per liter
PA	3-pyridinecarboxamide
PAM	Polyamide membrane
PDA	Polydopamine
pM	Picomole per liter
p-NPP	P-nitrophenylpalmitate
ppm	Parts per million
ppb	Parts per billion
PVA	Polyvinyl alcohol

QCM	Quartz crystal microbalance
QD	Quantum dot
RIfS	Reflectometric interference spectroscopy
RTP	Phosphorescence
SERS	Surface-enhanced Raman scattering
SPR	Surface plasmon resonance
ssDNA	Single-stranded DNA
TCP	2,4,6-trichlorophenol
TSA	Transition state analogue
WGA	Wheat germ agglutinin

Contents

1 Introduction

Molecularly imprinted polymers (MIPs) are smart materials formed in the presence of a template molecule. After polymerization, complementary cavities with the desired shape and functional groups are formed in the imprinted materials. Nowadays, molecular imprinting is widely used for the preparation of tailor-made materials with high recognition capability towards target molecules, ranging from small organic molecules to biomacromolecules [1, 2].

Bioassays are commonly used approaches for the determination of bioactive small molecules, peptides, proteins, nucleic acids, and drugs in complex biological samples. The key requirements of bioassays are specific recognition elements that

are capable of binding the analytes with high affinity and selectivity. Traditionally used recognition elements for bioassays are antibodies, receptors, enzymes, nucleic acids, and the like. These native biological materials possess excellent binding selectivity and affinity. However, most of them suffer from common disadvantages including high cost to produce, poor physical/mechanical stability, and low resistance to harsh conditions (e.g., high temperature, pressure, acids, bases, and some organic solvents). With similar specific binding and affinity properties for target molecules, MIPs have shown distinct advantages in that they are easy to produce and have high stability under various buffer conditions [1–3].

In early studies, MIPs have been used to detect the target molecules in a format similar to conventional immunoassays. The polymers were labelled with enzymes or fluorophores, which allow for detection by colorimetric, fluorescent, or chemiluminescent signals. In recent years, a number of new bioassays have been developed by integrating the MIP material with a transducer, which can provide faster analysis with a direct readout without the need for labor-intensive sample preparation. In these assays, MIPs show additional advantages over the native biomolecules because the transduction mechanism can be directly built into the material itself. Molecular recognition of an analyte leads to changes of the optical or other properties of the material, thus providing a direct readout [4].

Commonly used physicochemical transducing systems include optical, electrochemical, thermometric, piezoelectric, magnetic, and the like. Luminescent optical assays transform the analyte–receptor binding events into measurable light signals, such as light absorption, fluorescence/phosphorescence, bio/chemiluminescence, reflectance, Raman scattering, or refractive index. The advantages of luminescent optical assays include high sensitivity, flexibility, environmental stability, ease of miniaturization, inexpensiveness, and nondestructive analyte analysis [5–9].

Biotransformation is a process whereby a substance is transformed into another by a specific biochemical reaction. Enzymes are ubiquitous natural biocatalysts for catalyzing most biotransformation processes in cells and organisms. Without these enzymes, many biotransformation reactions would not take place effectively. However, enzymes are basically expensive compared with chemical catalysts and the stability and recovery of enzymes are relatively low. To address such an issue, many efforts have been made in creating artificial enzyme mimics or so-called bioinspired catalysts. MIPs, taking advantage of the molecular recognition ability, stability, and low cost, have been engineered as a powerful tool to promote biotransformation with enzymelike specificity and activity [10–12].

In this chapter, a number of the latest important examples of how MIPs have been used in place of antibodies or receptors and provided exciting performances in bioassays are reviewed. MIP-based bioassays that convert the rebinding of template to the imprinted cavities into measurable luminescent signals are first introduced and discussed. Then in the following parts, several MIP-based biotransformation reactions that show encouraging results are summarized. Finally, some remaining issues for further development of MIP-based bioassays and applications of MIPs for biotransformation in complex systems are briefly discussed.

2 MIPs as Tools for Bioassays

2.1 MIP-Based Fluorescent or Phosphorescent Bioassays

Fluorescent nanomaterials, as well as organic fluorophores, have both been used in the development of MIP-based bioassays to provide fluorescent signals (see Fig. 1a). Quantum dots (QDs) are semiconductor nanocrystals (2–10 nm in diameter) that provide narrow, symmetrical, and tunable emission spectra [13–16]. CdSe/ZnS QDs have been embedded in MIPs or used to prepare CdSe@SiO_2@MIP core-shell nanoparticles for the measurement of uracil and caffeine [17, 18]. By anchoring a MIP matrix (CDs@MIP) on the surface of highly luminescent carbon dots (CDs), a fluorescence optosensor for dopamine was also developed recently [19]. The resulting composite showed high selectivity for dopamine and high photostability. The relative fluorescence intensity of CDs@MIP decreased linearly with the increasing dopamine in the concentration range of 25–500 nM with a detection limit of 1.7 nM. The proposed method was successfully applied for the determination of trace dopamine in human urine samples. Liu et al. introduced graphene oxide (GO) to MIP to provide a large specific surface area and increase the mass-transfer rate [20]. Then they further used ionic liquid to improve the fluorescence stability of QDs by virtue of its high thermal and chemical stability. The ionic liquid MIP/GO/QDs composites thus stabilized offer highly selective and sensitive specific recognition of vitamin E. The relative fluorescence intensity of MIP decreased linearly with the increasing concentration of vitamin E in the range of 0.023–920 μM with a detection limit of 3.5 nM.

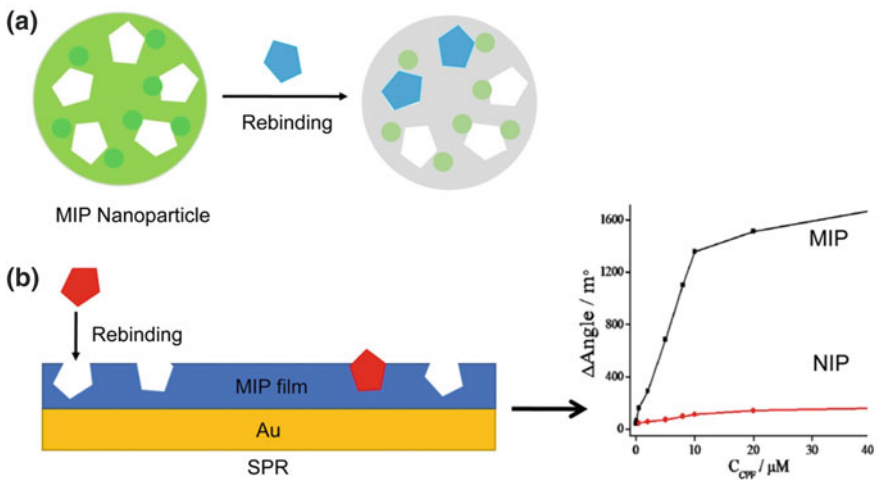

Fig. 1 Schematic illustration of the working principles of MIP-based bioassays. Measurement of target analytes by using **a** QDs embedded in MIP nanoparticles; **b** surface plasmon resonance spectroscopy (the figure on the *right* is adapted from Ref. [45])

For protein analysis, Zhang et al. [21] synthesized MIP-coated CdTe QDs composite for selective recognition of cytochrome c by sol-gel reaction. The fluorescence of MIP-coated QDs was quenched by the template. Under optimum conditions, the linear range for cytochrome c detection is from 0.97 to 24 μM, and the detection limit is 0.41 μM. Later, the same group further anchored MIP on the surface of denatured bovine serum albumin (dBSA) modified CdTe QDs [22]. The dBSA was used not only for modification of the surface defects of the QDs, but also as assistant monomers to create effective recognition sites. The resultant artificial receptors showed linear responses to the template lysozyme in the range from 0.014 to 8.5 μM, and the detection limit was 6.8 nM. Similar QD/MIPs composites were prepared by Lee et al. [23] for several protein biomarkers using phase inversion of poly(ethylene-co-vinylalcohol) solutions. QD fluorescence quenching was observed on binding of analytes to the composite MIPs in a concentration-dependent manner. The composite MIP particles were used for the quantitative detection of amylase, lipase, and lysozyme in real saliva samples.

Inoue et al. [24] synthesized a MIP capable of transducing specific protein-binding events into fluorescent signal change by using dansylethylenediamine-conjugated O-acryloyl L-hydroxyproline. Human serum albumin (HSA) was used as a model target protein and HSA-imprinted polymers were prepared on glass substrates. Specific fluorescence changes were observed for HSA binding on the imprinted polymer thin film. By contrast, the responses for other proteins, including BSA, chymotrypsin, lysozyme, and avidin are much weaker.

Yin et al. [25] prepared a MIP nanocomposite for specific recognition and capture of benzo[a]pyrenediol epoxide (BPDE)–DNA adduct. Then they further developed a fluorescently imaged particle-counting immunoassay (FIPCIA) for ultrasensitive detection of BPDE–ssDNA adducts using a laser scanning confocal microscope. The number of countable fluorescent dots is proportional to the content of BPDE–ssDNA adducts in the DNA sample. The MIP-based FIPCIA method can sensitively detect BPDE–DNA adducts at concentrations as low as 18 pM in human lung carcinoma A549 cells.

Banerjee et al. [26] developed a MIP-based fluorescent assay by anchoring the MIP layer on the surface of functionalized unilammelar fluid vesicles. Using small peptides as templates, they have photopolymerized diacetylene-containing vesicles and generated imprinted polydiacetylene patches in the membrane. All binding sites are exposed to the surface and show high rebinding affinity for the template. The amphiphilic carboxyfluorescein coembedded into the fluid determined osteogenic precursor cell (DOPC) membrane offers signals by changing the emission intensity in the presence of analytes.

Gultekin et al. [5] have proposed a novel thiol ligand-capping method with polymerizable methacryloylamido-cysteine attached to gold nanoparticles. Using methacryloylamidohistidine-Pt(II) as a new metal-chelating monomer, they have constructed a surface MIP shell for cholic acid via metal coordination–chelation interactions. The cholic acid can simultaneously chelate to Pt(II) metal ion and fit into the shape-selective cavity in the nanoshell. The cholic acid level in blood serum and urine was determined by the prepared Au nanosensor.

In addition to fluorescence intensity detection, fluorescence polarization analysis was also combined with MIP nanoparticles for the direct detection of target analytes [27]. Water-compatible MIP nanoparticles were synthesized with enrofloxacin (ENRO) as the imprinting template. Fluorescence polarization measurements allow the direct determination of the amount of ENRO and other structurally related piperazine-based fluoroquinolones (FQs) that bind to the MIP. The assay was applied to determine FQs in tap water and milk by simply adding a known amount of MIP. In tap water, a low limit of detection of 0.1 nM for ENRO was achieved with 5 mg/mL of MIP. In milk, ENRO and danofloxacin, whose maximum residue limits (MRLs) have been fixed at 0.28 and 0.08 mM, respectively, could be selectively measured and distinguished from other families of antibiotics.

MIP techniques are also combined with room temperature phosphorescent detection. The long lifetime of phosphorescence avoids interference from autofluorescence and scattering of the biomatrix. Alvarez et al. [6] generated thin molecularly imprinted films by polymerization on glass slides. The layer exhibited intense phosphorescence upon binding with analyte with a maximum at 520 nm for an excitation wavelength of 314 nm. The detection limit achieved 22 μg/L of propranolol, and the response was linear at least up to 1 mg/L of propranolol. The probes were reusable and had been successfully applied to urine sample analysis.

By surface-graft imprinting using vinyl-modified Mn-doped ZnS QDs as supports, phosphorescent MIP for bovine hemoglobin was developed by Tan et al. [28]. The small particle sizes and the nontoxicity of the MIP–QDs composites allowed for good dispersibility and stability in an aqueous solution. Linear correlations were obtained for bovine hemoglobin over the concentration range from 0.1 to 5.0 μM and with >90 % recoveries for urine and serum samples.

Dan et al. [29] constructed an enhanced MIP-based room temperature phosphorescence (RTP) probe by combining the RTP of Mn-doped ZnS QDs and two-fragment imprinting. Fragments or structurally similar parts of the target analytes were used as the dummy templates. Polyethyleneimine-capped Mn-ZnS QDs were embedded into MIPs by the hydrolysis of tetraethoxysilane to provide the binding sites to interact with the carboxyl groups of templates. The rebinding of the target analytes to the recognition sites modulated the selective aggregation of Mn-ZnS QDs in QDs–MIPs and resulted in the RTP enhancement. The method could be used for the selective enhanced RTP detection of nonphosphorescent analytes without any derivatization and inducers. Using domoic acid as an example, the RTP enhancement two-fragment imprinting silica was about 2 times that of one-fragment imprinting silica and 4 times that of the nonimprinting silica. The two-fragment imprinting silica exhibited the linear RTP enhancement to domoic acid in the range of 0.25–3.5 μM in buffer and 0.25–1.5 μM in the shellfish sample. The limit of detection was 67 nM in buffer and 2.0 μg/g wet weight (w/w) in the shellfish sample.

In another study, a polyamide membrane-wheat germ agglutinin-polyvinyl alcohol-affinity adsorption imprinting (PAM-WGA-PVA-AAI) phosphorescence sensor has been developed for determination of trace alkaline phosphatase (AP) [30]. By labelling goat antihuman AP antibody (AbAP) using Morin-SiO_2, the

PAM-AP-AbAP-Morin-SiO_2 formed by the immunoreaction between AbAP and AP in PAM-WGA-PVA-AAI due to the affinity between AbAP and AP was stronger than that between AP and WGA. The product could emit room temperature phosphorescence (RTP) because of the heavy atom effect of Pb^{2+}. The detection limit achieved 7.2×10^{-19} mol/L). The method has been applied to the determination of trace AP in human serum and the results agreed well with those obtained by enzyme-linked immunoasssay (ELISA).

2.2 MIP-Based Bioassay by Measurement of Diffraction Signals or Surface-Enhanced Raman Scattering Signals

MIPs have also been incorporated into photonic crystals to provide a sensing platform for the template analyte. By combination of colloidal-crystal and molecular-imprinting techniques, Hu et al. [31] prepared two imprinted photonic-hydrogel films with theophylline and (1R,2S)-(-)-ephedrine as template molecules, respectively. The imprinted photonic polymer consists of a three-dimensional (3D), highly ordered, and interconnected macroporous array with a thin hydrogel wall, where nanocavities complementary to analytes are distributed. The polymer can quickly and directly report the molecular recognition event based on Bragg diffractive shifts due to the lattice change of their 3D-ordered macroporous arrays upon rebinding to the target molecules. The method was highly sensitive and specific, which provided a rapid and handy approach for stimulant assay and drug analysis in athletic sports.

A micropatterned MIP transmissive 2D diffraction grating (DG) was developed by Barrios et al. as a label-free enrofloxacin sensor [7]. Polymeric gratings are prepared by using microtransfer molding based on SiO_2/Si molds. MIP 2D-DGs exhibit 2D optical diffraction patterns and the refractive index of the micropatterned MIP material was estimated to be 1.486 via solvent index matching experiments. Target-molecule detection was demonstrated based on the changes in diffraction efficiency.

Liu et al. [32] developed a molecularly imprinted photonic crystal (MIPC) to detect the degradation product of nerve agents. Mono-dispersed poly-methyl methacrylate colloidal particles with the diameter of 280 nm were used to fabricate a closely packed colloidal crystal array (CCA), and a methyl phosphonic acid (MPA) imprinted hydrogel was prepared within the CCA. The diffraction intensity of the MIPC decreased significantly upon the MPA adsorption with a limit of detection (LOD) of 10 μM. Furthermore, the diffraction intensity decreased and blue shifted with the increase of temperature, and decreased and red shifted with the increase of ionic strength. At higher pH, the diffraction intensity increased without obvious diffraction shift. The MIPC provides an indirect path to detect nerve agents (Sarin, Soman, VX, and R-VX) by monitoring the MPA released from the hydrolysis of nerve agents, with LODs of 3.5, 25, 75, and 75 μM for Sarin, Soman, VX, and R-VX, respectively.

Bioassays that can be read directly by the naked eye without the requirement of expensive equipment are of particular interest for rapid and in situ detection. Bai et al. [33] developed a "Molecularly Imprinted Polymer Gel Laser Diffraction Sensor" (MIP-GLaDiS) to detect viruses. They employed a "double imprinting" method in which a virus-bioimprinted hydrogel was further micromolded into a diffraction grating sensor by using imprint-lithography techniques. A simple laser transmission apparatus was used to measure diffraction, and the system can read by the naked eye to detect the apple stem pitting virus (ASPV) at concentrations as low as 10 ng/mL.

A colorimetric MIPC sensor was developed by Zhang et al. [34] for the sensitive and selective chiral recognition of amino acids. The sensor was fabricated by infiltrating a polystyrene photonic crystal template with precursor and imprinting molecules, followed by a thermal polymerization. After removal of templates, the resulted MIPC consists of a 3D, highly ordered, and interconnected macroporous array. Rebinding the target amino acids induces visible color changes and readable optical signals through the diffraction peak shifts of the material. A function relationship was found between the diffraction peak shift and the concentration of l-pyroglutamic acid (l-Pga) in the range of 0.01–0.50 mM at pH 4. The chiral recognition process accompanied with a gradual color change of MIPC can be easily visualized with the naked eye. The developed method has been applied to detect l-Pga in monosodium glutamate samples.

Surface-enhanced Raman scattering (SERS) has attracted considerable attention in recent years. The combination of MIP with SERS measurement was first reported by Wulff et al. [35]. By using SERS, target analytes can be detected based on the specific vibrational spectra characteristics of the compound adsorbed on the MIP. In early studies, Kantarovich et al. [36] developed a MIP-based SERS biochip by printing the MIP solution droplets on SERS-active surfaces using a pipette or a nano fountain pen. Later they fabricated a chemical nanosensor based on composite MIP particles and SERS for (S)-propranolol with a detection limit of 0.1 μM [37, 38].

Recently, Liu et al. [39] reported on MIP-based assay for another drug, theophylline, by imprinting the target molecules on the surface of silver nanoparticles (AgNPs) and measurement of the SERS signals. The AgNPs were located around the recognition cavities through the in situ reduction of the theophylline–silver complex. So the resultant polymer matrix provided both molecular recognition ability and SERS active surfaces. SERS signals of the theophylline molecules captured on the surface of the silver nanoparticles have a dose–response relationship to the target analytes and good reproducibility. The SERS intensity should be correlated to the amount of theophylline re-bound and could be quantitatively measured. The intensity of the fingerprint Raman band of theophylline at 567 cm^{-1} increases gradually with the increasing aliquots of the concentration of theophylline whereas the broad band at 2935 cm^{-1} remains nearly constant. The intensity ratio of the Raman band of I567/I2935 was used for relative quantification of the compound, which increased linearly with the concentrations of theophylline below 100 mM. The limit of detection for theophylline is estimated to be as low as

3.5 mM. The assay could distinguish theophylline from the closely related structure caffeine due to the variations of molecular size and shape as well as the different affinity to silver ions.

2.3 MIP-Based Surface Plasmon Resonance Bioassays

Surface plasmon resonance (SPR) is a commonly used technique in bioassays. As shown in Fig. 1b, target analytes in liquid samples are recognized and captured on the surface of metal and subsequently produce a local increase in the refractive index at the metal surface. It allows rapid, label-free, and realtime monitoring of the binding events [40, 41]. MIP films have been combined with SPR for bioassays. Many efforts have been made to increase the sensitivity of these methods in the detection of small molecules (<1000 Da). Matsui et al. [42] reported an SPR sensor with high sensitivity to a low-weight molecular dopamine by preparing a MIP gel with embedded AuNPs on a gold substrate of a chip. The Au–MIP/MIP-coated sensor chip even showed a significant shift of SPR angle to a nanomolar sample, suggesting that cooperative use of an analyte-binding macromolecule and an Au nanoparticle was effective for development of sensitive sensor chips. Izenberg et al. [43] tried to amplify the signal by a secondary molecular recognition event between a water-soluble processable star MIP and the analyte first captured by the SPR sensor. On the other hand, some researchers try to utilize the effect of the electronic coupling between the localized plasmon of the gold nanoparticles and the surface plasmon wave to enhance the SPR response.

A structural SPR sensor was developed by Tokareva et al. for the detection of cholesterol [44]. A plasmon-band shift of 56 nm was observed after the rebinding of 1 mM cholesterol due to the changing of the interaction between 10-nm-thick gold nanoislands and 2-nm-diameter nanoparticles that sandwiched the MIP. A novel label-free and high-throughput SPR detection sensor was reported by Huang et al. using a microfluidic system with integrated MIP films designed for detection of multiple biomolecules (progesterone, cholesterol, and testosterone) [45].

Lautner et al. [46] prepared avidin-imprinted microstructures to bind avidin. The dissociation constants were found in the submicromolar range (125 nM). The MIPs were able to discriminate among functional homologues of avidin, such as neutravidin, extravidin, and streptavidin. Lysozyme-imprinted poly(ethylene glycol dimethacrylate-N-methacryloyl-l-histidine methylester) nanoparticles were prepared and attached on the SPR sensor surface by Sener et al. [47]. The nanosensor is able to detect lysozyme in chicken eggwhite with lysozyme concentration as low as 32.2 nM. The detection limit is 9.20 pM.

A Fab fragment-imprinted SPR chip was developed by Ert et al. [8] for the realtime detection of human immunoglobulin G (IgG). IgG in human plasma was measured and the detection limit found as 56 ng/mL. Dong et al. prepared an ultrathin imprinted film on a SPR sensor using malachite green (MG) as the template molecule [48]. The MIP-modified SPR sensor showed high sensitivity and selectivity as well as

good stability in detecting MG. The method offers a simple and rapid approach to prepare ultrathin MIP film as the recognition element of the SPR sensor.

Magnetic MIP nanoparticles were also employed for amplifying SPR responses [49]. The chlorpyrifos-imprinted Fe_3O_4@polydopamine nanoparticles (Fe_3O_4@PDA NPs) enable highly sensitive and selective detection of chlorpyrifos. There was a linear relationship between the SPR angle shift and the concentration over a range from 0.001 to 10 μM with a detection limit of 0.76 nM. Verma et al. [50] report a new technique for the detection of 3-pyridinecarboxamide (PA) using a SPR-based optical fiber sensor by combining colloidal crystal and molecular-imprinted hydrogel. The sensor works on a spectral interrogation technique. SPR spectra showed a red shift with increasing concentration of PA, which is due to the interaction of PA molecules over the specific binding sites caused by the molecular imprinting. The sensitivity of the sensor is found to be 1.483 nm/(mg/mL).

Abbas et al. [51] report a relatively fast and efficient plasmonic hotspot-localized surface imprinting of gold nanorods using reversible template immobilization and siloxane copolymerization. The technique enables fine control of the imprinting process at the nanometer scale and provides a nanobiosensor with high selectivity and reusability. The assay was applied to detect neutrophil gelatinase-associated lipocalin (NGAL), a biomarker for acute kidney injury, using localized SPR spectroscopy.

2.4 MIP-Based Quartz Crystal Microbalance Bioassays

Quartz crystal microbalance (QCM) is a type of mass-sensitive piezoelectric transducer that allows for label-free detection of the target analytes. Tai et al. developed a MIP-QCM assay for the detection of creatine kinases [52]. Linear epitope sequences were selected based on an artificial-epitope mapping strategy. Nine different MIPs corresponding to the selected peptides were synthesized and fabricated on QCM chips. The peptide-imprinting method provided more detailed information on the conformation changes than the bulk protein-imprinted method. Linear correlations were obtained for the CK-MB isozyme over the concentration range from 1.0 to 10 ng/mL and the limit of detection was observed to be 0.5 ng/mL.

Yaqub et al. [53] fabricated via in situ MIP synthesis directly on gold electrodes of QCM. The resultant label-free and robust biomimetic sensing material shows reversible and selective responses for chlorotriazine moieties with minor structural differences. A detection limit of 20 ppb for atrazine was attained while showing selectivity up to 9 times higher than its metabolites des-ethyl-atrazine, des-isopropyl-atrazine, des-ethyl-des-isopropyl-atrazine, and structural analogues like simazine and propazine. Furthermore, imprinted nanoparticles gave linear characteristics over a wide range and showed no saturation effects in comparison to bulk materials.

Schirhagl et al. [9] tried to transfer the selectivity of natural antibodies in a cheap, robust, and reusable polymer via a double-imprinting protocol. First, they used antibodies with the desired selectivity as the template to generate imprinted polymer particles. After removal of the antibodies, cavities remained that reproduced the size, shape, and surface chemistry of the antibodies. In a second imprinting step, the particles with cavities were pressed into a second polymer. After the second polymer was cured, the particles were removed, leaving positive structures behind that reacted with the desired antigen. Such a sensitive coating was applied to the surface of a QCM and incorporated into a microfluidic chip. An immunosensor for estradiol was fabricated having 6 times higher affinity to its antigen than to structurally related molecules. The method was applied to detect viruses in plasma and allergenic protein in bread extract.

QCM sensors coated with MIP were developed by Diltemiz et al. for the recognition of immunoglobulin M (IgM) and mannose [54]. QCM electrodes were modified with 2-propene-1-thiol to form mannose-binding regions on the QCM sensor surface. Then the methacryloylamidophenylboronic acid-mannose (MAPBA-mannose), preorganized monomer system, was prepared using the MAPBA monomer. The mannose-imprinted QCM electrodes showed homogeneous binding sites for mannose and heterogeneous binding sites for IgM. In another study, the combination of QCM with MIP achieved measurements of ephedrine in aqueous solution with a detection limit of $\sim$5 ppm [55]. The LODs for two folic acid metabolites were found to be 20 ppm for leucovorin and 1 ppm for anhydroleucovorin.

Reflectometric interference spectroscopy (RIfS) is a method based upon the shift of the interference patterns due to the uptake of an analyte by the recognition layer [56]. This shift corresponds to the optical thickness (the product of the physical thickness and the refractive index) change of the layer. The RIfS method is simple and robust with widely available materials as transducer substrates. Recently, a fiber Fabry–Pérot sensing probe based on an optical fiber tip coated with a MIP film was developed by Queir et al. for the detection of microcystin-LR (MCT), a hepatotoxin from cyanobacteria [57]. First, the MCT-imprinting sol–gel membrane was prepared and applied over the tip of the fiber by dip coating. The probe showed a linear response to MCT concentration within 0.3–1.4 μg/L with a sensitivity of -12.4 ± 0.7 nm L μg^{-1}. The method shows excellent selectivity for MCT against other species coexisting with the analyte in environmental waters. It was successfully applied to the determination of MCT in contaminated samples. The main advantages of the proposed optical sensor include high sensitivity and specificity, low cost, robustness, easy preparation, and preservation.

In another study, interference photolithography (holography) was employed for the first time to prepare MIP thin film photopatterning with interfering laser beams [58]. The holographic MIP films are capable of specifically binding the steroid testosterone, which results in a change in the polymer network and thus in the diffraction efficiency of the film. Based on this, target analyte testosterone is measured by diffraction analysis in the concentration range between 1 and 100 μM.

3 MIPs as Tools for Biotransformation

Different strategies have been employed to enable the application of MIPs in biotransformation. The traditional approach is to use a transition state analogue (TSA) as the template (Fig. 2). Wulff's group [59–61] and Resmini's group [62, 63] have pioneered in this area. Several polymers mimicking the hydrolytic activity of some enzymes have been synthesized using the TSA approximation, which stabilized the intermediate state and lowered the activation energy. Another option is to remove the end product from the equilibrium with an imprint that represents the shape of the end product. Ye and Mosbach [64] for the first time applied MIPs in a thermolysin catalyzed reaction between aspartic acid and phenylalanine methyl ester to give the sweetener aspartame, which shifted an unfavorable equilibrium towards product formation and considerably enhanced the product yields by 40 %.

With the development of the MIP technique in recent years, a number of elegant examples have demonstrated that employing MIPs in biotransformation reactions resulted in enhanced selectivity and/or activity. Some even surpassed those of the corresponding catalytic natural enzymes.

3.1 MIP-Based Hydrolysis Reaction

Keçili et al. [65] obtained a mimic of lipase enzyme by synthesizing a MIP on silylated magnetic iron nanoparticles using methacryloylamido serine (MASE), methacryloylamido histidine (MAH), and methacryloylamidoglutamic acid (MAGA)

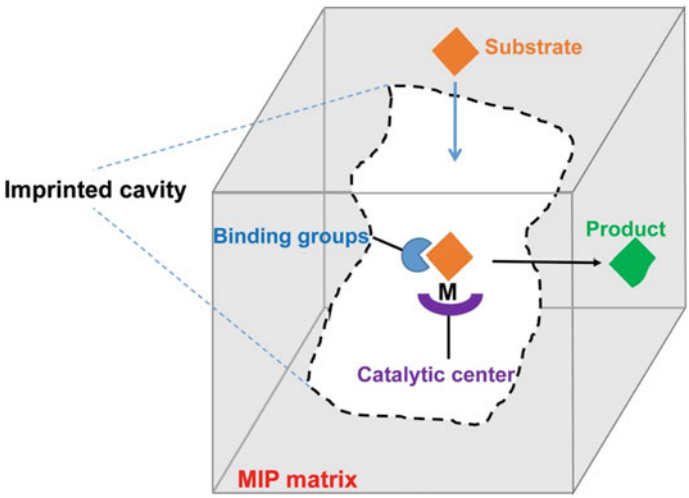

Fig. 2 Illustration of the principle of MIP-based biotransformation reactions

monomers, and p-nitrophenylpalmitate (p-NPP) which is a substrate of lipase as a template molecule. The resultant 50 nm-sized nanoparticles showed lipase activity, which could be easily removed from a reaction mixture and used repeatedly. Then they applied the p-NPP imprinted beads in a synthesis of biodiesel and methyl jasmonate [66]. The synthesized biomimetic artificial enzyme could be effectively used in transesterification reactions with a very high conversion rate, which is also highly thermal and chemically stable, low-cost, and reusable compared to natural lipase.

Li et al. [67] used temperature-dependent hydrophilicity and hydrophobicity of NIPAM to build up an "on/off"-switchable catalysis system with a smart enzyme-like imprinted polymer. At a temperature below its lower critical solution temperature (LCST), the polymer was capable of vigorously catalyzing for the hydrolysis of p-nitrophenyl acetate due to its hydrophilic networks, which enabled accessibility to the imprinted framework. By contrast, above the LCST, the dramatically decreased hydrophilicity caused shrinking of the imprinted networks, which inhibited the reactivity of the polymer. Later on, they fabricated a unique nanoreactor capable of running successive-reaction processes made of active MIPs containing AgNPs with two well-coupled templates, p-nitrophenyl acetate and p-nitrophenol [68]. The catalytic hydrolysis of the former by this nanoreactor led to the formation of the latter, which was further reduced by the nanoreactor to p-aminophenol.

3.2 MIP-Based Diels–Alder Reaction

Nicholls's group [69] presented a series of MIPs capable of catalyzing the Diels–Alder reaction between benzyl 1,3-butadienylcarbamate and N,N-dimethyl acrylamide. They found that the catalytic activity was significantly influenced by the choice of crosslinker and temperature, namely that polymer catalysis of the Diels–Alder reaction successfully enhanced the rate of the reaction up to 20-fold compared to the solution reaction at room temperature but was lowered at elevated temperature instead in contrast to the solution reaction. Molecular dynamics simulations were applied to investigate the equilibrium in the prepolymerization mixtures and the results illustrated the importance of different interactions of the template with functional monomer and crosslinker molecules, as well as interactions between the functional monomer and crosslinker.

3.3 MIP-Based Siloxane Bond Formation

Vincenzo et al. [70] reported the first example of biomimetic siloxane bond formation catalyzed by MIPs, which filled in the blank of MIPs suitable for organosilicon biotransformation. High-MAA–content MIPs prepared either via thermopolymerization or photopolymerization were observed to catalyze the

condensation of a model silanoltrimethylethoxysilane to the corresponding disiloxanehexamethyldisiloxane.

3.4 MIP-Based Oxidation and Reduction

Goretti et al. [71] synthesized MIPs that mimic chloroperoxidase for the oxidative dehalogenation of 2,4,6-trichlorophenol (TCP) using chloro-iron(III)-protoporphyrin IX as the catalytic center and simulating the amino acid residues of the enzyme with a combination of neutral and basic functional monomers (methacrylamide and 4-vinylpyridine, respectively). The template TCP was specifically adsorbed and underwent regioselective transformation by the polymers. The main oxidation product was 2,6-dichloro-1,4-benzoquinone, in accord with natural chloroperoxidase.

Sun et al. [72] prepared a series of MIPs by the polymerization of acrylamide and ethylene dimethacrylate in the presence of the template of o-, m-, or p-nitrobenzyl alcohol (NBA) and a $FeCl_3$ complex. The Fe(III)-MIP catalyst exhibited high catalytic activity and unique substrate recognition in the oxidation of benzyl alcohol derivatives.

Joanna et al. [73] chose four metal ions Cu^{2+}, Co^{2+}, Mn^{2+}, and Zn^{2+} among the microelements that are essential in the native enzymes for imprinting based on suspension polymerization of 4-vinylpyridine, acrylonitrile, and trimethylolpropanetrimethacrylate in the presence of the transition metal ions and 4-methoxybenzyl alcohol as a template. The Cu^{2+}, Co^{2+}, and Zn^{2+} imprinted MIPs showed catalytic activity for hydroquinone oxidation whereas the Mn^{2+} imprinted catalyst showed no activity due to the insufficient metal loading.

3.5 Other Reactions

Tada's group [74] designed a series of MIP–Ru complexes on oxide surfaces functioning as shape-selective catalysts for regioselective epoxidation and transfer hydrogenation. They utilized surface-attached Ru complexes with template ligands and inorganic/organic surface matrix overlayers to control the chemical environment around the active metal complex catalysts on oxide surfaces. Further advances such as the imprinting of a transition state structure or the addition of multiple binding sites could lead to systems that can achieve 100 % selective catalysis.

Meng et al. [75] prepared surface MIPs with silica microspheres as a supporting matrix using acrylamide as a functional monomer, ethylene glycol dimethacrylate as a crosslinker, azoisobutyronitrile as an initiator, and p-hydroxybenzoic acid as a template. The resultant MIPs selectively catalyzed the chlorination of toluene to para-chlorotoluene with a conversion ratio of 85.5 %. The molar ratio of para-chlorotoluene to o-chlorotoluene was 1.38, which was higher than that of traditional catalysts.

4 Conclusions and Future Trends

In summary, remarkable progress has been made in recent years in the development of MIP-based bioassays for the detection of both small bioactive molecules and biomacromolecules. MIP-based bioassays with optical signals exhibit excellent performance in comparison with traditional immunoassays. Recently published work has also shown many encouraging results of using MIPs for biotransformation. The advantages of using MIPs relative to proteins and peptides during catalysis include their facile and inexpensive preparation as well as improved stability to heat and organic solvents compared with their biological counterparts.

However, there are some remaining issues to be addressed in the future development of more practical MIP-based bioassays and applications of MIPs for biotransformation in complex systems. For further advances of MIP-based bioassays, the specificity and sensitivity need to be further improved by incorporation of more versatile functional monomers and signal enhancement mechanisms. Another important trend in this field goes towards simultaneous detection of multiple targets, which have not been well developed yet. Fabricating of MIP at the end of an optical fiber or on an appropriate substrate may generate very delicate probes or visible sensors and enable in situ and realtime measurement of the dynamic variations of many bioactive substances.

For the MIP-based biotransformation, in addition to the challenges to mimic natural processes more effectively, a key issue is to better understand and describe the mechanism of the reactions. Moreover, product inhibition has proven to be a serious problem for many MIP catalysts because of their rigidity, especially when the substrate, intermediate, and product are structurally similar. Although active sites in enzymes are flexible to adopt conformational changes to favor product release, the rigidity of MIP-binding sites often makes it difficult to achieve good turnover rates. The binding affinity of MIPs towards the products should be lower than the intermediates or transition states to ensure large turnover.

Finally, development of catalytic MIP-based bioassays may bring about significant improvement of the assay specificity or sensitivity in comparison to the solely binding-dependent assays. Detection of the products from the analyte conversion is also favorable to avoid interferences caused by nonspecific binding. Such a combination may play more important roles in future development.

References

1. Wulff G (1995) Molecular imprinting in cross-linked materials with the aid of molecular templates—a way towards artificial antibodies. Angew Chem Int Ed Eng 34(17):1812–1832
2. Mayes AG, Mosbach K (1997) Molecularly imprinted polymers: useful materials for analytical chemistry? Trac-Trend Anal Chem 16(6):321–332
3. Ge Y, Turner APF (2009) Molecularly imprinted sorbent assays: recent developments and applications. Chem-Eur J 15(33):8100–8107

4. Henry OYF, Cullen DC, Piletsky SA (2005) Optical interrogation of molecularly imprinted polymers and development of MIP sensors: a review. Anal Bioanal Chem 382(4):947–956
5. Gultekin A, Ersoz A, Denizli A, Say R (2012) Preparation of new molecularly imprinted nanosensor for cholic acid determination. Sensor Actuat B-Chem 162(1):153–158
6. Alvarez A, Costa JM, Pereiro R, Sanz-Medel A (2012) Reusable phosphorescent probes based on molecularly imprinted polymers for the determination of propranolol in urine. Sensor Actuat B-Chem 168:370–375
7. Barrios CA, Zhenhe C, Navarro-Villoslada F, Lopez-Romero D, Moreno-Bondi MC (2011) Molecularly imprinted polymer diffraction grating as label-free optical bio (mimetic) sensor. Biosens Bioelectron 26(5):2801–2804
8. Erturk G, Uzun L, Tumer MA, Say R, Denizli A (2011) F-ab fragments imprinted SPR biosensor for real-time human immunoglobulin G detection. Biosens Bioelectron 28(1):97–104
9. Schirhagl R, Qian JJ, Dickert FL (2012) Immunosensing with artificial antibodies in organic solvents or complex matrices. Sensor Actuat B-Chem 173:585–590
10. Meeuwissen J, Reek JN (2010) Supramolecular catalysis beyond enzyme mimics. Nat Chem 2 (8):615–621
11. Wiester MJ, Ulmann PA, Mirkin CA (2011) Enzyme mimics based upon supramolecular coordination chemistry. Angew Chem 50(1):114–137
12. Yin YZ, Dong ZY, Luo Q, Liu JQ (2012) Biomimetic catalysts designed on macromolecular scaffolds. Prog Polym Sci 37(11):1476–1509
13. Jin T, Fujii F, Sakata H, Tamura M, Kinjo M (2005) Amphiphilic p-sulfonatocalix [4] are ne-coated CdSe/ZnS quantum dots for the optical detection of the neurotransmitter acetylcholine. Chem Commun 34:4300–4302
14. Jin T, Fujii F, Sakata H, Tamura M, Kinjo M (2005) Calixarene-coated water-soluble CdSe-ZnS semiconductor quantum dots that are highly fluorescent and stable in aqueous solution. Chem Commun 22:2829–2831
15. Konishi K, Hiratani T (2006) Turn-on and selective luminescence sensing of copper ions by a water-soluble Cd10S16 molecular cluster. Angew Chem Int Ed 45(31):5191–5194
16. Basabe-Desmonts L, Reinhoudt DN, Crego-Calama M (2007) Design of fluorescent materials for chemical sensing. Chem Soc Rev 36(6):993–1017
17. Lin CI, Joseph AK, Chang CK, Lee YD (2004) Synthesis and photoluminescence study of molecularly imprinted polymers appended onto CdSe/ZnS core-shells. Biosens Bioelectron 20 (1):127–131
18. Lin CI, Joseph AK, Chang CK () Lee YD (2004) Molecularly imprinted polymeric film on semiconductor nanoparticles—analyte detection by quantum dot photoluminescence. J Chromatogr A 1027(1–2):259–262
19. Mao Y, Bao Y, Han DX, Li FH, Niu L (2012) Efficient one-pot synthesis of molecularly imprinted silica nanospheres embedded carbon dots for fluorescent dopamine optosensing. Biosens Bioelectron 38(1):55–60
20. Liu HL, Fang GZ, Zhu HD, Li CM, Liu CC, Wang S (2013) A novel ionic liquid stabilized molecularly imprinted optosensing material based on quantum dots and graphene oxide for specific recognition of vitamin E. Biosens Bioelectron 47:127–132
21. Zhang W, He XW, Chen Y, Li WY, Zhang YK (2011) Composite of CdTe quantum dots and molecularly imprinted polymer as a sensing material for cytochrome c. Biosens Bioelectron 26 (5):2553–2558
22. Zhang W, He XW, Chen Y, Li WY, Zhang YK (2012) Molecularly imprinted polymer anchored on the surface of denatured bovine serum albumin modified CdTe quantum dots as fluorescent artificial receptor for recognition of target protein. Biosens Bioelectron 31(1): 84–89
23. Lee MH, Chen YC, Ho MH, Lin HY (2010) Optical recognition of salivary proteins by use of molecularly imprinted poly(ethylene-co-vinyl alcohol)/quantum dot composite nanoparticles. Anal Bioanal Chem 397(4):1457–1466

24. Inoue Y, Kuwahara A, Ohmori K, Sunayama H, Ooya T, Takeuchi T (2013) Fluorescent molecularly imprinted polymer thin films for specific protein detection prepared with dansylethylenediamine-conjugated O-acryloyl L-hydroxyproline. Biosens Bioelectron 48:113–119
25. Yin JF, Wang ZX, Song MY, Zhao C, Wang HL (2013) Plastic antibody for DNA damage: fluorescent imaging of BPDE-dG adducts in genomic DNA. Analyst 138(17):4958–4966
26. Banerjee S, Konig B (2013) Molecular imprinting of luminescent vesicles. J Am Chem Soc 135(8):2967–2970
27. Ton XA, Acha V, Haupt K, Bernadette TSB (2012) Directfluorimetric sensing of UV-excited analytes in biological and environmental samples using molecularly imprinted polymer nanoparticles and fluorescence polarization. Biosens Bioelectron 36(1):22–28
28. Tan L, Rang CC, Xu SY, Tang YW (2013) Selective room temperature phosphorescence sensing of target protein using Mn-doped ZnS QDs-embedded molecularly imprinted polymer. Biosens Bioelectron 48:216–223
29. Dan L, Wang HF (2013) Mn-doped ZnS quantum dot imbedded two-fragment imprinting silica for enhanced room temperature phosphorescence probing of domoic acid. Anal Chem 85 (10):4844–4848
30. Liu JM, Cui ML, Wang XX, Lin LP, Jiao L, Zhang LH, Zheng ZY, Huang LZ (2013) A highly selective affinity adsorption imprinting phosphorescence sensor for determination of trace alkaline phosphatase and prediction of human diseases. Sensor Actuat B-Chem 186: 521–527
31. Hu XB, Li GT, Li MH, Huang J, Li Y, Gao YB, Zhang YH (2008) Ultrasensitive specific stimulant assay based on molecularly imprinted photonic hydrogels. Adv Funct Mater 18 (4):575–583
32. Liu F, Huang SY, Xue F, Wang YF, Meng ZH, Xue M (2012) Detection of organophosphorus compounds using a molecularly imprinted photonic crystal. Biosens Bioelectron 32(1): 273–277
33. Bai W, Spivak DA (2014) A double-imprinted diffraction-grating sensor based on a virus-responsive super-aptamer hydrogel derived from an impure extract. Angew Chem Int Ed 53 (8):2095–2098
34. Zhang YX, Zhao PY, Yu LP (2013) Highly-sensitive and selective colorimetric sensor for amino acids chiral recognition based on molecularly imprinted photonic polymers. Sensor Actuat B-Chem 181:850–857
35. Kostrewa S, Emgenbroich M, Klockow D, Wulff G (2003) Surface-enhanced Raman scattering on molecularly imprinted polymers in water. Macromol Chem Phys 204(3):481–487
36. Kantarovich K, Tsarfati I, Gheber LA, Haupt K, Bar I (2009) Writing Droplets of molecularly imprinted polymers by nano fountain pen and detecting their molecular interactions by surface-enhanced Raman scattering. Anal Chem 81(14):5686–5690
37. Bompart M, De Wilde Y, Haupt K (2010) Chemical nanosensors based on composite molecularly imprinted polymer particles and surface-enhanced Raman scattering. Adv Mater 22(21):2343–2348
38. Kantarovich K, Tsarfati I, Gheber LA, Haupt K, Bar I (2010) Reading microdots of a molecularly imprinted polymer by surface-enhanced Raman spectroscopy. Biosens Bioelectron 26(2):809–814
39. Liu P, Liu RY, Guan GJ, Jiang CL, Wang SH, Zhang ZP (2011) Surface-enhanced Raman scattering sensor for theophylline determination by molecular imprinting on silver nanoparticles. Analyst 136(20):4152–4158
40. Phillips KS, Cheng Q (2007) Recent advances in surface plasmon resonance based techniques for bioanalysis. Anal Bioanal Chem 387(5):1831–1840
41. Gordon R, Sinton D, Kavanagh KL, Brolo AG (2008) A new generation of sensors based on extraordinary optical transmission. Acc Chem Res 41(8):1049–1057
42. Matsui J, Akamatsu K, Hara N, Miyoshi D, Nawafune H, Tamaki K, Sugimoto N (2005) SPR sensor chip for detection of small molecules using molecularly imprinted polymer with embedded gold nanoparticles. Anal Chem 77(13):4282–4285

43. Izenberg NR, Murrray GM, Pilato RS, Baird LM, Levin SM, Van Houten KA (2009) Astrobiological molecularly imprinted polymer sensors. Planet Space Sci 57(7):846–853
44. Tokareva I, Tokarev I, Minko S, Hutter E, Fendler JH (2006) Ultrathin molecularly imprinted polymer sensors employing enhanced transmission surface plasmon resonance spectroscopy. Chem Commun 31:3343–3345
45. Huang SC, Lee GB, Chien FC, Chen SJ, Chen WJ, Yang MC (2006) A microfluidic system with integrated molecular imprinting polymer films for surface plasmon resonance detection. J Micromech Microeng 16(7):1251–1257
46. Lautner G, Kaev J, Reut J, Opik A, Rappich J, Syritski V, Gyurcsanyi RE (2011) Selective artificial receptors based on micropatterned surface-imprinted polymers for label-free detection of proteins by spr imaging. Adv Funct Mater 21(3):591–597
47. Sener G, Uzun L, Say R, Denizli A (2011) Use of molecular imprinted nanoparticles as biorecognition element on surface plasmon resonance sensor. Sensor Actuat B-Chem 160 (1):791–799
48. Dong JW, Peng Y, Gao N, Bai JL, Ning BA, Liu M, Gao ZX (2012) A novel polymerization of ultrathin sensitive imprinted film on surface plasmon resonance sensor. Analyst 137 (19):4571–4576
49. Yao GH, Liang RP, Huang CF, Wang Y, Qiu JD (2013) Surface plasmon resonance sensor based on magnetic molecularly imprinted polymers amplification for pesticide recognition. Anal Chem 85(24):11944–11951
50. Verma R, Gupta BD (2013) Fiber optic SPR sensor for the detection of 3-pyridinecarboxamide (vitamin B-3) using molecularly imprinted hydrogel. Sensor Actuat B-Chem 177:279–285
51. Abbas A, Tian LM, Morrissey JJ, Kharasch ED, Singamaneni S (2013) Hot spot-localized artificial antibodies for label-free plasmonic biosensing. Adv Funct Mater 23(14):1789–1797
52. Tai DF, Ho YF, Wu CH, Lin TC, Lu KH, Lin KS (2011) Artificial-epitope mapping for CK-MB assay. Analyst 136(11):2230–2233
53. Yaqub S, Latif U, Dickert FL (2011) Plastic antibodies as chemical sensor material for atrazine detection. Sensor Actuat B-Chem 160(1):227–233
54. Diltemiz SE, Hur D, Kecili R, Ersoz A, Say R (2013) New synthesis method for 4-MAPBA monomer and using for the recognition of IgM and mannose with MIP-based QCM sensors. Analyst 138(5):1558–1563
55. Kotova K, Hussain M, Mustafa G, Lieberzeit PA (2013) MIP sensors on the way to biotech applications: targeting selectivity. Sensor Actuat B-Chem 189:199–202
56. Belmont AS, Jaeger S, Knopp D, Niessner R, Gauglitz G, Haupt K (2007) Molecularly imprinted polymer films for reflectometric interference spectroscopic sensors. Biosens Bioelectron 22(12):3267–3272
57. Queiros RB, Silva SO, Noronha JP, Frazao O, Jorge P, Aguilar G, Marques PVS, Sales MGF (2011) Microcystin-LR detection in water by the Fabry-Perot interferometer using an optical fibre coated with a sol-gel imprinted sensing membrane. Biosens Bioelectron 26(9): 3932–3937
58. Fuchs Y, Soppera O, Mayes AG, Haupt K (2013) Holographic molecularly imprinted polymers for label-free chemical sensing. Adv Mater 25(4):566–570
59. Wulff G (2002) Enzyme-like catalysis by molecularly imprinted polymers. Chem Rev 102 (1):1–27
60. Liu JQ, Wulff G (2004) Molecularly imprinted polymers with strong carboxypeptidase a-like activity: combination of an amidinium function with a zinc-ion binding site in transition-state imprinted cavities. Angew Chem 43(10):1287–1290
61. Wulff G, Liu J (2012) Design of biomimetic catalysts by molecular imprinting in synthetic polymers: the role of transition state stabilization. Acc Chem Res 45(2):239–247
62. Resmini M (2012) Molecularly imprinted polymers as biomimetic catalysts. Anal Bioanal Chem 402(10):3021–3026
63. Bonomi P, Servant A, Resmini M (2012) Modulation of imprinting efficiency in nanogels with catalytic activity in the Kemp elimination. J Mol Recognit JMR 25(6):352–360

64. Ye L, Ramstrom O, Ansell RJ, Mansson MO, Mosbach K (1999) Use of molecularly imprinted polymers in a biotransformation process. Biotechnol Bioeng 64(6):650–655
65. Keçili R, Özcan AA, Ersöz A, Hür D, Denizli A, Say R (2010) Superparamagnetic nanotraps containing MIP based mimic lipase for biotransformations uses. J Nanopart Res 13(5): 2073–2079
66. Kecili R, Say R, Ersoz A, Hur D, Denizli A (2012) Investigation of synthetic lipase and its use in transesterification reactions. Polymer 53(10):1981–1984
67. Li SJ, Ge Y, Tiwari A, Wang SQ, Turner APF, Piletsky SA (2011) 'On/off'-switchable catalysis by a smart enzyme-like imprinted polymer. J Catal 278(2):173–180
68. Li SJ, Luo YY, Whitcombe MJ, Piletsky SA (2013) A successive-reaction nanoreactor made of active molecularly imprinted polymer containing Ag nanoparticles. J Mater Chem A 1 (47):15102–15109
69. Henschel H, Kirsch N, Hedin-Dahlström J, Whitcombe MJ, Wikman S, Nicholls IA (2011) Effect of the cross-linker on the general performance and temperature dependent behaviour of a molecularly imprinted polymer catalyst of a Diels-Alder reaction. J Mol Catal B Enzym 72 (3–4):199–205
70. Abbate V, Bassindale AR, Brandstadt KF, Taylor PG (2011) Biomimetic catalysis at silicon centre using molecularly imprinted polymers. J Catal 284(1):68–76
71. Diaz-Diaz G, Blanco-Lopez MC, Lobo-Castanon MJ, Miranda-Ordieres AJ, Tunon-Blanco P (2012) Hemo-acrylic polymers as catalyst for the oxidative dehalogenation of 2,4,6-trichlorophenol. Chloroperoxidase's mimic imprinting effects. J Mol Catal A-Chem 353:117–121
72. Sun WQ, Tan R, Zheng WG, Yin DH (2013) Molecularly imprinted polymer containing Fe (III) catalysts for specific substrate recognition. Chin J Catal 34(8):1589–1598
73. Czulak J, Jakubiak-Marcinkowska A, Trochimczuk A (2013) Polymer catalysts imprinted with metal ions as biomimics of metalloenzymes. Adv Mater Sci Eng. doi:10.1155/2013/464265
74. Muratsugu S, Tada M (2013) Molecularly imprinted Ru complex catalysts integrated on oxide surfaces. Acc Chem Res 46(2):300–311
75. Meng MJ, Bao LL, He MQ, Sun KY, Li WB, Zhao DX, Feng YH, Yan YS (2014) Preparation, characterization, and adsorption performance of p-hydroxybenzoic acid imprinted polymer and selective catalysis of toluene to para-chlorotoluene. J Appl Polym Sci. doi:10.1002/App.40118

Adv Biochem Eng Biotechnol (2015) 150: 227–231
DOI 10.1007/978-3-319-20729-2

Index